
# EFFECTS OF TEMPERATURE AND STEAM ENVIRONMENT ON FATIGUE BEHAVIOR OF THREE SIC/SIC CERAMIC MATRIX COMPOSITES

THESIS

Vipul Sharma, 2nd Lieutenant, USAF

AFIT/GAE/ENY/08-S02

**DEPARTMENT OF THE AIR FORCE**
**AIR UNIVERSITY**

## AIR FORCE INSTITUTE OF TECHNOLOGY

**Wright-Patterson Air Force Base, Ohio**

The views expressed in this thesis are those of the author and do not reflect the official policy or position of the United States Air Force, Department of Defense, or the U.S. Government.

AFIT/GAE/ENY/08-S02

# EFFECTS OF TEMPERATURE AND STEAM ENVIRONMENT ON FATIGUE BEHAVIOR OF THREE SIC/SIC CERAMIC MATRIX COMPOSITES

THESIS

Presented to the Faculty

Department of Aeronautical and Astronautical Engineering

Graduate School of Engineering and Management

Air Force Institute of Technology

Air University

Air Education and Training Command

In Partial Fulfillment of the Requirements for the

Degree of Master of Science in Aeronautical Engineering

Vipul Sharma, B.S.

2nd Lieutenant, USAF

September 2008

AFIT/GAE/ENY/08-S02

# EFFECTS OF TEMPERATURE AND STEAM ENVIRONMENT ON FATIGUE BEHAVIOR OF THREE SIC/SIC CERAMIC MATRIX COMPOSITES

Vipul Sharma, B.S.

2nd Lieutenant, USAF

Approved:

| | |
|---|---|
| Marina Ruggles-Wrenn, PhD (Chairman) | Date |
| Geoff Fair, PhD (Member) | Date |
| Richard Hall, PhD (Member) | Date |

## Abstract

The fatigue behavior of two woven SiC-SiNC ceramic matrix composites (CMCs) was investigated at 1300 °C in laboratory air and in steam. The first composite (C1) consists of a PIP SiNC matrix reinforced with Sylramic (Syl) fibers woven in a five-harness satin weave fabric and coated with a proprietary dual-layer interface. The second composite (C2) consists of a modified PIP SiNC matrix reinforced with Sylramic-iBN (Syl-iBN) fibers woven in a five-harness satin weave fabric and coated with a proprietary dual-layer interface. The tensile stress-strain behavior was investigated and the tensile properties measured at 1300°C. Tension-tension fatigue behavior was studied for fatigue stresses ranging from 100 to 180 MPa at 1300 °C in air and in steam. The presence of steam caused noticeable degradation in fatigue performance of both composites at 1300°C. The fatigue limit of the composite C1 (based on a run-out condition of $2 \times 10^5$ cycles) was 100 MPa (53% UTS at 1300°C) in both air and steam. The fatigue limit of the composite C2 was 160 MPa (66% UTS) in air and 140 MPa (58% UTS) in steam. The retained strength and modulus of all specimens that achieved run-out were characterized. Specimens of both composites tested in air retained 100% of their tensile strength, while the specimens of both composites tested in steam retained only about 90% of their tensile strength.

**Acknowledgments**

I would like to express my sincere appreciation to the following people for their help during the course of this thesis work: Lab technicians Sean Miller, Barry Page, and Chris Zickefoose for helping me in repair and maintenance of the MTS machines. 1st Lt Tufan Yeleser of the Turkish Air Force for showing me how to use the equipment necessary to complete research. To my family and friends for your love and support. I would like to express my extreme gratitude to my thesis advisor Dr. Marina Ruggles-Wrenn who demonstrated great patience, and was always there to guide and help me get back on course when I needed it.

Vipul Sharma

## Table of Contents

Page

## List of Figures

Page

## List of Tables

Page

# EFFECTS OF TEMPERATURE AND STEAM ENVIRONMENT ON FATIGUE BEHAVIOR OF THREE SIC/SIC CERAMIC MATRIX COMPOSITES

## I. Introduction and Background

> "It is a truism that technological development depends on advances in the field of materials. One does not have to be an expert to realize that a most advanced turbine or aircraft design is of no use if adequate materials to bear the service loads and conditions are not available. Whatever the field may be, the final limitation on advancement depends on materials" [21].

Advances in materials and our understanding of their properties have provided the basis for much of our technological development over the years. This is particularly true in the case of the aerospace industry. While some advances in aircraft performance can be attributed to improvements in areas such as design technique and manufacturing methods, over the years the biggest factor influencing cutting-edge aeronautical technology has been the application of new materials.

Composite materials made their appearance in commercial airplanes with the introduction of the Boeing 707 in the 1950s. Today, composites make up a large percentage of aircraft structural components. Composites comprise 9% of the aircraft structural weight in the Boeing 777. Boeing is predicting that 50% of the material used on the 787 Dreamliner, scheduled for delivery in 2010, will be composites [2]. Fighter aircraft produced in the late 1970s such as the F-15 and F-16 incorporated about 1-2% composites into the airframe of by weight. The use of composites increased greatly in the next generation of fighter aircraft, so much that the F/A-18E/F and F-22A are

approximately 25% composites by weight [35]. Composites are now being considered for use in areas where metals have traditionally been used, such as turbine engines.

The US Air Force, and the aerospace industry as a whole, has a strong interest in the continued development of composites. Advances in propulsion technologies have raised the demand for materials that have to perform at high loads while at high temperatures. The US Air Force Integrated High Performance Turbine Engine Technology (IHPTET) program was established in 1987 with a goal to double aircraft propulsion capability [27:3]. This led to an increased interest Ceramic Matrix Composites (CMCs), which exhibit and maintain high strength at elevated temperatures. Many potential applications for CMC's include combustor liners and turbine vanes. Ceramic Matrix Composites, while capable of withstanding high temperatures, also exhibit high fracture toughness, thermal conductivity and low densities [14, 29, 33, 34]. Ceramic Matrix Composites, which were introduced in the late 1970's are currently being considered for potential applications such as combustor liners and turbine vanes [11, 38]. It is likely that CMCs will be used in propulsion components of reusable launch vehicles [41]. In these applications the CMCs will be subjected to varying temperatures, pressures, and degrading environments like water vapor. Such environments can cause rapid oxidation which is a primary mechanism of environmental degradation of CMCs [5]. Therefore thermodynamic stability of CMCs is a vital issue.

Ceramics are typically inorganic materials processed at high temperatures falling into two classes: Traditional and advanced. Traditional ceramics are monolithic in form and are exemplified by bricks, pottery, and tiles. Advanced ceramics are characterized by the fact that their production generally utilizes a chemical processing route [5:47]. Continuous fiber ceramic composites (CFCCs) are advanced ceramics. Both traditional and advanced ceramics are known for their ability to withstand high temperatures, however, both types of ceramics are also characterized by their brittle nature. CFCCs are composed of a ceramic matrix reinforced with high aspect ratio ceramic fibers allowing them to exhibit less brittle behavior than other ceramics. The fiber bundles are the primary load bearing mechanism whereas the matrix is responsible for transferring the load amongst the fibers. These characteristics allow CFCCs to display non-catastrophic failure modes as compared to monolithic ceramics. CMCs are continuous fiber ceramic composites designed to withstand high temperature environments allowing CMCs to be used in applications where monolithic ceramics cannot survive.

CMC matrices are usually capable of withstanding high temperatures and are composed of one or more metals combined with a nonmetal such as oxygen, carbon, nitrogen, or boron. Figure 1 shows maximum service temperatures for different materials.

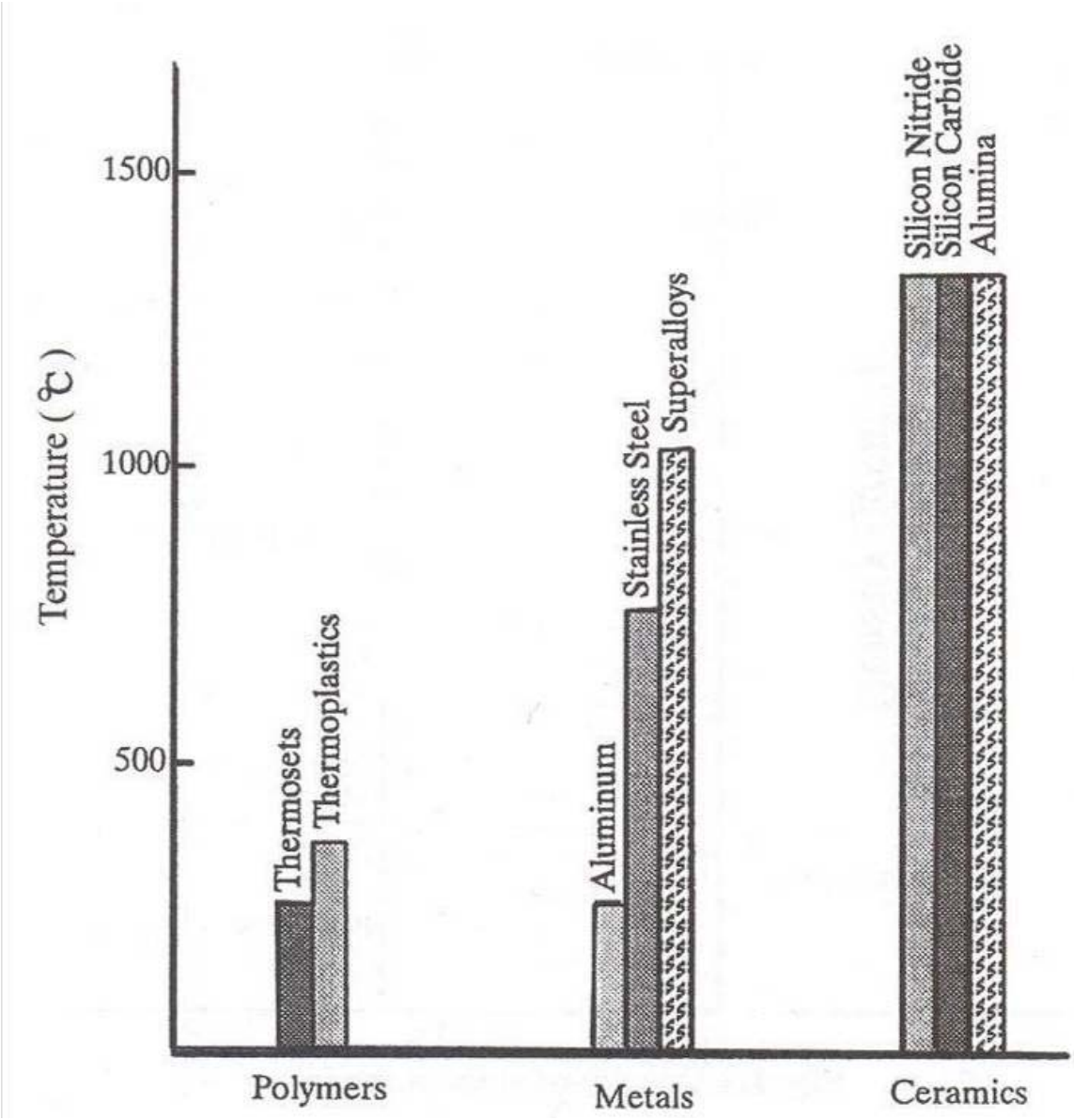


**Figure 1. Maximum Material Service Temperatures [5:5 ]**

CMC matrices are categorized as oxide or non-oxide matrices. Oxide matrices are oxidization resistant. Alumina is an example of an Oxide matrix. Silicon based Non-oxide matrices are susceptible to oxidation at high temperatures and therefore rely on a layer of Silica ($SiO_2$) to prevent from oxidation. Silicon Carbide is an example of a non-

oxide matrix. The oxidation resistance mechanisms of both oxide and non-oxide matrices highlight another function of the matrix; the matrix is supposed to protect the fibers from the environment.

Fibers are categorized by their diameter size. A monofilament is a continuous fiber with a diameter greater than 100μm [5:47]. A multifiber tow is a bundle of individual fibers. These individual fiber diameters range from 5-15 μm. Fibers are also denoted as oxide and non-oxide fibers. Oxide fibers are oxidation resistant similar to their matrix counterparts. Additionally oxide fibers are produced with relatively constant diameters variations on the order of ~1μm. Nextel 610, 650 and 720 developed by 3M are examples of oxide fibers. Table 1 lists CMC fiber properties.

**Table 1. Properties of Ceramic Fibers [7].**

| Fiber Property | CMC Benefit |
|---|---|
| • High Modulus | • Improves CMC stiffness and reduces matrix stresses |
| • High As-Produced Strength | • Improves CMC toughness and ultimate strength |
| • High Thermomechanical Stability | • Improves CMC as-fabricated strength, CMC strength retention and creep resistance during service |
| • High Oxidative Stability | • Improves CMC service life in oxidizing environments |
| • Small Diameter | • Improves matrix strength and facilitates fabrication of thin and complex-shaped CMCs |
| • Low Density | • Improves CMC specific properties for weight-sensitive applications and reduces stresses in CMC rotating components |
| • Low Cost | • Reduces CMC cost and improves CMC commercial viability |

Non-oxide fibers are susceptible to oxidation and are usually covered by a protective coating. At high temperatures these coatings often demonstrate poor oxidation resistance thus exposing the fiber itself to the oxidizing environment. Sylramic™ is a SiC fiber manufactured by ATK-COI Ceramics.

The region where the matrix bonds to the fiber is known as the interface. Interface bonds are usually characterized as weak or strong. Weak interfacial bonds allow for the matrix and fiber bond to come undone. This behavior is known as debonding. During debonding, a growing crack is deflected around the fiber allowing it to remain intact. Crack deflection, fiber bridging, fiber pullout and fiber fracture occur after debonding. CMCs with weak interfacial bonds, therefore, demonstrate non-catastrophic failure.

Strong interface bonds do not allow for crack deflection. A crack, therefore, will grow from the matrix into the fiber resulting in catastrophic failure. Figure 2 shows crack growth in weak and strong interface bond CMCs.

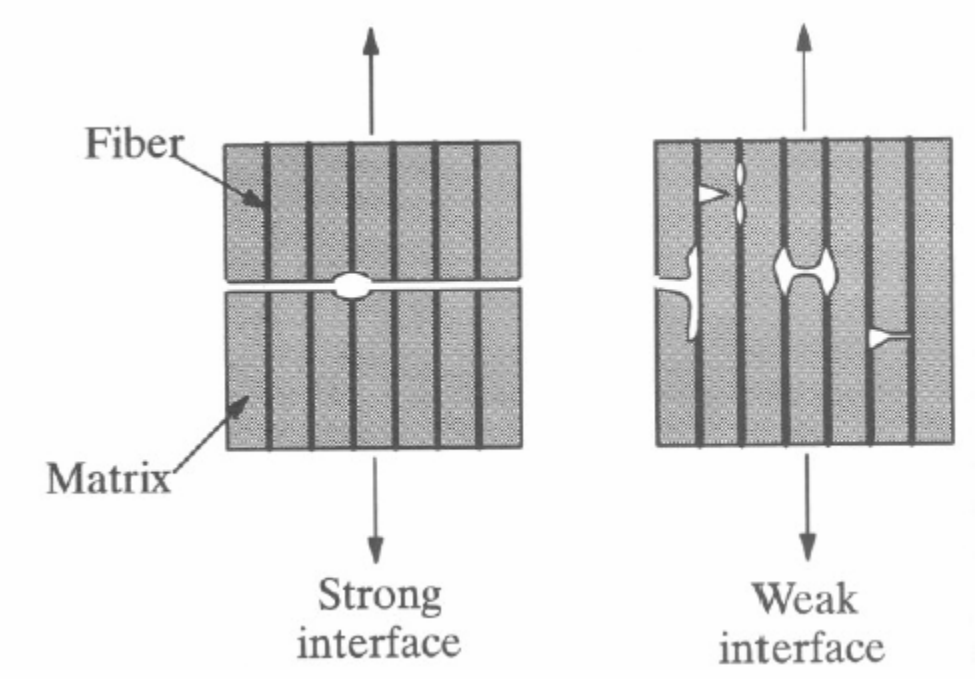


**Figure 2. Failure of a CMC as a function of interfacial bond [5:170].**

### 1.1. Silicon Carbide-Silicon Carbide CMCs

SiC/SiC CMCs consist of a Silicon Carbide fiber in a Silicon Carbide matrix. SiC/SiC composites are capable of withstanding temperatures up to 1500 $^{o}$C [32]. They can be manufactured through a variety of different methods including sinteringChemical Vapor Infiltration (CVI), Chemical Vapor Deposition (CVD) and polymer impregnation/pyrolysis (PIP) [5:20, 32].

The SiC fibers currently used in SiC/SiC CMCs are third generation fibers. First generation SiC fibers had a Young's modulus of ~220 GPa and decomposed beyond

1100 °C. Second generation SiC could withstand higher temperatures but would creep at ~1200 °C and third generation SiC fibers are prepared at approximately 1600-2000 $^{o}$C and therefore are able to operate at very high temperatures. Their diameter is approximately 15 μm. In bulk form they are reported to have a Young's modulus of ≈400 GPa or approximately twice that of steel [3, 16, 32]. The high stiffness of the third generation fiber reduces their weaveability and they exhibit low strain at failure [32].

SiC/SiC CMCs utilize an interphase to help protect the fibers from the effects of oxidation. The interphases can be composed of hexagonal BN, $(PyC\text{-}SiC)_n$, and $(BN\text{-}SiC)_n$ multilayered interphases. Of the aforementioned coatings, BN is one of the most commonly used. BN coatings crack at high temperatures and oxidize at 1000 $^{o}$C to form $BN_2O_3$ which then reacts with the SiO and $SiO_2$ already present in the matrix and fibers to form Borosilicate glass. BN coating degradation allows moisture to penetrate and damage the SiC fibers [46].

In tension tests SiC/SiC CMCs often demonstrate two zones of linear deformation. In the first zone, the load is being evenly distributed amongst the fibers and matrix. The stress strain curve departs linearity when matrix cracking first occurs. Additional load is thrown onto the fibers and the CMC demonstrates another region of linear behavior until failure. The modulus of the second linear region is lower than the modulus of the first linear region due to the fact that the fibers in SiC/SiC CMCs demonstrate higher failure strains than the matrix [5:238].

SiC/SiC CMCs show a high creep tolerance [34] however they are vulnerable to cyclic fatigue. McNulty *et al.* stated that Nicalon™-fiber-reinforced CMCs tested at

room temperature demonstrated a fatigue limit of 65-80% of their Ultimate Tensile Strength (UTS) [24]. Kalluri *et al.* and Mizuno *et al.* conducted fatigue testing of SiC/SiC CMCs at temperatures ranging from 1000-1200 $^{o}$C and found that the fatigue limit dropped to 30-50% of the UTS [20, 29].

McNulty and Mizuno observed that fatigue failure is due to the fact that the cyclic loading and unloading led to repeated opening and closing of crack surfaces. This cyclic opening and closing leads to reduced shear strength and slip of interfaces between the fiber and the matrix in the $0^{o}$ bundles. Interface slip causes interphase degradation. At both room and high temperature this leads to degradation of the fiber [29]. High temperatures also cause interphase degradation which may lead to the oxidation of the fibers.

Whether in monotonic tension or cyclic fatigue, the fibers of 2 dimensional (2D) CMCs first develop cracks in the $90^{o}$ fibers. As load increases in the case of monotonic tension tests or as cycling increases in the case of fatigue tests, these cracks then propagate through the $0^{o}$ fibers. This increases the load on the $0^{o}$ fibers. When the cracks in the $90^{o}$ fibers reach crossover points they transfer into the $0^{0}$ fiber [6, 7, 16, 20, 29].

Crack growth in the matrix and degradation of fibers during cyclic loading leads to an increased permanent strain in hysteresis loops which indicates the presence of permanent damage to the CMC and a decreased Young's Modulus. This increase in strain is known as ratcheting. Previous studies of cyclic loading on SiC/SiC CMCs report that the majority of damage to the composite occurs during the first cycle [6, 22, 28].

## II. Materials and Specimens

The three different ceramic composites studied in this work had a silicon-nitrogen-carbon (Si-N-C) matrix reinforced with SiC fibers. The first composite was reinforced with Sylramic™ fibers woven in a five harness satin weave (5HSW) fabric. The second composite was reinforced with Sylramic-iBN fibers (i. e. treated Sylramic™ fibers that possess an in situ BN coating) woven in a five harness satin weave (5HSW) fabric. The third composite was reinforced with Nicalon™ fibers woven in an eight harness satin weave (8HSW) fabric.

The commercial Sylramic™ SiC fiber is produced by ATK-COI Ceramics. It is derived from polymers at low temperatures and then pyrolyzed and sintered at high temperatures using boron-containing sintering aids [21]. The sintering process results in very strong fibers that are dense, oxygen-free, and nearly stoichiometric. They also display an optimum grain size that is beneficial for high tensile strength, good creep resistance, and good thermal conductivity [41].

The Nicalon™ fiber is manufactured by Nippon Carbon (Tokyo, Japan). Properties of Sylramic™ and Nicalon™ fibers are listed in Table 2 [33] together with the properties of Hi-Nicalon™ fibers also developed for load bearing applications.

**Table 2. Properties of Nicalon™, Hi-Nicalon™, and Sylramic™ fibers [33].**

| Property | Nicalon™ | Hi-Nicalon™ | Sylramic™ |
|---|---|---|---|
| Diameter (μm) | 14.00 | 14.00 | 12.00 |
| Density (g/cm$^3$) | 2.55 | 2.74 | 3.10 |
| Tensile Strength (GPa) | 3.00 | 2.80 | 2.60 |
| Young's Modulus (GPa) | 220.00 | 270.00 | 390-420 |
| Failure Strain (%) | 1.40 | 1.00 | 0.60 |

Sylramic-iBN fiber is a new type of small-diameter (10-μm) SiC fiber that was developed at the NASA Glenn Research Center. It is produced by subjecting commercially available Sylramic™ SiC fibers, fabrics, or preforms to a specially designed high-temperature treatment in a controlled nitrogen environment for a specific time. It can be used in a variety of applications, but it has the greatest advantage as a reinforcement for SiC/SiC ceramic composites that are targeted for long-term structural applications at temperatures higher than the capability of metallic superalloys. The NASA-developed treatment allows the excess boron in the fiber bulk to diffuse to the fiber surface where it reacts with nitrogen to form an in situ boron nitride (BN) coating on the fiber surface. The removal of boron from the fiber bulk allows the retention of high tensile strength while significantly improving creep resistance and electrical conductivity [41]. In addition, as shown in Figure 3, these improvements allow the fiber to display the best rupture strength at high temperatures in air for any available SiC fiber. Finally, for CMC applications under oxidizing conditions, the formation of an in situ BN surface layer creates a more environmentally durable fiber surface because a more oxidation-resistant BN is formed [7,42].

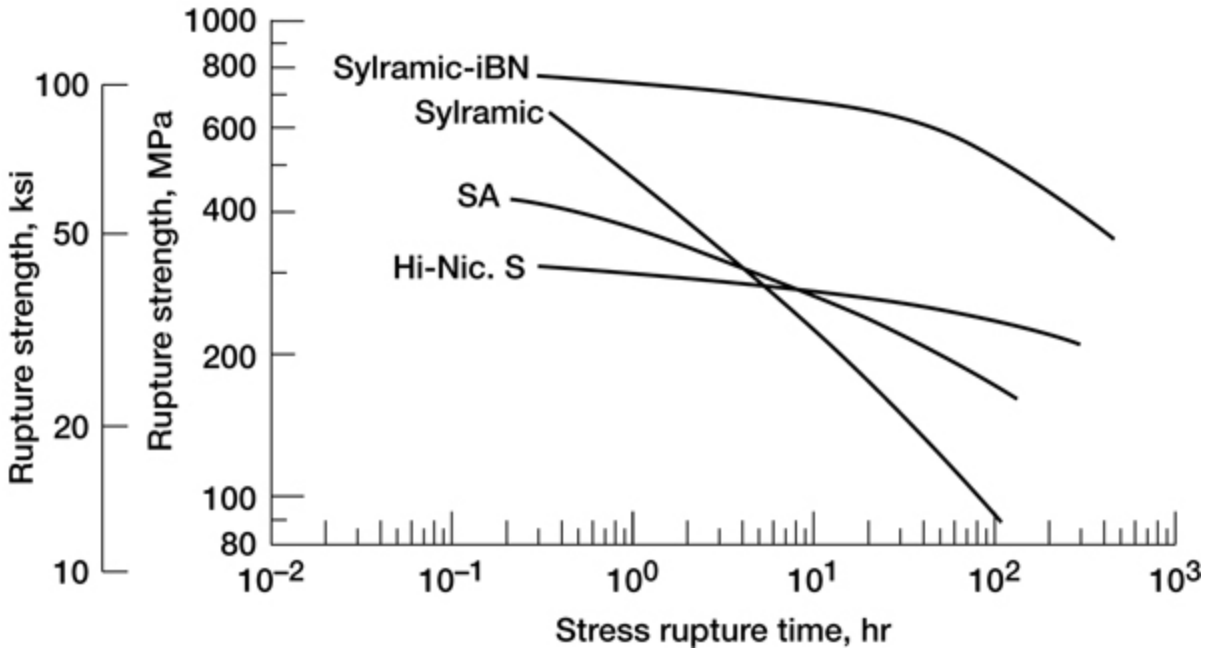


**Figure 3. Rupture strength behavior for various high-performance SiC fibers at 1400 °C in air. SA, Tyranno SA fiber from UBE Industries; Hi-Nic. S, Hi-Nicalon Type S fiber from Nippon Carbon [47].**

The three SiC/SiNC composites investigated in this study were processed by using polymer infiltration and pyrolysis (PIP) method. Polymer infiltration and pyrolysis processing method allows near-net-shape molding and fabrication producing almost fully dense composites [6, 12, 24, 39, 41]. In PIP, the fibers are first infiltrated with an organic polymer. The assembly is heated to fairly high temperatures (> 1000 °C in some cases). During this treatment the polymer is pyrolyzed to form a ceramic matrix. Because of the relatively low yield of polymer to ceramic, several infiltrations are generally used to densify the composites. As a large amount of shrinkage and matrix cracking occurs

during the pyrolysis process; particulate fillers can be added to the polymer to reduce shrinkage and to stiffen the matrix material in the composite [13].

For proprietary reasons only a brief description of these materials can be given. The first composite, referred to as C1 in this document, was reinforced with Sylramic™ fibers. The woven 5HSW fiber fabric was coated with a proprietary dual-layer interface. The composite was infiltrated with a mixture of polymer, filler particles and solvent. During pyrolysis under nitrogen at temperatures > 1000 °C, the polymer was pyrolyzed to an amorphous SiNC ceramic matrix. The infiltration and pyrolysis procedure was repeated several times to increase the density of the matrix.

The second composite, referred to as C2 in this document, consisted of Sylramic-iBN fibers and a proprietary dual-layer interface in a modified PIP SiNC matrix. The third composite, referred to as C3 in this document, consisted of Nicalon™ fibers and a proprietary dual-layer interface in a PIP SiNC matrix.

## 2.1. Test Specimens

Test specimens used in this research were provided by the Air Force Research Laboratory Materials and Manufacturing Directorate located at Wright Patterson Air Force Base OH. The dog-bone shaped specimens of composites C1 and C2 were machined to specifications in Figure 4. The composite C3 specimens were straight sided with dimensions shown in Figure 5.

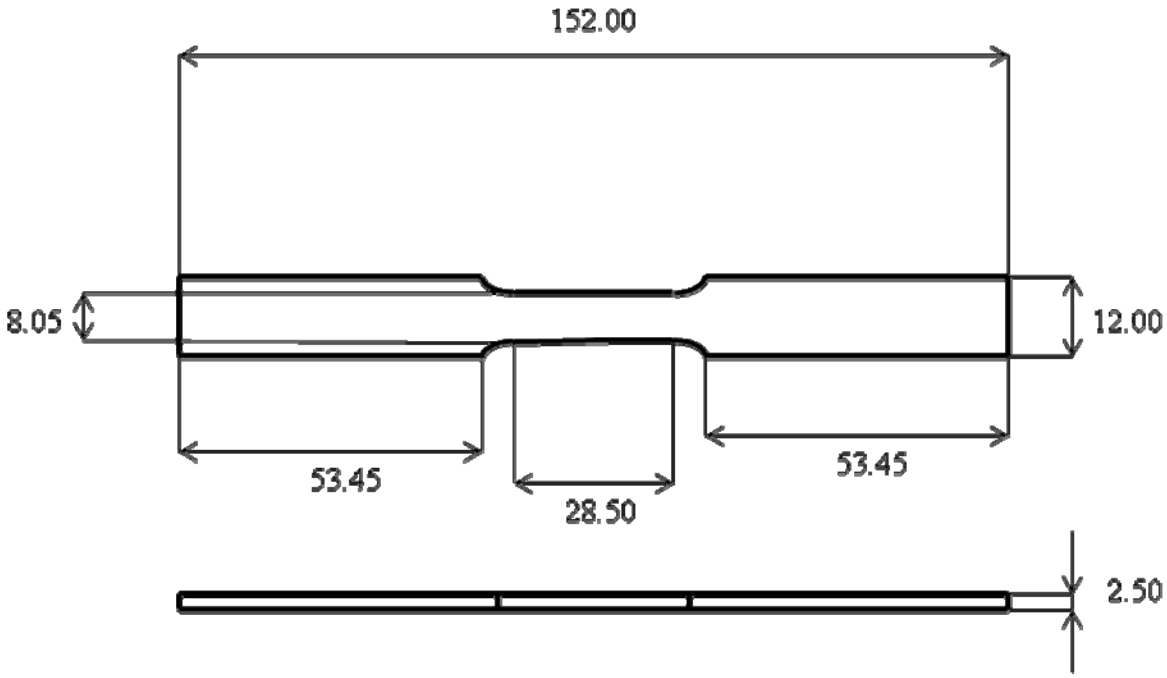


**Figure 4. Composites C1 and C2 test specimen, all dimensions in mm.**

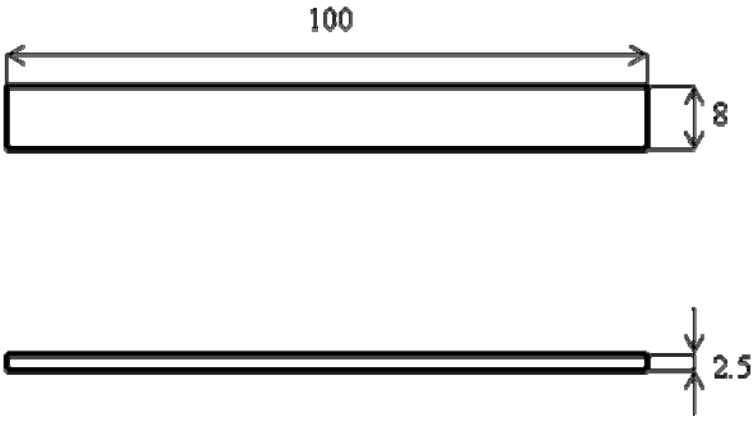


**Figure 5. Composite C3 test specimen, all dimensions in mm.**

Fiberglass tabs were attached to the grip sections of the specimens with M-Bond 200 adhesive. The tabs protected the surface of the specimen from the rough, surfalloy grips. Fiberglass tables of 1/16-in. thickness were used for specimens of composites C1 and C2. Fiberglass tables of 1/4-in. thickness were used for specimens of composite C3.

Figure 6 shows a tabbed specimen of composite C1. A tabbed specimen of composite C3 is depicted in Figure 7.

**Figure 6. Tabbed specimen for Composites C1 and C2.**

**Figure 7. Composite C3 tabbed test specimen**

# III. Experimental Arrangements and Test Procedures

## 3.1. Mechanical Testing Equipment

### 3.1.1. MTS Machines

MTS System Corporation model 810 5 kip and 22 kip servo-hydraulic machines were used for all mechanical tests, and an MTS Test Star IIs digital controller used for input signal generation and data acquisition. MTS system software and Multi-Purpose Testware (MPT) were used to program and execute tests. The hydraulic grips were coated with a Surfalloy grip texture in order to prevent slipping. Gripping pressure was set to 3 MPa on the 22 kip machine and 8 MPa on the 5 kip machine. Grips on both machines were chilled by a Neslab HX-75 chiller which continuously circulated deionized water through the wedge grips to keep the grips at temperatures under 177 °C. A low contact force, uniaxial, air-cooled, high temperature MTS Extensometer (Model 632.53E-14) was used for strain measurement.

### 3.1.2 Environmental Testing Equipment

The MTS machines were equipped with several additional pieces of equipment which helped to maintain the necessary environmental controls. The 5 kip mechanical testing station was equipped with a compact, dual zone AMTECO Hot-Rail Furnace controlled by an MTS Model 409.83B Temperature Controller. The 22 kip mechanical testing station was equipped with an MTS hot rail furnace which was also controlled by an MTS Model 409.83B Temperature Controller. The furnaces were both fitted with two R-type thermocouples, which provided chamber temperature to the controller. The

controller applied a PID control algorithm to the furnaces elements with a feedback loop from the control thermocouples.

An AMTECO HRFS-STMGEN Steam Generation System provided steam for all tests in steam environment. For these tests the specimens were placed inside a cylindrical alumina susceptor with end caps. The susceptor was then placed inside the oven and connected to a feeding tube which pumped in a continuous stream of steam at a slightly positive pressure. This would expel the dry air creating a nearly 100% steam environment inside the susceptor.

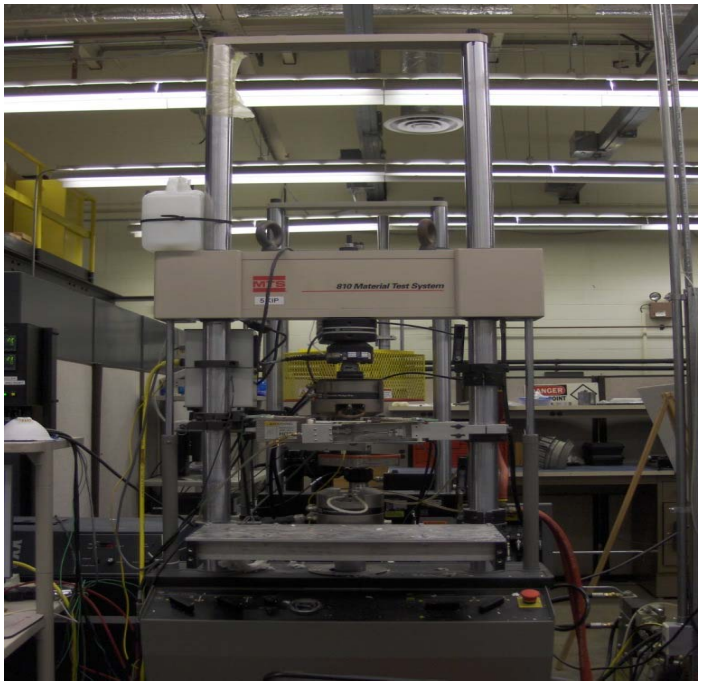


**Figure 8. MTS System Corporation model 810 5 kip servo-hydraulic machine.**

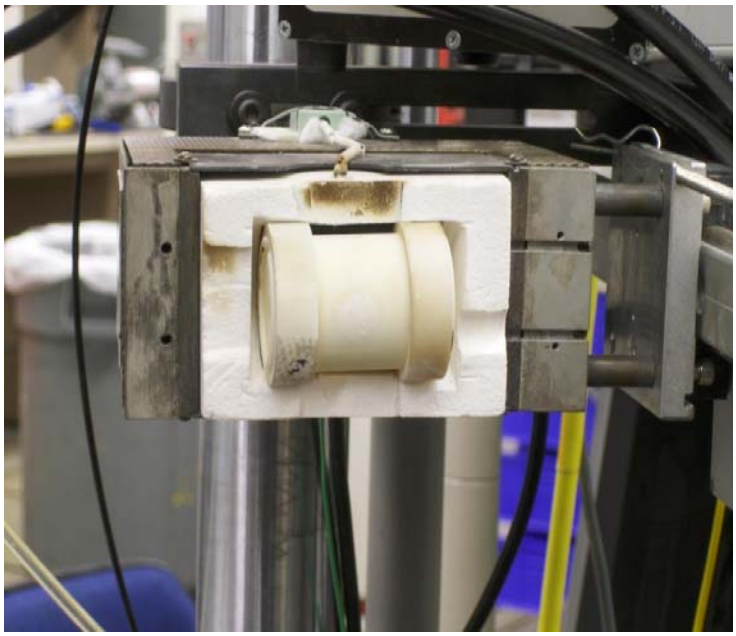

**Figure 9. Susceptor inside Amteco Hot Rail Furnace.**

## 3.2. Test Procedures

### 3.2.1 Mechanical Testing Equipment - Calibration

Prior to the start of the testing program, various components of the mechanical testing equipment needed to be calibrated. The load cell and extensometer were calibrated by MTS and AFIT technicians. The grip alignment was verified and, if necessary adjusted by AFIT technicians. Next, the MTS controller was tuned for displacement (stroke) and force control.

The furnace temperature controller was calibrated to maintain the desired test temperature of the specimen. One specimen was instrumented with two R-type thermocouples. The specimen was mounted into the MTS machine following a procedure used in a typical experiment. The furnace temperature was slowly raised with the MTS System Software until the specimen temperature reached 1300°C. This temperature was held for 8 h to demonstrate that the temperature controller could maintain stable temperatures within ± 5°C of the nominal. For 1300°C tests in air conducted on the 22-kip MTS machine, the furnace set points were 1196°C and 1183°C. For 1300°C tests in air conducted on the 5-kip MTS machine. For 1300°C tests in steam, the furnace set points were 1300°C and 1300°C. The difference is set points can be attributed to the addition of the alumina susceptor and the continuous flow of the relatively cold (300°C) steam.

### 3.2.2 Mechanical Test Preparation

Prior to testing, the servo-hydraulic machine was warmed up. This ensured that the hydraulic fluid was up to operating temperature and that the gains for the controller determined in tuning would be accurate. The MTS function generator was used to cycle the actuator in displacement control mode for at least 15 min. A saw tooth waveform with amplitude of ±0.1 inch was used.

While the hydraulics were warming up, the specimen test section width and thickness were measured with a Mitutoyo Corporation Digital Micrometer (model NTD12-6”C). Based on these measurements the cross-sectional area of the test section

was calculated, which was then used to determine the maximum and minimum loads for the particular test.

Next the specimen was placed in the grips. A grip pressure of 8 MPa was used for all tests conducted on the 5-kip MTS testing machine. A grip pressure of 3 MPa was used for all tests conducted on the 22-kip MTS testing machine. The top grip was closed while in displacement control and the load cell auto-zeroed. Control mode was switched to force and the bottom grip was closed. For tests conducted in steam, the susceptor was closed around the specimen and the oven was pulled forward into position making sure that the steam tube was inserted into the opening in the back of the susceptor. The extensometer was mounted on the specimen. Then the oven sides were completely closed around the specimen and clearances for the extensometer rods were checked. The water chiller was turned on and the cooling water temperature set to 15°C. The water lines for each grip were opened fully and the air cooling line for the extensometer was opened to 30 psi.

Next the MPT software was opened and the test procedure was written. A sample test procedure can be seen in Figure 10. Lastly, the test procedure was started and heating of the specimen began. For testing in steam, the steam generator was turned on right after the test started. In all tests, the furnace temperature was ramped to 1100°C in 25 min. Then, the furnace temperature was ramped more slowly (25 min) to 1300 °C. Once the test temperature was reached the specimen was allowed to thermally stabilize for 25 min prior to applying the mechanical loading.

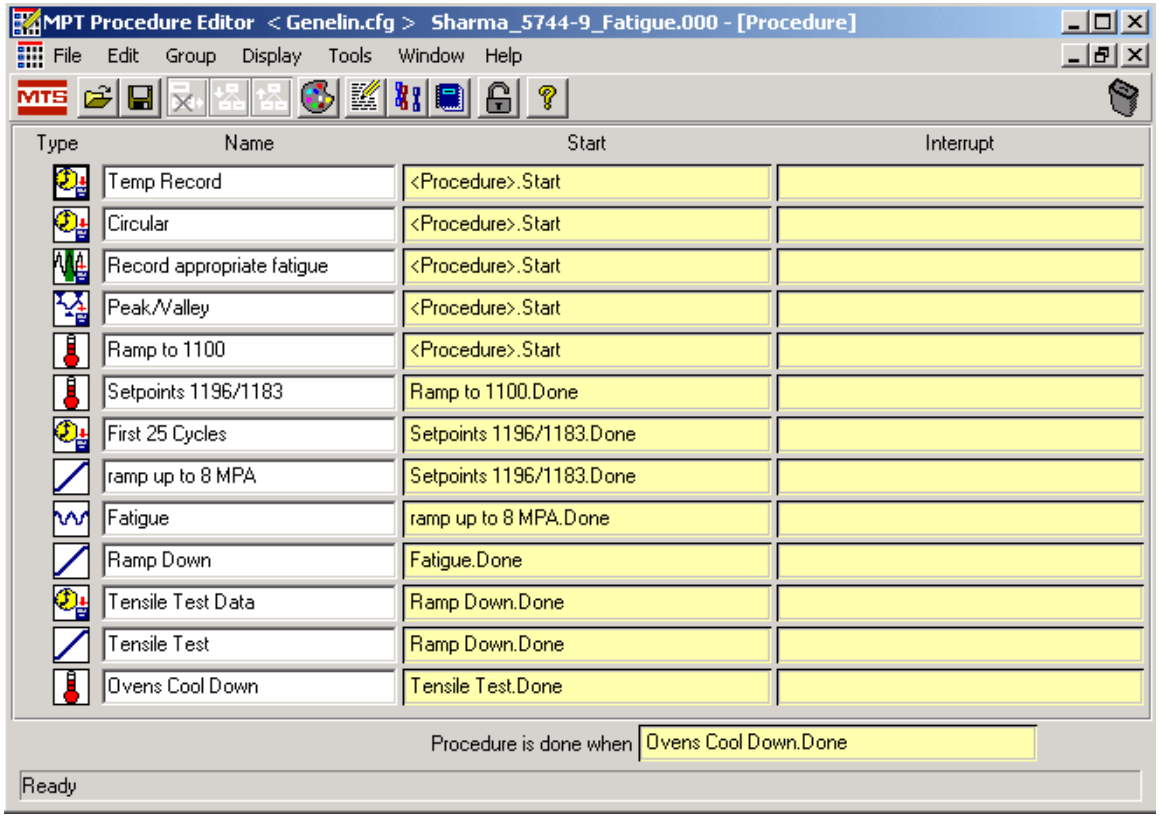


**Figure 10. Sample MPT test procedure.**

In the case of composite C3 the specimens were subjected to mechanical loading at 23 °C, but prior to that were aged for 8 h at 815 °C in air or in steam. The experimental set-up used for testing at elevated temperature in air or in steam described above was used to age the C3 specimens. In this case the temperature was increased at the rate of 30 °C /min. Once the desired aging temperature 815 °C was reached, the specimen was allowed to thermally stabilize for 15 min prior to starting the 8-h aging period.

### 3.2.3 Monotonic Tensile Test

For composites C1 and C2 all monotonic tensile tests to failure were conducted at 1300 °C in laboratory air. For composite C3 all monotonic tensile tests to failure were conducted at 23 °C in laboratory air. All monotonic tensile tests were conducted in displacement control at a constant displacement rate of 0.05 mm/s. Time, displacement, displacement command, strain, and force were recorded at a rate of 100 Hz for the duration of the test.

### 3.2.4 Tension-Tension Fatigue Test

Tension-tension fatigue tests with an R ratio (ratio of minimum stress to maximum stress) of 0.05 were conducted in load control with the frequency of 1.0 Hz. Fatigue run-out was set to 200000 cycles. Prior to cycling, load was raised to the minimum fatigue stress over 20 s. Time, cycle number, strain, displacement, force, force command, and temperature were measured and recorded during each test. "Peak and valley" data was collected for all cycles. For selected cycles, the data was recorded at a rate of 32 Hz. The cycles selected for collecting the full cyclic loop data were: (i) the first 25 cycles, (ii) every $100^{th}$ cycle for cycles 100 to 5000, (iii) every $500^{th}$ cycle for cycles 5000 to 25000, and (iv) data was recorded every $5000^{th}$ cycle for cycles 25000 to 200000.

The specimens that achieved fatigue run-out were unloaded to a small positive load of 1.5 N over 20 s. To determine the retained tensile strength and modulus, specimens that achieved run-out were subjected to tensile test to failure at the

temperature of the fatigue test. The tensile test was conducted according to the procedure described in section 3.2.3 above.

### 3.2.5 Microstructural Characterization

Post-test microstructure was first examined with the optical microscope. Digital pictures of each half of the failed specimens were taken for documentation. After observations by the optical microscope, the specimens were prepared for examination with the SEM. One half of the failed specimen was selected and the fracture surface was cut off with a Sherline Model 5410 diamond saw. The cut was made ~2mm behind the damage zone of the specimen. The fracture surface was then mounted onto a 12.4mm SEM specimen stage with silver paint. In addition, a section of the failed specimen located directly behind the fracture surface was also cut off and polished for viewing with the SEM.

# IV. Results and Discussion

## 4.1. Chapter Overview

Section 4.2 discusses the tensile stress-strain behavior and tensile properties at 1300 °C of composites C1 and C2. Section 4.3 discusses composite C1 and C2 tension-tension fatigue behavior in both air and steam at 1300 °C. Section 4.4 presents concluding remarks on the fatigue performance of composites C1 and C2 in air and steam environments at 1300 °C. Secition 4.5 discusses the effects of aging at 815 °C in both air and steam on the tensile properties of composite C3. Section 4.6 presents concluding remarks on the effects of aging at 815 °C in both air and steam environments on composite C3. Section 4.7 discusses the microstructural characterization of composites C1, C2, and C3.

## 4.2. Composites C1 and C2 - Tensile Stress-Strain Behavior and Tensile Properties at 1300 °C

As-processed specimens of composite C1 and composite C2 were tested in monotonic tension to failure at 1300°C in laboratory air. The tests were conducted in displacement control at a constant displacement of 0.05 mm/s. Elastic modulus, ultimate tensile strength (UTS), and failure strain obtained for each composite are presented in Table 3. The stress-strain curves obtained for composites C1 and C2 are shown in Figure. 11.

**Table 3. Tensile Properties of composites C1 and C2 at 1300 °C**

| Specimen Number | Elastic Modulus (GPa) | UTS (MPa) | Failure Strain (%) |
|---|---|---|---|
| *Composite C1* | | | |
| 6310-2-1 | 134 | 185 | 0.16 |
| *Composite C2* | | | |
| 5744-1 | 135 | 241 | 0.27 |

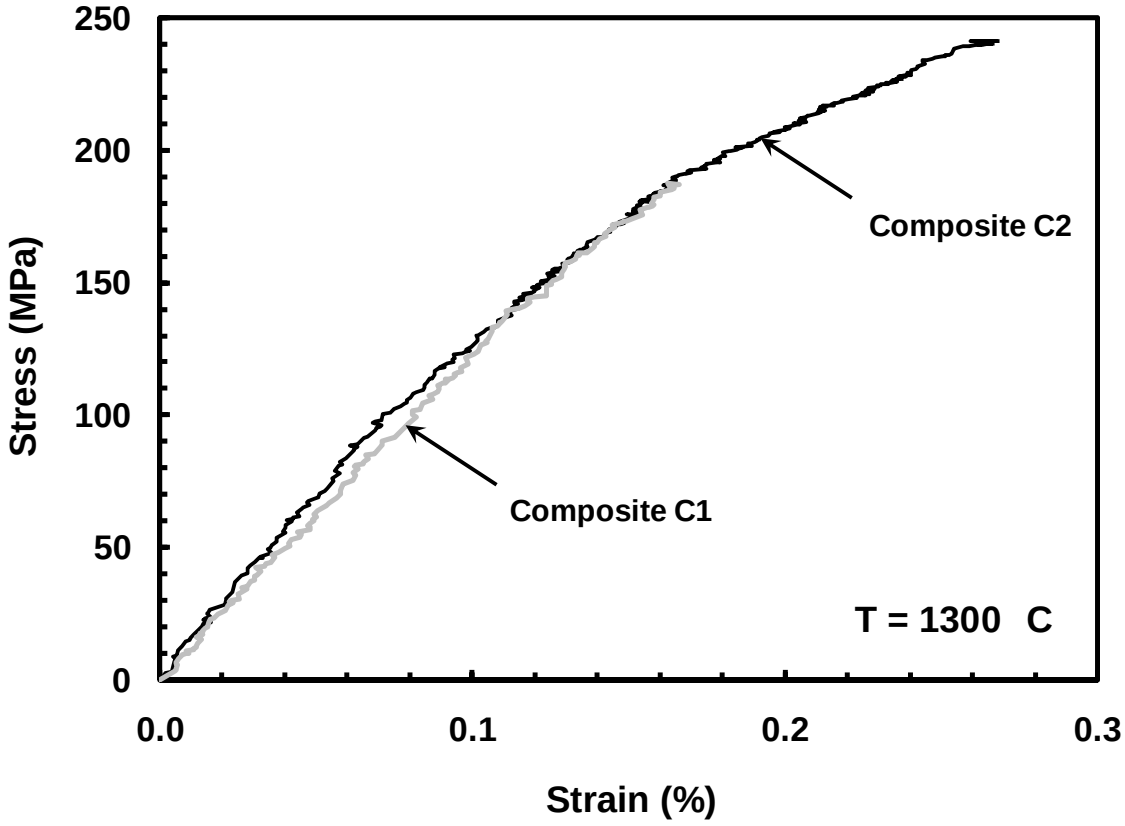


**Figure 11. Tensile stress-strain curves for composites C1 and C2 at 1300 °C.**

It is seen in Figure 11 that the tensile stress-strain curve for composite C1 is nearly linear to failure. A slight decrease in slope occurs at the stress of ~140 MPa.

Conversely, the stress-strain curve obtained for composite C2 departs from linearity at the stress of ~100 MPa, as evidenced by a noticeable decrease in slope. Immediately after this change in slope, the near linear stress-strain behavior resumes and continues until the stress reaches ~180 MPa, where another decrease in slope takes place. This stress–strain behavior indicates composite damage (most likely matrix cracking) at each change in slope. Progressive matrix cracking and crack deflection are the mechanisms likely responsible for a considerably larger tensile failure strain and a somewhat higher tensile strength exhibited by composite C2.

### 4.3. Composites C1 and C2 Tension-Tension Fatigue Behavior in Air and in Steam at 1300 °C

Tension-tension fatigue tests with a ratio, R = 0.05 of minimum stress to maximum stress, were performed at 1300°C in air and in steam environments for composites C1 and C2. Results are summarized in Table 4, where test environment is shown together with the maximum stress level and number of cycles to failure for each composite. Results are also presented in Fig. 12 as stress vs cycles to failure (S-N) curves for both composites and both environments.

**Table 4. Summary of fatigue tests for composites C1 and C2 at 1300 °C in laboratory air and in steam environments.**

| Specimen Number | Test Environment | Initial Modulus (GPa) | Max Stress (MPa) | Cycles to Failure |
|---|---|---|---|---|
| *Composite C1* | | | | |
| 6310-2-9* | Air | 133 | 100 | >200,000* |
| 6310-2-8 | Air | 148 | 120 | 28,515 |
| 6310-2-7 | Air | 148 | 140 | 10,104 |
| 6310-2-6* | Steam | 129 | 100 | >200,000* |
| 6310-1-2* | Steam | 149 | 100 | >200,000* |
| 6310-2-5 | Steam | 133 | 120 | 14,688 |
| 6310-2-2 | Steam | 134 | 140 | 2,328 |
| *Composite C2* | | | | |
| 5744-3* | Air | 95.9 | 140 | >200,000* |
| 6312-2* | Air | 141 | 140 | >200,000* |
| 5744-9* | Air | 132 | 160 | >200,000* |
| 5744-6 | Air | 110 | 180 | 22,807 |
| 5744-2* | Steam | 131 | 140 | >200,000* |
| 5744-10* | Steam | 130 | 140 | >200,000* |
| 5744-4 | Steam | 114 | 160 | 153,142 |
| 5744-5 | Steam | 103 | 180 | 5,764 |

* indicates a run-out

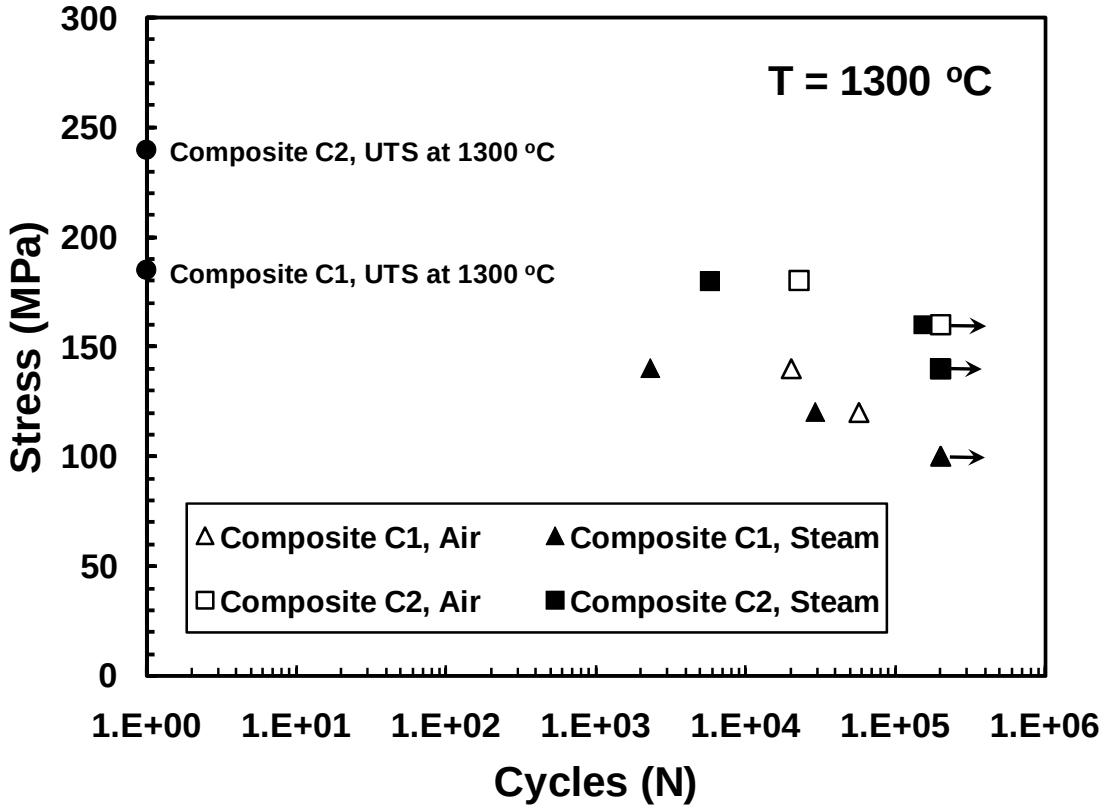


**Figure 12. Fatigue S-N curves for composites C1 and C2 at 1300 °C in laboratory air and in steam environments.**

At 1300°C in air the fatigue limit was 100 MPa (54 %UTS at 1300°C) for composite C1 and 160 MPa (66 %UTS at 1300°C) for composite C2. Presence of steam (a highly oxidizing environment) causes noticeable degradation in fatigue performance. Although for composite C1 the fatigue limit at 1300°C in steam was the same as that at 1300°C in air (100 MPa), fatigue lifetimes obtained at maximum stress levels above 100 MPa were significantly lower in steam than in air. The reduction in fatigue lifetime due to steam was 49% for the maximum stress of 120 MPa and 77% for the maximum stress of 140 MPa. In contrast, the fatigue limit of composite C2 at 1300°C in steam was only 140 MPa (58 %UTS at 1300°C), which is below the 160 MPa fatigue limit obtained at 1300

°C in air. The presence of steam also resulted in considerable decrease in fatigue lifetimes obtained for maximum stress levels > 140 MPa. The reduction in fatigue lifetime due to steam was 23% for the maximum stress of 160 MPa and 75% for the maximum stress of 180 MPa.

The full cycle stress-strain measurements collected for selected cycles (see test procedure described in Section 3.4.4) afforded the ability to evaluate the change in elastic modulus during cyclic fatigue. For each cycle, where the full stress-strain hysteresis loop data were recorded, the elastic modulus was calculated as the slope of the linear elastic region of the loading stress-strain curve. A reduction in elastic modulus reflects the damage development during cycling. Damage was quantified by a normalized damage parameter $D_E$ defined as [R1, R2]:

$$D_E = 1 - \frac{E}{E_0}$$

where $E_o$ is the initial modulus and $E$ is the modulus at a given number of cycles. Damage parameter as a function of fatigue cycles in air and in steam is presented in Figures 13a and 13b for composites C1 and C2, respectively.

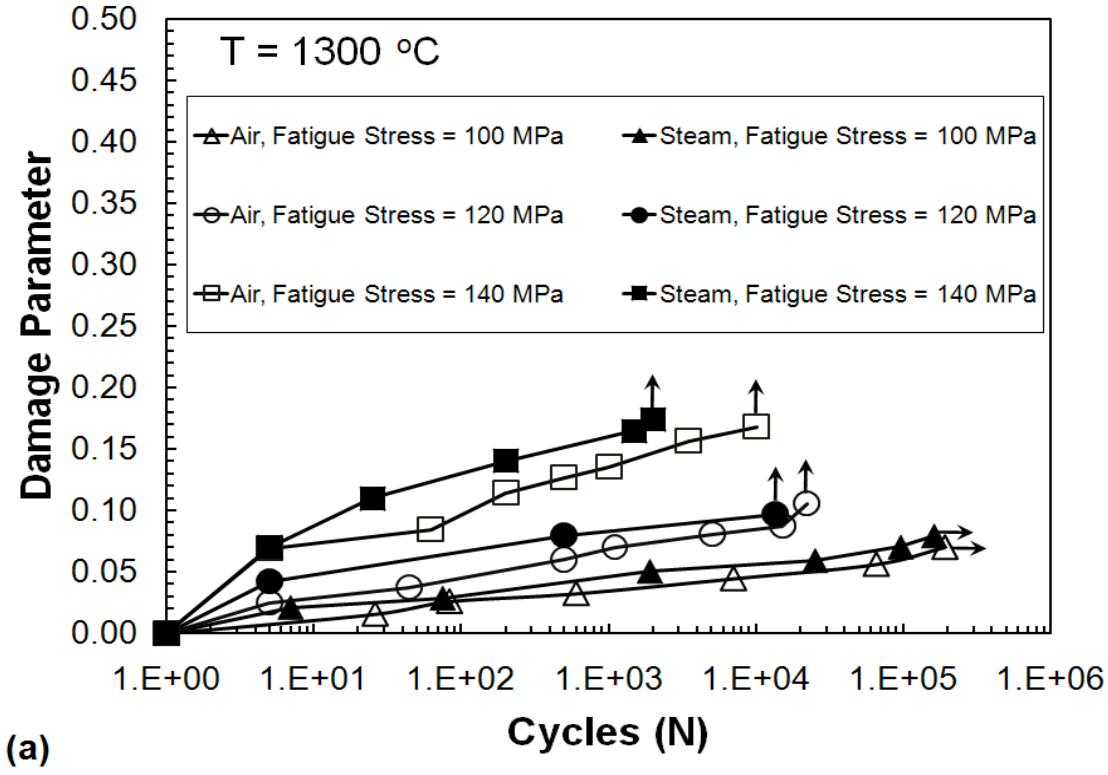


(a)

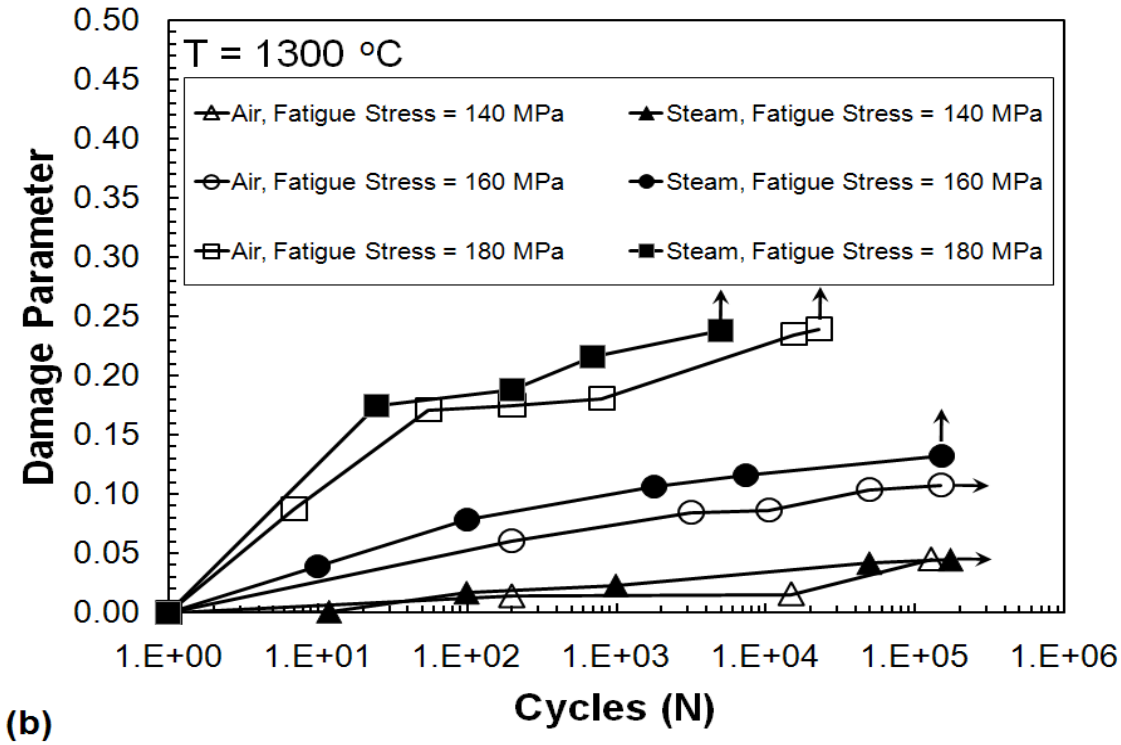


(b)

**Figure 13. Damage parameter vs. cycle numbers at 1300 °C in air and in steam for: (a) composite C1 and (b) composite C2.**

It is seen that the damage parameter increases with higher fatigue stress. Both composites C1 and C2 demonstrate that they experience more permanent damage as the maximum fatigue stress increases. Moreover, composites C1 and C2 also show that tests conducted in steam are more damaging than tests conducted in air.

Composite C1 obtained run-out for fatigue tests with maximum fatigue stress $\sigma$ = 100 MPa in both air and steam environments. For run-out in air composite C1 demonstrated a 6.8% reduction in elastic modulus whereas composite C1 demonstrated a 7.9% reduction in elastic modulus in steam. At maximum fatigue stress $\sigma$ = 140 MPa composite C1 exhibited a 16.8% reduction in elastic modulus in air and a 17.4% reduction in elastic modulus in steam.

Composite C2 achieved run-out in both air and steam for fatigue tests conducted with maximum fatigue stress $\sigma$ = 140 MPa and demonstrated a 4.5% reduction in elastic modulus in both air and steam. For tests conducted with a maximum fatigue stress $\sigma$ = 140 MPa composite C2 demonstrated a 23.9% reduction in elastic modulus in air and 23.8% reduction in elastic modulus in steam

Maximum and minimum cyclic strains as functions of cycle number for fatigue tests conducted at 1300°C in laboratory air and steam are presented in Figs. 14(a) and 14(b) for composites C1 and C2, respectively.

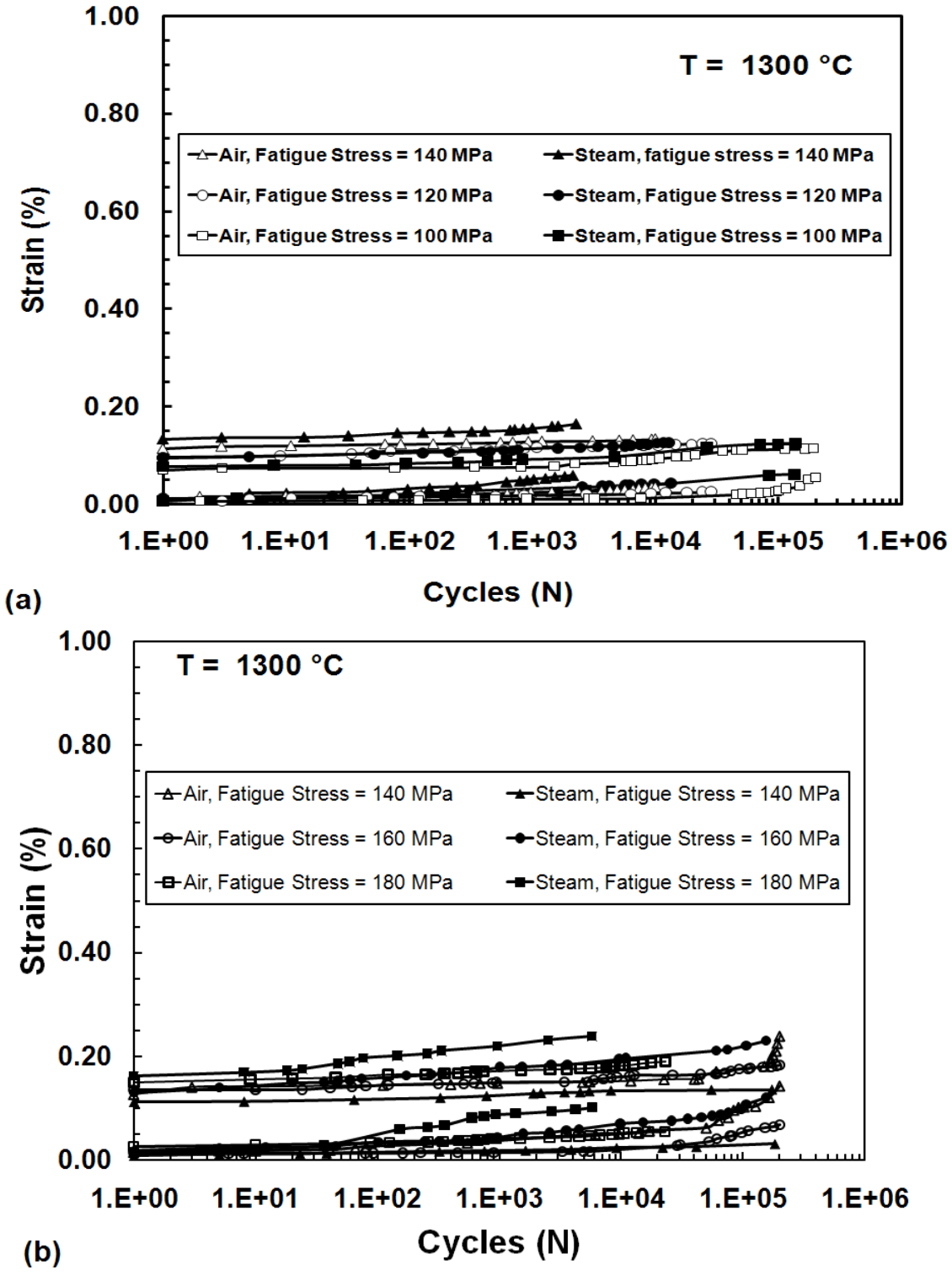


**Figure 14. Maximum and minimum strains as functions of cycle number at 1300°C in air and in steam for: (a) composite C1 and (b) composite C2.**

It is seen that composite C1 produced virtually no ratcheting in all fatigue tests conducted in air and in fatigue tests conducted in steam with maximum stress levels < 140 MPa. Minimal ratcheting is observed in the fatigue test conducted in steam with the maximum stress of 140 MPa. Yet even in the 140 MPa test in steam, there is little change in accumulated strain for up to 1000 cycles, only then does ratcheting begin. Maximum strains accumulated in fatigue tests by composite C1 were limited to 0.16%, which is also the failure strain obtained in tension test.

Results shown for composite C2 in Figure 9(b) reveal that ratcheting takes place in fatigue tests conducted in steam with the maximum stress levels of 160 and 180 MPa. Earlier onset of ratcheting (after approximately 100 cycles) is observed in the 180 MPa test than in the 160 MPa test, where the ratcheting commences after about 10000 cycles. Surprisingly, ratcheting is also observed in the 140 MPa test conducted in air. In this case the increase in the accumulated strain is seen after about 100000 cycles. However, it should be noted that the maximum strains accumulated in fatigue tests by composite C2 are limited to 0.24%, which is also the failure strain obtained in tension test. The strong interface bond, typical in SiC/SiC ceramic composites is likely responsible for minimal amounts of ratcheting observed for composites C1 and C2.

Evaluation of retained properties is useful in assessing the damage state of the composite subjected to prior loading. Retained strength and stiffness of the specimens, which achieved fatigue run-out, are summarized in Table 5 for both composites C2 and C2. Note that the modulus retention was calculated by comparing the modulus obtained

in tensile test conducted after survival of 200,000 fatigue cycles to the modulus of that same specimen obtained from the elastic portion of the loading stress-strain curve of the first cycle.

**Table 5. Retained properties of the composite C1 and composite C2 specimens subjected to prior fatigue at 1300 °C in laboratory air and in steam environments.**

| Specimen number | Fatigue stress (MPa) | Retained modulus (GPa) | Modulus retention (%) | Retained strength (MPa) | Strength retention (%) | Failure strain (%) |
|---|---|---|---|---|---|---|
| *Composite C1, Prior Fatigue in Air* | | | | | | |
| 6310-2-9 | 100 | 122 | 91.2 | 206 | ≥100 | 0.20 |
| *Composite C1, Prior Fatigue in Steam* | | | | | | |
| 6310-2-6 | 100 | 115 | 89.1 | 170 | 91.9 | 0.15 |
| 6310-1-2 | 100 | 133 | 90.5 | 209 | ≥100 | 0.19 |
| *Composite C2, Prior Fatigue in Air* | | | | | | |
| 5744-3 | 140 | 86.3 | 90.0 | 246 | ≥100 | 0.32 |
| 6312-2 | 140 | 128 | 90.8 | 227 | 94.2 | 0.18 |
| 5744-9 | 160 | 115 | 87.1 | 252 | ≥100 | 0.26 |
| *Composite C2, Prior Fatigue in Steam* | | | | | | |
| 5744-2 | 140 | 119 | 90.8 | 215 | 89.2 | 0.17 |
| 5744-10 | 140 | 120 | 92.3 | 193 | 80.2 | 0.09 |

Tensile stress-strain curves obtained for the composite C1 specimens subjected to prior fatigue at 1300 °C in air and in steam are presented in Figure 15 together with the tensile stress-strain curve for the as-processed material. Effects of prior fatigue in air and in steam on tensile stress-strain behavior of composite C2 are typified in Figure 16 where the tensile stress-strain curve for the as-processed material is presented for comparison.

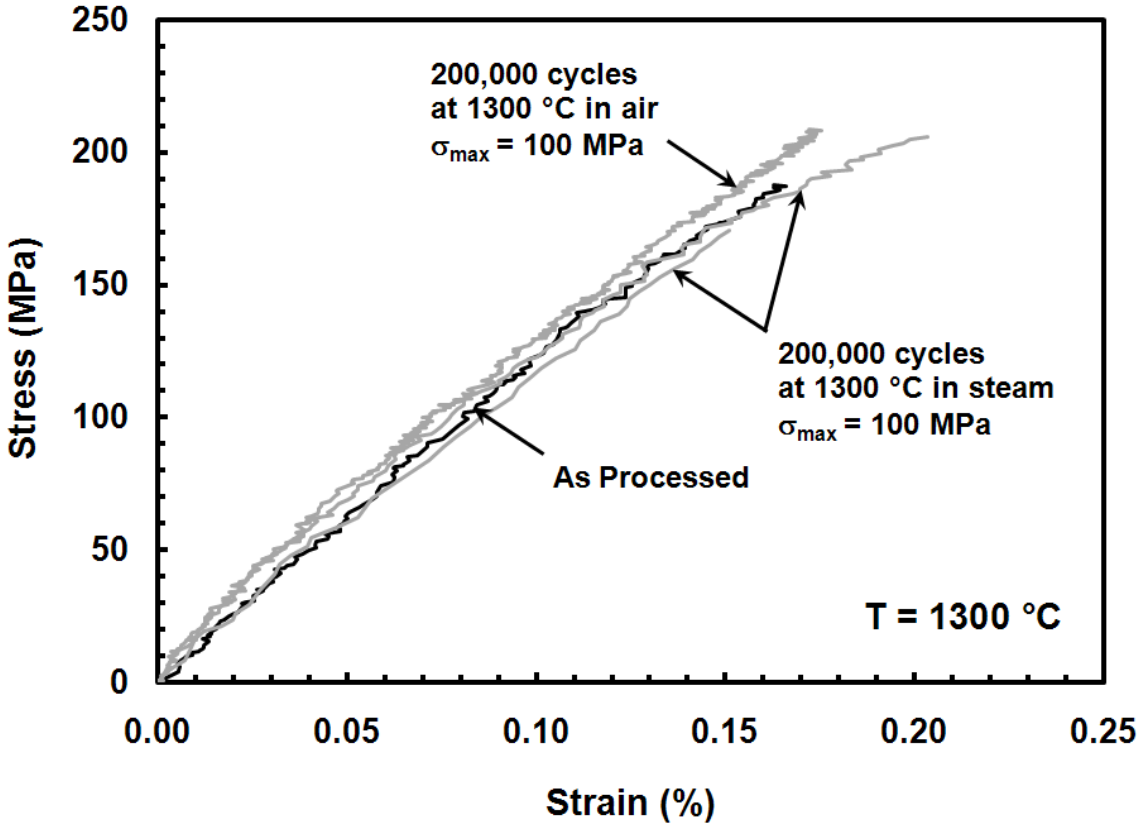


**Figure 15. Effects of prior fatigue at 1300 °C in air and in steam on tensile stress-strain behavior of composite C1.**

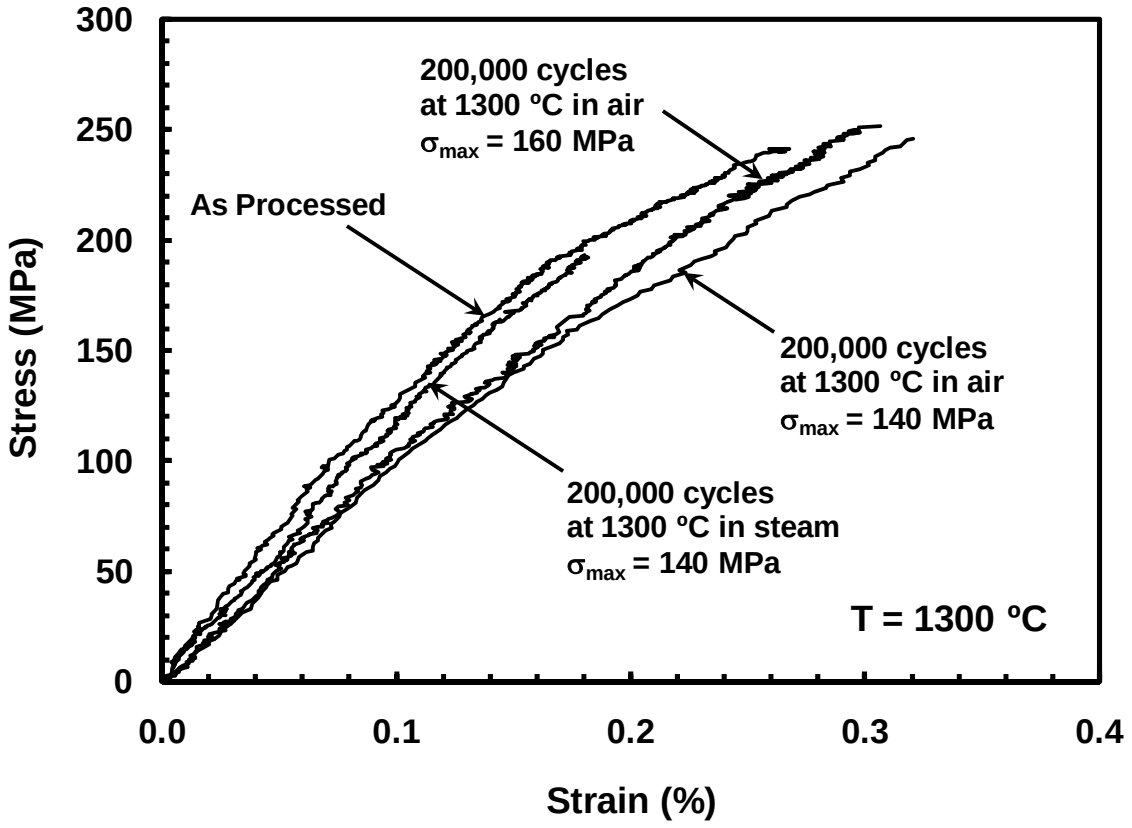


**Figure 16. Effects of prior fatigue at 1300 °C in air and in steam on tensile stress-strain behavior of composite C2.**

It is seen that on the average composite C1 exhibited no loss of tensile strength due to prior fatigue in air or in steam. However, stiffness loss of up to 11% was observed. Full retention of tensile strength suggests that no fatigue damage occurred to the fibers. The reduction in stiffness is most likely due to additional matrix cracking. Effects of prior fatigue in air on tensile properties of composite C2 were similar. On the average composite C2 retained 100 % of its tensile strength after 200,000 fatigue cycles at 1300 °C in air. Stiffness loss was near 10% for specimens pre-fatigued with the maximum stress level of 140 MPa and 13% for specimens pre-fatigued with the maximum stress of

160 MPa. Conversely, prior fatigue in steam caused reduction of both strength and stiffness of composite C2. Average strength loss in steam reached 15% and stiffness loss, 10%. In this case, the loss of strength may be associated with the environmental degradation of the fibers, while both fiber degradation and progressive matrix cracking may account for the loss of stiffness.

### 4.4 Conclusion on Fatigue Performance of Composites C1 and C2

Both composites C1 and C2 seem to demonstrate excellent fatigue behavior in air and steam environments at 1300$^{o}$C. In both air and steam environments composite C1 demonstrated a fatigue limit which was approximately 54% of its UTS. In steam composite C2 demonstrated an endurance limit approximately 58% of its UTS and in air composite C2 demonstrated an endurance limit approximately 66% of its UTS. All endurance limits are higher than values found in previous values for cyclic fatigue of SiC/SiC CMCs in high temperature.

Steam degraded the fatigue performance of both Composites C1 and C2. Composite C1 specimens tested in steam at a fatigue stress of 120 and 140 MPa demonstrated shorter lifetimes than specimens tested in air. Composite C2 specimens tested in steam at fatigue stresses of 160 and 180 MPa demonstrated shorter lifetimes tested in air.

Composite C2 produced a fatigue limit 60% higher than Composite C1 in air and 40% higher in steam. This superior fatigue performance can be attributed to the processing differences between composites C1 and C2 discussed in chapter 2.

## 4.5. Composite C3 – Effects of Aging at 815 °C in Air and in Steam on Tensile Properties and Stress-Strain Behavior at 23 °C

Baseline tensile properties of composite C3 were established in two tension to failure tests were conducted at 23 °C. Note that these tensile tests as well as all other tensile tests discussed in this Section were conducted in accordance with the procedure described in Section 3.4.3. The average elastic modulus was 91.6 GPa, the average UTS was 312 MPa, and the average failure strain was 0.61%.

The objective of this part of the overall research effort was to evaluate the effects of prior isothermal aging at 815 °C in air and in steam environments on tensile properties and on stress-strain behavior of composite C3. To accomplish this, two as-processed specimens were aged for 8 h at 815°Cin air and one as-processed specimen was aged for 8 h at 815 °C in steam. Then the aged specimens were subjected to tension tests to failure at 23 °C.

It is recognized that the presence of oxygen and/or molecules of water in a testing environment severely degrades the performance of SiC/SiC CMCs. The environmental degradation is accelerated if matrix cracks allow the load-bearing fibers and interface material to be exposed to the oxidizing environment. To accelerate the environmental degradation of composite C3 during no-load exposure at 815 °C in air and in steam, four C3 as-processed specimens were subjected to 10 tension-tension fatigue cycles with the maximum stress of 125 MPa conducted according to the procedure described in Section 3.4.4. It is expected that fatigue loading promoted matrix cracking in these specimens, thereby opening pathways for molecules of oxygen and/or water to penetrate into the

specimen and to attack the fiber/matrix interface and the fibers. Then two of the pre-fatigued specimens were aged for 8 h at 815°Cin air and the other two pre-fatigued specimens were aged for 8 h at 815 °C in steam. Following aging all four specimens were tested in tension to failure at 23 °C.

It should be noted that specimens of composite C3 did not have constant width or constant thickness. When specimens were measured with a micrometer, it was found that the thickness of a given specimen varied by as much 0.10 mm and the width of a given specimen varied by as much as 0.10 mm. Not surprisingly all specimens failed at the location with the smallest cross sectional area, which was generally in the gage section of the specimen.

Results obtained for composite C3 are summarized in Table 6, where elastic modulus, UTS and failure strain of the aged specimens are given together with the tensile properties of the as-processed specimens.

**Table 6: Summary of room-temperature tensile properties for composite C3 as-processed specimens, C3 specimens subjected to prior aging at 815 °C, and C3 pecimens subjected to prior fatigue and aging at 815 °C.**

| Specimen Number | Prior Fatigue | Aging Environment | Modulus (GPa) | UTS (MPa) | Failure Strain (%) |
|---|---|---|---|---|---|
| 25 | No | N/A | 86.7 | 311 | 0.66 |
| 27 | No | N/A | 83.6 | 313 | 0.55 |
| 19 | No | Air | 84.0 | 234 | 0.34 |
| 20 | No | Air | 85.8 | 255 | 0.41 |
| 21 | No | Steam | 82.2 | 182 | 0.60 |
| 24 | Yes | Air | 84.6 | 210 | 0.32 |
| 26 | Yes | Air | 86.9 | 240 | 0.37 |
| 28 | Yes | Steam | 85.7 | 184 | 0.25 |
| 29 | Yes | Steam | 85.8 | 170 | 0.21 |

The stress-strain curves obtained for the as-processed composite C3 at 23 °C are presented in Figure 17. It is seen that these stress-strain curves are nearly bi-linear. The stress-strain curve continues in a linear fashion with the original slope (elastic modulus) until the stress of about 100 MPa, where a noticeable decrease in slope takes place indicating composite damage. Following this change in slope the stress-strain curve continues in a nearly linear fashion (with the reduced slope) until failure. Such stress-strain behavior is consistent with that reported earlier for a similar composite [22].

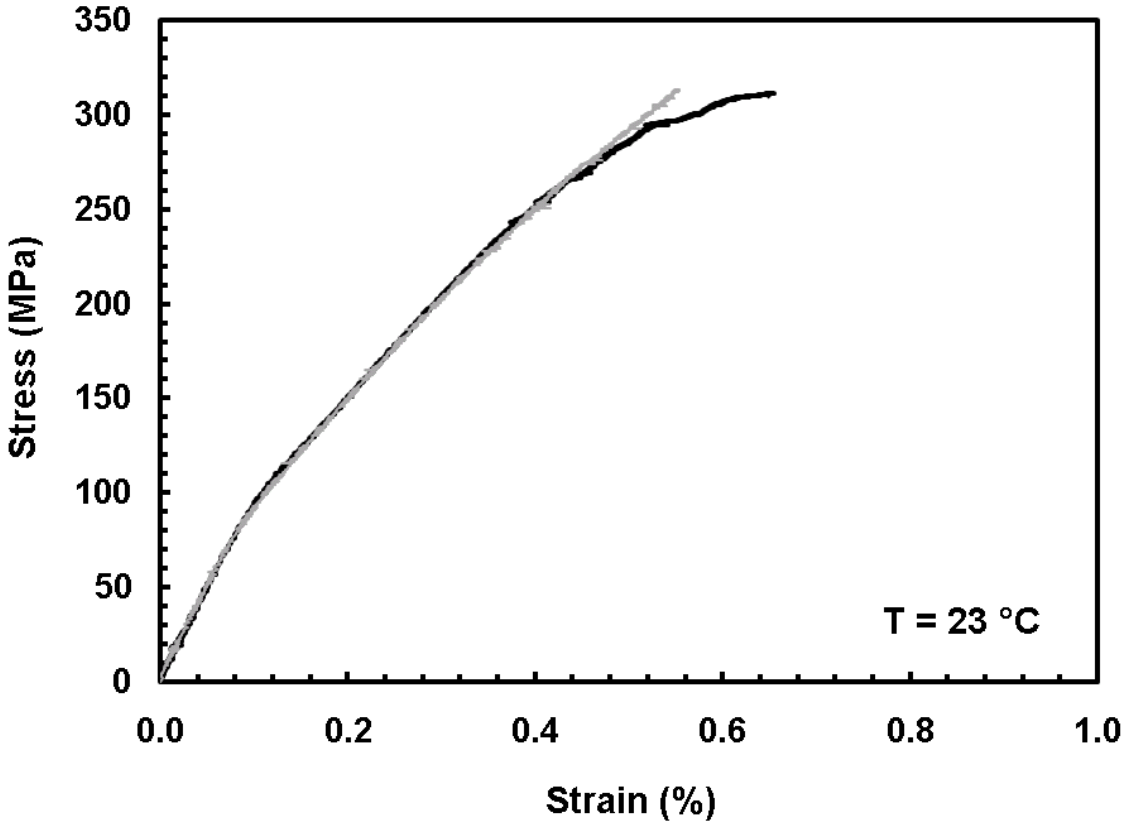


**Figure 17. Tensile stress-strain curves obtained for composite C3 at 23 °C.**

The stress-strain curves for the C3 specimens aged for 8 h at 815 °C in air are presented in Figure 18 together with the stress-strain curve obtained for the as-processed

C3 composite. As evidenced by the results in Table 6 and Figure 17, prior aging in air caused reduction in tensile strength of the composite C3, but had no effect on the elastic modulus or on the overall stress-strain behavior until failure. The stress-strain curves obtained for the aged material are virtually indistinguishable from the stress-strain curve for the as-processed material until the failure stress of the aged material is reached. Average reduction in strength due to prior aging was ~22%.

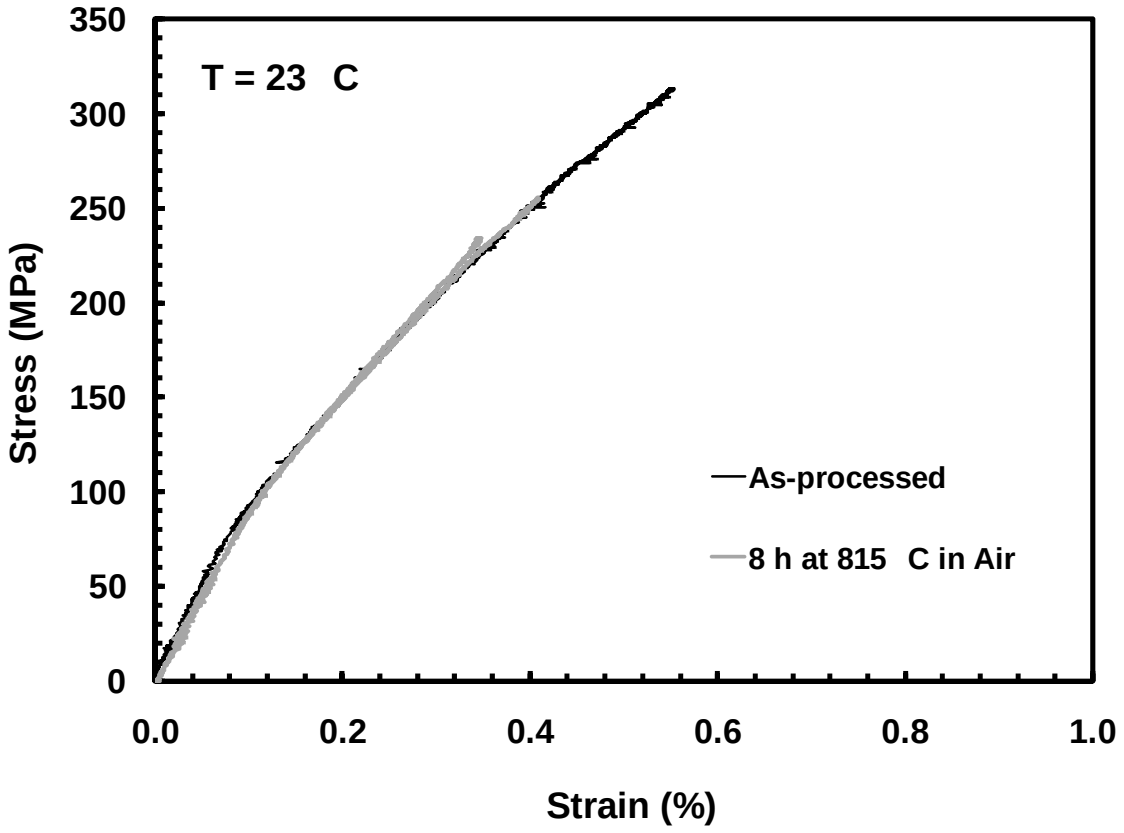


**Figure 18. Tensile stress-strain curves obtained at 23 °C for composite C3 aged for 8 h at 815 °C in air and for the as-processed composite C3.**

The stress-strain curves for the C3 specimens aged for 8 h at 815 °C in steam are presented in Figure 19 together with the stress-strain curve obtained for the as-processed C3 composite. Results in Table 6 and Figure 19 reveal that the effects of prior aging for 8

h at 815 °C in steam are significantly different from the effects of prior aging in air. As in the case of prior aging in air, prior aging in steam caused reduction in tensile strength, but prior aging in steam also has a dramatic effect on the overall stress-strain behavior. The stress-strain behavior of the aged material becomes markedly nonlinear as the stress exceeds 100 MPa. Appreciable inelastic strains accompany moderate increase in stress. Reduction in strength due to prior aging in steam was nearly 42%. However, the elastic modulus was largely unaffected by prior aging in steam.

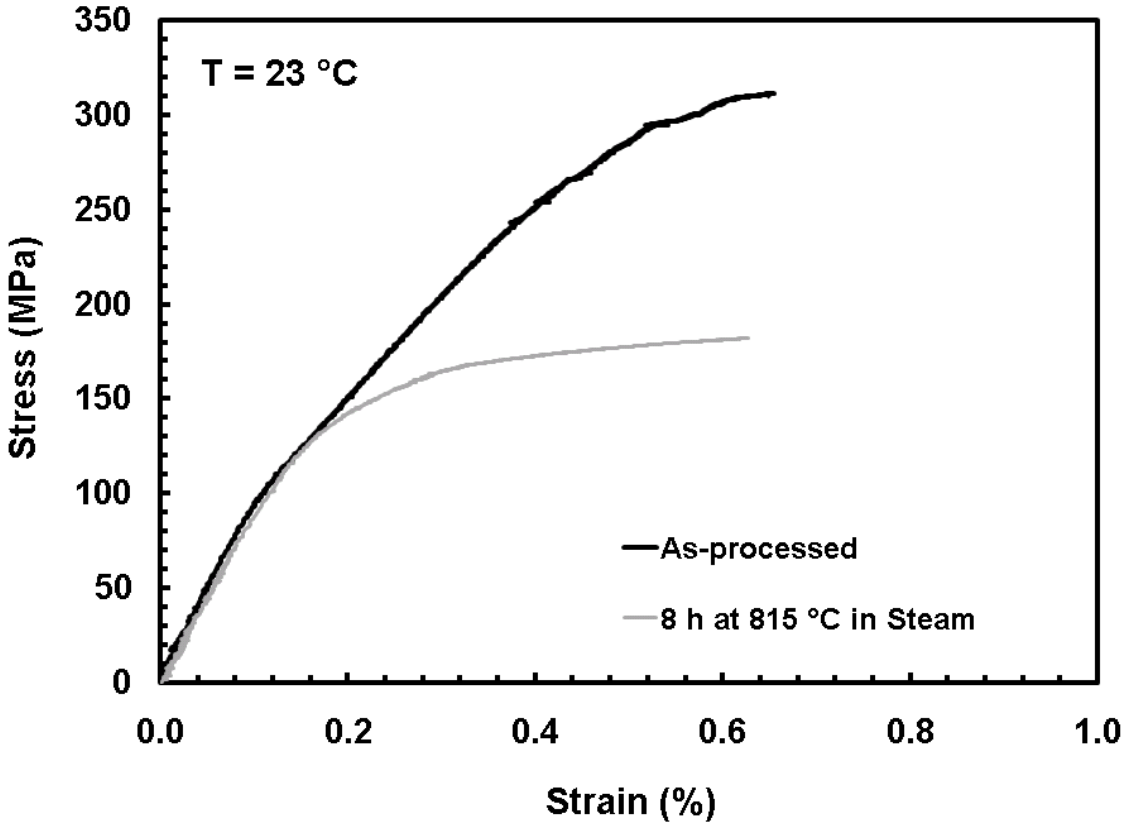


**Figure 19. Tensile stress-strain curves obtained at 23 °C for composite C3 aged for 8 h at 815 °C in steam and for the as-processed composite C3.**

The stress-strain curves for the pre-fatigued C3 specimens aged for 8 h at 815 °C in air are presented in Figure 20 together with the stress-strain curve for the specimen aged in air (but not subjected to fatigue before aging) and the stress-strain curve for the as-processed C3 composite. It is seen that prior aging in air has qualitatively similar effects on the pre-fatigued and on the as-processed specimens. Prior fatigue at 23 °C followed by aging at 815 °C in air caused a ~28%.reduction in the tensile strength of the composite C3, but had virtually no effect on the elastic modulus or on the overall stress-strain behavior until failure. The stress-strain curves obtained for the aged material are essentially the same as the stress-strain curve for the as-processed material until the failure stress of the aged material is reached.

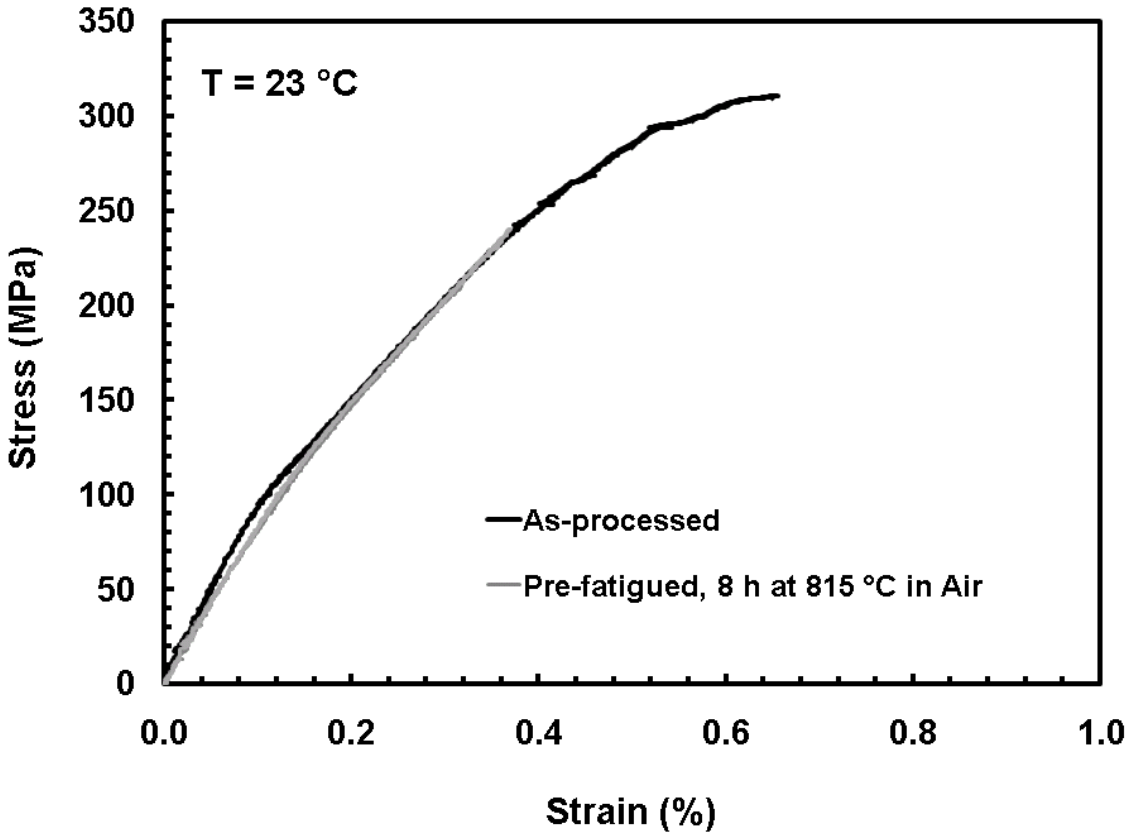


**Figure 20. Tensile stress-strain curves obtained at 23 °C for pre-fatigued C3 specimens aged for 8 h at 815 °C in air and for the as-processed composite C3.**

The stress-strain curves for the pre-fatigued C3 specimens aged for 8 h at 815 °C in steam are presented in Figure 21 together with the stress-strain curve for the specimens aged in steam (but not subjected to fatigue before aging) and the stress-strain curve obtained for the as-processed C3 composite. It is seen that prior fatigue followed by aging in steam caused a ~43%.reduction in the tensile strength, which was close to the 42% reduction in strength due to prior aging in steam alone. The elastic modulus remained largely unaffected by the combination of prior fatigue and aging in steam. However, the stress-strain behavior of the specimens subjected to prior fatigue followed by aging in steam was noticeably different from that exhibited by the specimens

subjected to prior aging alone. Pre-fatigued specimens produced the stress-strain curves that were nearly linear for stresses < 100 MPa. At the stress of about 100 MPa a slight nonlinearity develops, then the stress-strain curve continues in a nearly linear fashion (albeit with a lower slope) to failure. Strains to failure produced by the pre-fatigued specimens were about one third of the failure strain produced by the specimen subjected to prior aging alone.

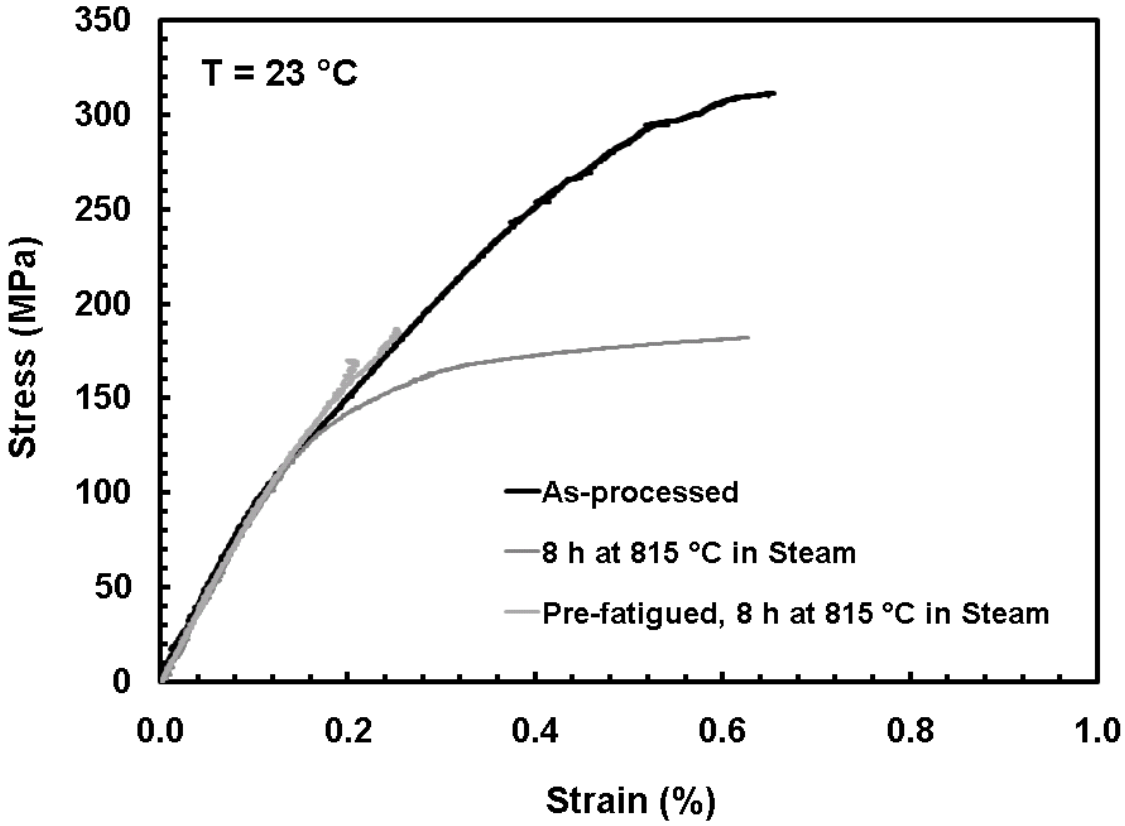


**Figure 21. Tensile stress-strain curves obtained at 23 °C for pre-fatigued C3 specimens aged for 8 h at 815 °C in steam, for as-processed C3 specimens aged for 8 h at 815 °C in steam, and for the as-processed composite C3.**

## 4.6 Summary of Results for Composite C3

Exposure to high temperature seems to adversely affect the mechanical properties of composite C3. Specimens aged in air at 815 °C for 8 hours demonstrated a 22% reduction in UTS as compared to the as processed specimens. Specimens aged in steam showed a larger reduction in strength (42%) as compared to the as processed specimens.

Pre-fatiguing for 10 cycles seems to have little effect on the mechanical properties of composite C3. Specimens pre-fatigued and then aged in air demonstrated a 28% reduction in strength as compared to the as processed materials. This reduction in strength is slightly greater than the reduction in strength exhibited by specimens aged in steam but not subjected to pre-fatiguing.

Specimens pre-fatigued then aged in steam demonstrated a 43% reduction in UTS compared to the as processed specimen. This is 1% more than the 42% reduction in UTS demonstrated by the specimens aged in steam but not subjected to pre-fatiguing. Moreover, specimens pre-fatigued then aged in steam demonstrated average failure strains 0.37% lower than specimens aged in steam.

## 4.7 Microstructural Characterization

### 4.7.1. Composite C1 Microstructural Characterization

Optical micrographs of composite C1 fatigue tests in steam are presented in Figure 22-23 and optical micrographs of composite C1 fatigue tests in air are presented in Figure 24-25. Specimens tested in both air and steam display very flat fracture surfaces with minimal fiber pullout.

Composite C1 does not demonstrate a clear correlation between the damage zone and stress level the specimen was tested at or environment the specimen was tested in. Specimens tested in air and steam demonstrate discoloration on the surface. Figures 23 and 25 show that the damage zone seems is contained to the fracture surface. Additional optical micrographs can be found in the appendix.

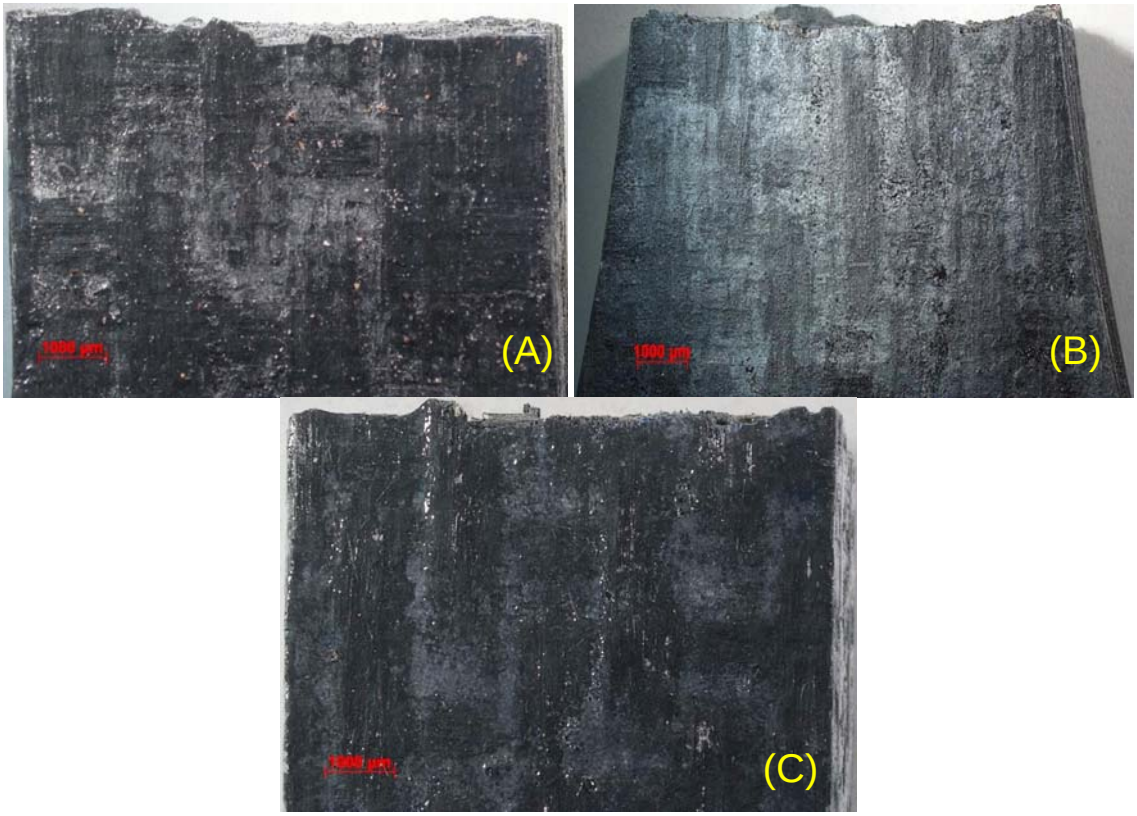


**Figure 22. Fracture surfaces of composite C1 specimens obtained in fatigue testing in steam at 1300 $^{o}$C, Maximum Fatigue Stress Level: 140 MPa (A), 120 MPa (B), and 100 MPa (C).**

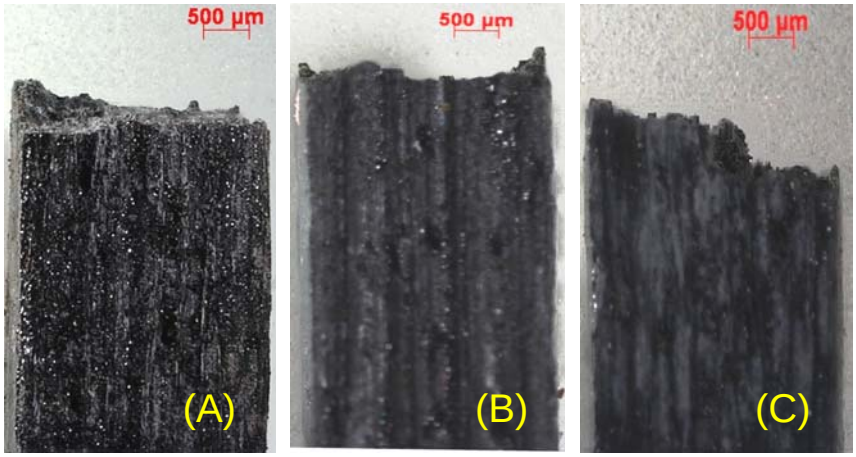


**Figure 23. Fracture surfaces of composite C1 specimens obtained in fatigue testing in steam at 1300 $^{o}$C, Maximum Fatigue Stress Level: 140 MPa (A), 120 MPa (B), and 100 MPa (C).**

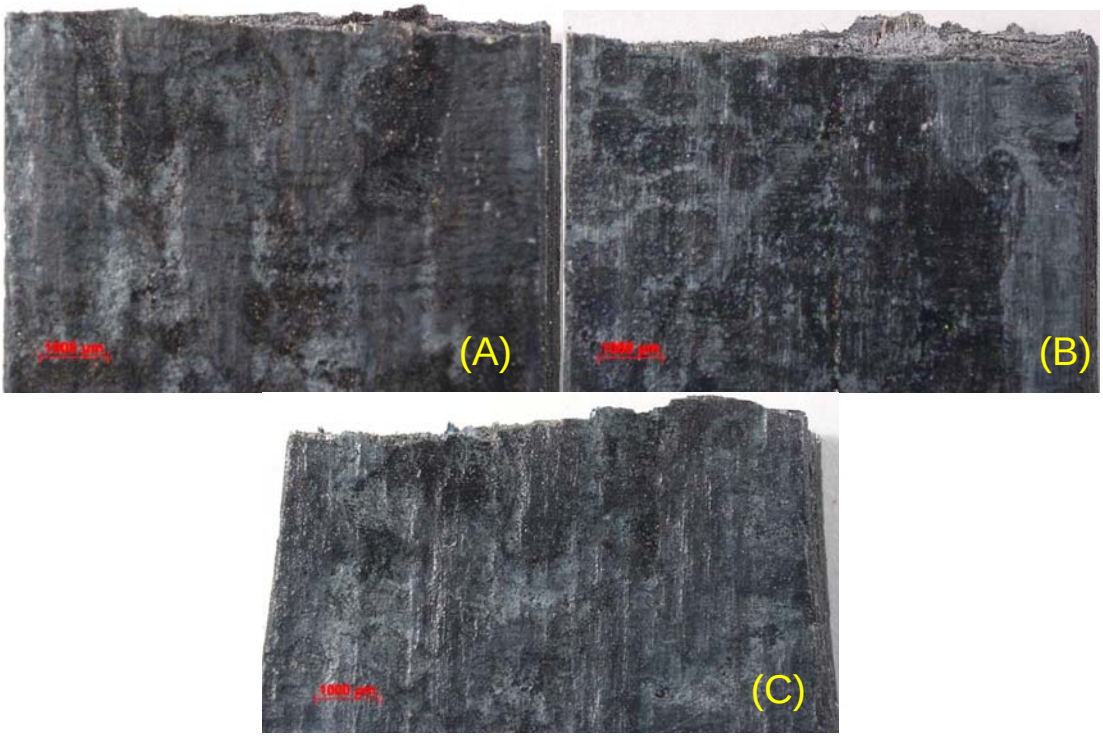


**Figure 24. Fracture surfaces of composite C1 specimens obtained in fatigue testing in air at 1300 $^{o}$C, Maximum Fatigue Stress Level: 140 MPa (A), 120 MPa (B), and 100 MPa (C).**

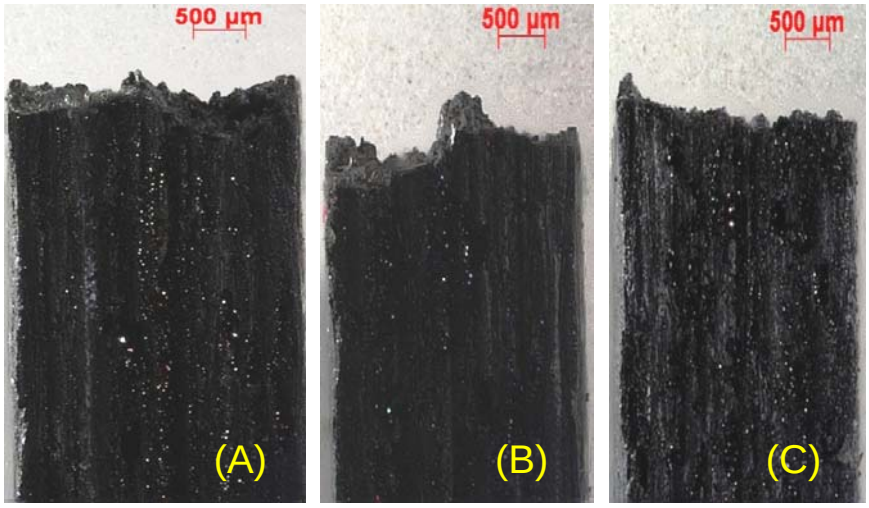


**Figure 25. Fracture surfaces of composite C1 specimens obtained in fatigue testing in air at 1300 $^{o}$C, Maximum Fatigue Stress Level: 140 MPa (A), 120 MPa (B), and 100 MPa (C).**

Figure 26(A) shows the entire face of the polished virgin specimen and highlights voids in the material. Figure 26(B) shows relatively good matrix infiltration, however, it also shows a varying diameter size in the 0° fibers which is a typical characteristic of SiC fibers. The voids in the matrix are most likely due to manufacturing defects. Figure 28(C) shows the fiber coating.

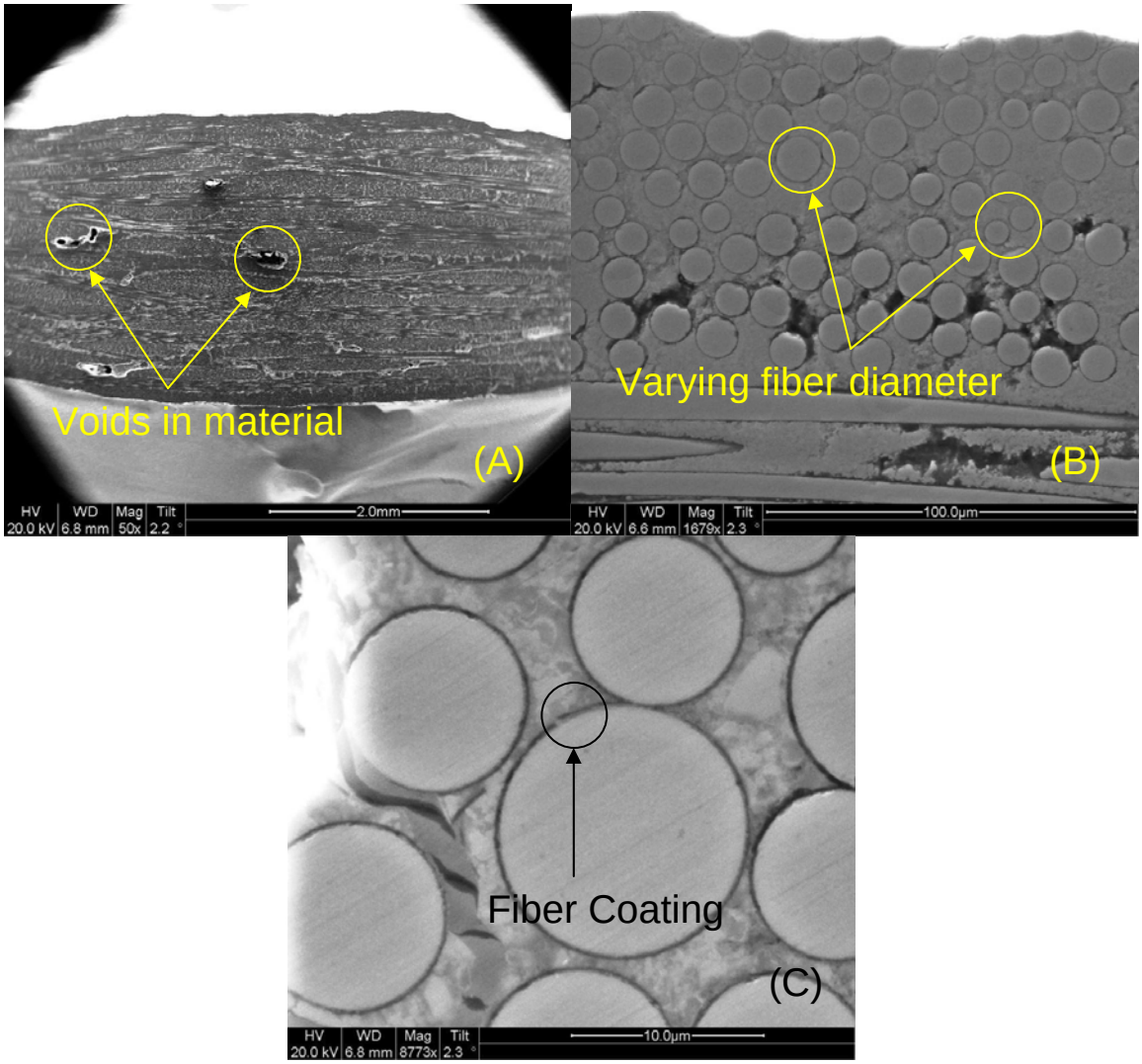


**Figure 26. SEM micrographs of composite C1 polished virgin specimen.**

Figure 27 shows SEM micrographs of the C\composite C1 as processed specimen. Figure 27(B) shows fracture of the 0 and $90^{o}$ fibers. Figure 27(C) shows minimal fiber degradation.

Figure 28 shows SEM micrographs of the polished composite C1 as processed tensile test specimen. Figure 28(A) shows the general trend of the fracture surface. Although the fracture surface does not show individual fiber pullout it does show a varying topography which is due to fiber bundle pullout. This is a trend displayed by all composite C1 and C2 fracture surfaces. Figure 28(B) shows a tow of 0° fibers amongst tows of 90° fibers. The image shows that the surface is littered with debris. Photoelectron spectroscopy was not carried out in this study and the properties of the debris, therefore, could not be determined. Figure 28(B) further demonstrates fiber bundle pull-out. Figure 28(C) shows individual fibers from the fracture surface. The fibers maintain their shape and show little physical degradation, however, some fibers show a degradation of their coating. Additionally the fibers seem to be covered with some sort of glassy film. This may be a result of oxidation of the formation of borosilicate glass during fatigue.

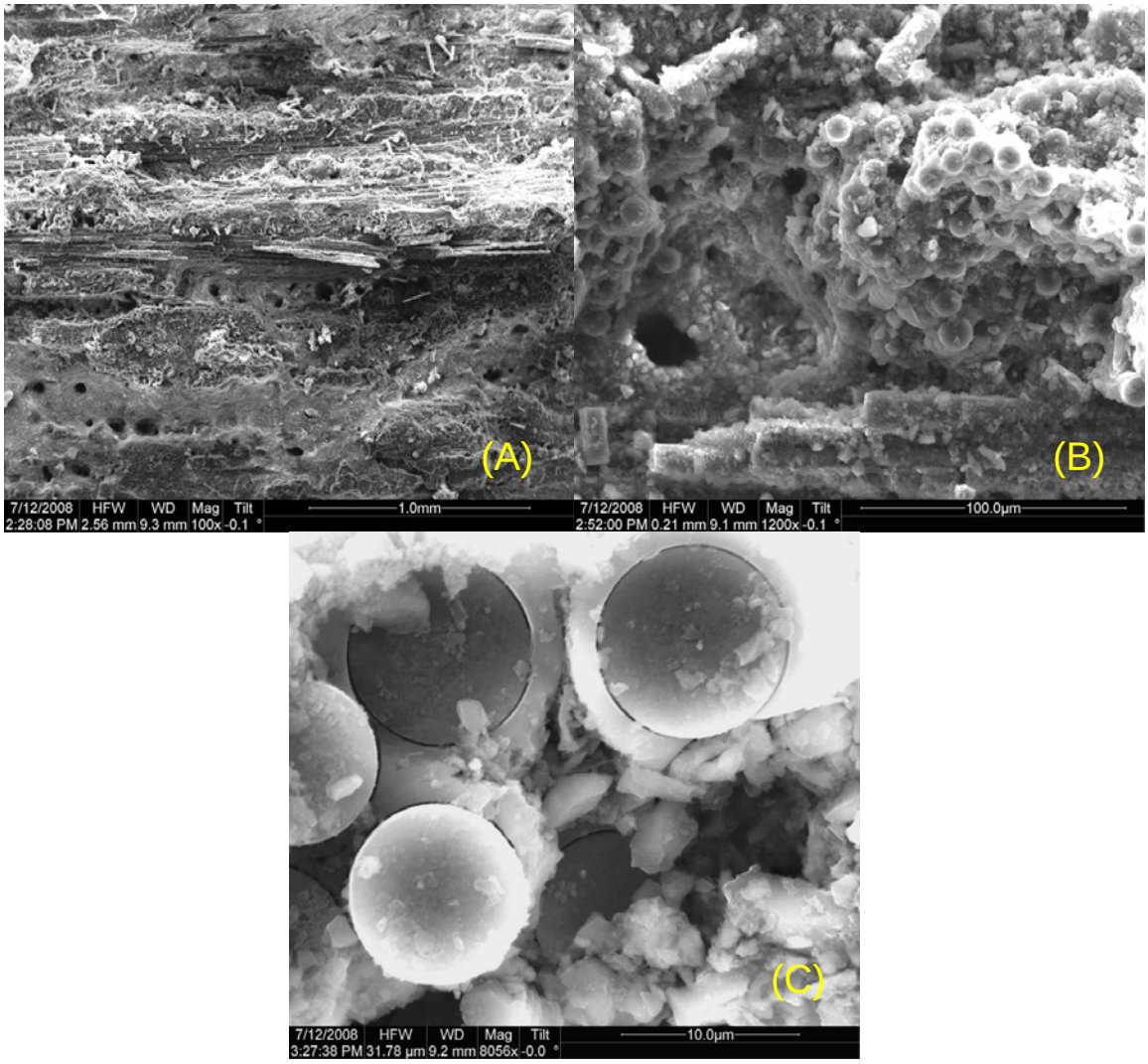


**Figure 27. Fracture surface SEM micrographs of the as processed composite C1 specimen which was subjected to a monotonic tension test to failure. (A) Overall fracture surface, (B) 0° and 90° fibers, (C) 0°fibers at higher magnification.**

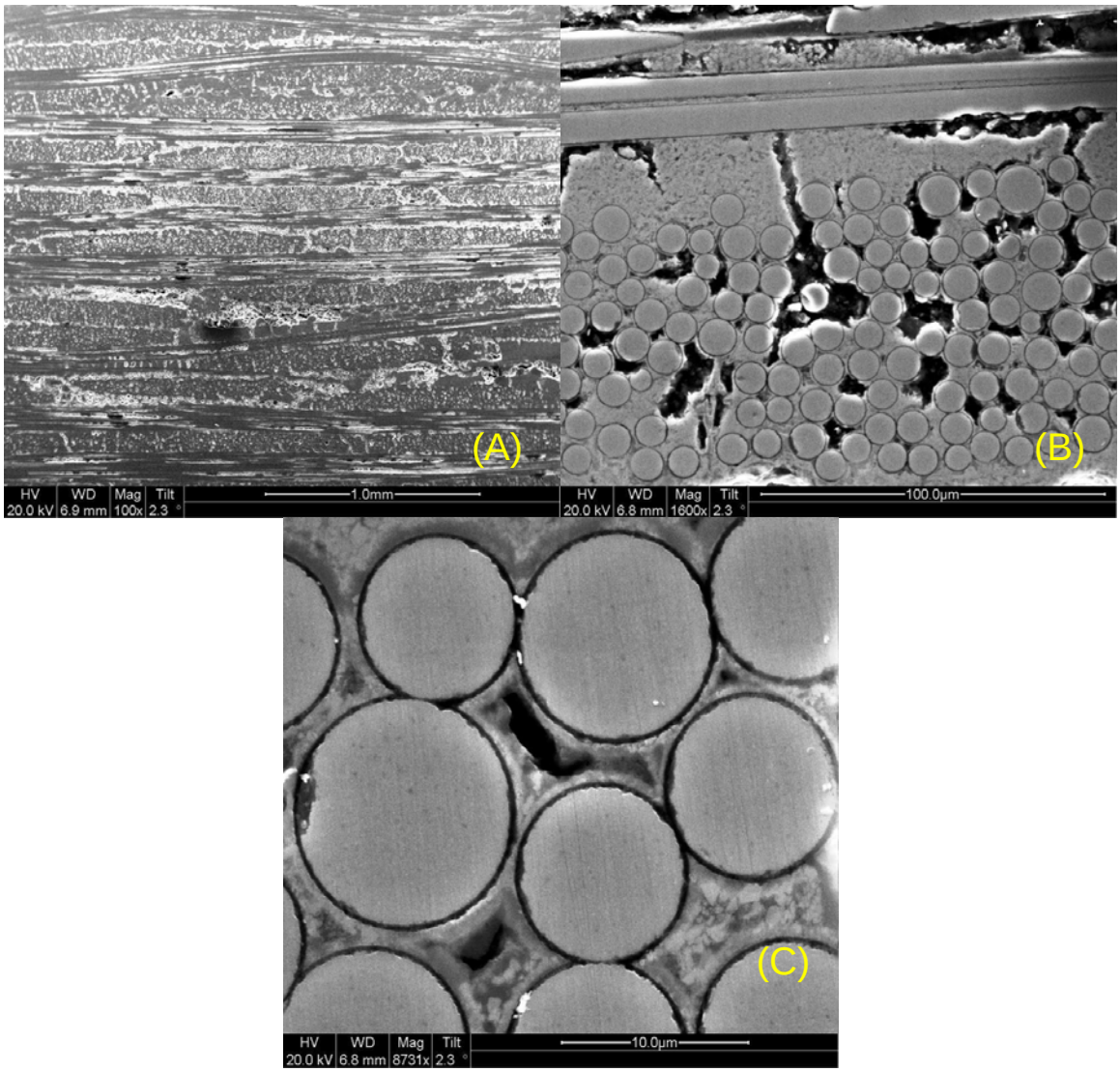


**Figure 28. SEM micrographs of polished as processed composite C1 specimen subjected to a monotonic tension test to failure at 1300°C in laboratory air. (A) Overall view, (B) 0° and 90° fibers, (C) $0^{o}$ fibers at higher magnification**

Figure 29 shows SEM Micrographs of the fracture surface from the composite C1 specimen subjected to fatigue with a maximum stress of 140 MPa in steam environment. Figure 29(B) shows cracking in the 90° fibers in a matrix rich region. Figure 29(C) shows severe damage to the fiber. The fiber coating is absent and the glassy overcoat is also seen. Figure 30 shows SEM micrographs of polished material taken from the composite C1 specimen fatigued in steam at 140 MPa. Unlike Figure 28(B), Figure 30(B) shows regions where it is difficult to differentiate fiber coatings and it appears as if the matrix is directly bonded to the fiber. This is indicative of regions where oxidation has occurred. Figure 30(B) also shows cracks propagating from the $90^{o}$ tows into the $0^{o}$ fiber tows. Figure 30(C) shows oxidation of the matrix and interphase. Interphase oxidation allows for damage mechanisms to penetrate the matrix and attack the fibers which weakens them and thus expedites material failure.

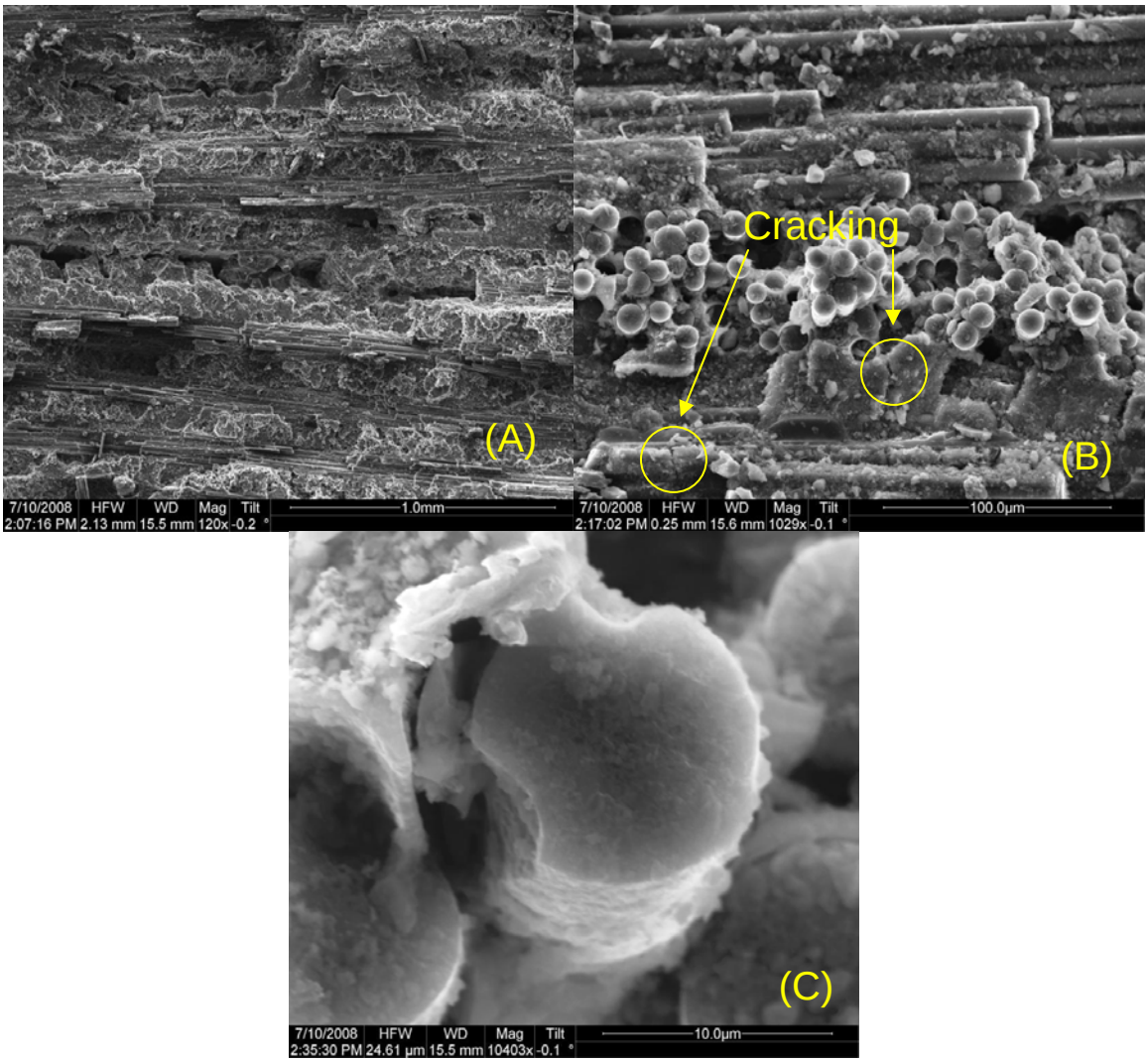


**Figure 29. Fracture surface SEM micrographs of composite C1 specimen fatigued in a steam environment at 1300°C with a maximum fatigue stress σ = 140MPa. (A) Overall fracture surface, (B) 0° and 90° fibers, (C) 0° fiber at higher magnification.**

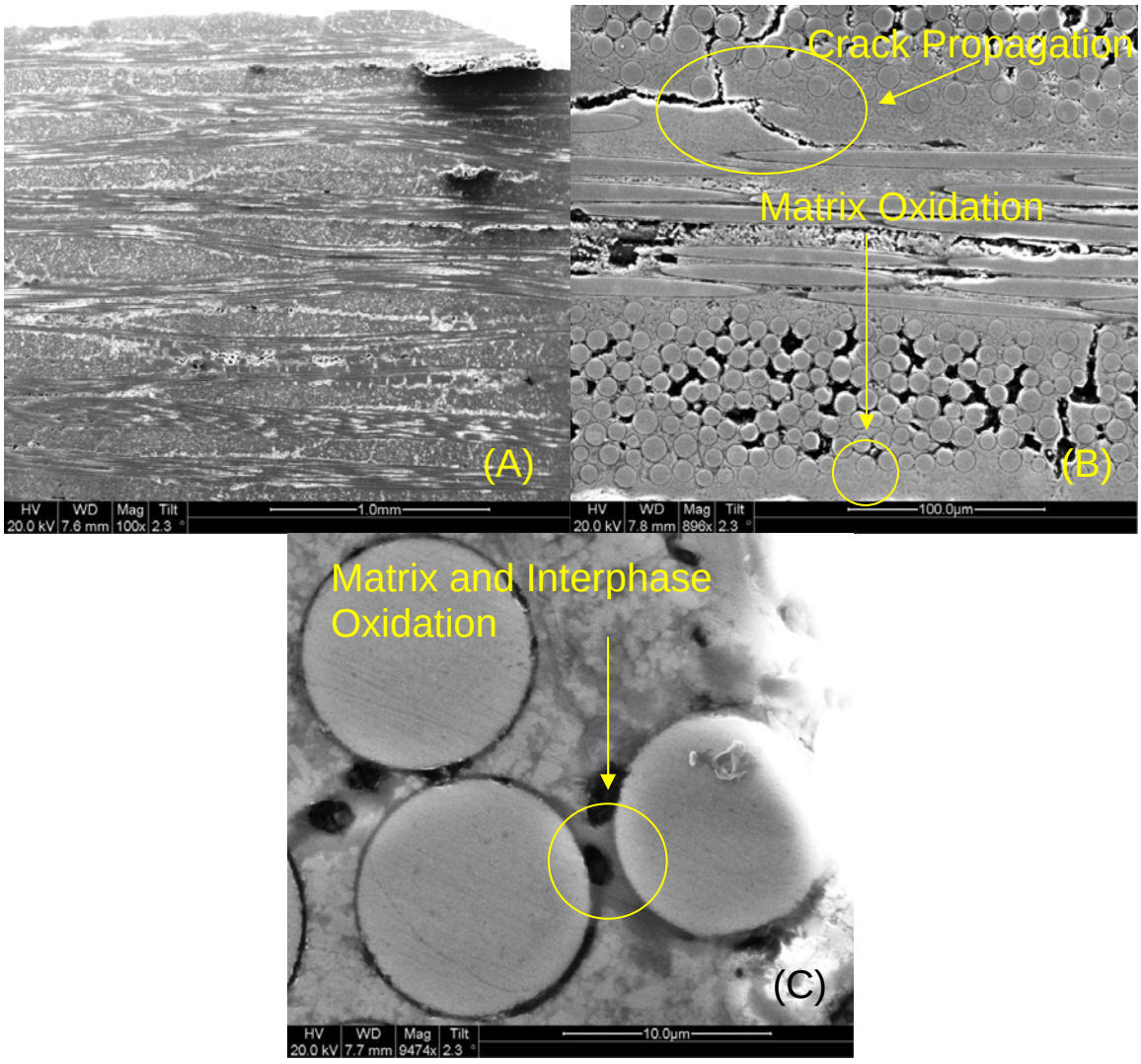


**Figure 30. SEM micrographs of polished composite C1 specimen fatigued in a steam environment at 1300°C with a maximum fatigue stress σ = 140MPa. (A) Overall fracture surface, (B) 0° and 90° fibers, (C) 0° fiber at higher magnification.**

Figure 31 shows fracture surface SEM micrographs of the composite C1 specimen fatigued in air at 1300°C with a maximum stress level $\sigma = 140$ MPa. Figure 31(B) shows individual fiber pullout, however, the pullout length is quite short and only visible under the SEM. Figure 31(C) shows fibers where the interphase cannot be seen and the fibers show degradation. Additionally the fibers and surrounding matrix area show a lot of deposited debris.

Figure 32 shows SEM micrographs of the polished material from the composite C1 specimen fatigued in an air environment at 1300°C with a maximum stress level of 140 MPa. Figure 34(B) shows a fairly large region of Matrix oxidation. The porous matrix region seen towards the bottom third of figure 32(B) cannot be explained. Figure 32(C) shows degradation of the fiber coatings as well as matrix and interphase oxidation. The oxidation does not appear to be as severe as it was in Figure 30(C) and the fibers seem to be relatively intact and free of any major damage.

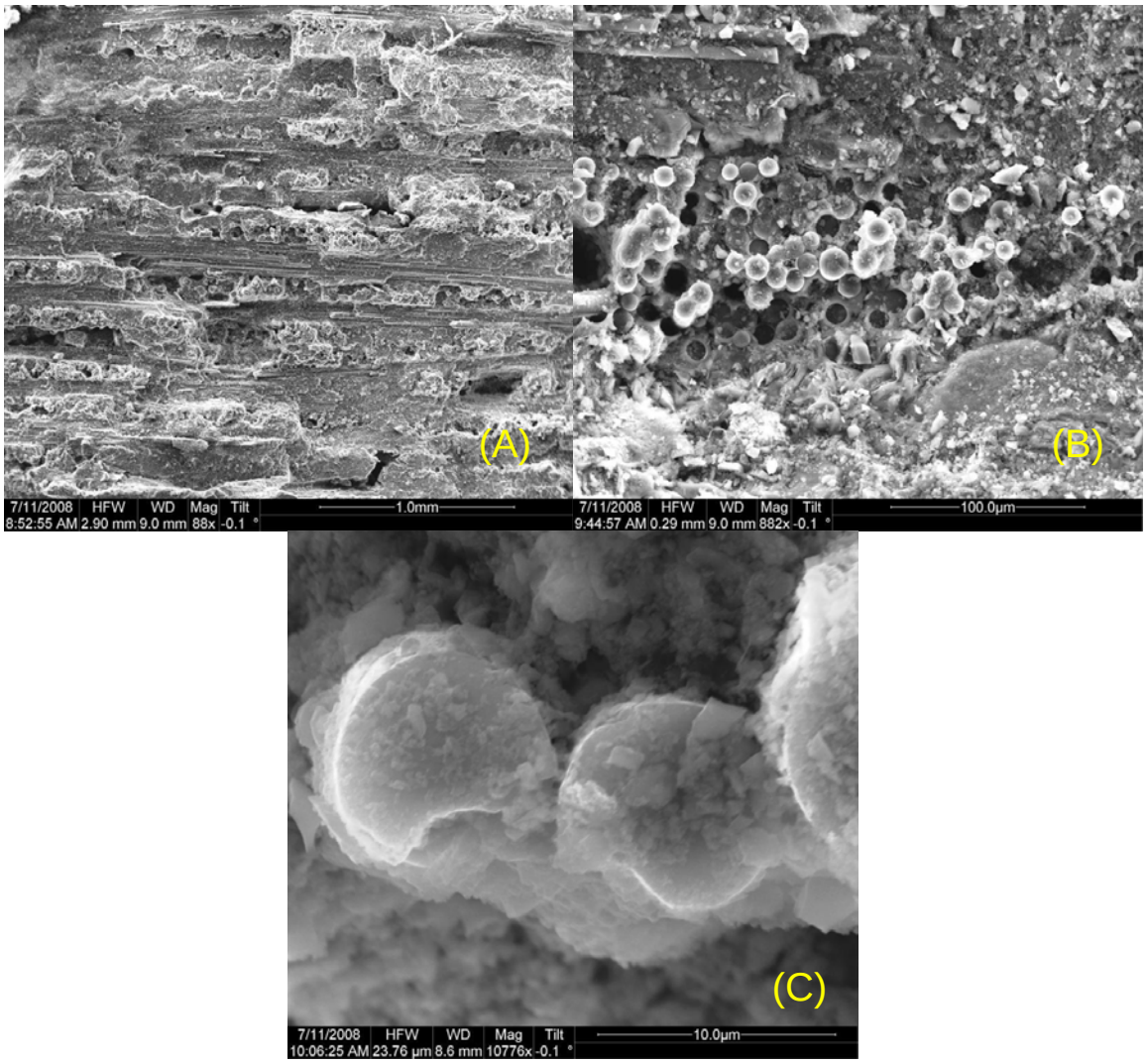


**Figure 31. Fracture surface SEM micrographs of composite C1 specimen fatigued in laboratory air at 1300°C with a maximum fatigue stress σ = 140MPa. (A) Overall fracture surface, (B) 0° and 90° fibers, (C) 0° fiber at higher magnification.**

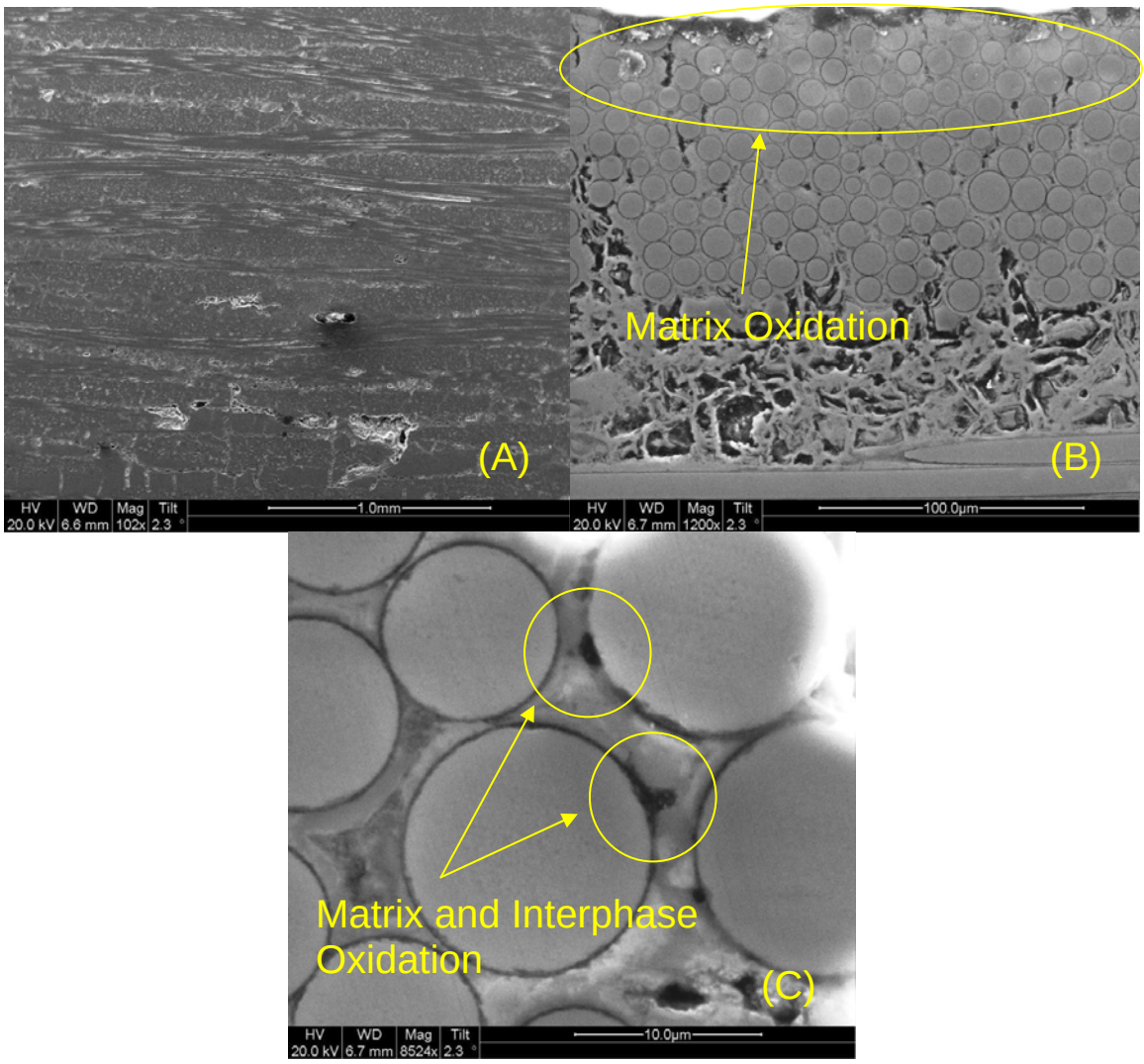


**Figure 32. SEM micrographs of polished composite C1 specimen that was fatigued in laboratory air at 1300°C with a maximum fatigue stress σ = 140MPa. (A) Overall fracture surface, (B) 0° and 90° fibers, (C) 0° fiber at higher magnification.**

Figure 33 shows fracture surface SEM micrographs of the composite C1 specimen fatigued in steam at 1300°C at a maximum stress value of 100 MPa. Figure 33(A) shows a characteristic representation of the fracture surface. Figure 33(B) shows a 90° fiber tow amongst several 0° fiber tows. Several of the fibers in the 90° tow have failed. Additionally a glass like substance which covers many of the 0° fibers. As previously mentioned, spectroscopy could not be conducted and therefore the composition of the substance could not be determined. The substance most probably formed when the specimen fractured and the surface was exposed to the high temperature oxidizing environment. Figure 33(C) shows several fibers demonstrating little or no degradation. The fiber coatings are still relatively intact although in some areas the matrix in between the fibers seems to have completely disintegrated.

Figure 34 shows SEM micrographs of the polished composite C1 specimen fatigued in steam at 1300°C with a maximum stress of 100 MPa. It is difficult to discern an area of matrix or interphase oxidation in Figure 34. Figure 34(B) however shows cracking in the $0^{o}$ fiber tows and very large voids in the matrix material of the $90^{o}$ fiber tows. In figure 34(C) the fiber coating is not clearly visible, however the fibers appear to be undamaged.

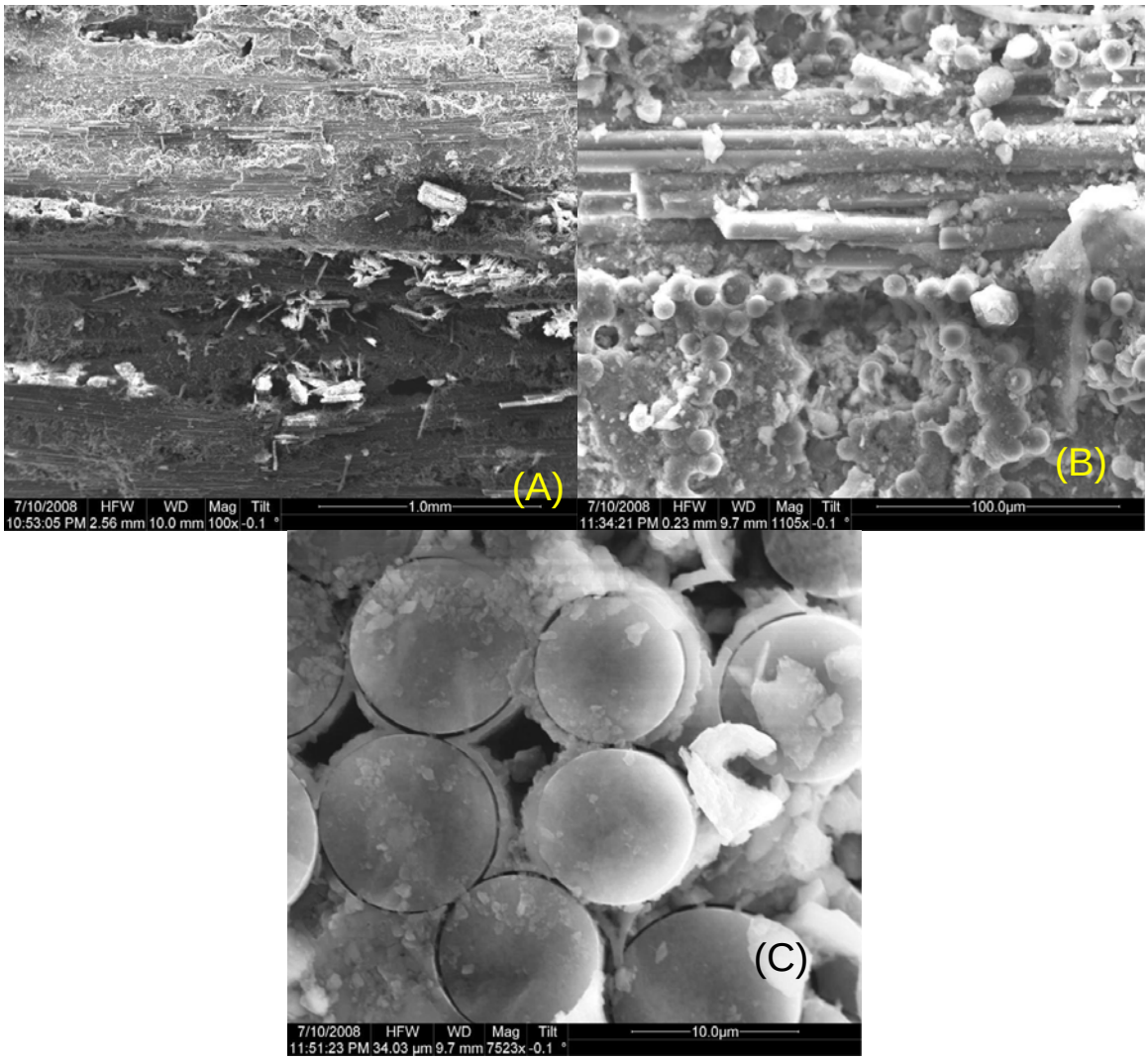


**Figure 33. Fracture surface SEM micrographs of composite C1 specimen fatigued in a steam environment at 1300°C with a maximum fatigue stress σ = 100MPa. (A) Overall fracture surface, (B) 0° and 90° fibers, (C) 0° fiber at higher magnification.**

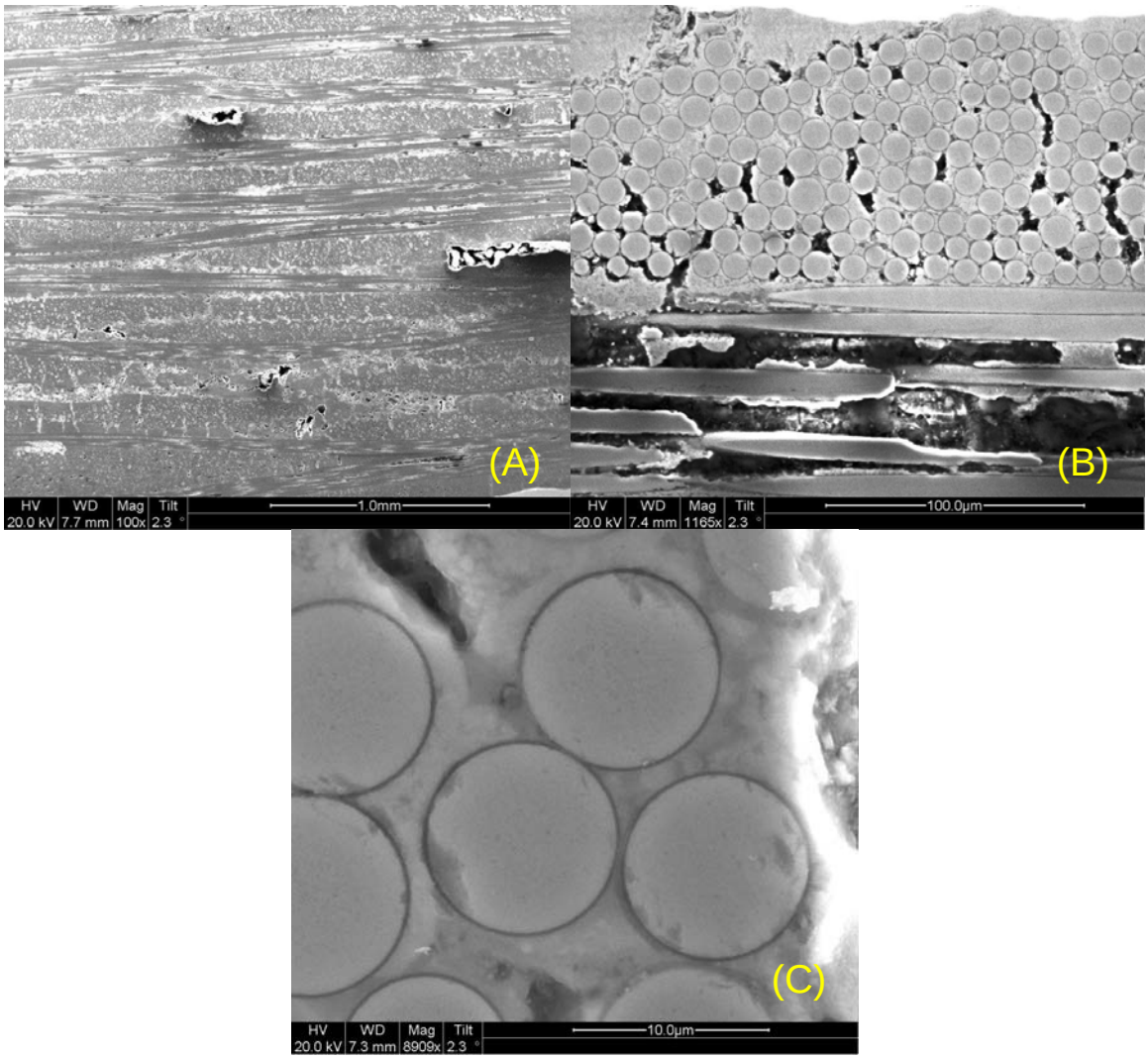


**Figure 34. SEM micrographs of polished composite C1 specimen that was fatigued in a steam environment at 1300°C with a maximum fatigue stress σ = 100MPa. (A) Overall fracture surface, (B) 0° and 90° fibers, (C) 0° fiber at higher magnification.**

Figure 35 shows SEM micrographs of the fracture surface of the Composite C1 specimen fatigued in air at 1300°C with a maximum fatigue stress of 100 MPa. The fracture surface looks very similar to the fracture surfaces of other specimens from composite C1. Once again, the fibers themselves show little or no degradation.

Figure 36 shows SEM micrographs of polished Composite C1 fatigued in air at 1300°C with a maximum fatigue stress of 100 MPa. Figure 36(B) shows cracking in the matrix region. Figure 36(C) shows that the fibers and the interphase with no visible damage mechanisms.

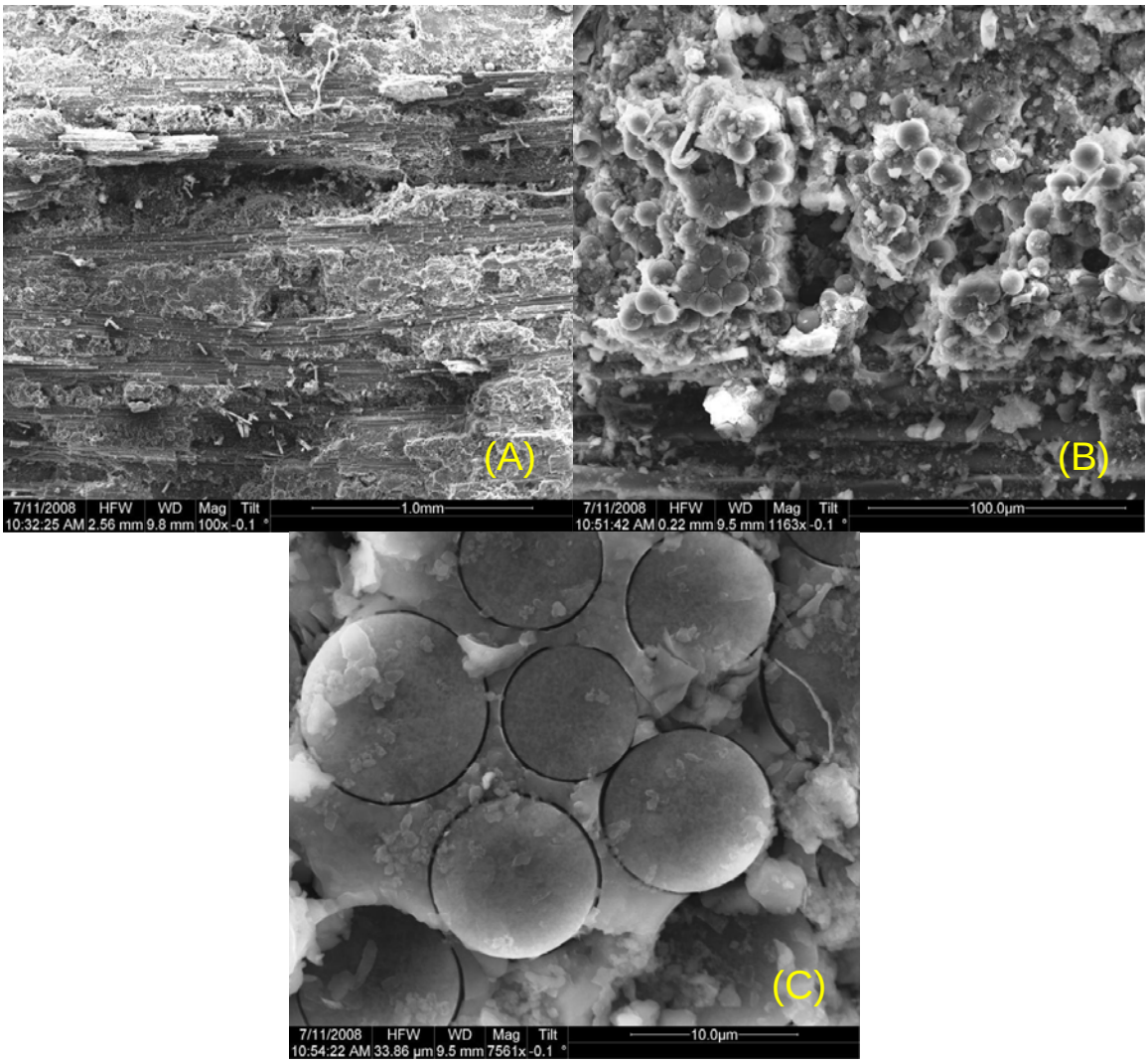


**Figure 35. Fracture surface SEM micrographs of composite C1 specimen fatigued in laboratory air at 1300°C with a maximum fatigue stress σ = 100MPa. (A) Overall fracture surface, (B) 0° and 90° fibers, (C) 0° fiber at higher magnification.**

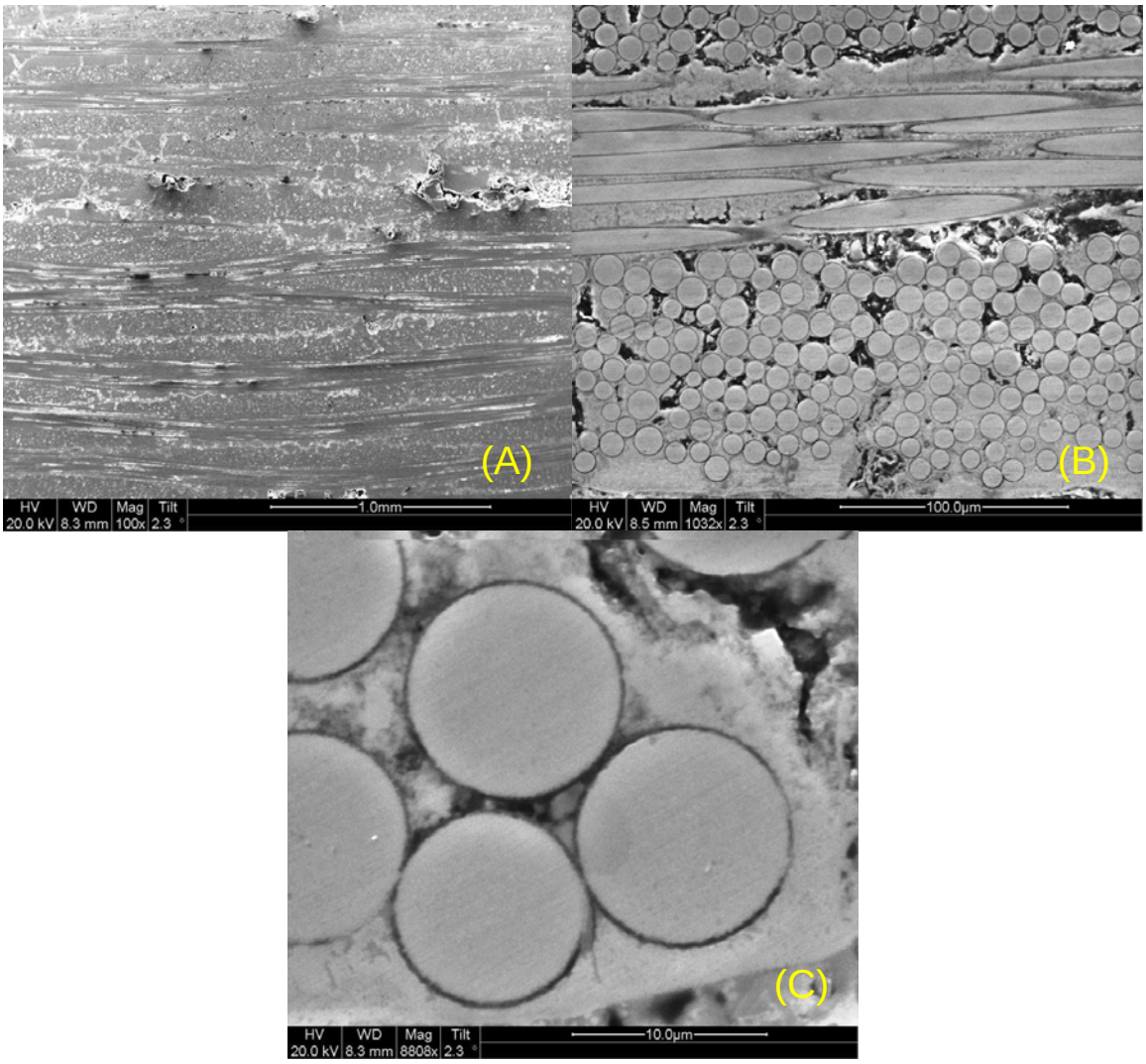


**Figure 36. SEM micrographs of polished composite C1 specimen that was fatigued in laboratory air at 1300°C with a maximum fatigue stress σ = 100MPa. (A) Overall fracture surface, (B) 0° and 90° fibers, (C) 0° fiber at higher magnification.**

### 4.7.2. Composite C2 Microstructural Characterization

Optical micrographs of composite C2 fatigue tests in steam are presented in Figure 37-38 and optical micrographs of composite C2 fatigue tests in air are presented in Figure 39-40. composite C2 specimens also display very flat fracture surfaces with minimal fiber pullout.

A white residue is visible on the surface of composite C2 specimens fatigued in steam. There appears to be a correlation between the amount of time spent in the oxidizing steam environment and the amount of residue on the surface of the specimen. Figure 37(A) and 38(A) shows far less residue accumulation than the specimen from Figures 37(C) and 38(C). The specimens fatigued in air showed slight discoloration with some of their fibers turning blue The cause of the blue residue could not be determined. Additional optical micrographs for Material 2 can be found in the appendix.

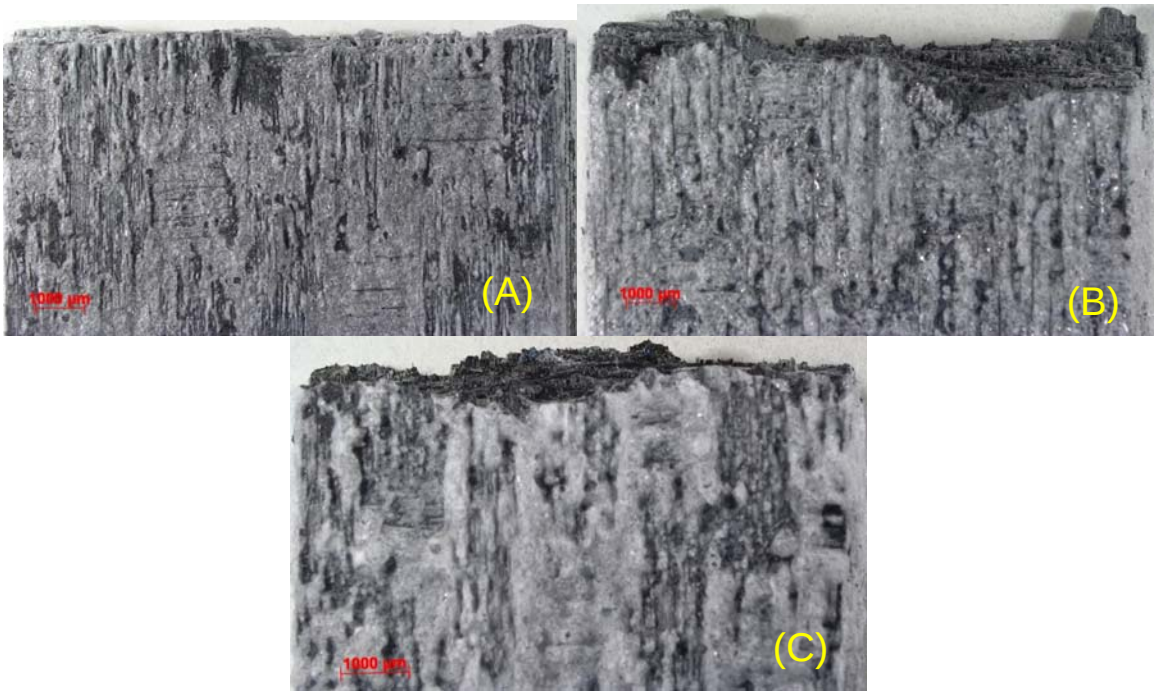


**Figure 37. Fracture surfaces of composite C2 specimens fatigued in a steam environment at 1300 $^{o}$C, Maximum Fatigue Stress Level: (A)180 MPa, (B) 160 MPa, and (C) 140 MPa.**

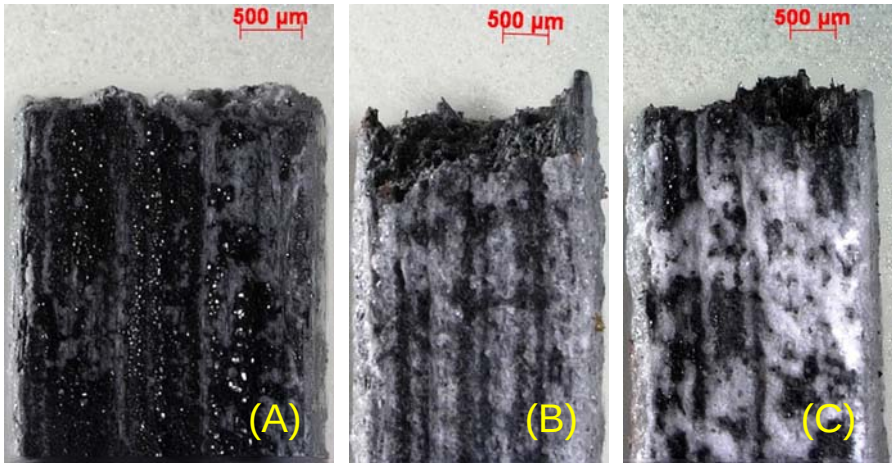


**Figure 38. Fracture surfaces of composite C2 specimens fatigued in a steam environment at 1300 $^{o}$C, Maximum Fatigue Stress Level: (A) 180 MPa, (B) 160 MPa, and (C) 140 MPa.**

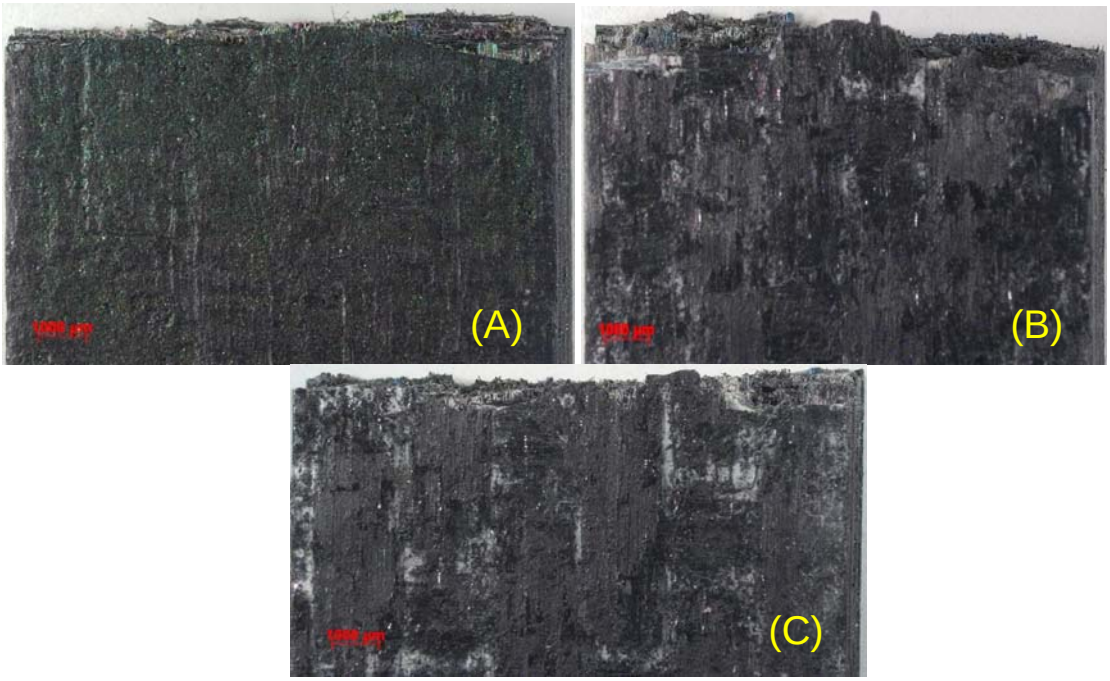


**Figure 39. Fracture surfaces of composite C2 specimens fatigued in air at 1300 °C, Maximum Fatigue Stress Level: (A) 180 MPa, (B) 160 MPa, and 140 MPa (C).**

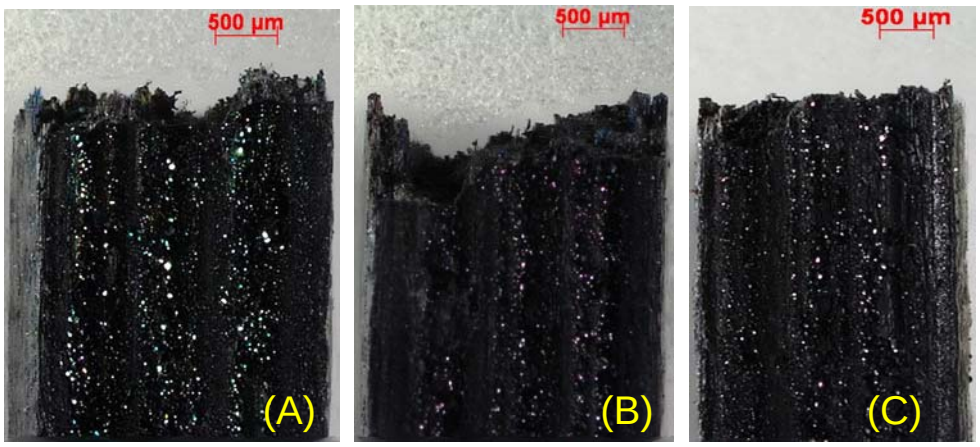


**Figure 40. Fracture surfaces of composite C2 specimens obtained in fatigue testing in air at 1300 °C, Maximum Fatigue Stress Level: (A) 180 MPa, (B) 160 MPa), and (C) 140 MPa.**

Figure 41 shows SEM micrographs of a polished virgin composite C2 specimen. The images show relatively good matrix infiltration. Figure 41(A) is a general representation of the polished face of the specimen and shows voids similar to those seen

in composite C1. Figure 41(B) shows varying fiber diameters which were also seen in composite C1. Finally Figure 41(C) shows individual fibers with fiber coatings visible.

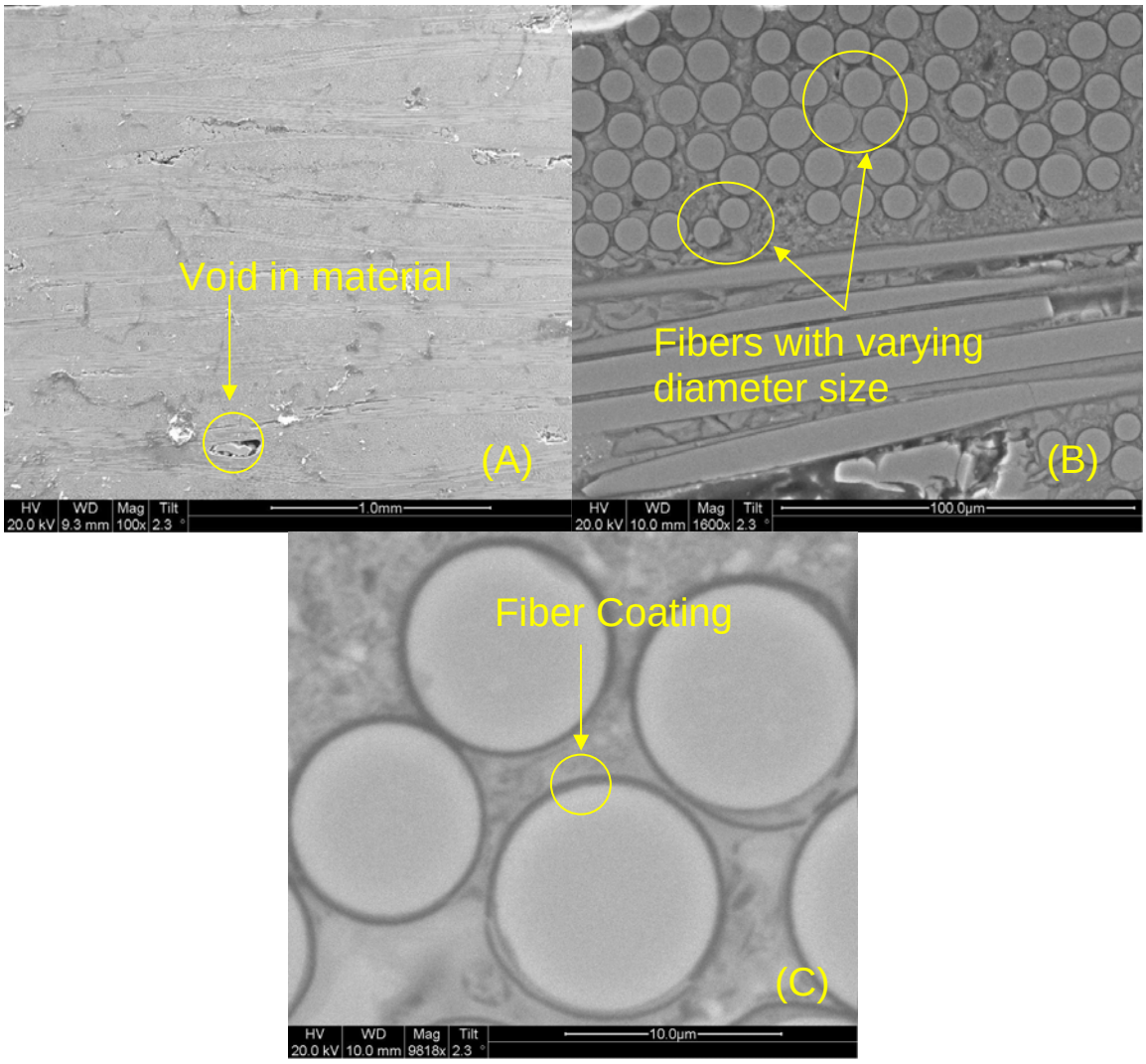


**Figure 41. SEM micrographs of composite C2 polished virgin specimen.**

Figure 42 shows fracture surface SEM micrographs of the as processed composite C2 specimen subjected to a monotonic tension test to failure. Figure 43 shows SEM micrographs of polished material of the as processed composite C2 specimen subjected to a monotonic tension test to failure.

Figure 42(A) shows typical characteristics of the fracture surface which is mostly planar and shows little fiber pull out. Figure 42(B) shows 0 and $90^{o}$ fibers on the fracture surface. No individual fiber pull-out can be seen in the $0^{o}$ fibers, however, fiber bundle pull-out is evident. Similarly the $90^{o}$ fibers show failure and fiber bundle fracture. Fiber 43(C) shows individual fibers where the fiber coating seems to have experienced severe degradation. This, damage, however may have occurred during the fracture surface's exposure to the high temperature environment after failure.

Figure 43(A) shows a characteristic representation of the polished surface where voids in the material can be seen. Figure 43(B) shows areas of matrix oxidation along the edge of the specimen. Figure 43(C) shows further evidence of matrix oxidation.

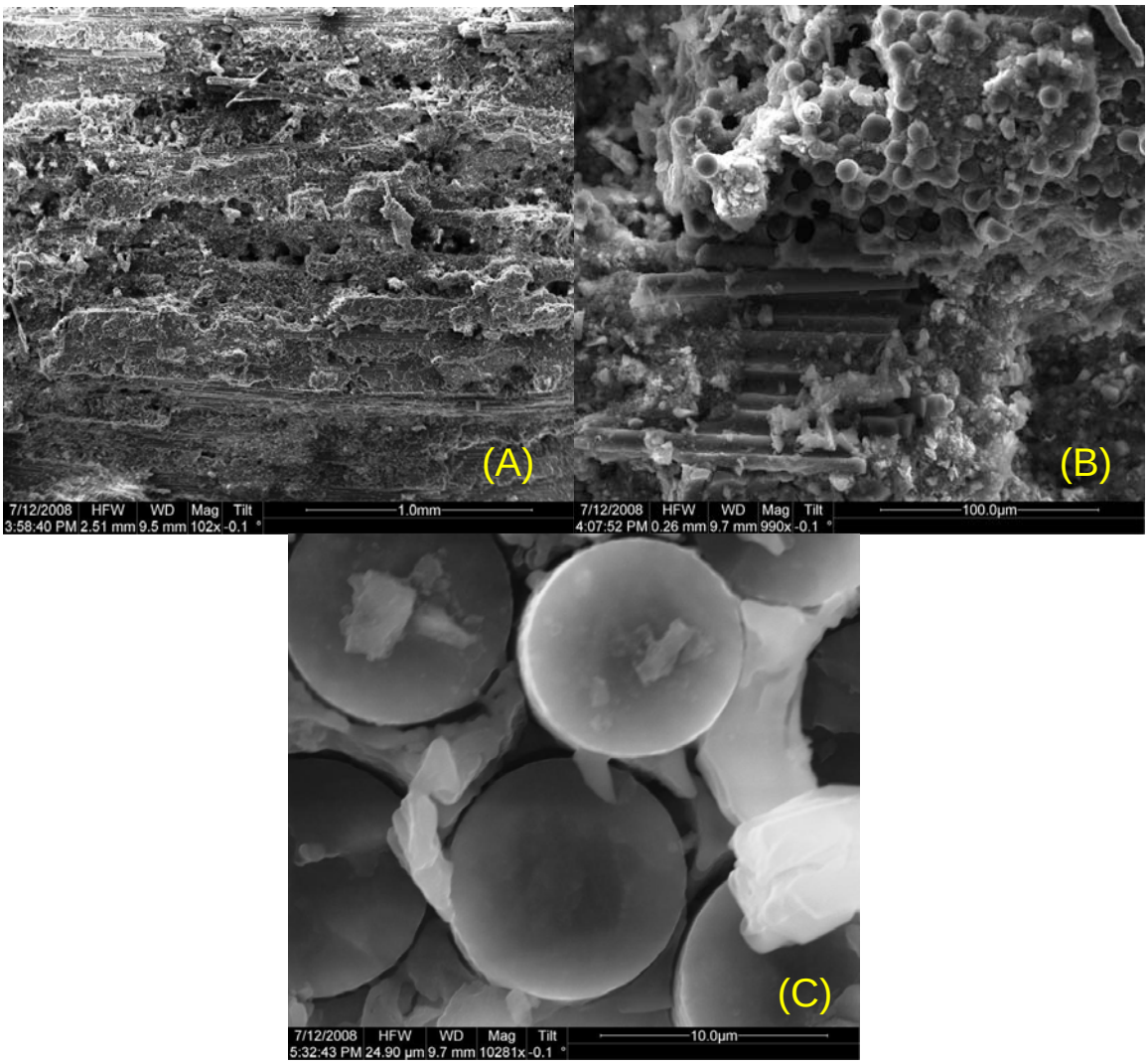


**Figure 42. Fracture surface SEM micrographs of the as processed Composite C2 specimen which was subjected to a monotonic tension test to failure. (A) Overall fracture surface, (B) 0° and 90° fibers, (C) 0°fibers at higher magnification.**

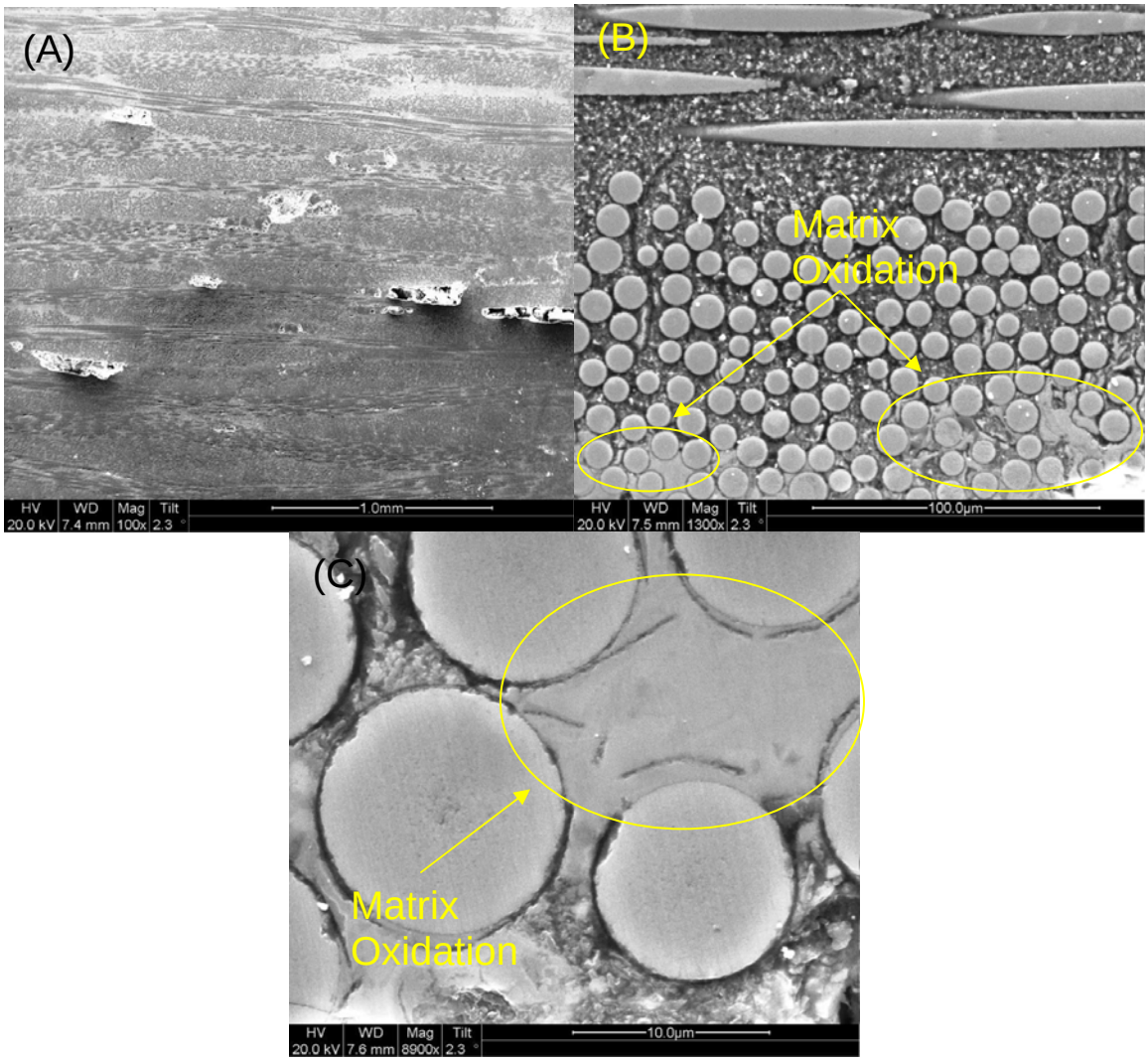


**Figure 43. SEM micrographs of polished as processed composite C1 specimen subjected to a monotonic tension test to failure at 1300°C in laboratory air. (A) Overall view, (B) 0° and 90° fibers, (C) $0^{o}$ fibers at higher magnification**

Figure 44 and 45 show SEM micrographs of the fracture surface and polished material of the composite C2 specimen fatigued tested at 1300 $^{o}$C in a steam environment with a maximum stress level $\sigma = 140$ MPa. Figure 44(A) shows a characteristic representation of the fracture surface. The fracture surface shows areas where a glassy residue has been deposited on the material. This glassy substance is shown in greater magnification in figure 44(B) and 44(C). Even though the fibers are covered by the glassy substance, there are areas in figure 44(C) which show fiber coating degradation.

Figure 45(B) shows that matrix oxidation is contained to areas within 50 μm of the edge of the specimen. Additionally, Figure 45(B) shows that the matrix is virtually free of cracking. The specimen shown in figure 45 achieved run-out in steam environment. The SEM micrographs of the composite C1 specimen which achieved run-out in steam are given in Figure 34 and they show matrix cracking.

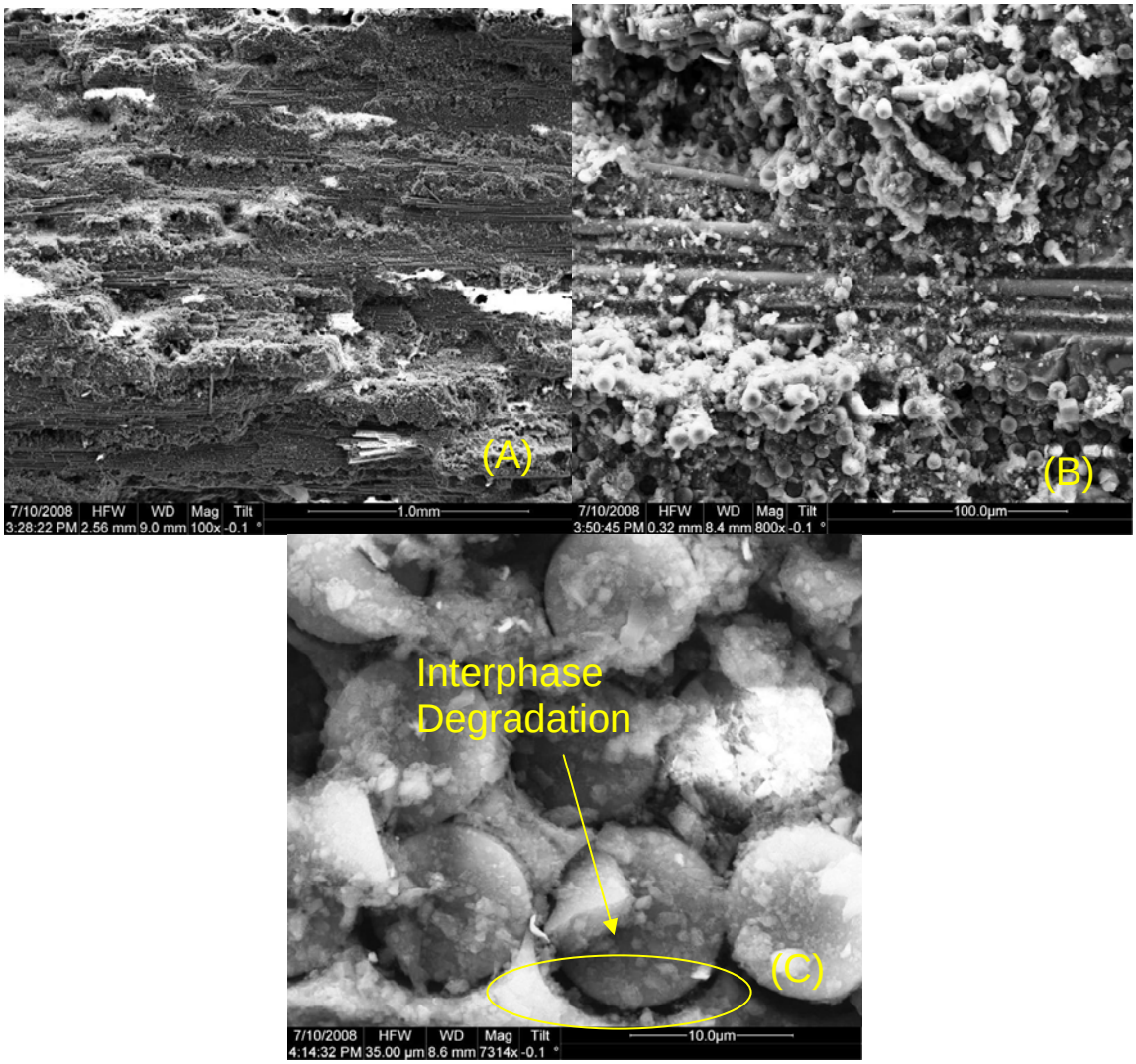


**Figure 44. Fracture surface SEM micrographs of composite C2 specimen fatigued in a steam environment at 1300°C with a maximum fatigue stress σ = 140MPa. (A) Overall fracture surface, (B) 0° and 90° fibers, (C) 0° fiber at higher magnification.**

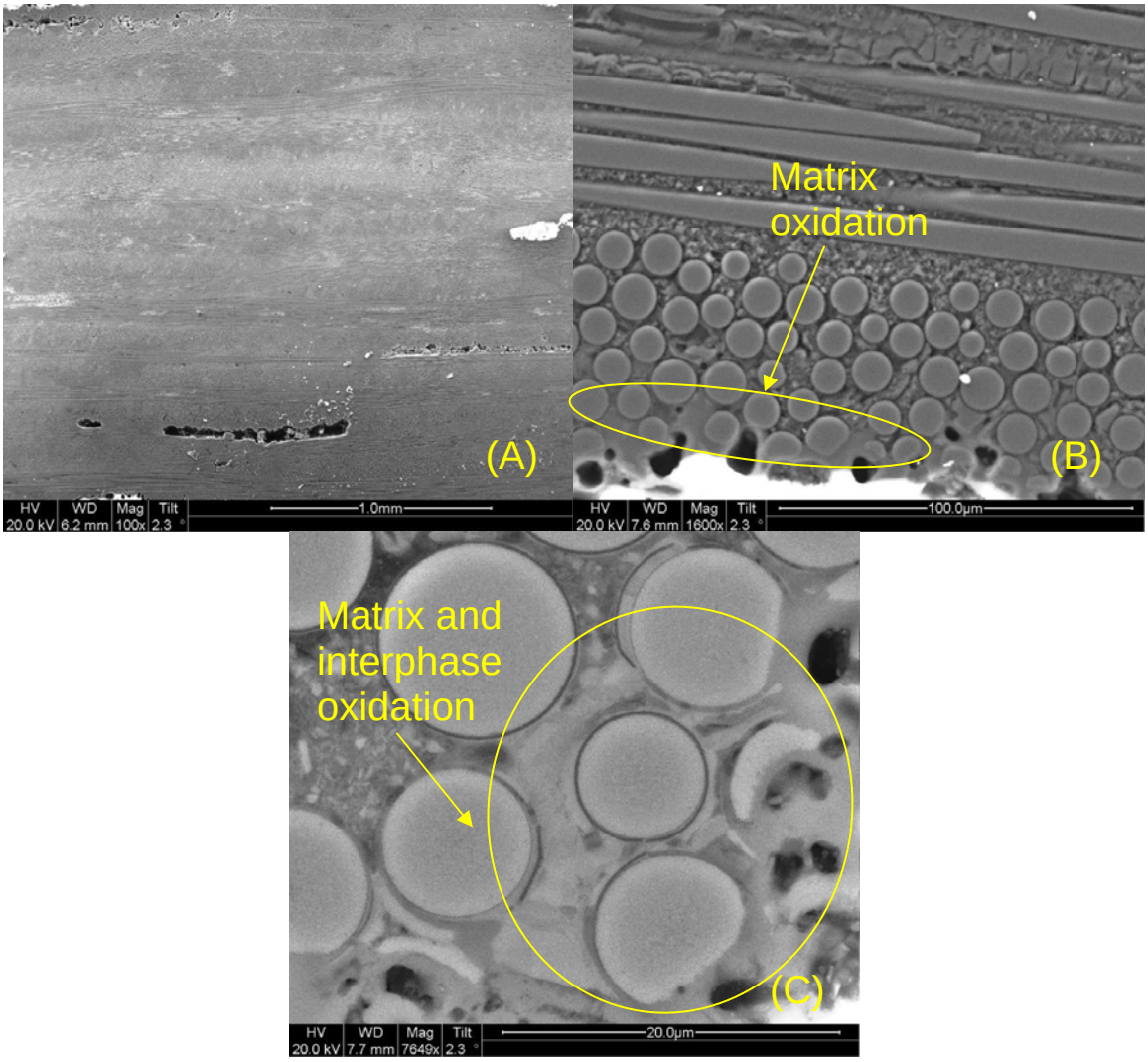


**Figure 45. SEM micrographs of polished composite C2 specimen that was fatigued in a steam environment at 1300°C with a maximum fatigue stress σ = 140MPa. (A) Overall fracture surface, (B) 0° and 90° fibers, (C) 0° fiber at higher magnification.**

Figure 46 and 47 show SEM micrographs of the fracture surface and polished material from the composite C2 specimen fatigued in air at 1300 $^{o}$C with a maximum fatigue stress $\sigma$ = 140 MPa. Figure 46(A) shows the planar fracture surface, Figure 46(B) shows pull-out of fiber bundles and that there is no pull-out of individual fibers. Figure 46(C) shows an area of fiber-interphase oxidation. The fiber coatings are not visible, however, the fibers seem to be undamaged and maintain their round shape.

Figure 47(A) shows that the material contains voids just as all other specimens viewed under the SEM. Figure 47(B) shows that there is a region of matrix oxidation on the edges of the specimens however it is smaller than the regions shown in Figures 45(B). This indicates that matrix oxidation is exacerbated in the presence of moisture. Figure 47(C) also shows that the matrix oxidation region for the Composite 2 specimen tested in air with maximum fatigue stress level of 140 MPa is smaller than that of its steam counterpart.

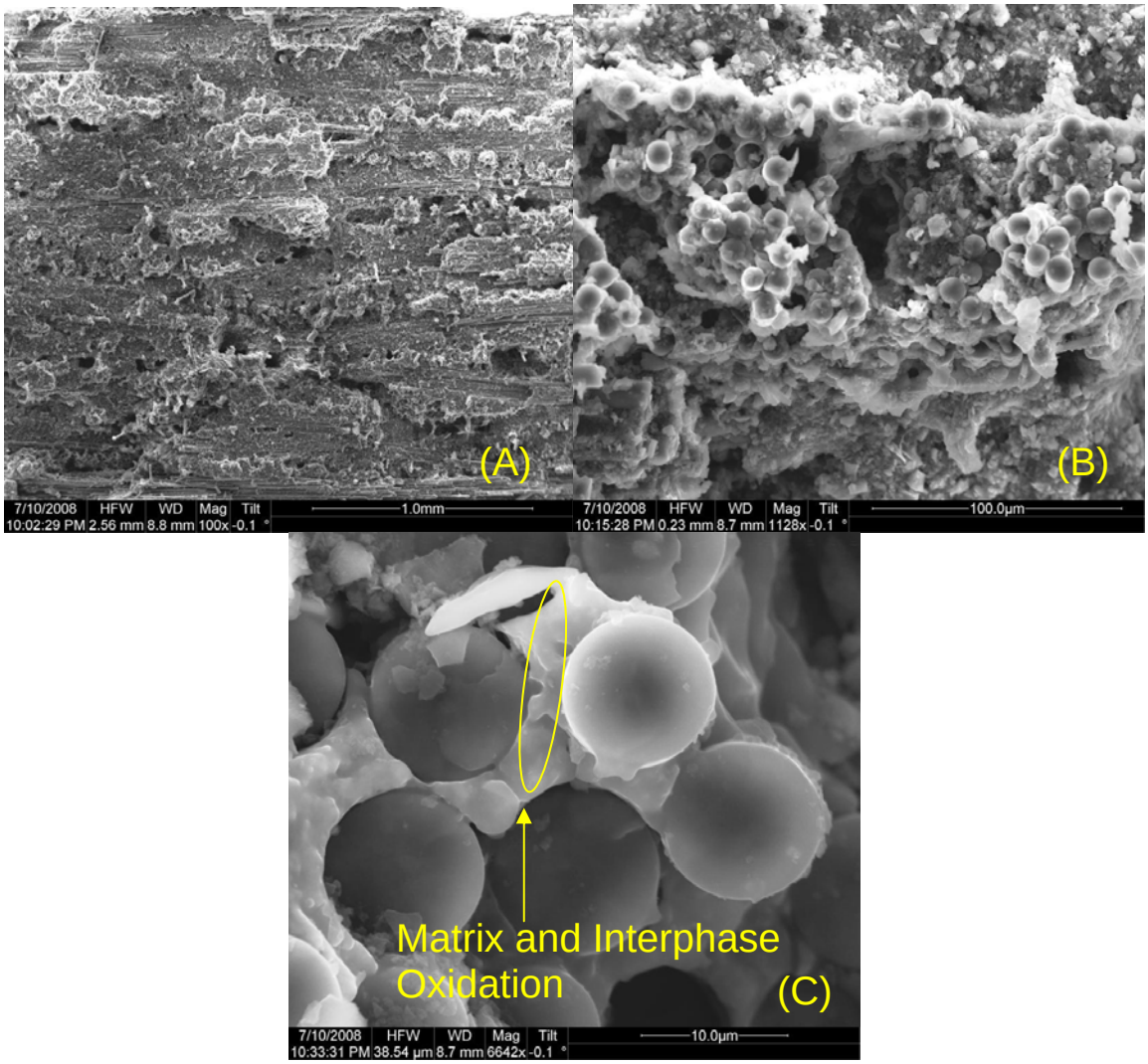


**Figure 46. Fracture surface SEM micrographs of composite C2 specimen fatigued in laboratory air at 1300°C with a maximum fatigue stress σ = 140MPa. (A) Overall fracture surface, (B) 0° and 90° fibers, (C) 0° fiber at higher magnification.**

.

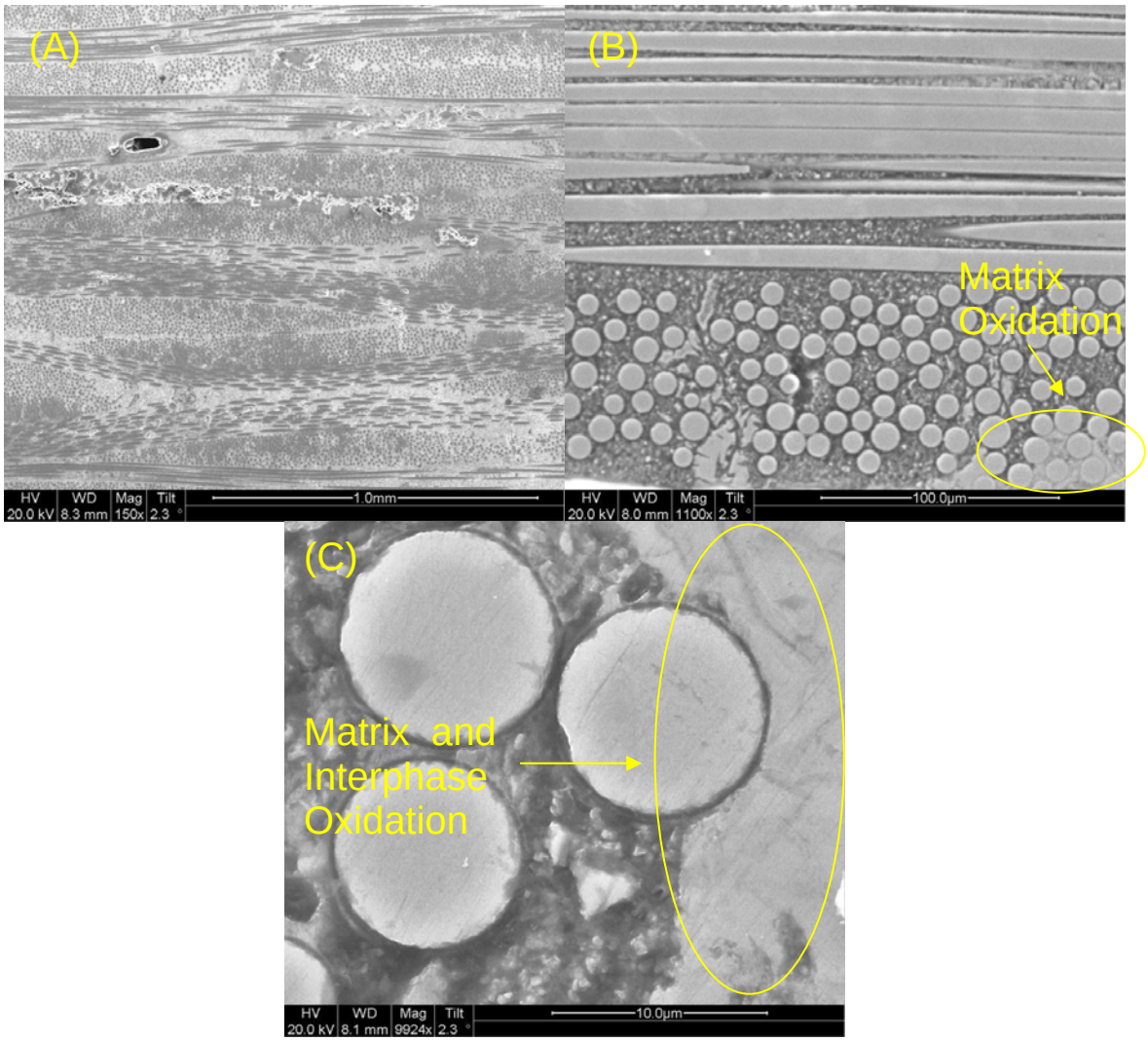


**Figure 47. SEM micrographs of polished composite C2 specimen that was fatigued in laboratory air at 1300°C with a maximum fatigue stress σ = 140MPa. (A) Overall fracture surface, (B) 0° and 90° fibers, (C) 0° fiber at higher magnification**

Figures 48 and 49 show the fracture surface and polished specimen of the composite C2 specimen fatigued in steam at 1300 $^{o}$C with a maximum fatigue stress of 180 MPa. Figure 48(A) shows pull-out of 0$^{o}$ fiber bundles. Figure 48(B) shows fractures of the 0$^{o}$ and 90$^{o}$ fiber bundles and figure 48(C) shows fiber interphase degradation as well as matrix and interphase oxidation.

Figure 49(A) shows the polished surface of the specimen. Figure 49(B) shows that the oxidized area of the specimen seems to be substantially smaller than the oxidized areas in figure 45(B) and 47(B). Unlike the oxidation regions in Figure 45(B) and 47(B), the oxidation region in 49(B) is not continuous. This specimen exhibited the shortest lifetime of all composite C2 specimens.

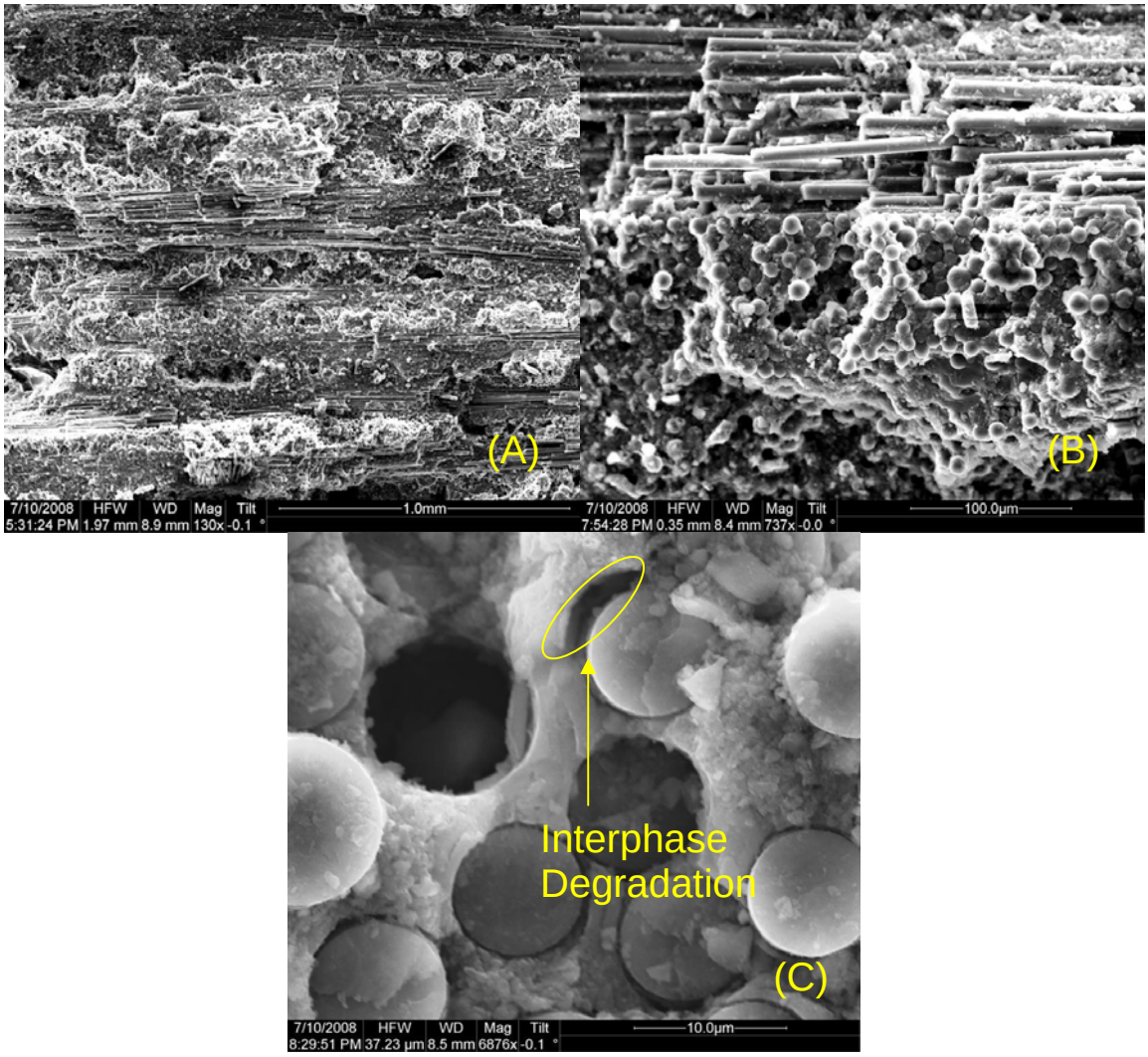


**Figure 48. Fracture surface SEM micrographs of composite C2 specimen fatigued in a steam environment at 1300°C with a maximum fatigue stress σ = 180MPa. (A) Overall fracture surface, (B) 0° and 90° fibers, (C) 0° fiber at higher magnification.**

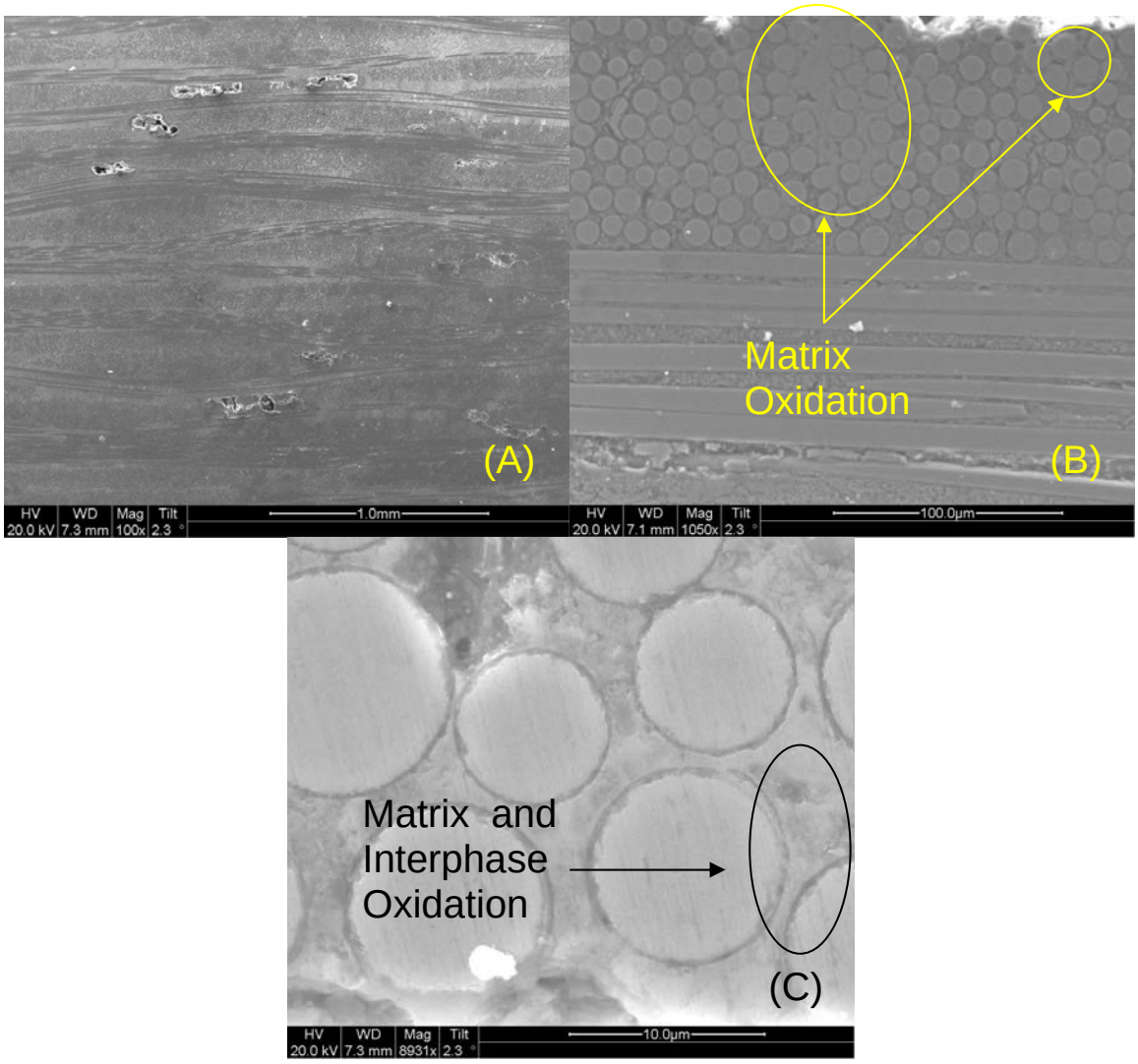


**Figure 49. SEM micrographs of polished composite C1 specimen that was fatigued in a steam environment at 1300°C with a maximum fatigue stress σ = 180MPa. (A) Overall fracture surface, (B) 0° and 90° fibers, (C) 0° fiber at higher magnification.**

Figure 50 and 51 show the fracture surface and polished specimen for the composite C2 specimen fatigued in air at 1300 $^{o}$C with a maximum fatigue stress of 180 MPa. Figure 50(A) shows a typical representation of the fracture surface. Figures 50(B) and 50(C) show that the fracture surface is much more glassy than any previous specimens. This cannot be explained at this time. Figure 50(B) also shows fracture in the 90$^{o}$ fiber bundles.

Figure 51(B) shows discontinuous oxidation regions similar to figure 49(B). Figure 51(C) shows almost small amounts of matrix and interphase oxidation.

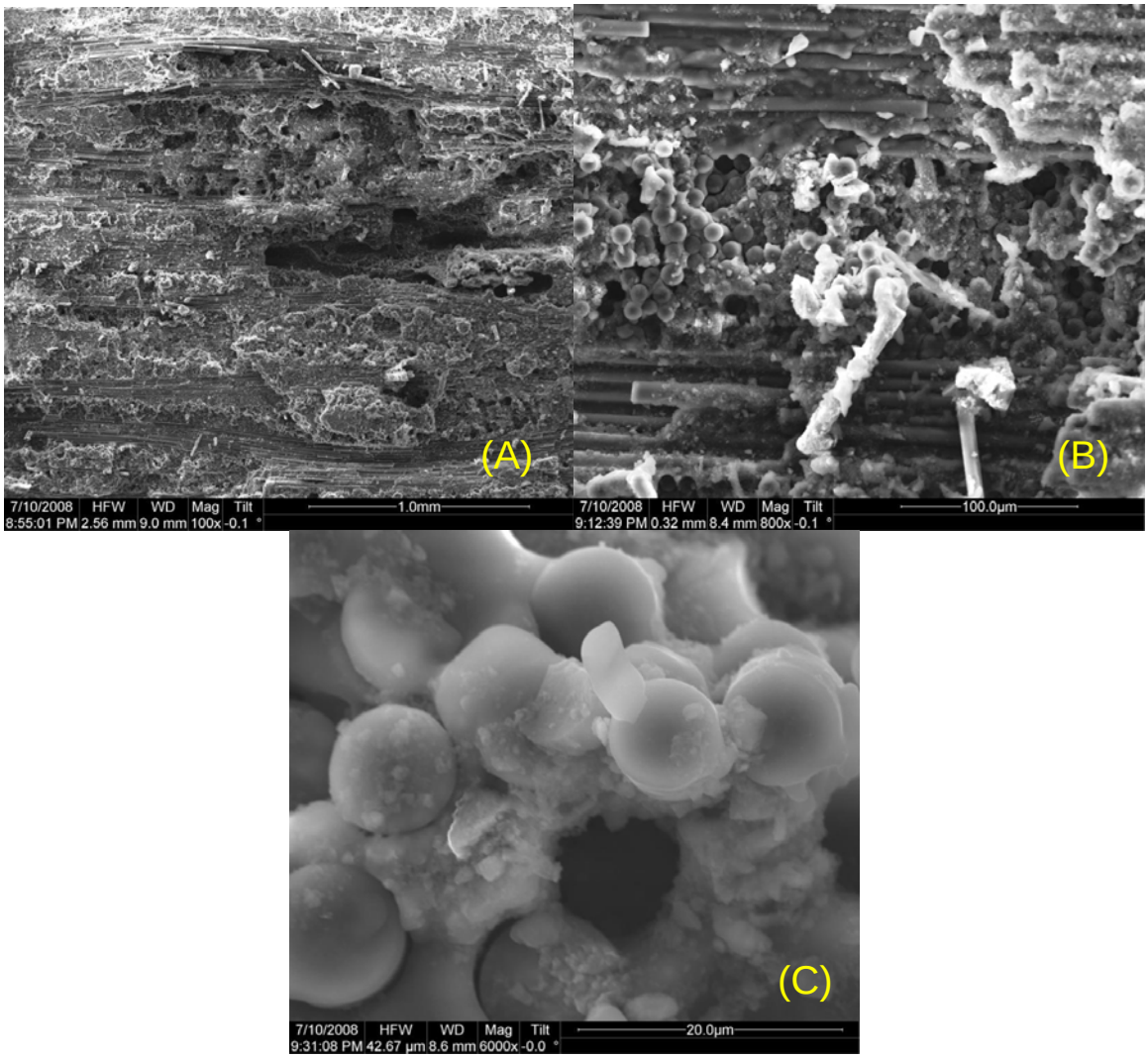


**Figure 50. Fracture surface SEM micrographs of composite C2 specimen fatigued in laboratory air at 1300°C with a maximum fatigue stress σ = 180MPa. (A) Overall fracture surface, (B) 0° and 90° fibers, (C) 0° fiber at higher magnification.**

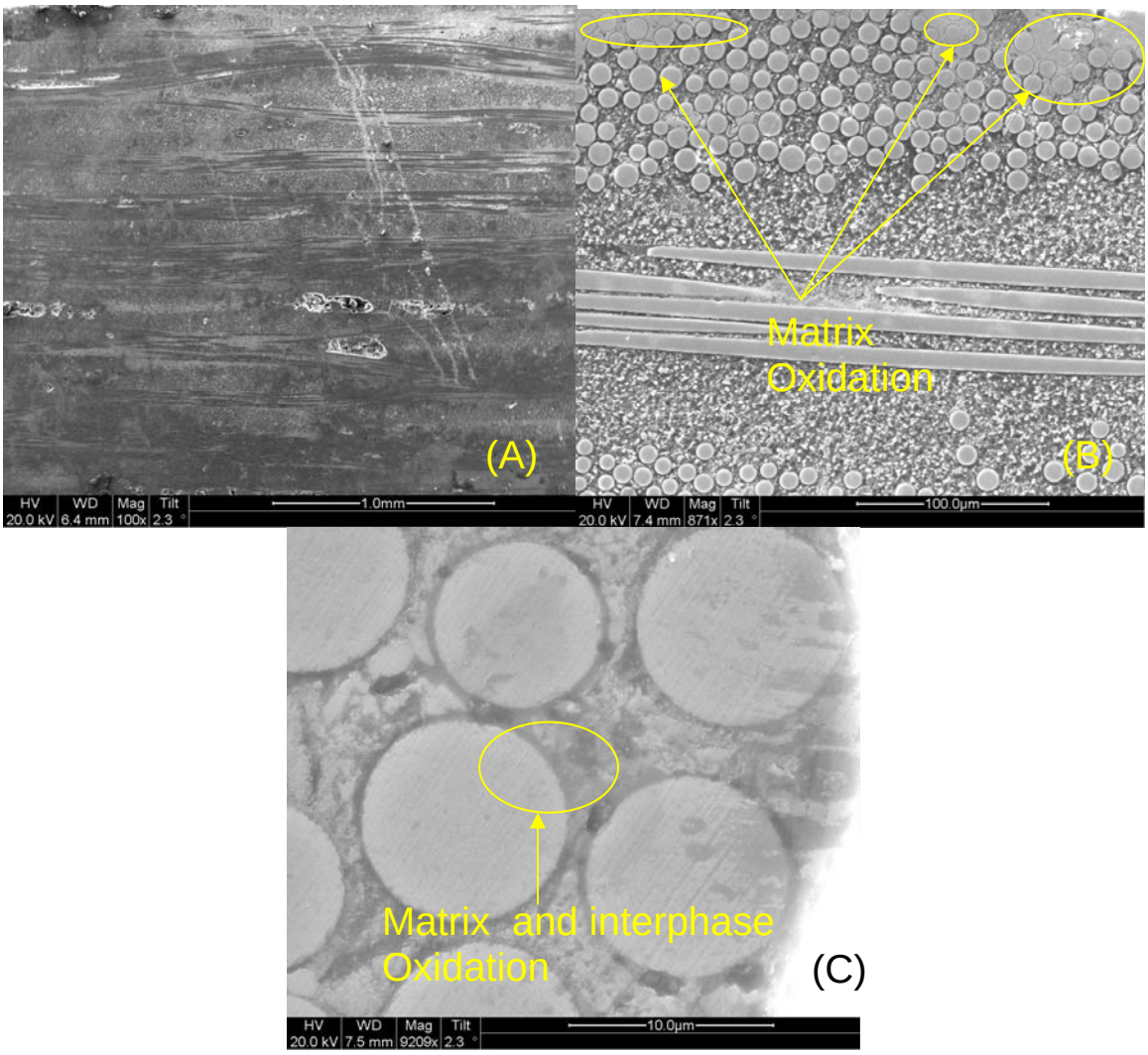


**Figure 51. SEM micrographs of polished composite C2 specimen that was fatigued in laboratory air at 1300°C with a maximum fatigue stress σ = 180MPa. (A) Overall fracture surface, (B) 0° and 90° fibers, (C) 0° fiber at higher magnification.**

### 4.7.3. Composite C3 Microstructural Characterization

Figure 52 shows optical micrographs of the fracture surface from the as processed composite C3 specimen subjected to a monotonic tensile test to failure. The fracture surface is significantly more brushy than fracture surfaces of composites C1 and C2. Figure 52(B) shows that the damage zone stretches approximately 2 mm past the fracture surface.

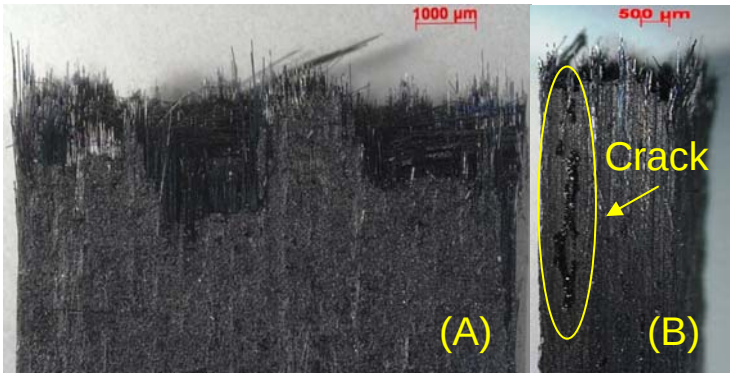


**Figure 52. Optical micrographs of as processed composite C3 specimen subjected to a monotonic tension test in laboratory air.**

Figure 53 shows optical micrographs of the composite C3 specimen aged in steam at 815°C for 8 hours, then subjected to a monotonic tension test. The fracture surface demonstrates some fiber pull-out, however, it is less brushy than the micrographs shown in figure 52. Figure 53(A) shows the material is slightly discolored when compared to figure 52(A). Figure 53(B) shows the damage zone extends approximately 2 mm past the fracture surface. Other micrographs of the specimen do not show extension of the damage zone past the fracture surface. These can be seen in the appendix.

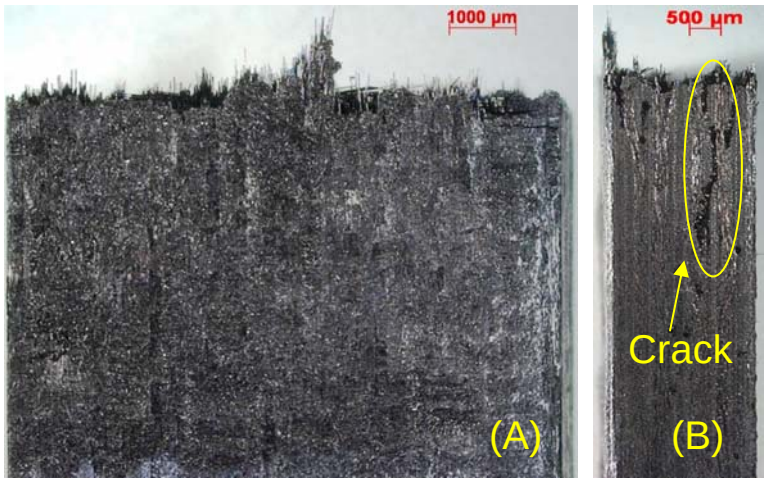


**Figure 53. Optical micrographs of composite C3 specimen aged for 8 hours in steam environment at 815°C and then subjected to a monotonic tension test to failure at 23°C.**

Figure 54 shows optical micrographs of the composite C3 specimen aged in air at 815 $^{o}$C for 8 hours then subjected to a monotonic tension test to failure. The fracture surface is less brushy than the fracture surface of as processed specimen but it is comparable to the fracture surface in Figure 53. Figure 54(A) shows the specimen exhibits slight discoloration and seems to demonstrate areas of "pitting" across the surface. Figure 54(B) shows damage to the material well below the fracture surface. Unlike in figures 52 and 53, the crack in figure 54(B) does not originate at the fracture surface. The reasoning behind this crack formation is not understood.

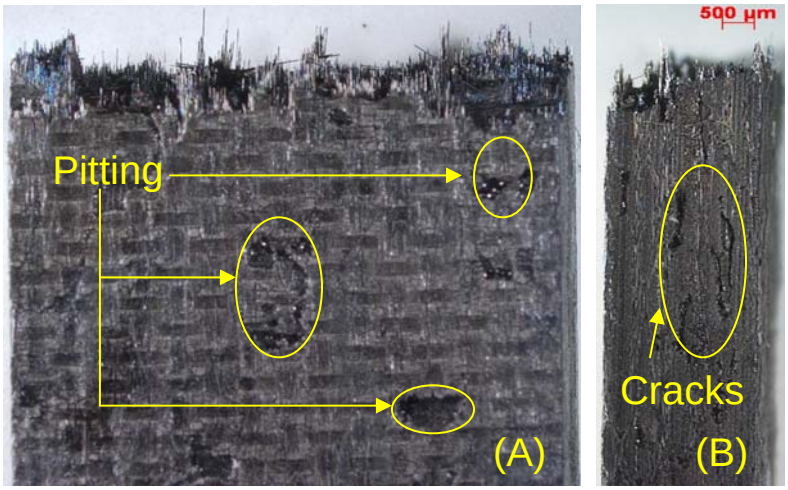


**Figure 54. Optical micrographs of composite C3 specimen aged for 8 hours in air environment at 815°C and then subjected to a monotonic tension test to failure at 23°C.**

Figure 55 shows optical micrographs of the composite C3 specimen pre-fatigued, aged in steam at 815 $^{o}$C for 8 hours, and then subjected to a monotonic tension test to failure. The fracture surface is brushy and similar in appearance to the fracture surfaces of the specimens aged in air and steam without pre-fatiguing. The specimen exhibits less surface flaws than the specimens shown in Figures 53 and 54.

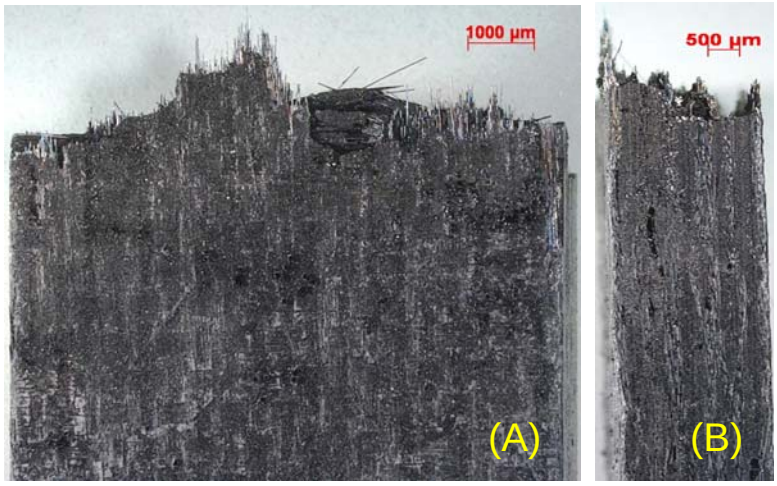


**Figure 55. Optical micrographs of composite C3 specimen pre-fatigued, aged for 8 hours in steam environment at 815°C and then subjected to a monotonic tension test to failure at 23°C.**

Figure 56 shows optical micrographs of the Composite C3 specimen pre-fatigued, aged in air at 815 $^{o}$C for 8 hours, and then subjected to a monotonic tension test to failure. The specimen shows a brushy fracture surface similar to other pre-fatigued and aged specimens. Figure 56(B) shows a crack longer than 2 mm extending from the fracture surface along the side of the specimen.

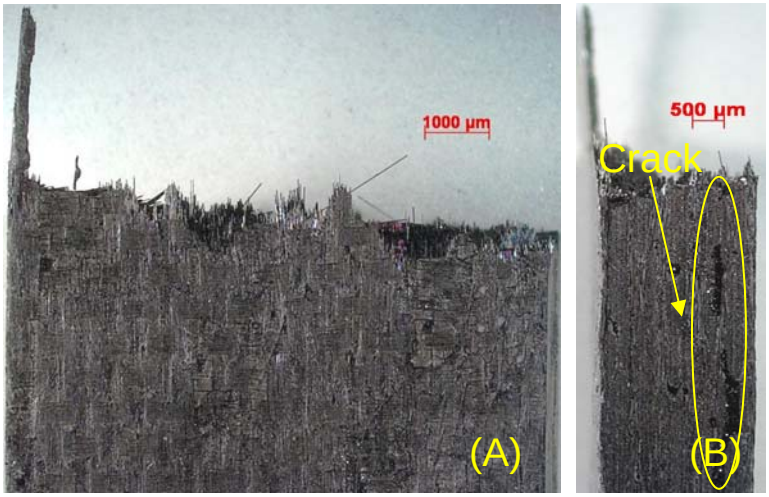


**Figure 56. Optical micrographs of composite C3 specimen pre-fatigued, aged for 8 hours in air environment at 815°C and then subjected to a monotonic tension test to failure at 23°C.**

Figure 57 shows SEM micrographs of a Composite C3 virgin polished specimen. Figure 57(A) shows that the virgin material contains voids in the matrix. Figure 57(B) shows that these voids are prevalent in both the 0$^{o}$ and 90$^{o}$ bundles and that the fibers demonstrate varying diameter size. Figure 57(C) shows a Nicalon™ fiber encased in its fiber coating.

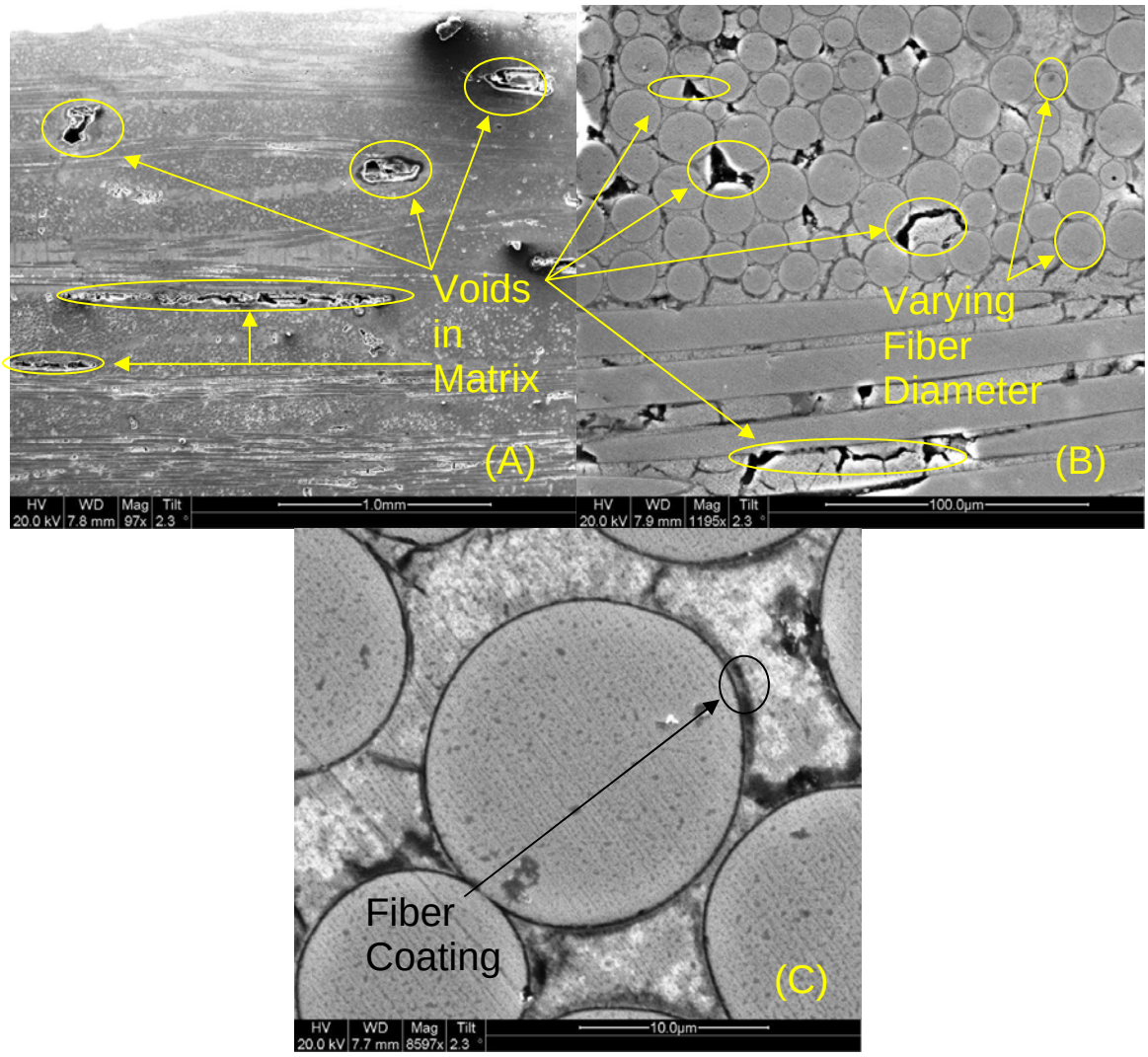


**Figure 57. SEM micrographs of composite C3 polished virgin specimen.**

Figures 58 and 59 show SEM micrographs of the fracture surface and polished material from the composite C3 as-processed specimen. Figure 59(A) shows the fracture surface was very brushy and extensive fiber pull-out occurred in the $0^{o}$ fibers. Additionally the $90^{o}$ fibers exhibit debonding and fan out near their respective failure regions. Figure 58(B) shows that both $0^{o}$ and $90^{o}$ fibers are covered with debris. This may be residue from the fiber coating or matrix. Since the specimen in figure 58 is as

processed, the residue is not due to the effects of oxidation. Figure 58(B) also shows several fibers that have sustained damage. This is a departure from behavior demonstrated by Materials 1 and 2 where fibers on the fracture surface still maintained their shape. Figure 58(C) shows two fibers covered with the aforementioned debris. Figures 59(A), 59(B), 59(C) are very similar to figure 57(A), 57(B), and 57(C) and show no new characteristics.

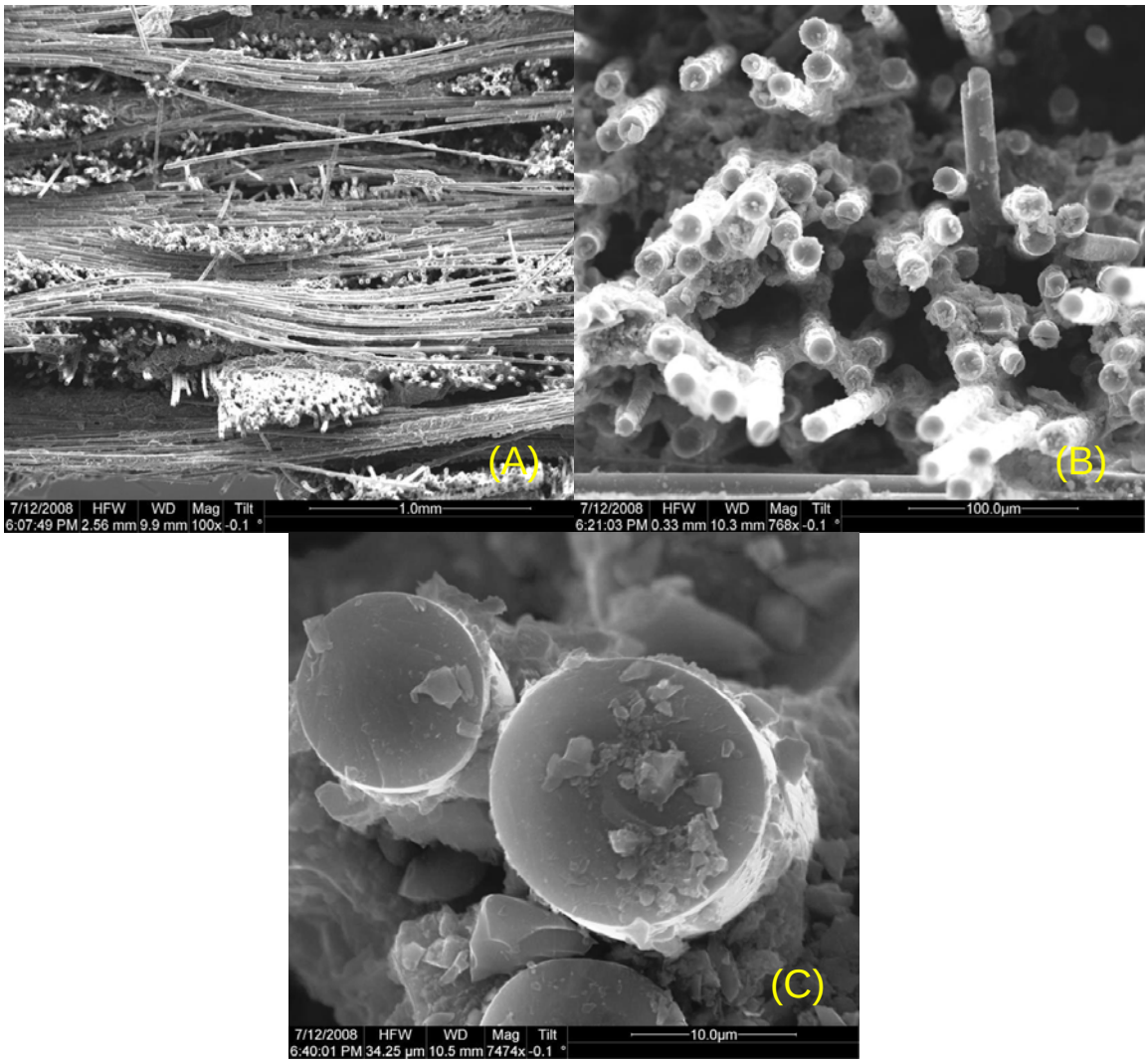


**Figure 58. SEM micrographs of fracture surface of the as processed composite C3 specimen that was subjected to a monotonic tension test to failure. (A) Overall fracture surface, (B) 0° fibers, (C) 0° fiber at higher magnification.**

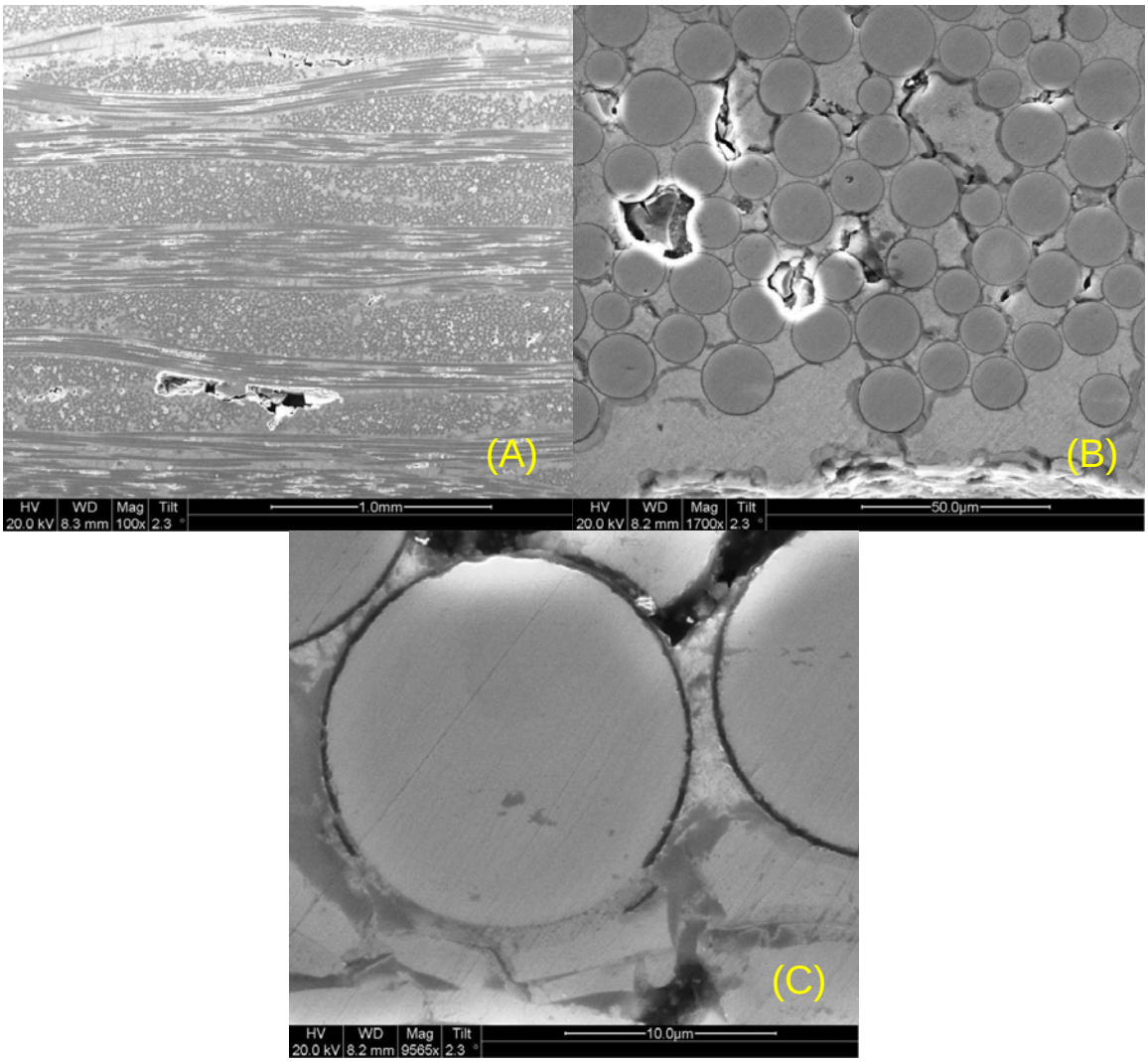


**Figure 59. SEM micrographs of polished as processed composite C3 specimen that was subjected to a monotonic tension test to failure. (A) Overall view, (B) 0° fibers, (C) 0° fibers at higher magnification.**

Figure 60 and 61 show SEM micrographs of the fracture surface and polished material of the composite C3 specimen aged in steam at 815 $^{o}$C for 8 hours and then subjected to a monotonic tension test to failure. The fracture surface exhibits fiber pull-out, however, the fiber surface is less brushy than the fiber surface of the as processed specimen. This behavior was also seen in the optical micrographs of composite C3 specimens. Figure 60(C) shows three 0$^{o}$ fibers. The exterior of the fibers are void of any matrix or interphase materials, however, matrix material is still seen in the region between the fibers.. The angle of the fibers makes it difficult to determine whether this material is the matrix, fiber interphase, or both.

Figure 62(A) shows that the polished surface seems similar to the polished virgin material. Voids in the matrix are visible in both the 0$^{o}$ and 90$^{o}$ fiber tows. Figure 62(B) shows regions of matrix oxidation. These oxidation regions show a maximum penetration distance of approximately 50 μm. Figure 62(C) shows a fiber along the upper edge of the specimen covered in a glassy residue. The surrounding matrix and interphase show signs of oxidation.

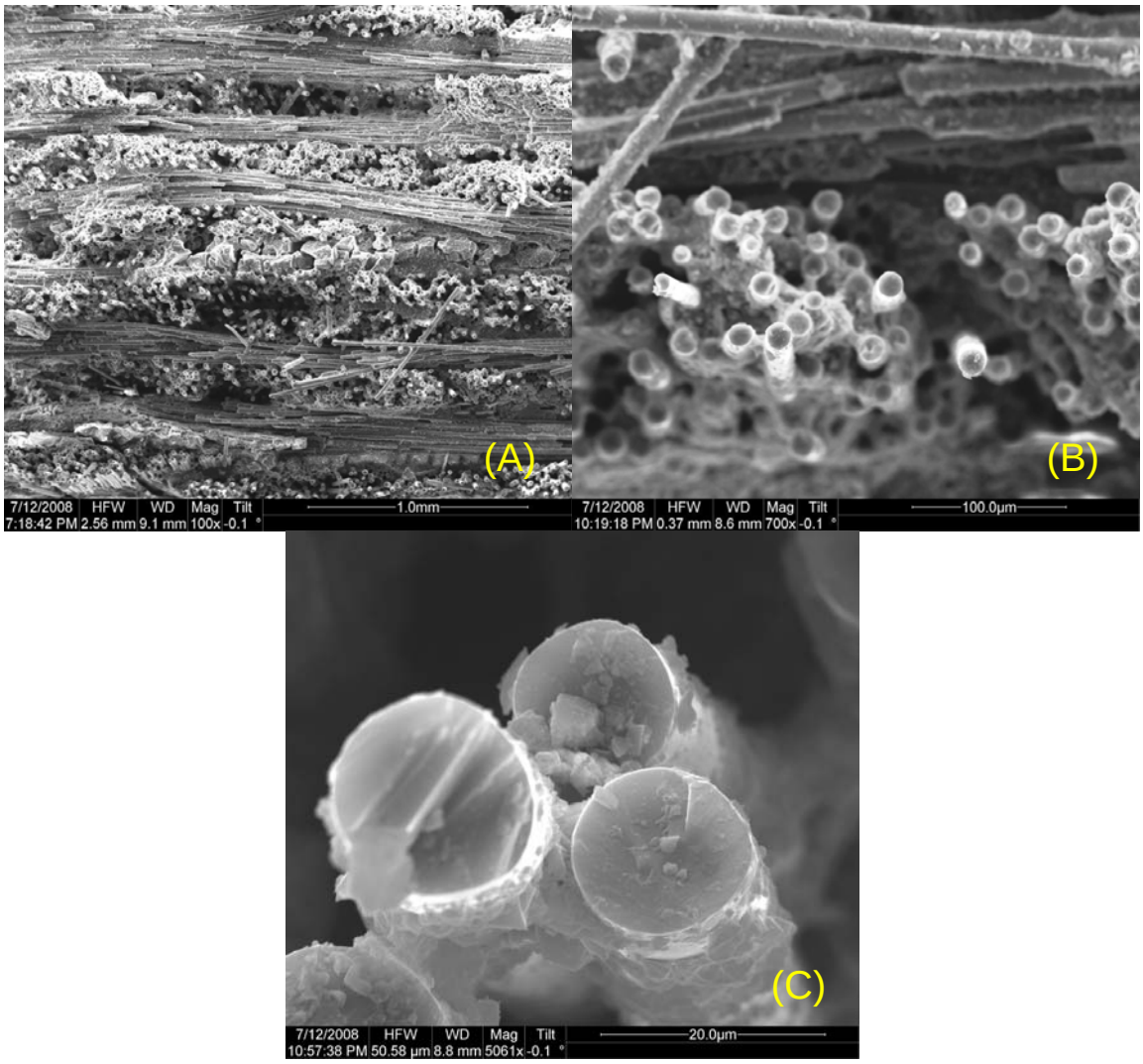


**Figure 60. SEM micrographs of fracture surface of composite C3 specimen that was aged in a steam environment at 815 °C for 8 hours, and then subjected to a monotonic tension test to failure. (A) Overall fracture surface, (B) 0° fibers, (C) 0° fiber at higher magnification.**

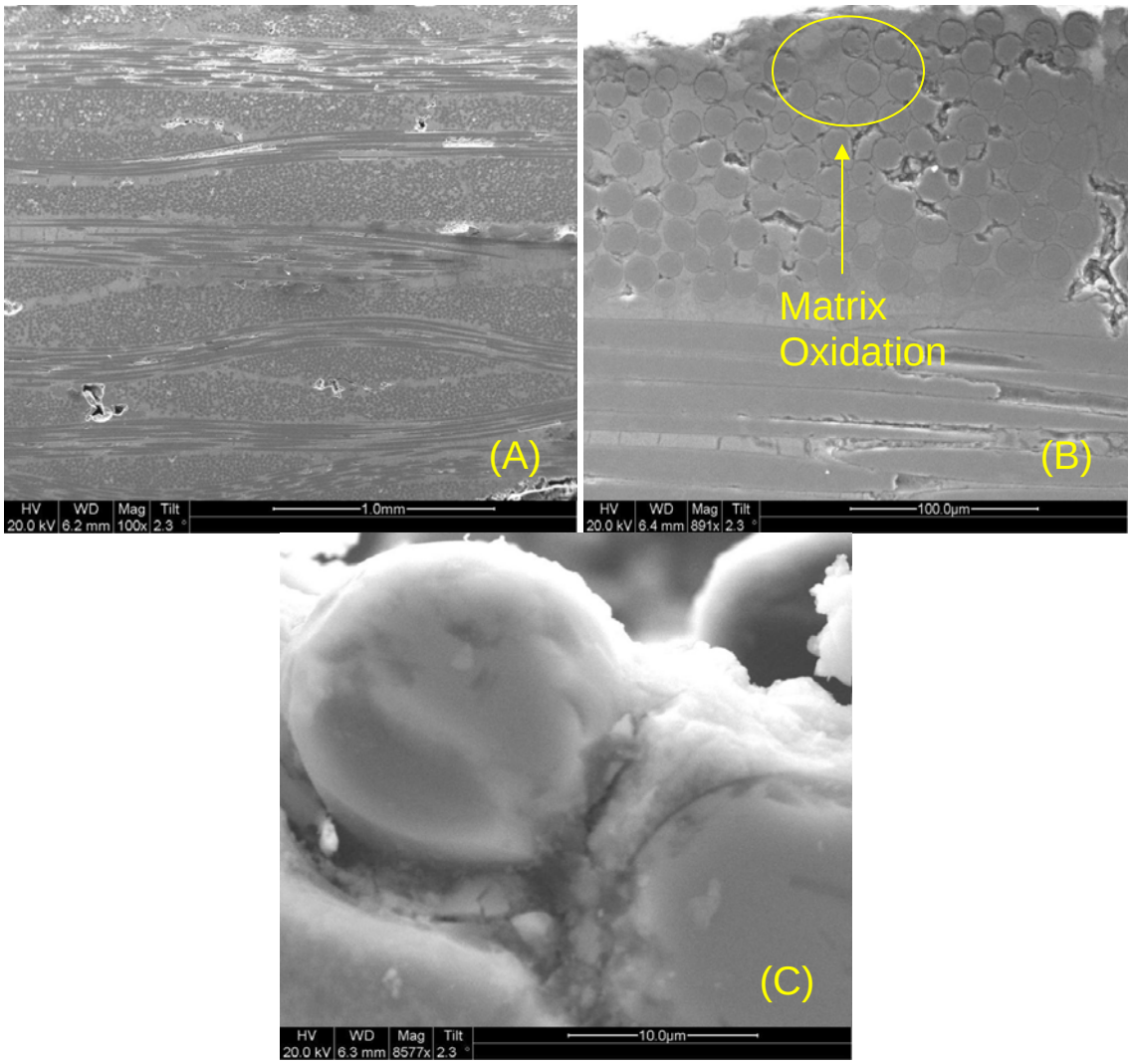


**Figure 61. SEM micrographs of polished composite C3 specimen that was, aged in a steam environment at 815 $^{o}$C for 8 hours, and then subjected to a monotonic tension test to failure. (A) Overall view, (B) 0° fibers, (C) 0° fibers at higher magnification.**

Figures 62 and 63 show SEM micrographs of the fracture surface and polished material from the composite C3 specimen aged in air at 815°C for 8 hours and then subjected to a monotonic tension test to failure. Once again the fracture surface is less brushy than the fracture surface of the as processed specimen. Figure 62(A) shows a $0^o$ fiber bundle protruding from the fracture surface. This is in stark contrast to the as processed specimen where individual fibers demonstrated pull out. Figure 62(B) displays several $0^o$ fibers. Figure 62(C) shows a severely damaged $0^o$ fiber. The cause of this damage is unknown.

Figure 63(A) is indicative of the entire polished surface. Figure 63(B) shows no visible signs of matrix oxidation which indicates superior performance as compared to the specimen aged in steam. Figure 63(C) shows $0^o$ fibers demonstrating no visual sign of matrix or interphase oxidation.

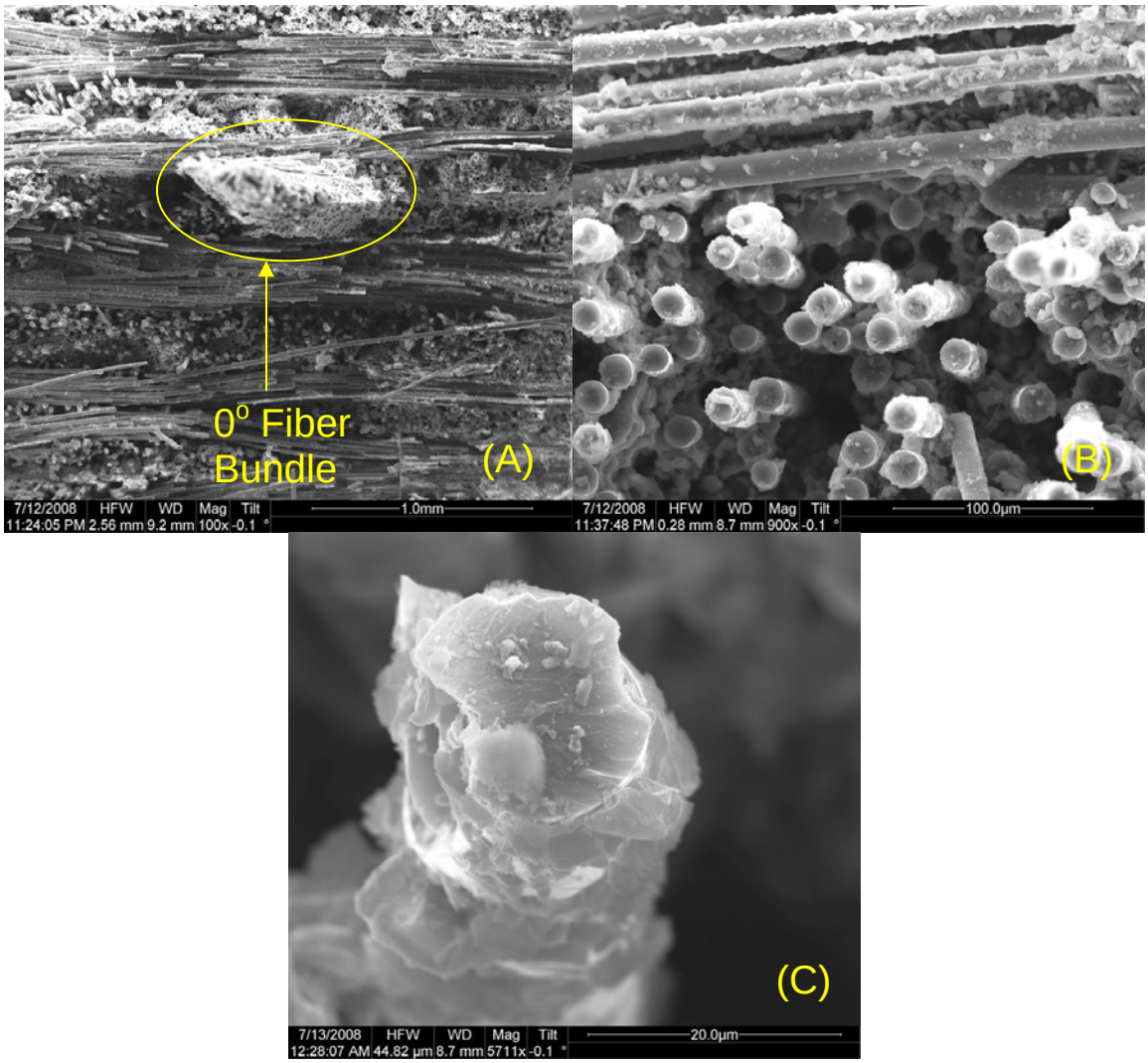


**Figure 62. SEM micrographs of fracture surface of composite C3 specimen that was aged in air at 815 °C for 8 hours, and then subjected to a monotonic tension test to failure. (A) Overall fracture surface, (B) 0° fibers, (C) 0° fiber at higher magnification.**

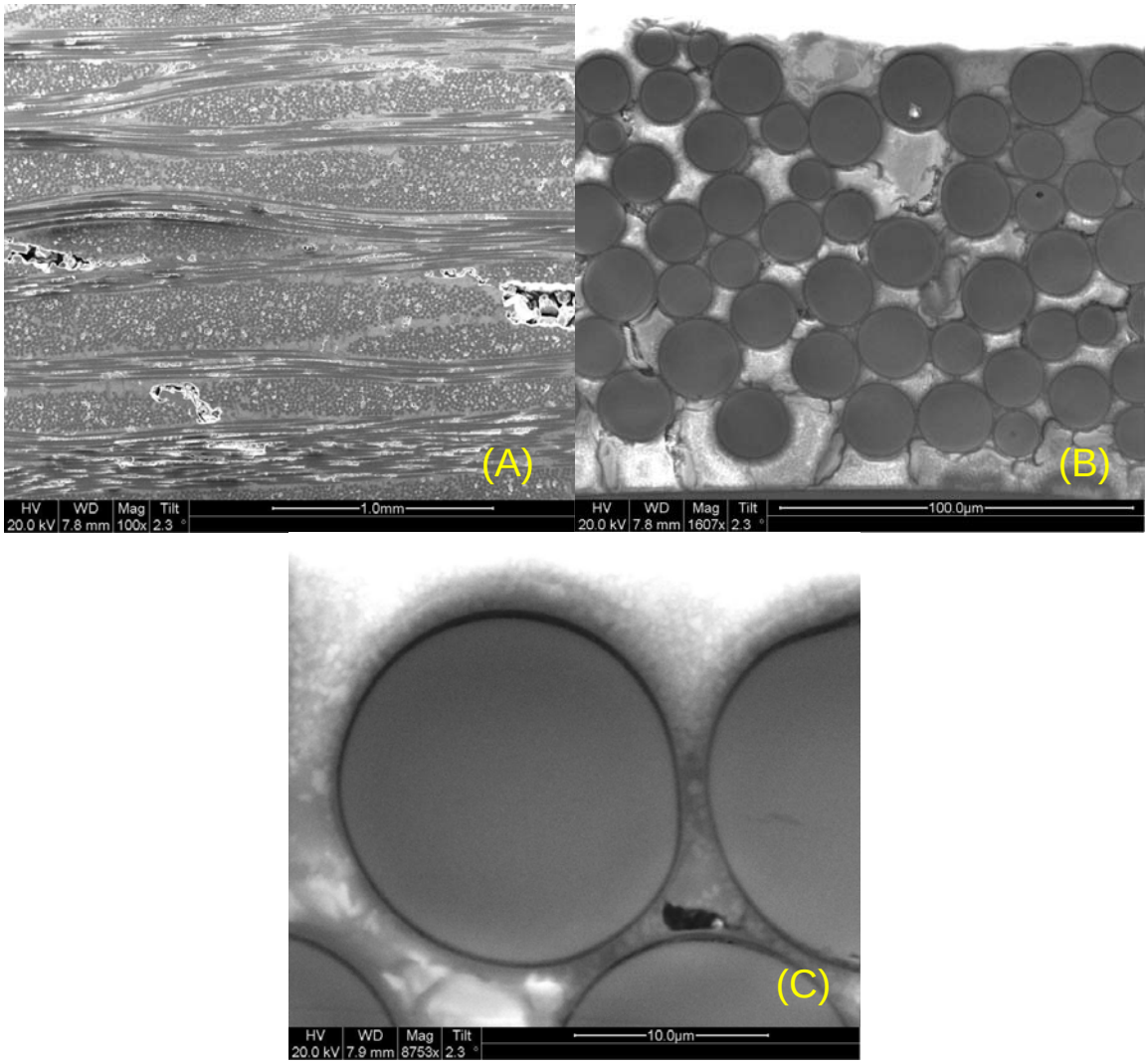


**Figure 63. SEM micrographs of polished composite C3 specimen that was aged in air at 815 $^{o}$C for 8 hours, and then subjected to a monotonic tension test to failure. (A) Overall view, (B) 0° fibers, (C) 0° fibers at higher magnification.**

Figure 64 and 65 show SEM micrographs of the fracture surface and polished material from the Composite C3 specimen pre-fatigued, aged in steam at 815 $^{o}$C for 8 hours, and then subjected to a monotonic tensile test to failure. Figure 65(A) shows the general characteristics of the fracture surface which looks similar to the fracture surfaces in Figures 60(A) and 62(A). Figure 64(B) shows a 0$^{o}$ fiber bundle where a few fibers exhibit damage mechanisms. Figure 64(C) shows two damaged 0$^{o}$ fibers. The cause of this damage is not fully understood.

Figure 65(A) shows the general characteristics of the polished surface which shows increased cracking in the 90$^{o}$ fiber bundles. Figure 65(B) shows that there is little visual evidence of oxidation. The pre-fatigued specimen aged is steam shows more cracking and voids in the matrix than the specimen aged in steam but not subjected to pre-fatiguing. The fact that the specimen shows more cracking and matrix degradation, yet shows less signs of oxidation may be explained by the fact that the specimen failed outside of the thermal gage section. Although the specimen conducts heat, the temperature will decrease significantly as the distance from the thermal gage section increases. This specimen failed right above the bottom grip where the temperature was most likely not high enough to oxidize the material. Figure 65(C) shows a 0$^{o}$ fiber showing no sign of matrix or interphase oxidation.

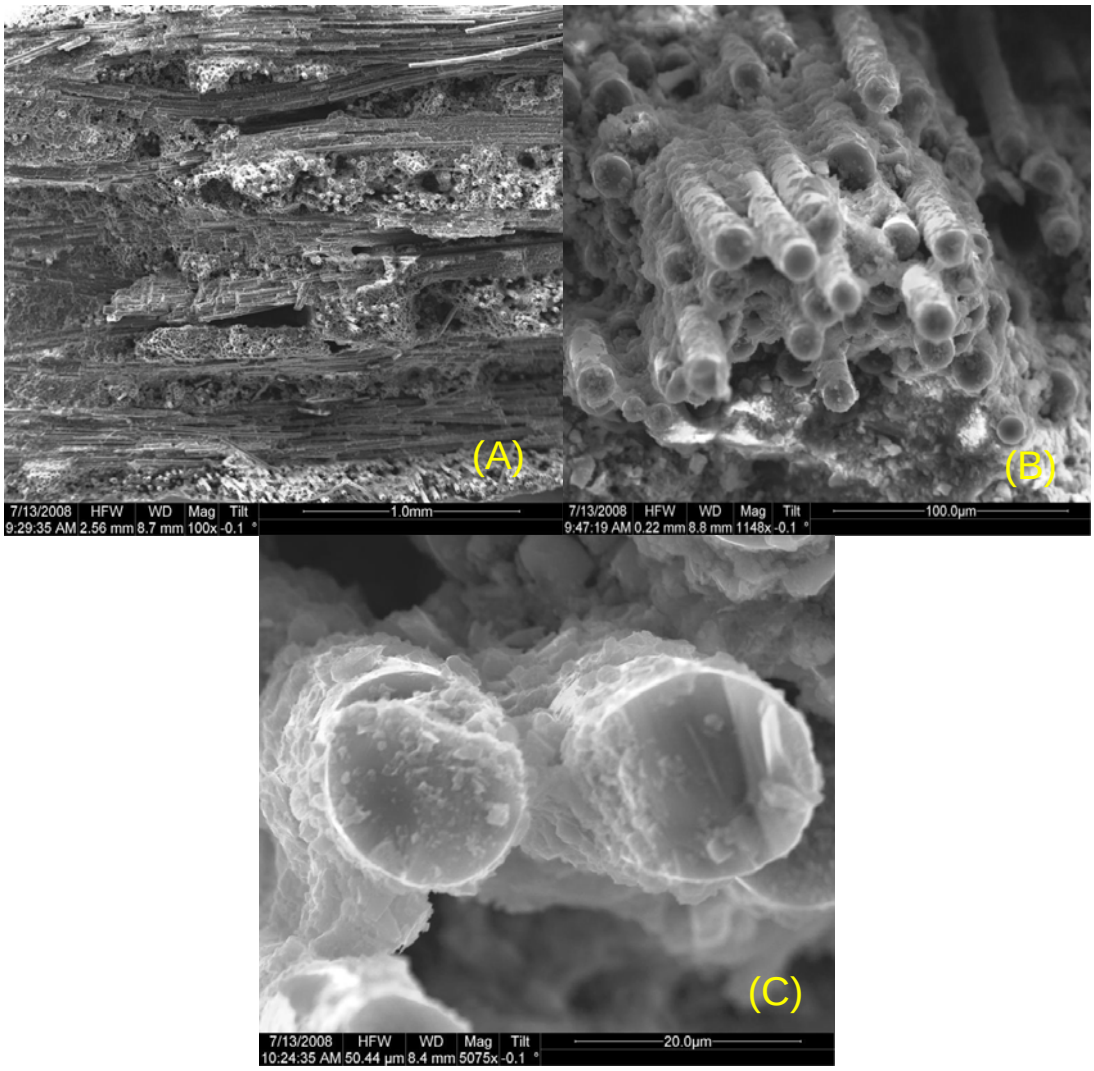


**Figure 64. SEM micrographs of fracture surface of composite C3 specimen that was pre-fatigued, aged in a steam environment at 815 °C for 8 hours, and then subjected to a monotonic tension test to failure. (A) Overall fracture surface, (B) 0° fibers, (C) 0° fiber at higher magnification.**

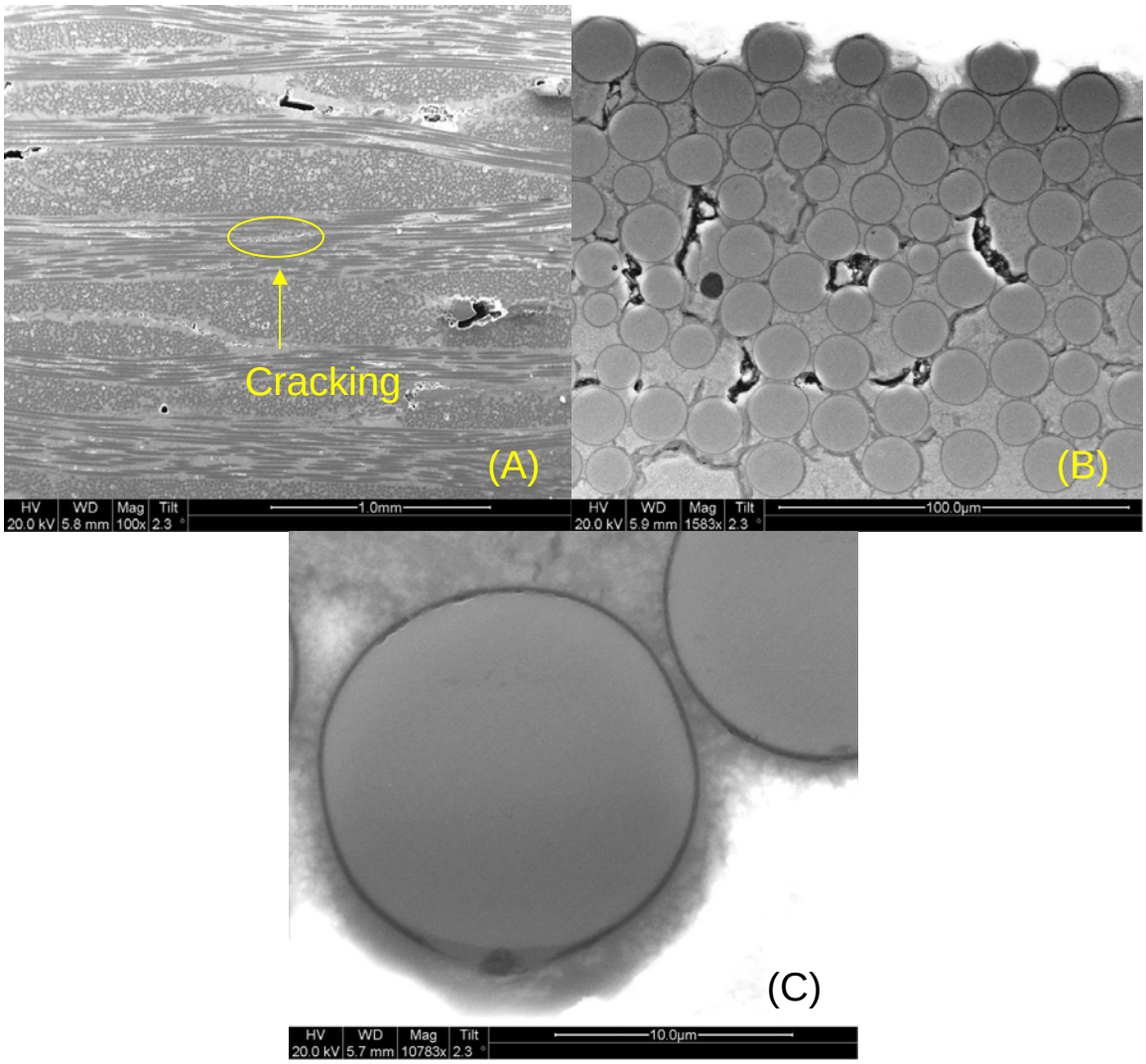


**Figure 65. SEM micrographs of polished Composite C3 specimen that was pre-fatigued, aged in a steam environment at 815 °C for 8 hours, and then subjected to a monotonic tension test to failure. (A) Overall view, (B) 0° fibers, (C) 0° fibers at higher magnification.**

Figures 66 and 67 show SEM micrographs of the fracture surface and polished material from the Composite C3 specimen prefatigued, aged in air at 815$^{o}$ C for 8 hours, and then subjected to a monotonic tension test to failure. The fracture surface as seen in Figure 66(A) shows less fiber pullout than the fracture surface of the as processed specimen. Figure 66(B) shows failure in both 0$^{o}$ and 90$^{o}$ fiber bundles. Figure 66(C) shows a severely damaged 0$^{o}$ fiber similar to the one seen in figure 64(C).

Figure 67(A) shows the presence of cracking in the 90$^{o}$ fiber bundles. Just as in Figure 66(B), Figure 68(B) shows no evidence of matrix or fiber oxidation. Figure 66(C) shows a 0$^{o}$ fiber showing no sign of interphase degradation.

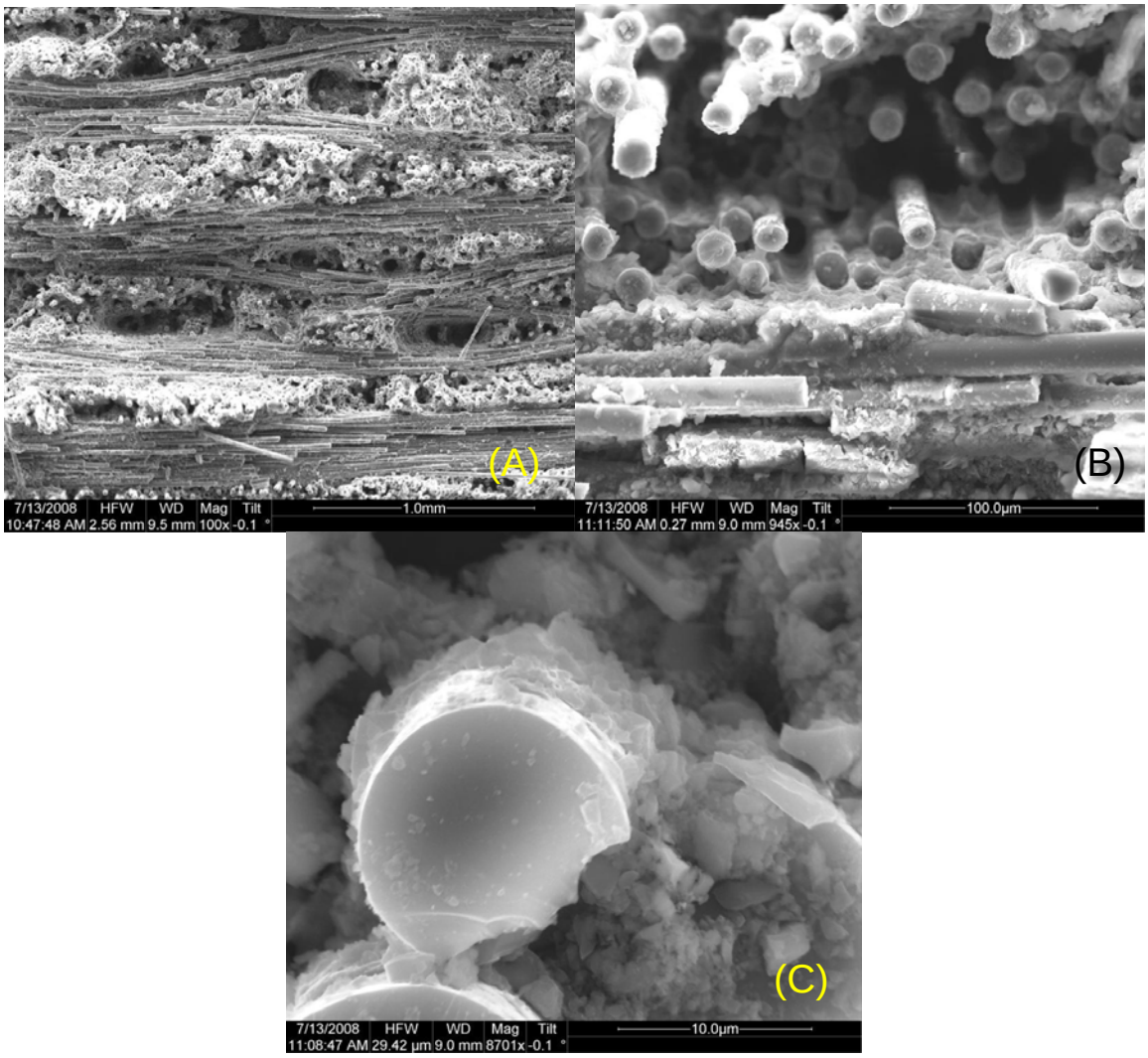


**Figure 66. SEM micrographs of fracture surface of composite C3 specimen that was pre-fatigued, aged in air at 815 °C for 8 hours, and then subjected to a monotonic tension test to failure. (A) Overall fracture surface, (B) 0° fibers, (C) 0° fiber at higher magnification.**

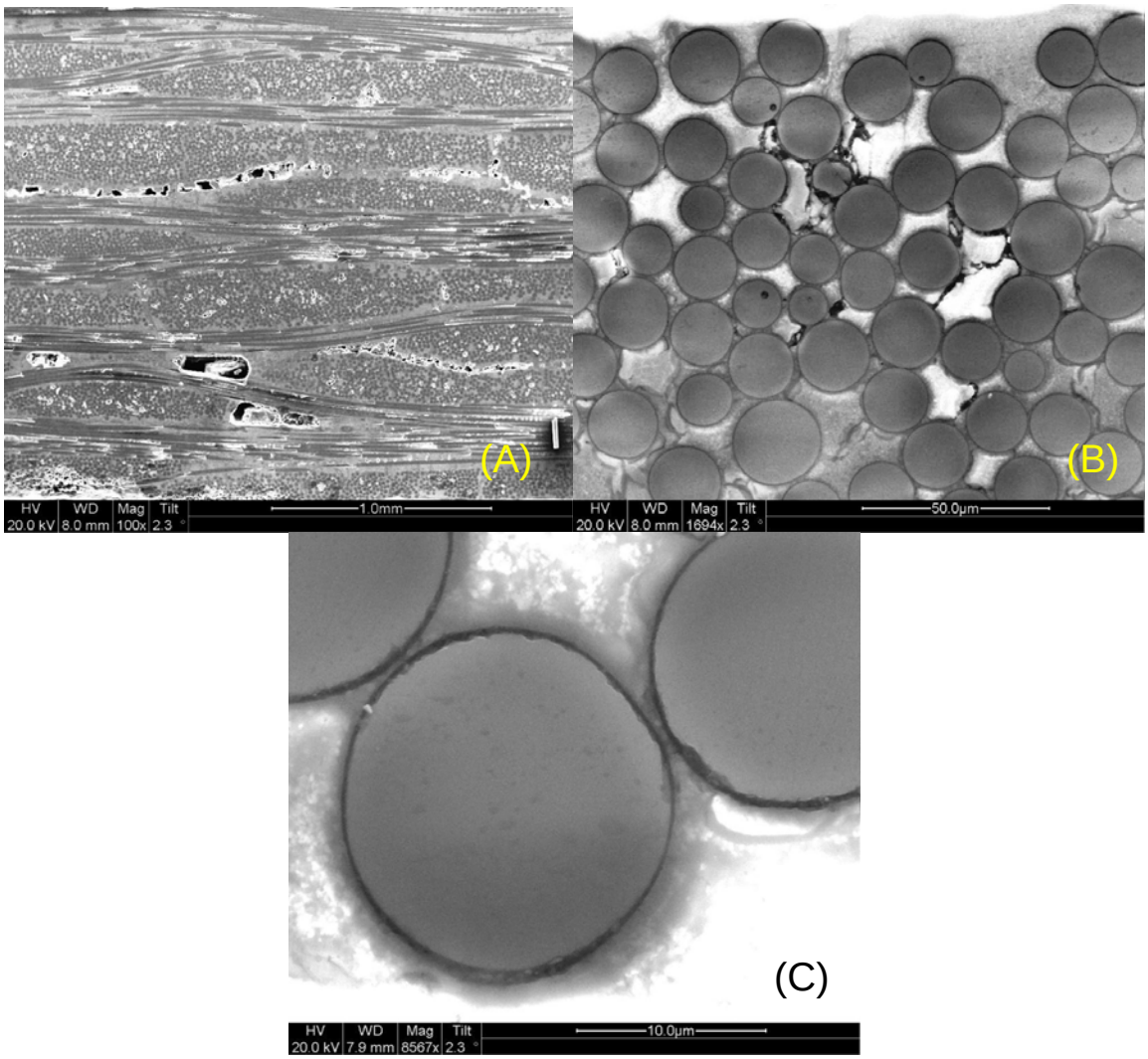


**Figure 67. SEM micrographs of polished composite C3 specimen that was pre-fatigued, aged in air at 815 $^{o}$C for 8 hours, and then subjected to a monotonic tension test to failure. (A) Overall view, (B) 0° fibers, (C) 0° fibers at higher magnification.**

# V. Conclusions and Recommendations

## 5.1 Conclusions

The two SiC/SiC CMC systems reinforced with Sylramic™ fibers demonstrate excellent fatigue resistance in both air and steam environments at 1300 °C. Fatigue life of both CMCs decreased as fatigue stress increased. The presence of steam degraded the fatigue resistance of both materials. In air, the fatigue limit for composite C1 was 100 MPa (54% UTS) and the fatigue limit for composite C2 was 160 MPa (66% UTS). In steam, the fatigue limit of composite C1 was 100 MPa (54% UTS) and the fatigue limit of composite C2 was reduced to 140 MPa (58% UTS).

Both Composites C1 and C2 demonstrated minimal strain ratcheting, but a decrease in stiffness with fatigue cycles was observed. While both composites C1 and C2 demonstrated excellent fatigue resistance at high temperature, fatigue performance of composite C2 was superior to that of composite C1. Composite C2 also produced a higher value of UTS than composite C1. Furthermore, in steam fatigue limit of composite C2 was some 40% higher than that of composite C1. Microstructural characterization of composites C1 and C2 revealed that nearly planar fracture surfaces were produced in all tests. Microstructural investigation also suggests that oxidation of these materials depends on time spent in an oxidizing environment under mechanical loading.

Tensile properties of composite C3 were significantly affected by prior aging for 8 h at 815 ° in air and in steam environments. Prior aging in air caused a 22% reduction in UTS and a 0.29% reduction in stiffness. Prior aging in steam resulted in a 42% loss in strength and a 3.46% loss in stiffness. Subjecting C3 specimens to 10 tension-tension fatigue cycles with the fatigue stress of 125 MPa followed by aging for 8 h at 815 ° in air and in steam resulted in further reductions in strength and stiffness of composite C3. For the pre-fatigued specimens aged in air the reduction in strength was 28%. In the case of the pre-fatigued specimens aged in steam, the strength loss was 43%. Pre fatigued specimens aged in both steam and air did not demonstrate a reduction in stiffness.

Microstructural characterization of composite C3 revealed that as-processed specimens produced brushy fracture surfaces with extensive fiber pull-out. Conversely, specimens subjected to prior aging produced fracture surfaces that were predominantly planar with isolated areas of fibrous failure. The aging environment or prior fatigue did not appear to significantly alter the appearance of the fracture surface.

## 5.2 Recommendations for future research

In order to get more reliable UTS values for composites C1 and C2, additional tensile tests should be carried out for each respective material. Moreover tests for Material 3 should be repeated using the dog-bone shaped specimens similar to those in ASTM Standard D 3552.

# Appendix

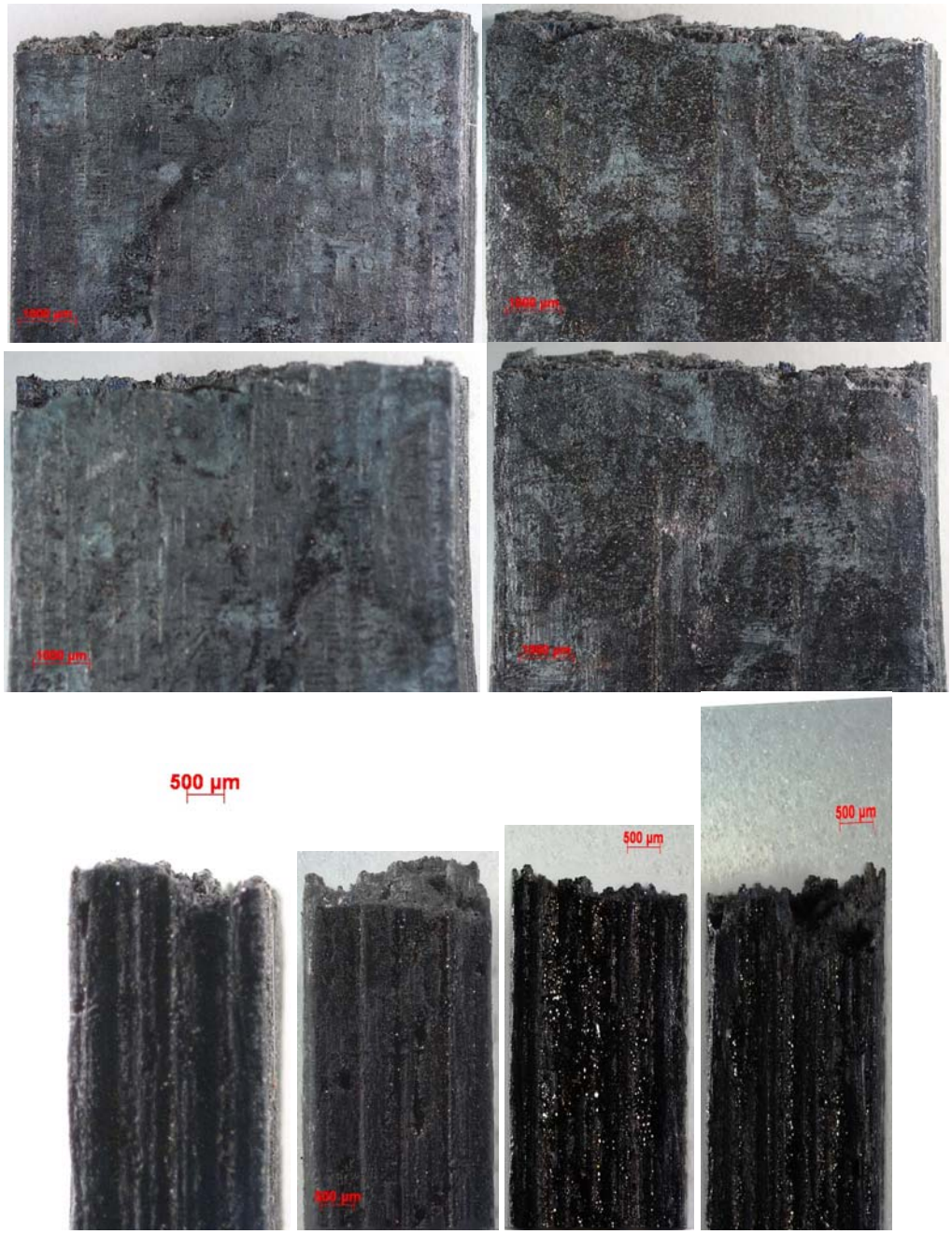


**Figure 68. Fracture Surface optical micrographs of as processed composite C1 specimen.**


**Figure 69. Fracture surface optical micrographs of composite C1 specimen fatigued in air at 1300 °C with maximum fatigue stress $\sigma_{max}$ = 100 MPa**

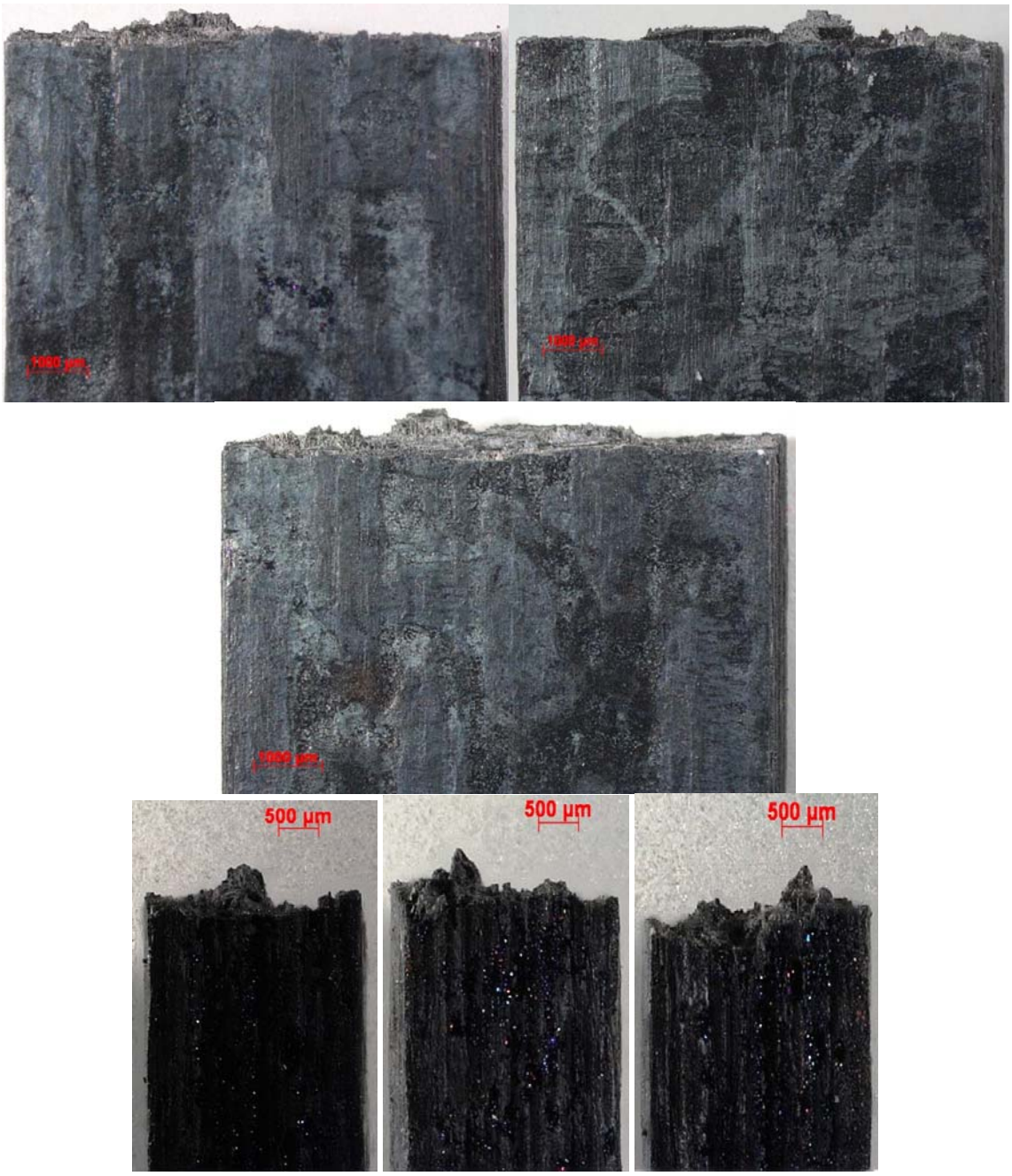


**Figure 70. Fracture surface optical micrographs of composite C1 specimen fatigued in air at 1300 °C with maximum fatigue stress $\sigma_{max}$ = 120 MPa**

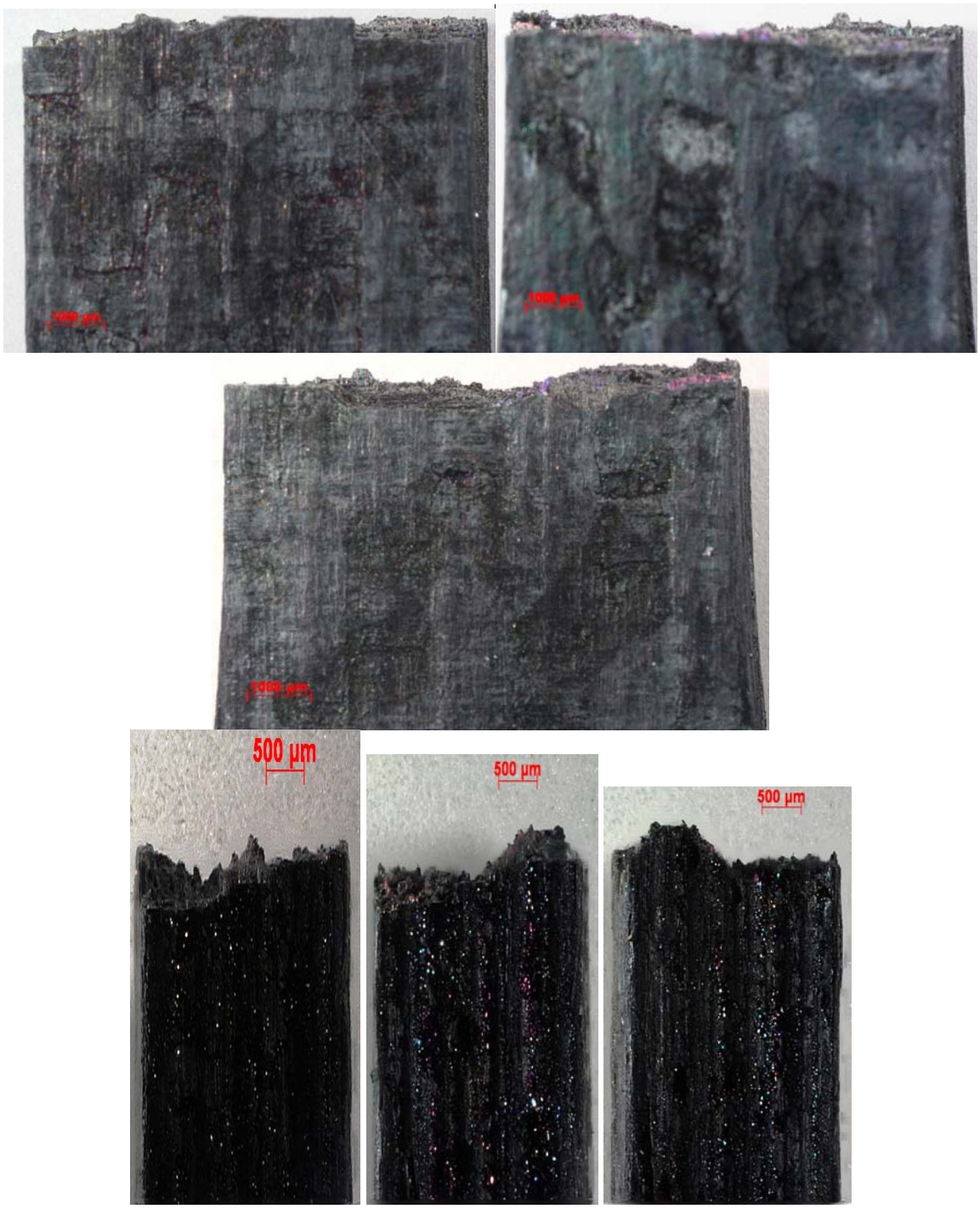


**Figure 71. Fracture surface optical micrographs of composite C1 specimen fatigued in air at 1300 °C with maximum fatigue stress $\sigma_{max}$ = 140 MPa**

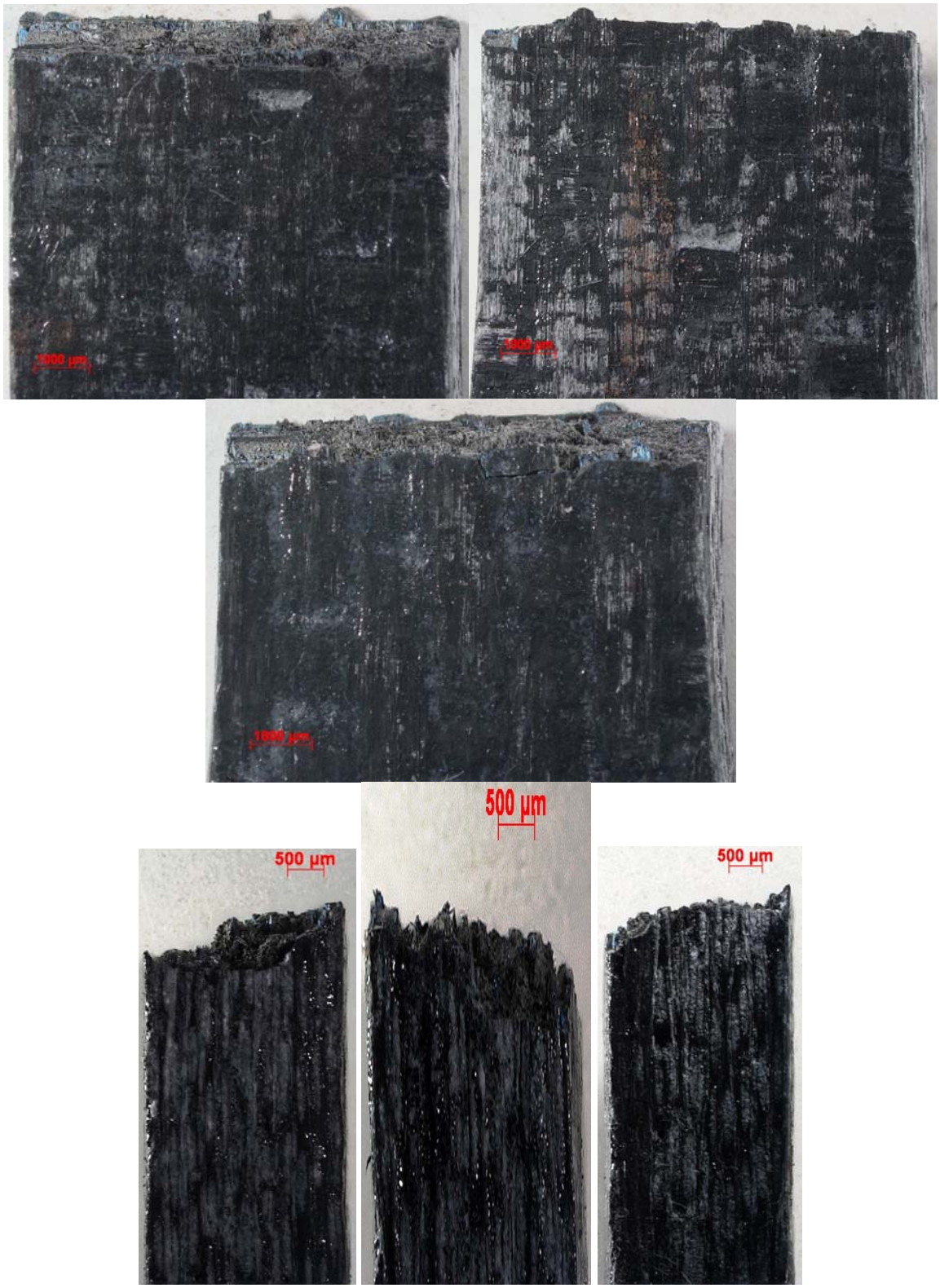


**Figure 72. Fracture surface optical micrographs of composite C1 specimen fatigued in steam at 1300 °C with maximum fatigue stress $\sigma_{max}$ = 100 MPa**


**Figure 73. Fracture surface optical micrographs of composite C1 specimen fatigued in steam at 1300 °C with maximum fatigue stress $\sigma_{max}$ = 120 MPa**

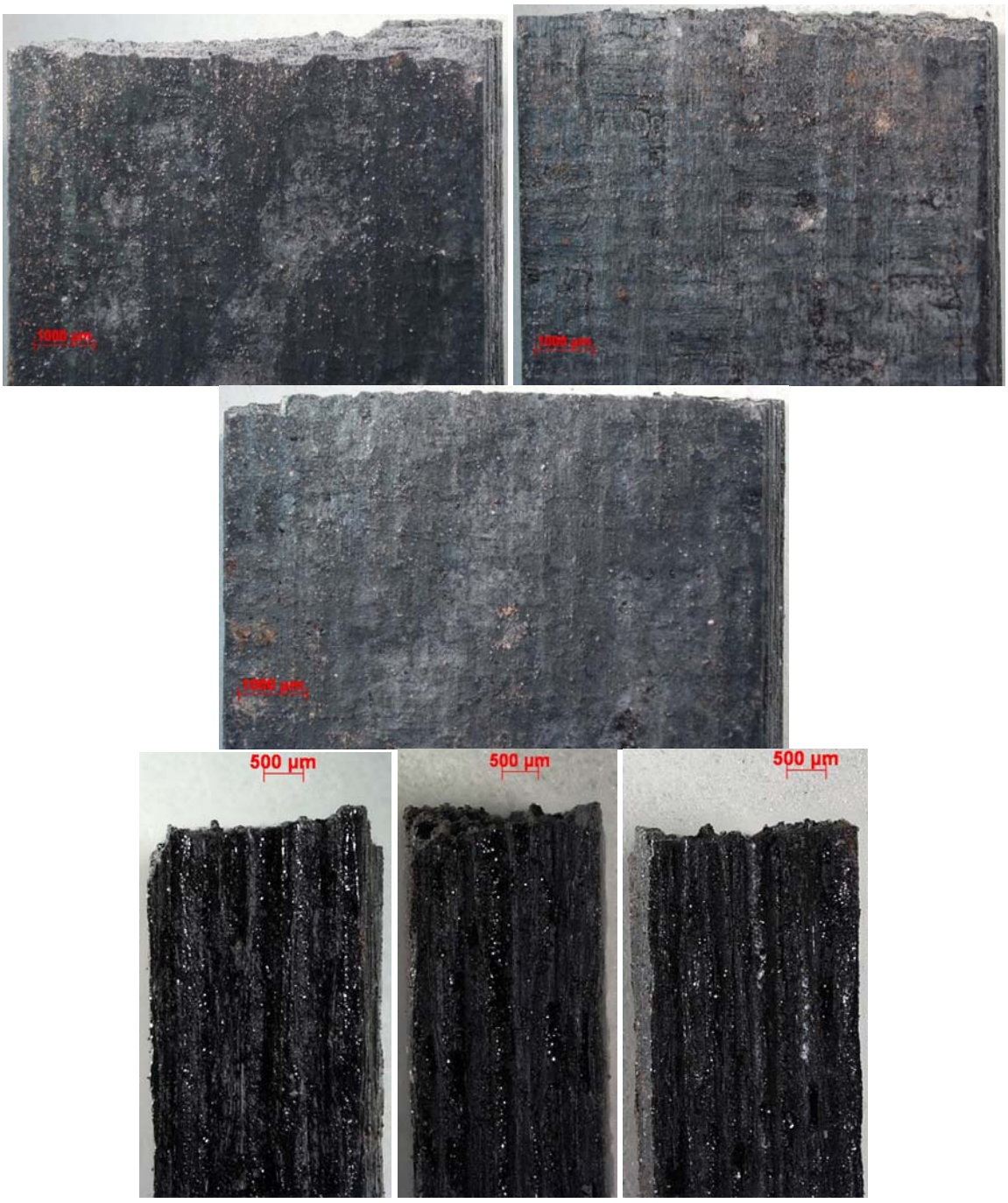


**Figure 74. Fracture surface optical micrographs of composite C1 specimen fatigued in steam at 1300 °C with maximum fatigue stress $\sigma_{max}$ = 140 MPa**

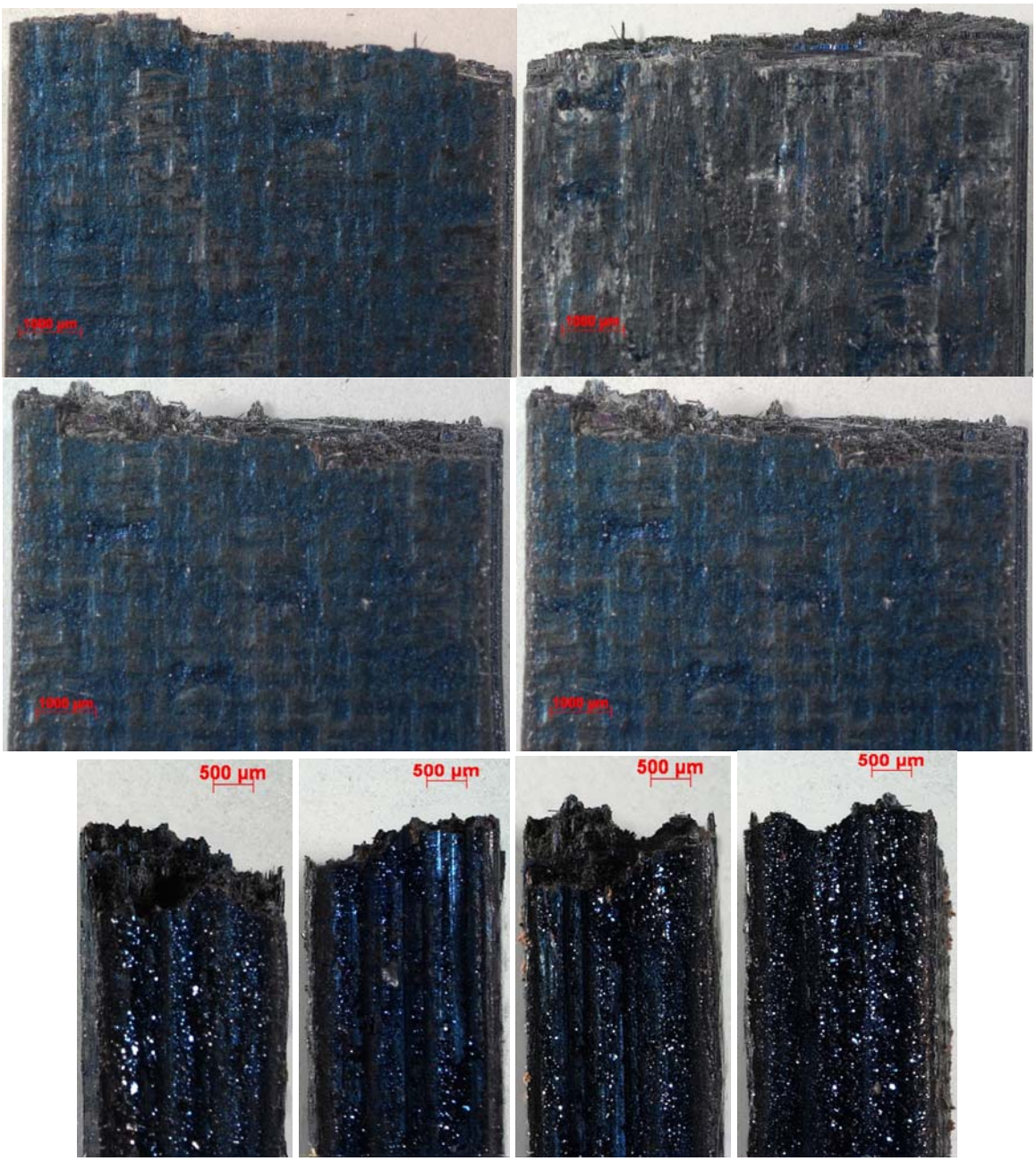


**Figure 75. Fracture Surface optical micrographs of as processed composite C2 specimen.**


**Figure 76. Fracture surface optical micrographs of composite C2 specimen fatigued in air at 1300 °C with maximum fatigue stress $\sigma_{max}$ = 140 MPa**

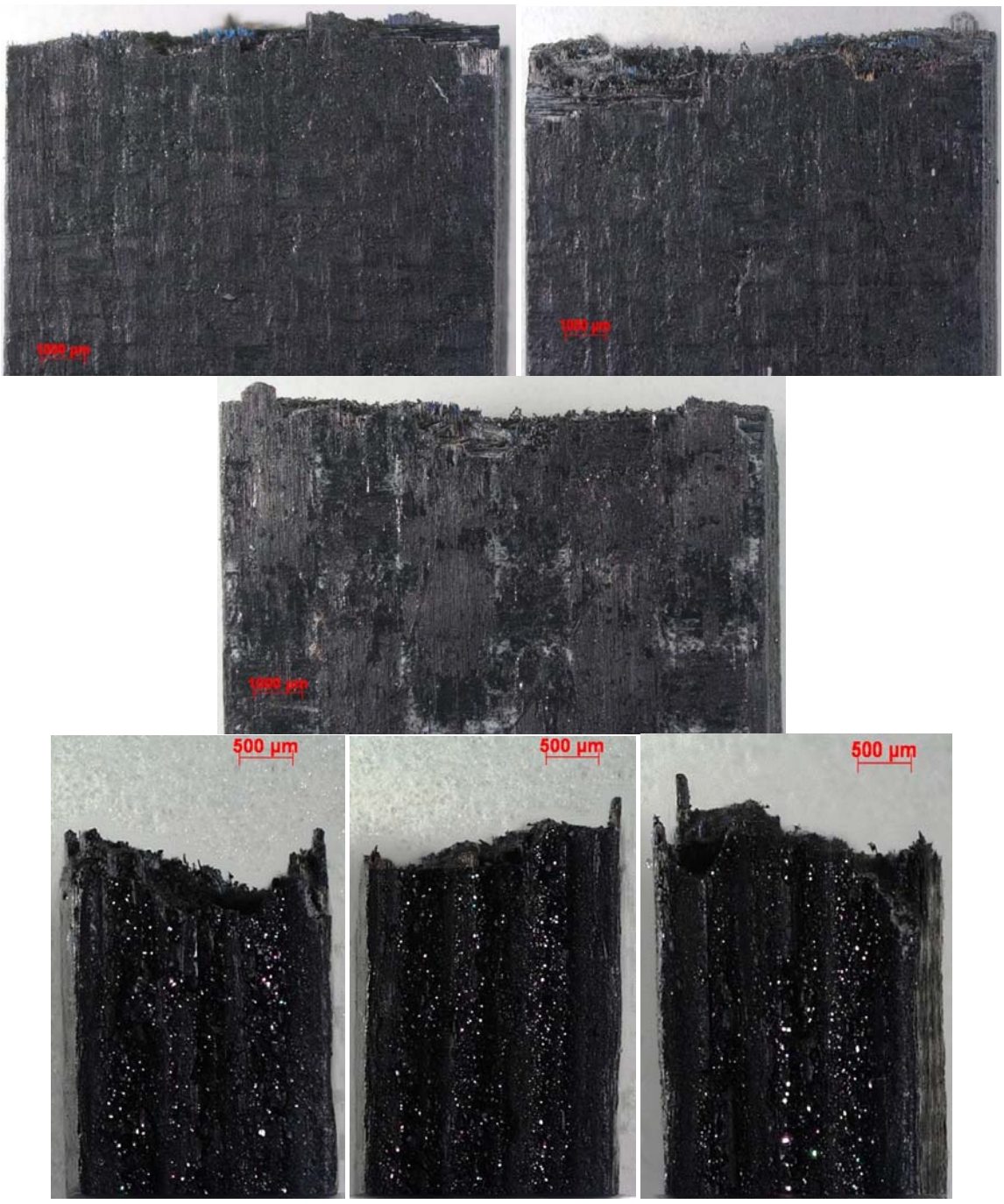


**Figure 77. Fracture surface optical micrographs of composite C2 specimen fatigued in air at 1300 °C with maximum fatigue stress $\sigma_{max}$ = 160 MPa**

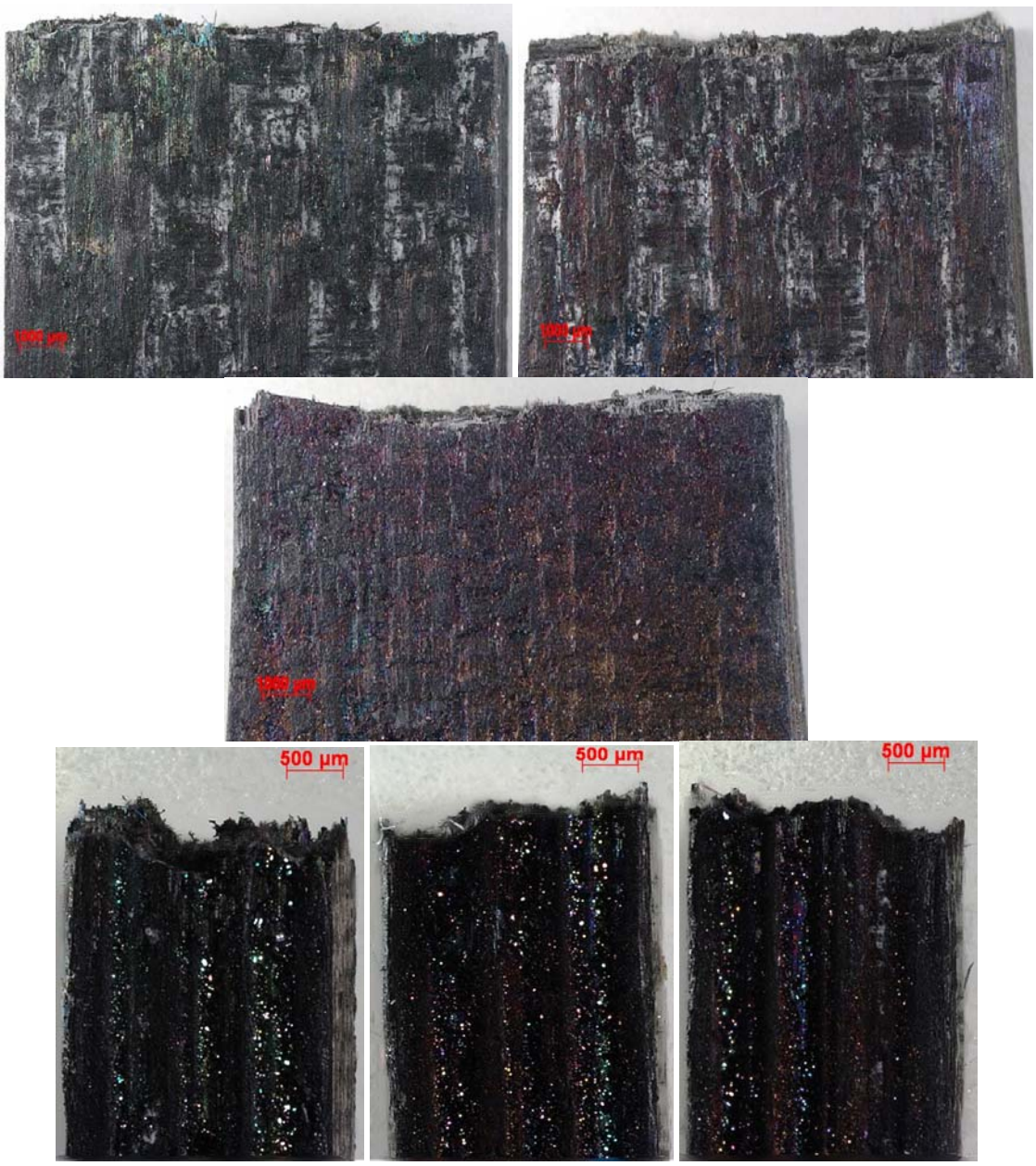


**Figure 78. Fracture surface optical micrographs of composite C2 specimen fatigued in air at 1300 °C with maximum fatigue stress $\sigma_{max}$ = 180 MPa**


**Figure 79. Fracture surface optical micrographs of composite C2 specimen fatigued in steam at 1300 °C with maximum fatigue stress $\sigma_{max}$ = 140 MPa**

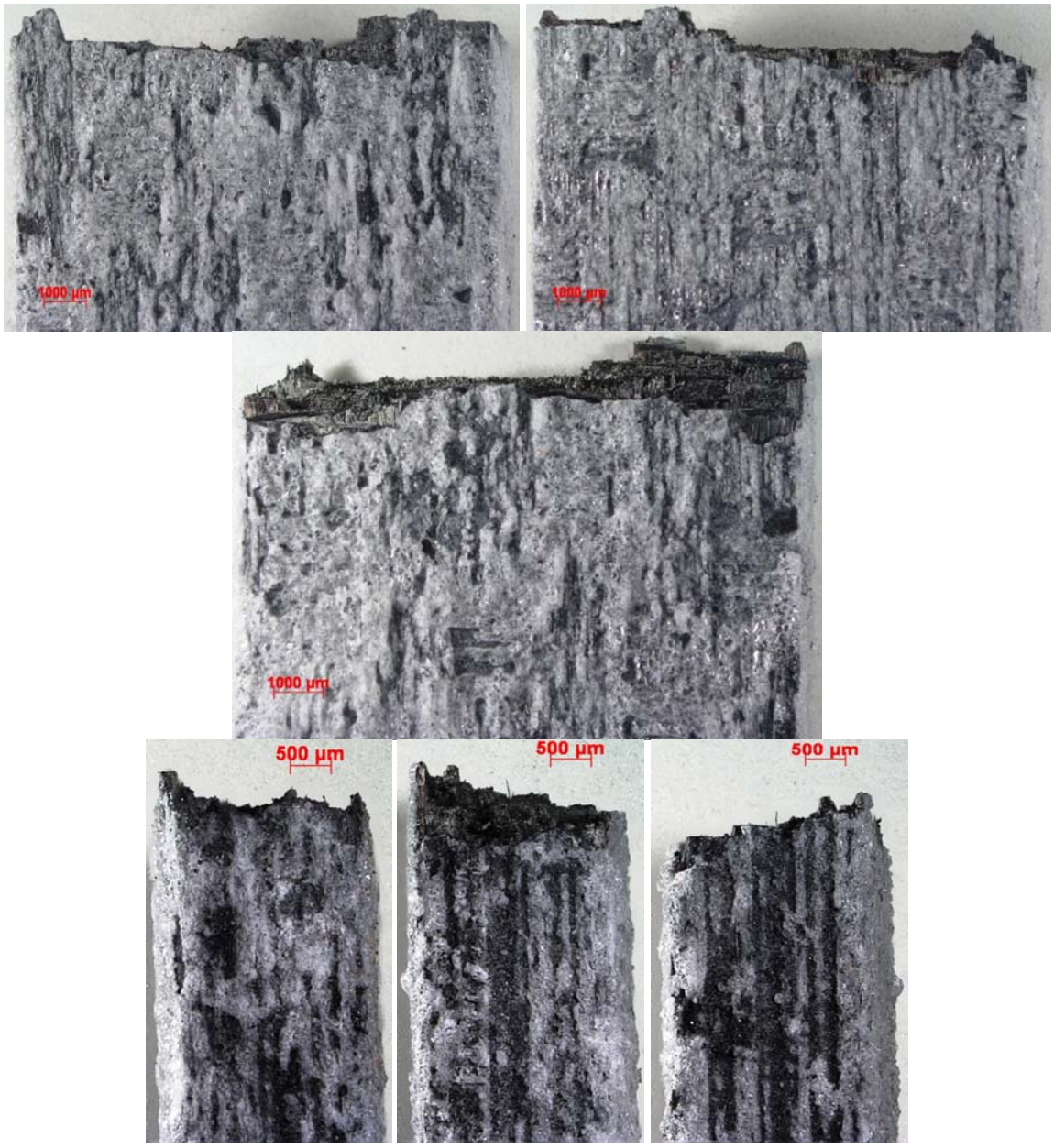


**Figure 80. Fracture surface optical micrographs of composite C2 specimen fatigued in steam at 1300 °C with maximum fatigue stress $\sigma_{max}$ = 160 MPa**

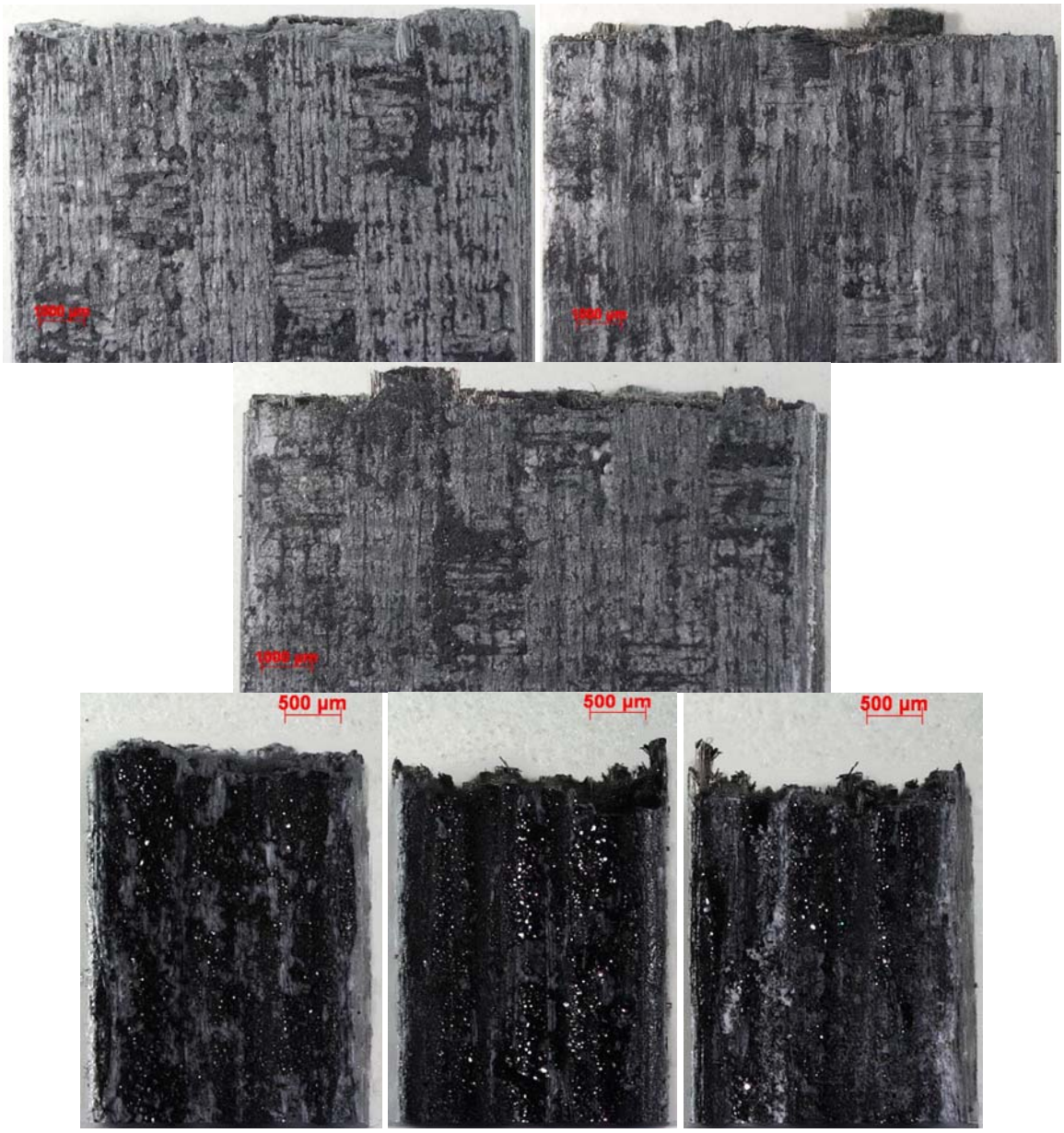


**Figure 81. Fracture surface optical micrographs of composite C2 specimen fatigued in steam at 1300 °C with maximum fatigue stress $\sigma_{max}$ = 180 MPa**

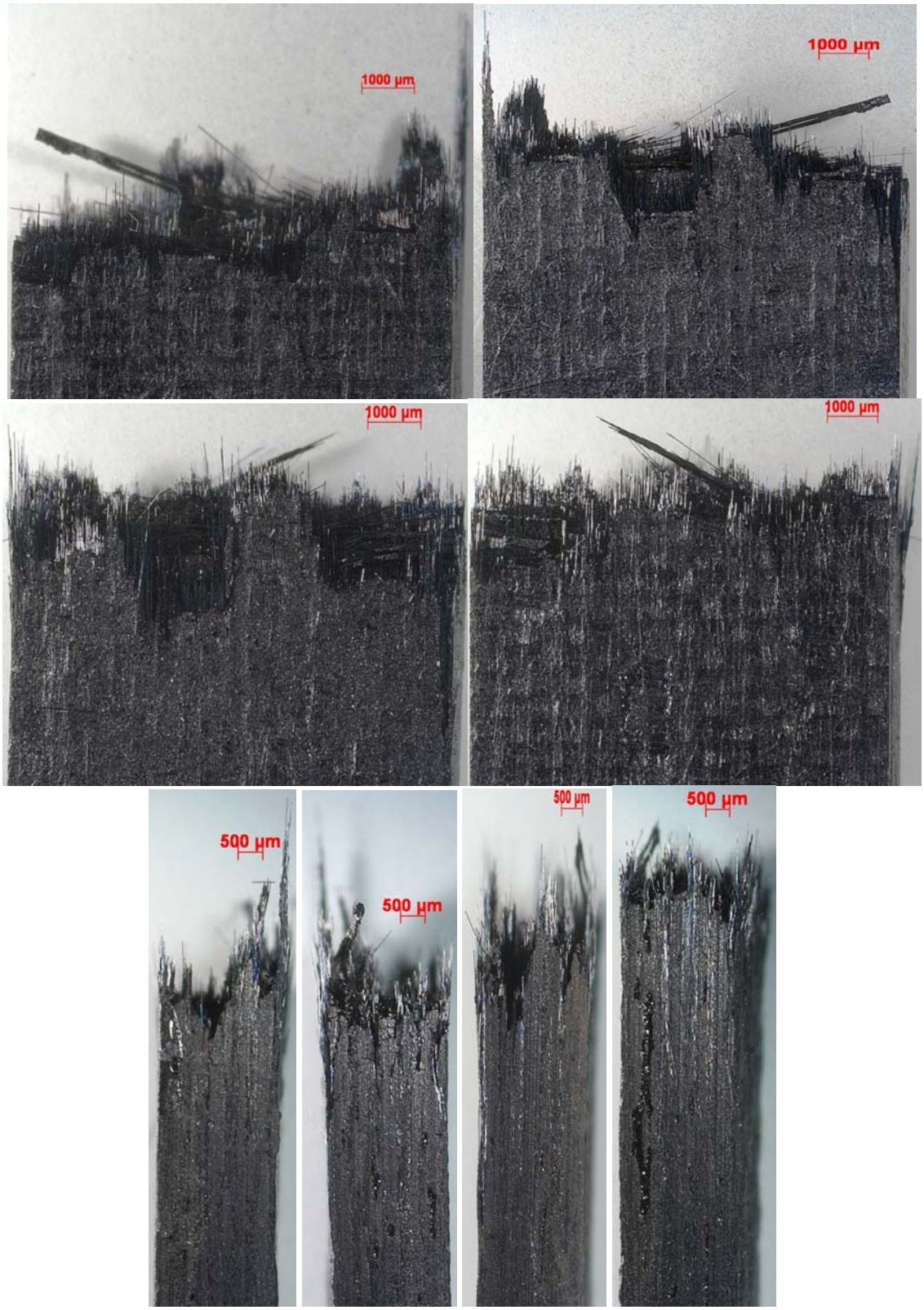


**Figure 82. Fracture surface optical micrographs of as processed composite C3 specimen.**

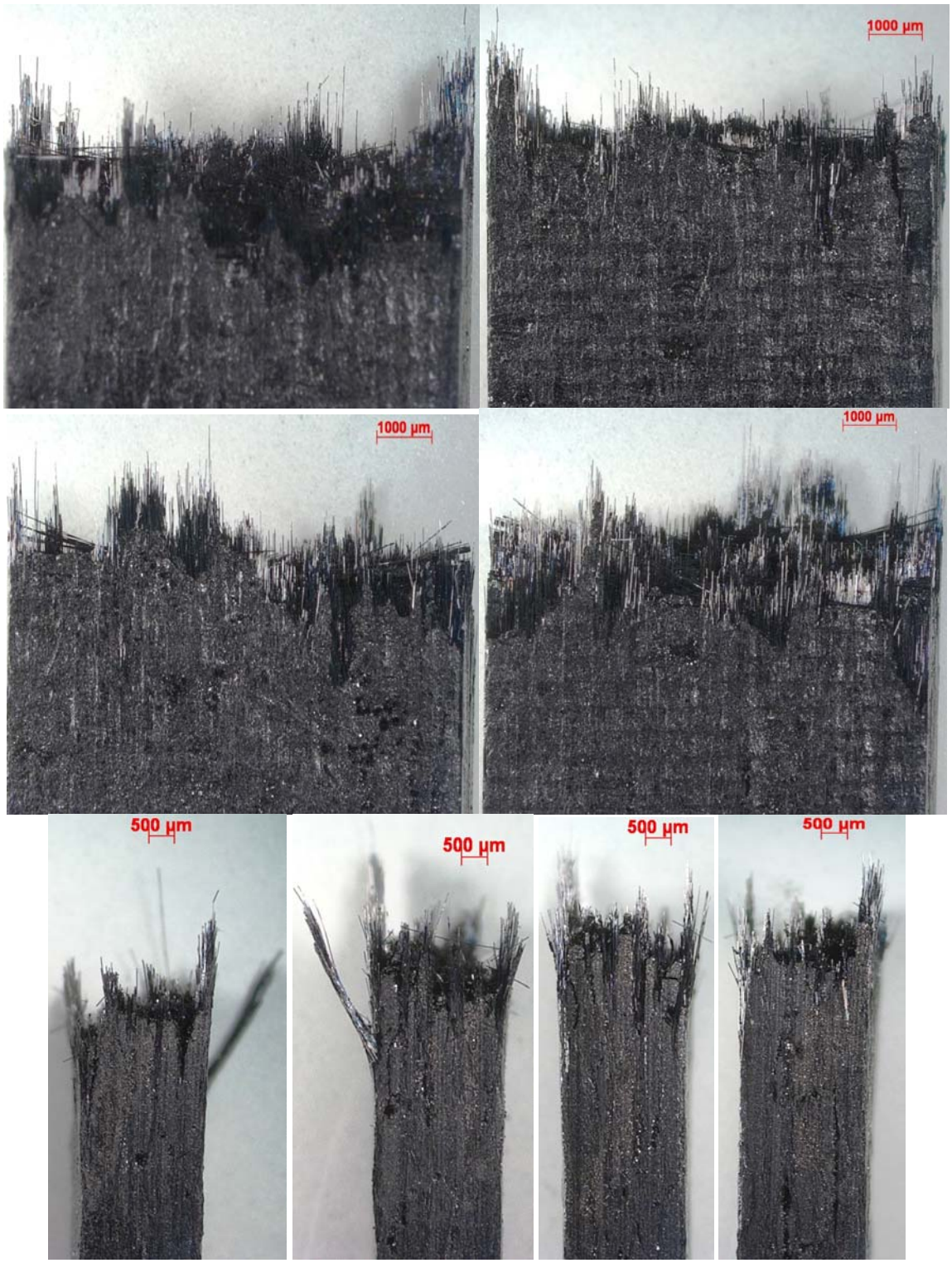


**Figure 83. Fracture surface optical micrographs of as processed composite C3 specimen.**

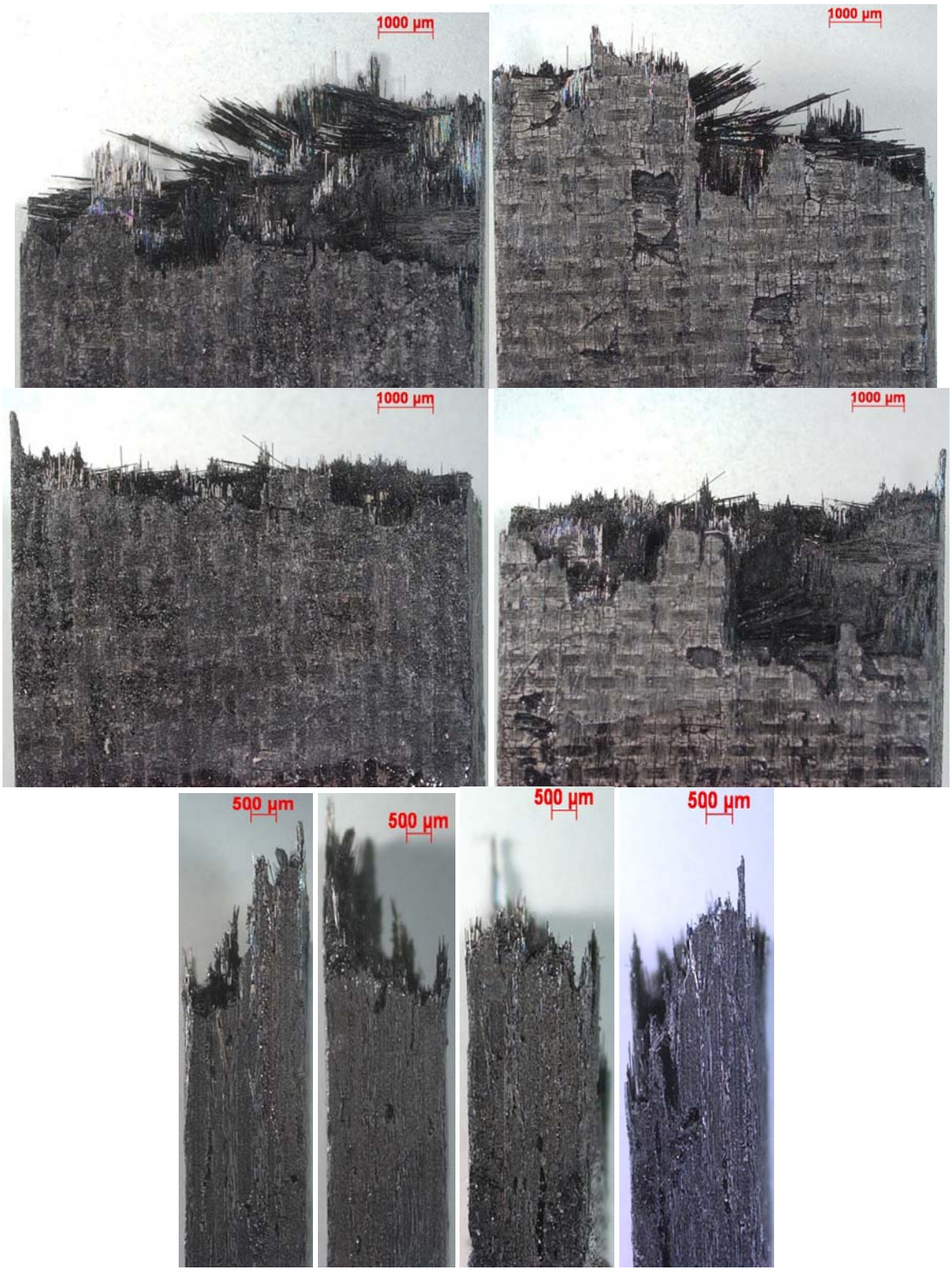


**Figure 84. Fracture surface optical micrographs of composite C3 specimen aged in air for 8 hours at 815 °C and subjected to a monotonic tension test to failure.**

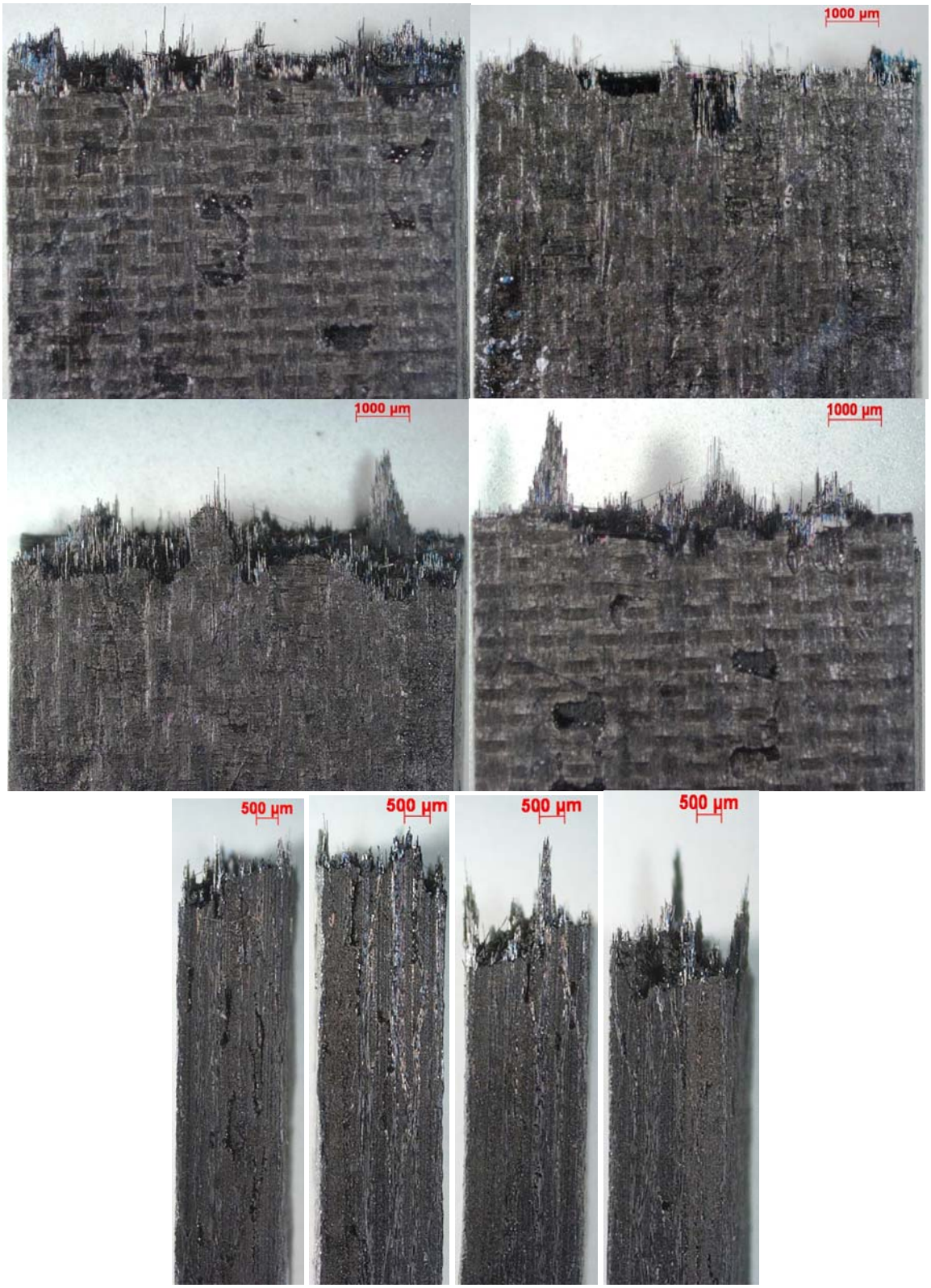


**Figure 85. Fracture surface optical micrographs of composite C3 specimen aged in air for 8 hours at 815 °C and subjected to a monotonic tension test to failure.**

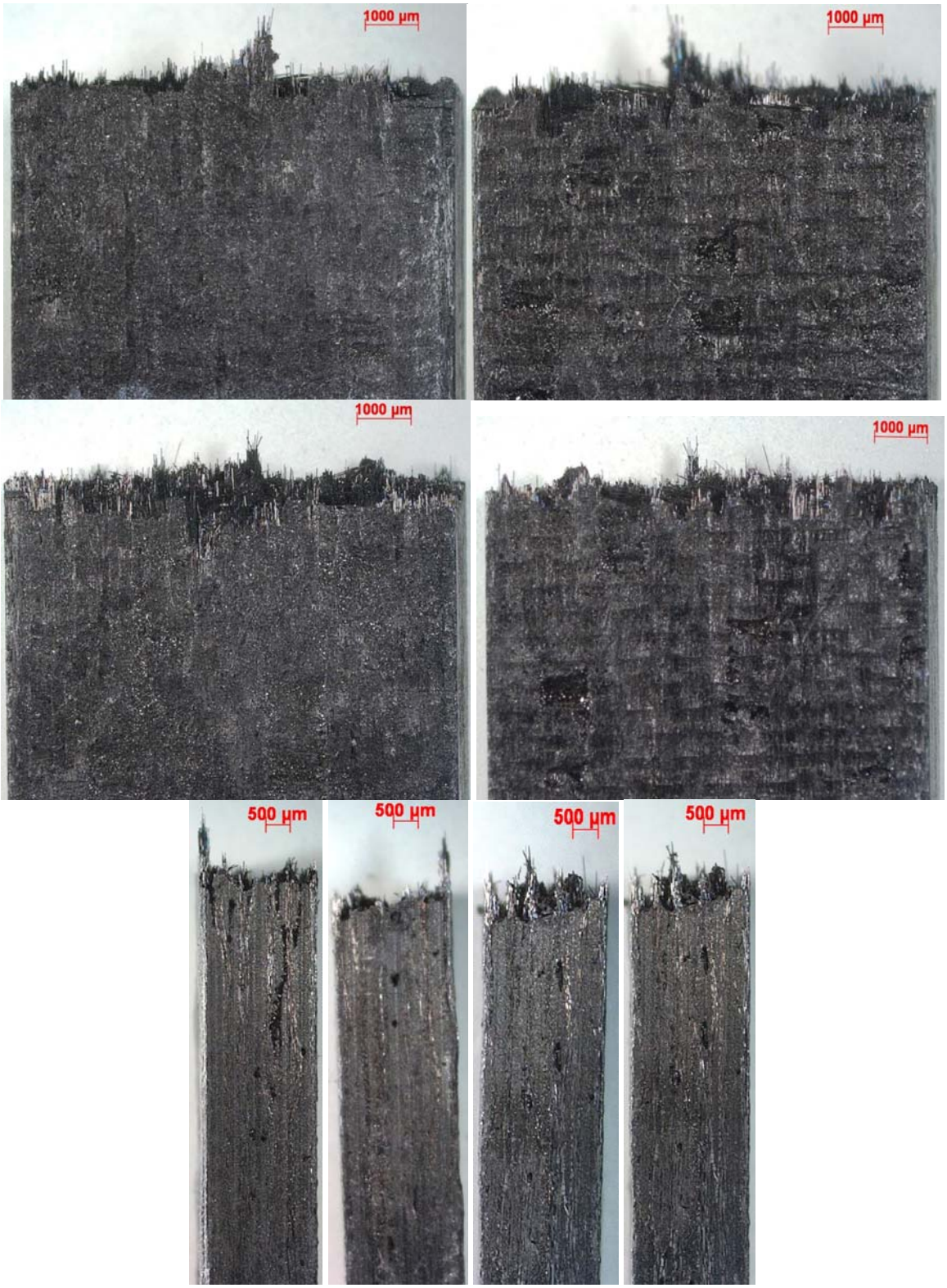


**Figure 86. Fracture surface optical micrographs of composite C3 specimen aged in steam for 8 hours at 815 °C and subjected to a monotonic tension test to failure.**

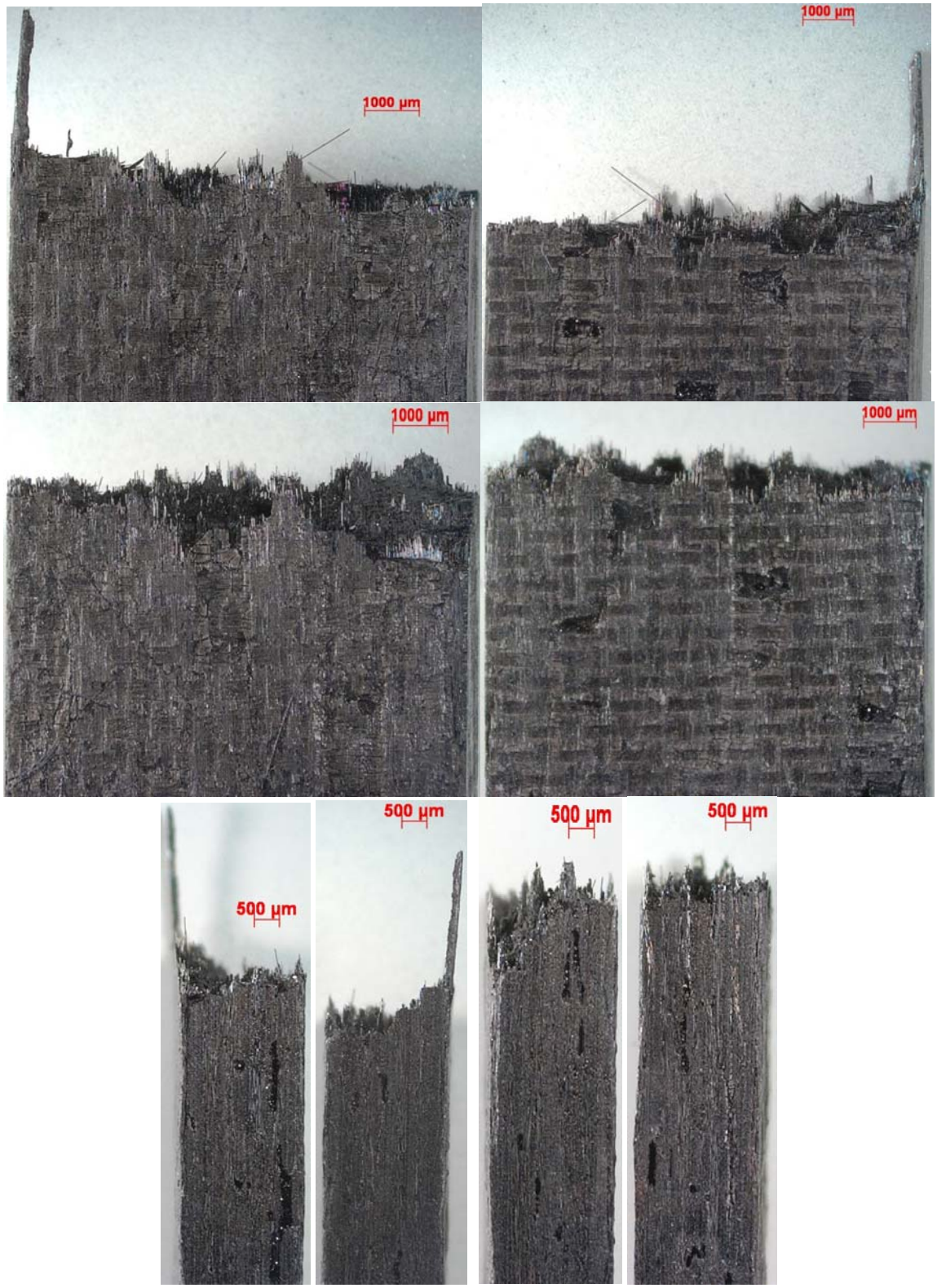


**Figure 87. Fracture surface optical micrographs of composite C3 specimen, pre-fatigued, aged in air for 8 hours at 815 °C, and subjected to a monotonic tension test to failure.**

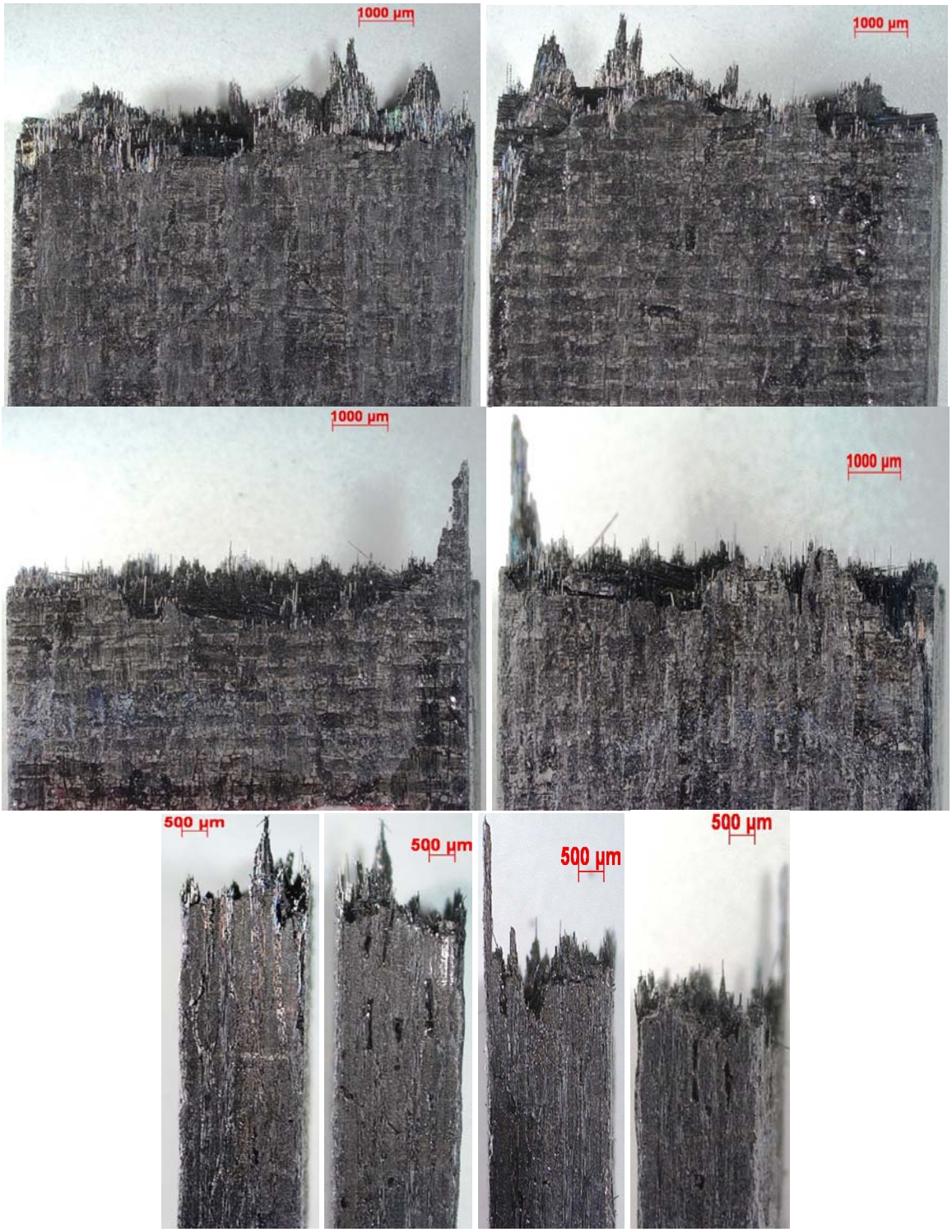


**Figure 88. Fracture surface optical micrographs of composite C3 specimen, pre-fatigued, aged in air for 8 hours at 815 °C, and subjected to a monotonic tension test to failure.**

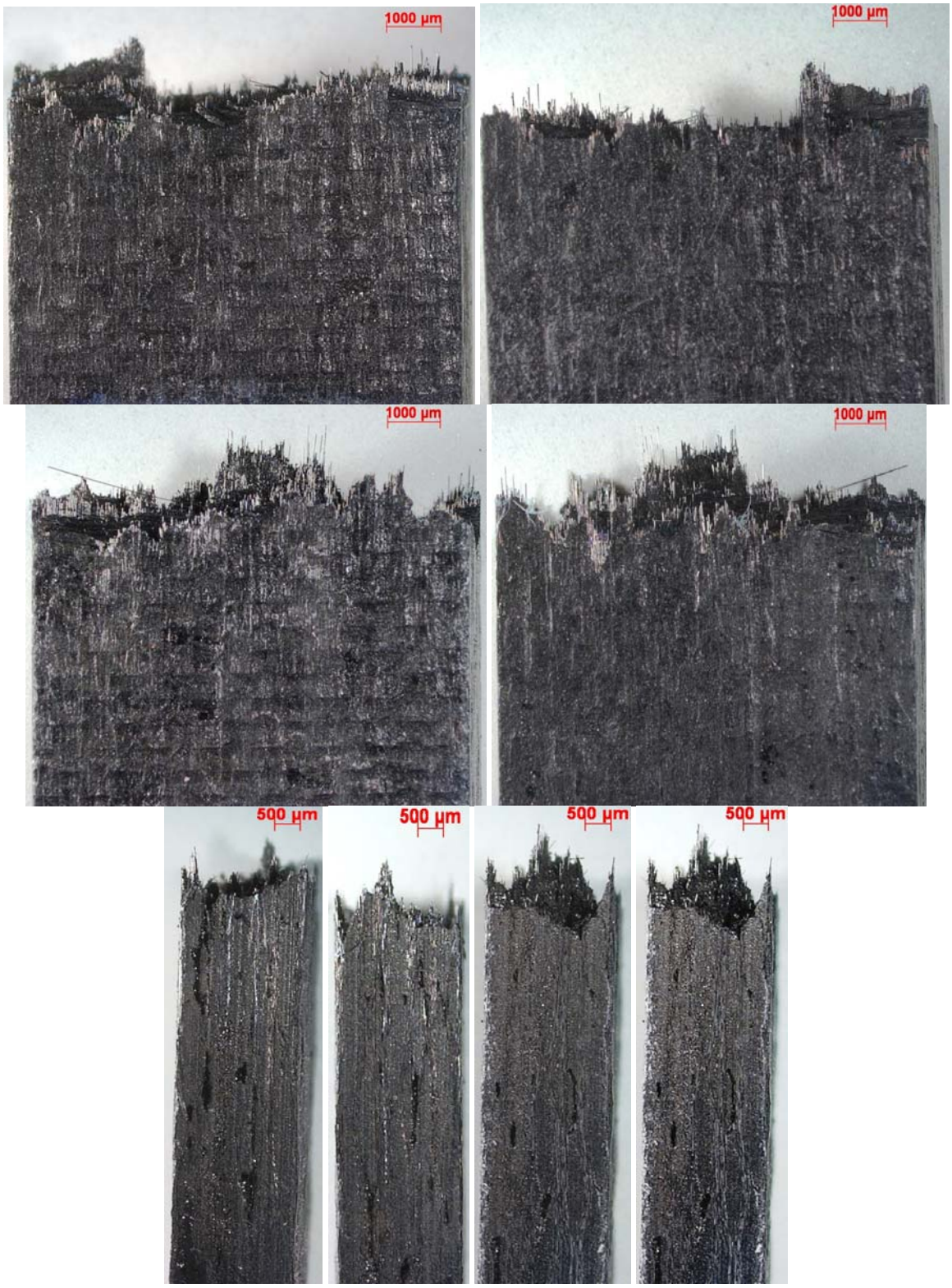


**Figure 89. Fracture surface optical micrographs of composite C3 specimen, pre-fatigued, aged in steam for 8 hours at 815 °C, and subjected to a monotonic tension test to failure.**

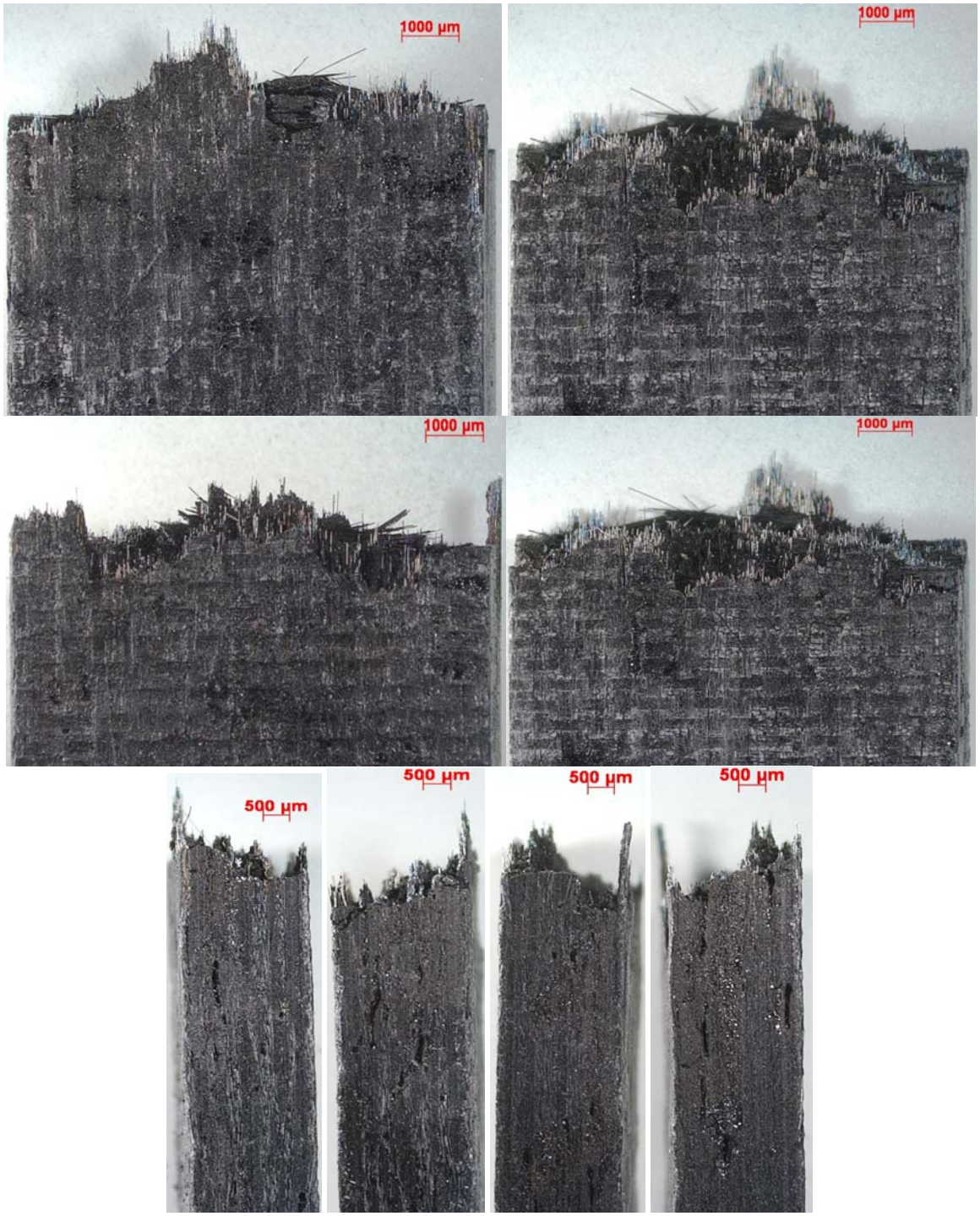


**Figure 90. Fracture surface optical micrographs of composite C3 specimen, pre-fatigued, aged in steam for 8 hours at 815 °C, and subjected to a monotonic tension test to failure.**

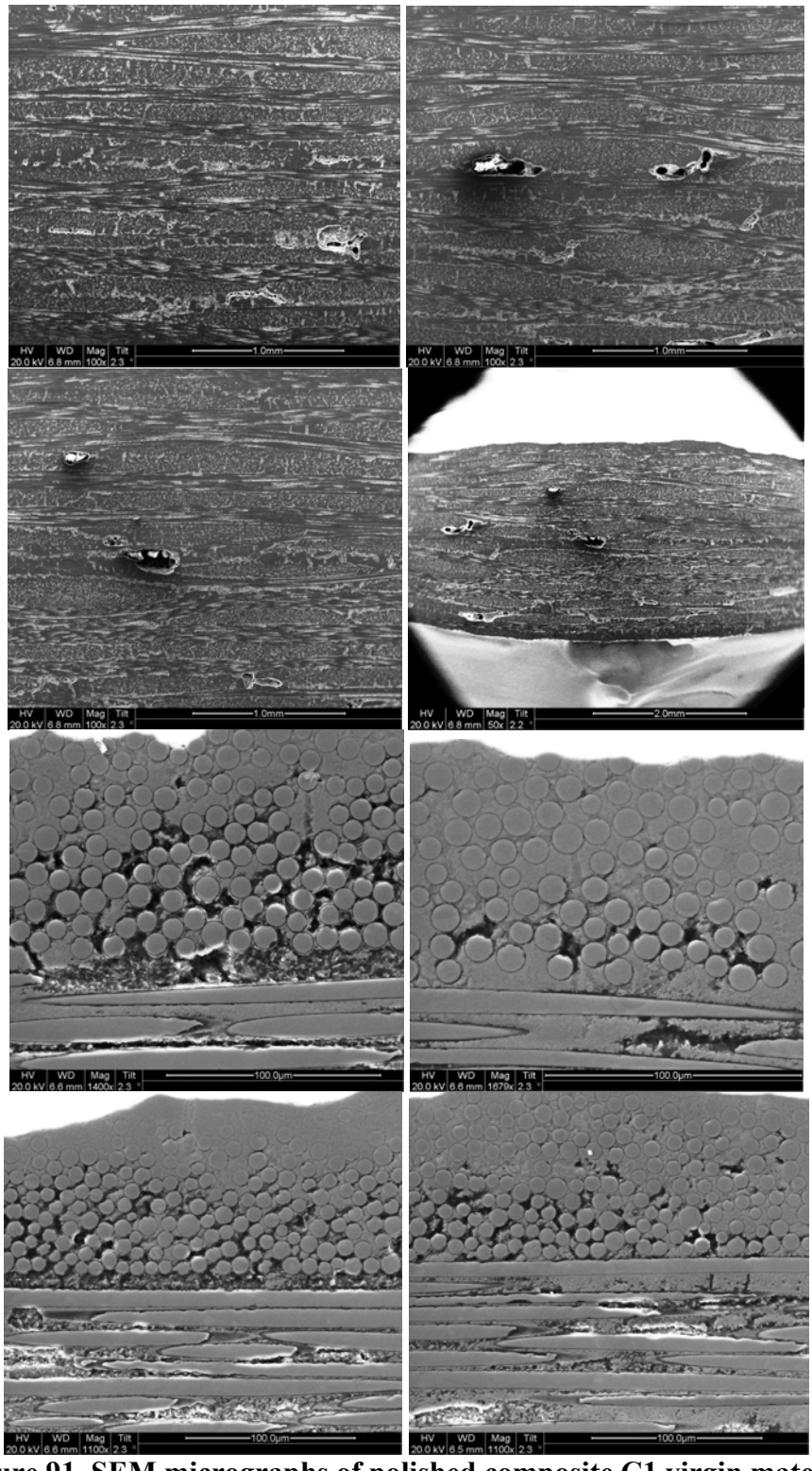

**Figure 91. SEM micrographs of polished composite C1 virgin material**

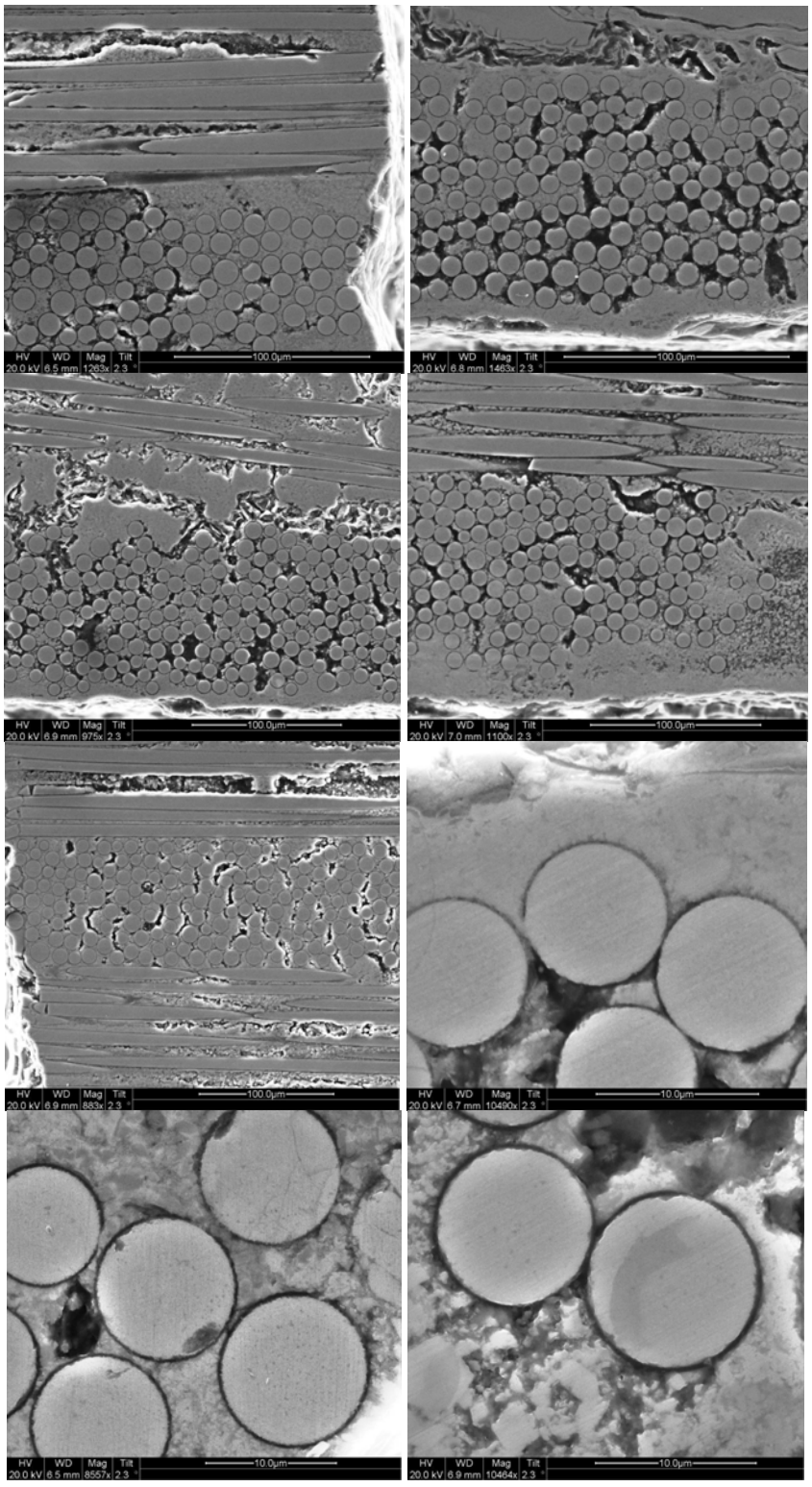


**Figure 92. SEM micrographs of polished composite C1 virgin material**

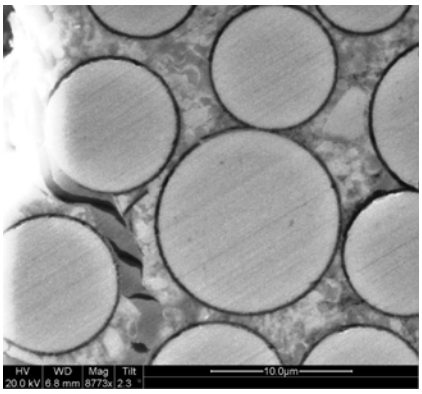


**Figure 93. SEM micrograph of polished composite C1 virgin material**

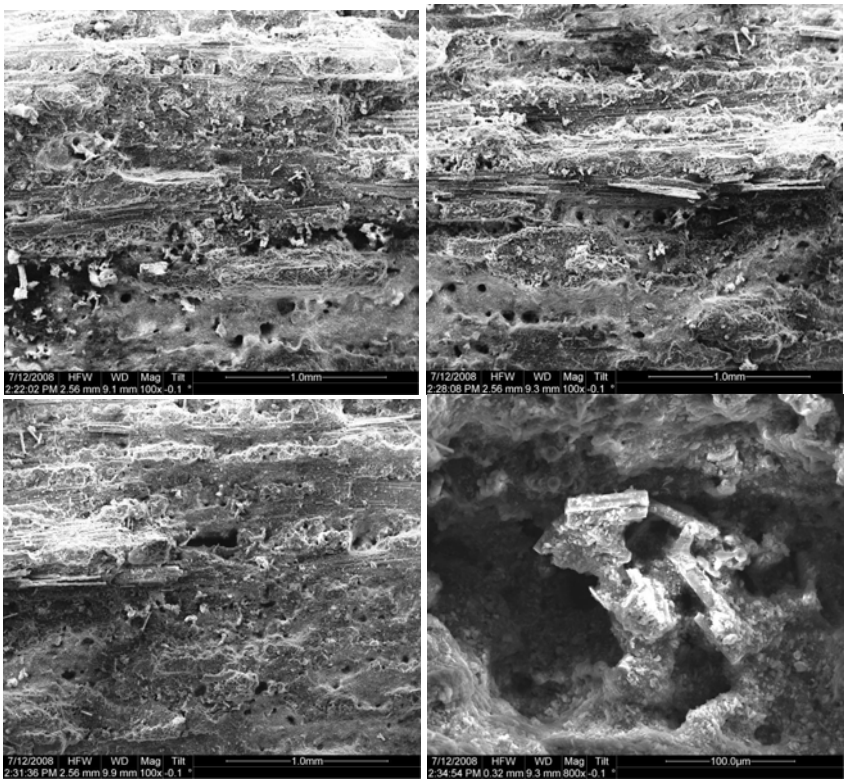


**Figure 94. Fracture surface SEM micrographs of as-processed composite C1 specimen**

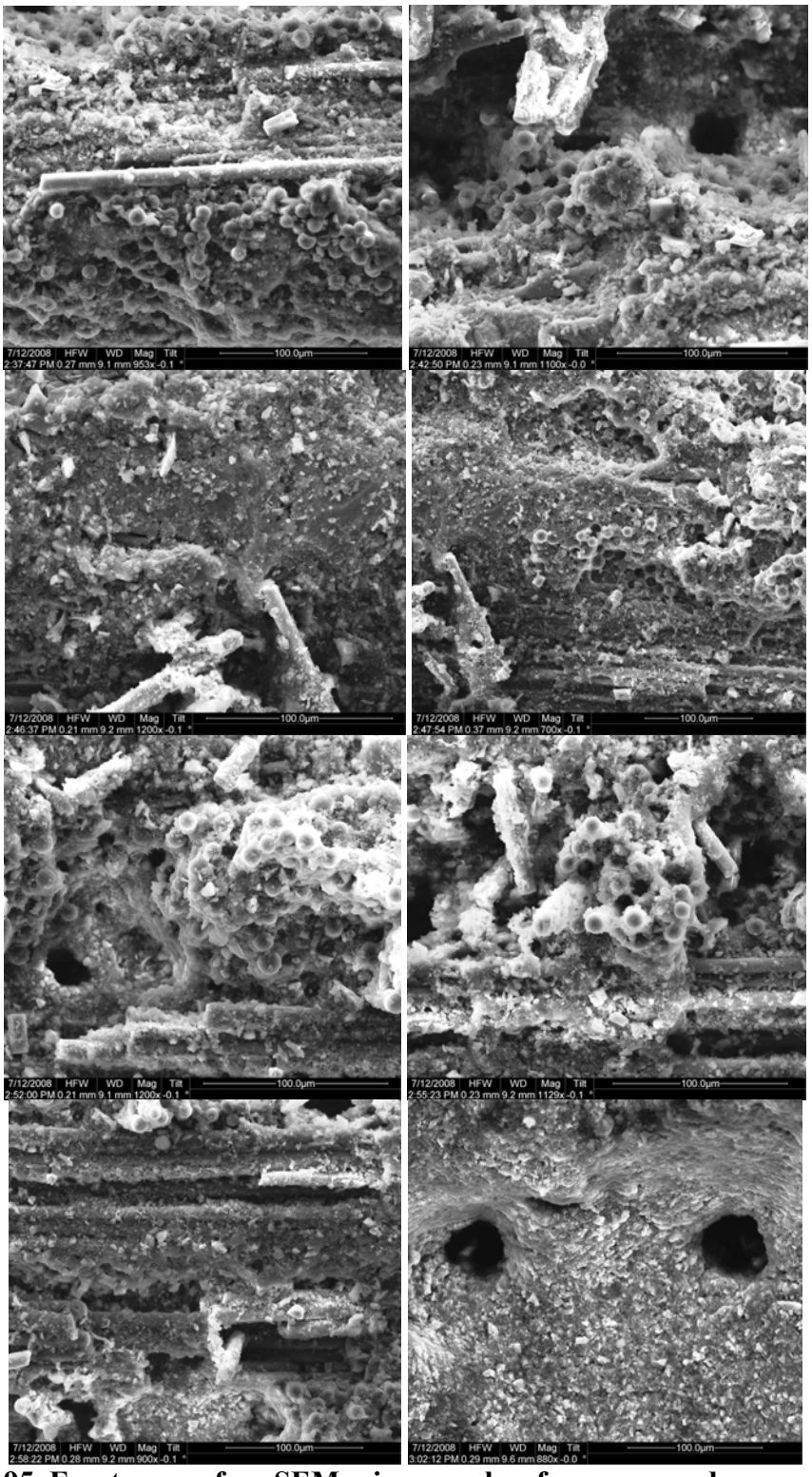


**Figure 95. Fracture surface SEM micrographs of as-processed composite C1 specimen**

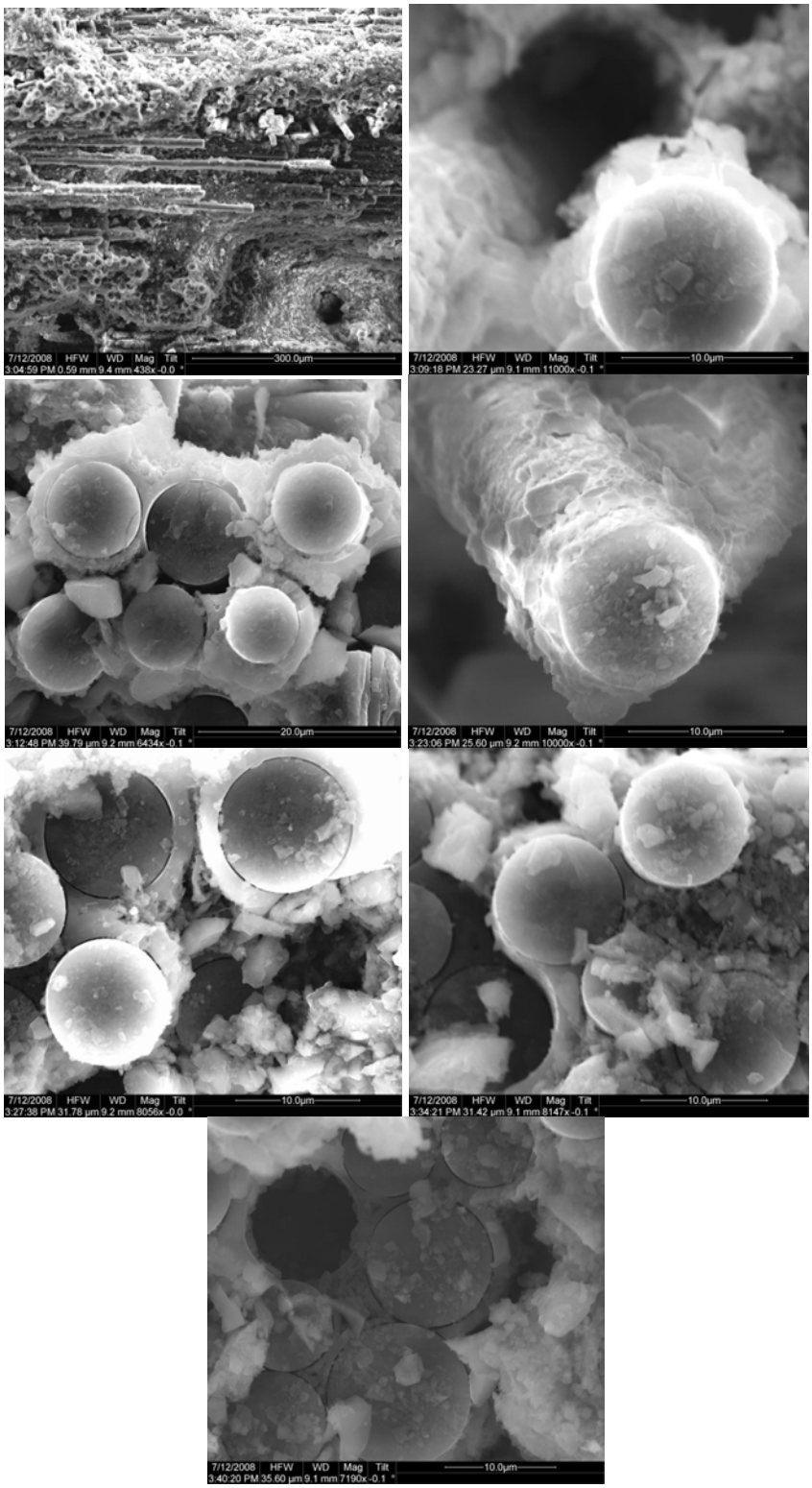


**Figure 96. Fracture surface SEM micrographs of as-processed composite C1 specimen**

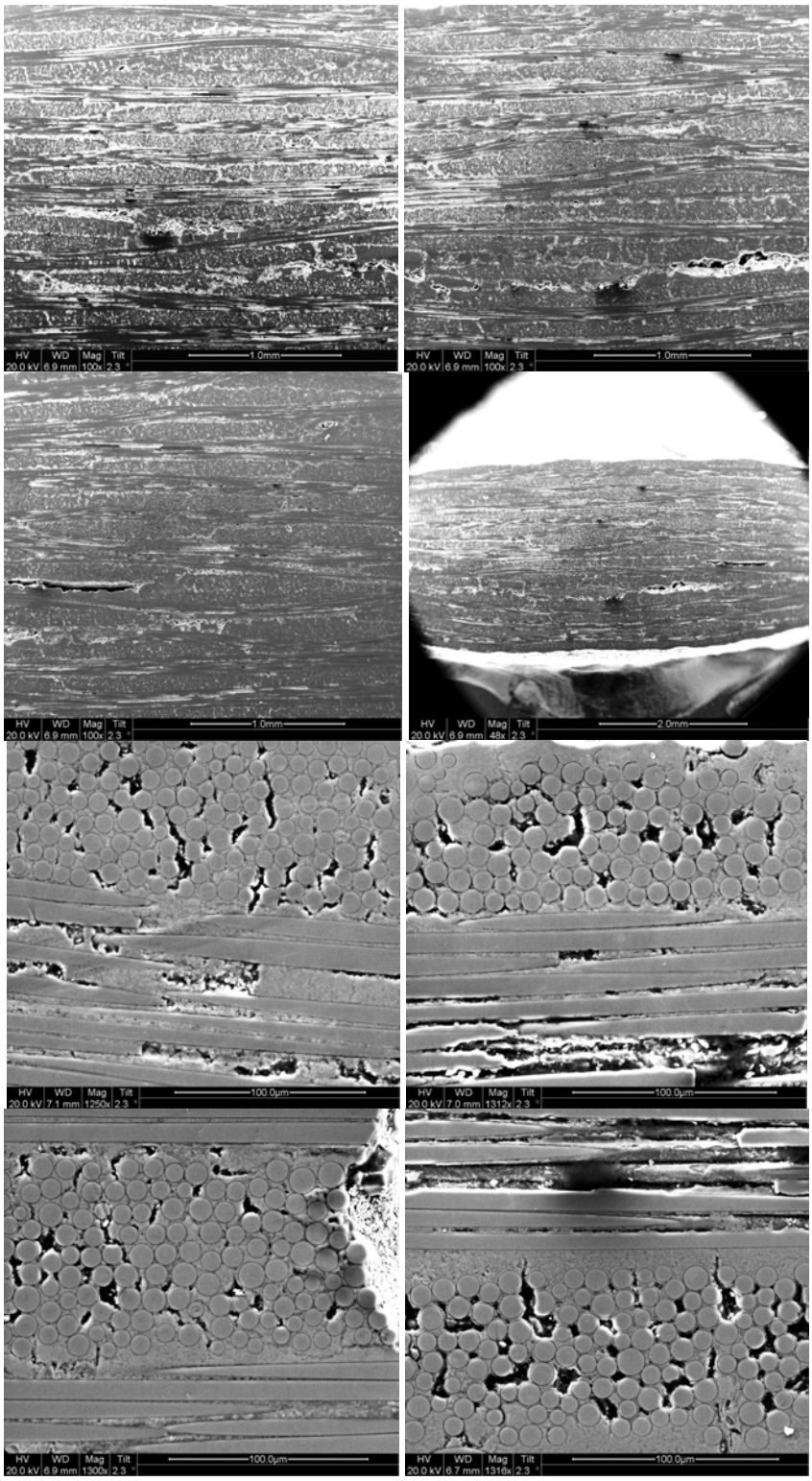

**Figure 97. SEM micrographs of polished as-processed composite C1 specimen**

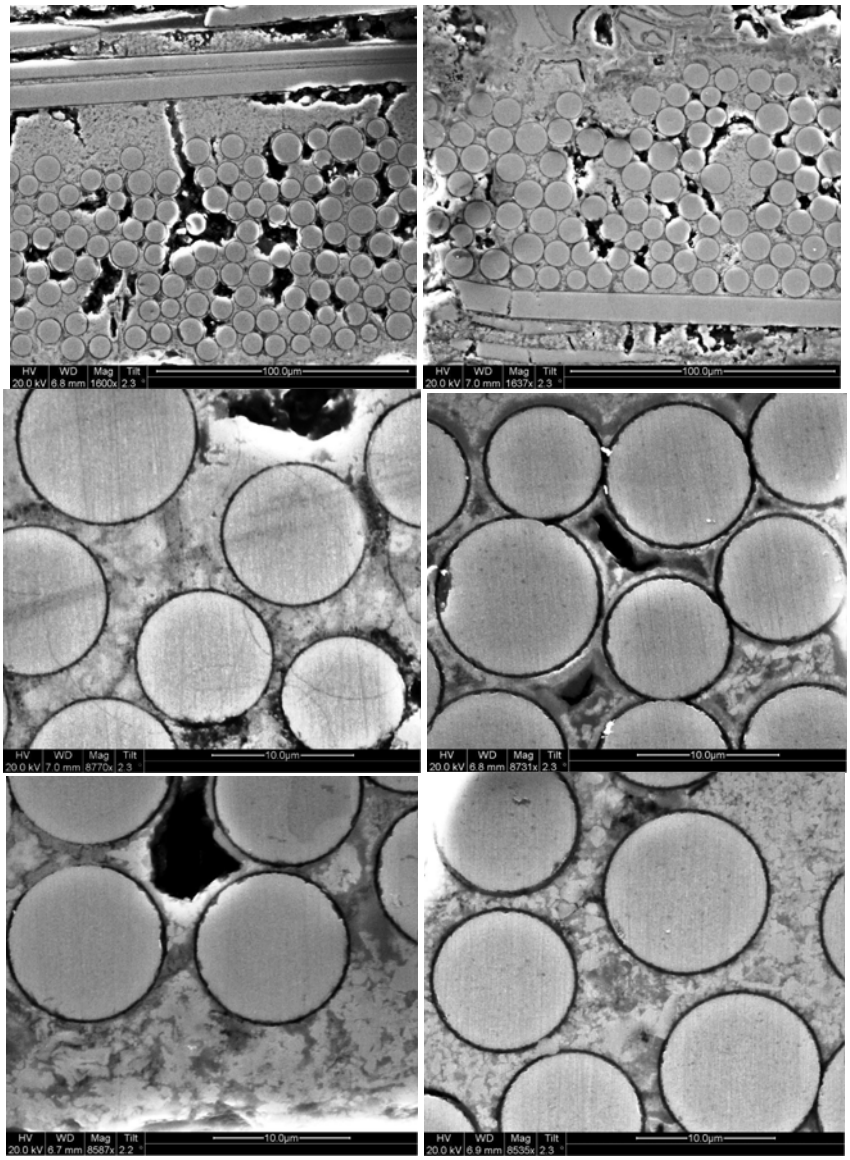


**Figure 98. SEM micrographs of polished as-processed composite C1 specimen**

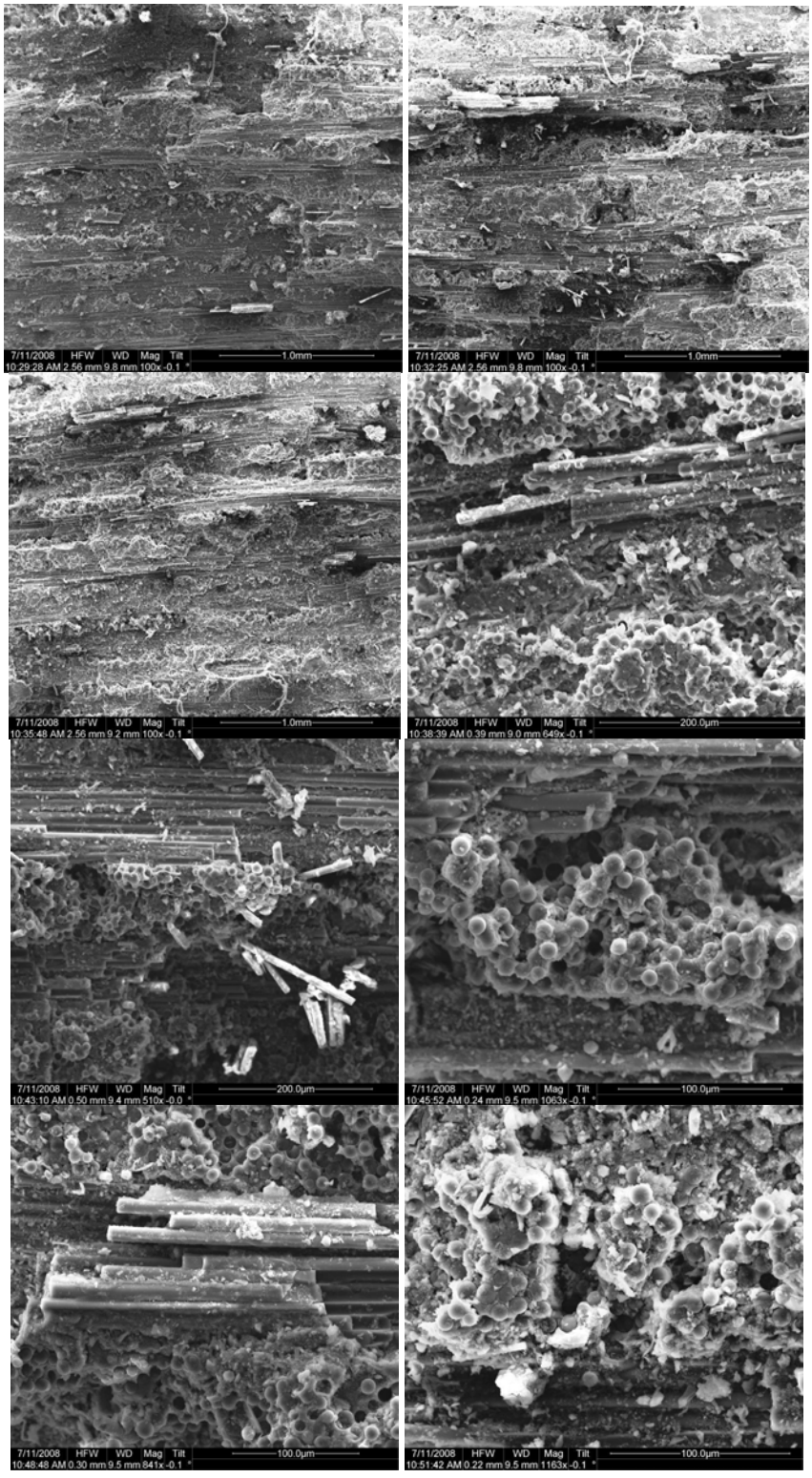

**Figure 99. Fracture surface SEM micrographs of composite C1 specimen tested at 1300 °C in air with maximum fatigue stress $\sigma_{max}$ = 100 MPa**

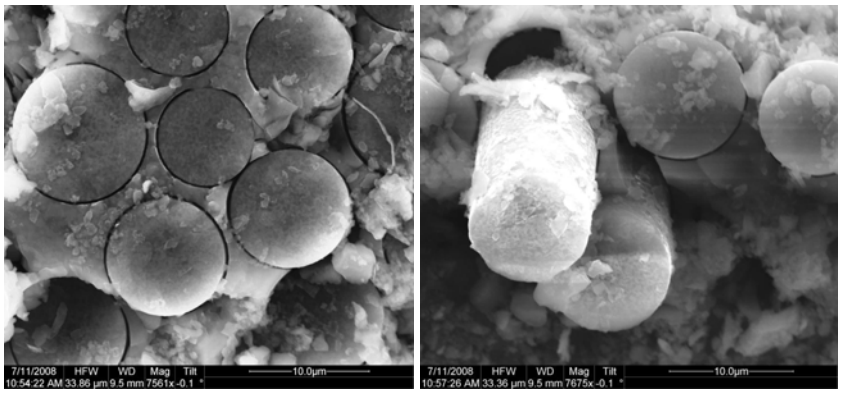

**Figure 100. Fracture surface SEM micrographs of composite C1 specimen tested at 1300 °C in air with maximum fatigue stress $\sigma_{max}$ = 100 MPa**

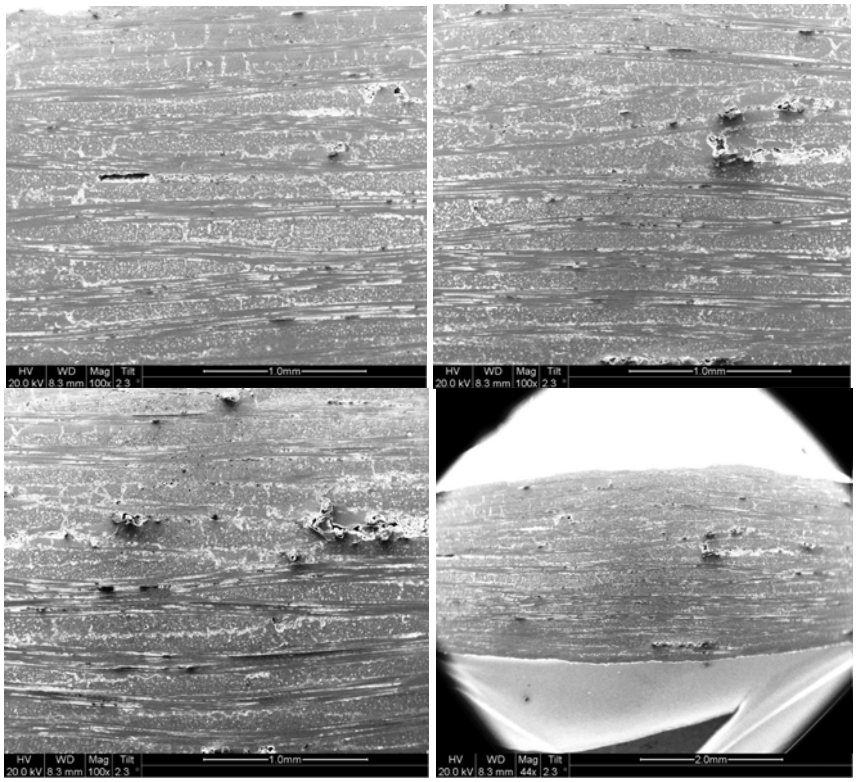

**Figure 101. SEM micrographs of polished material from composite C1 specimen tested at 1300 °C in air with maximum fatigue stress $\sigma_{max}$ = 100 MPa**

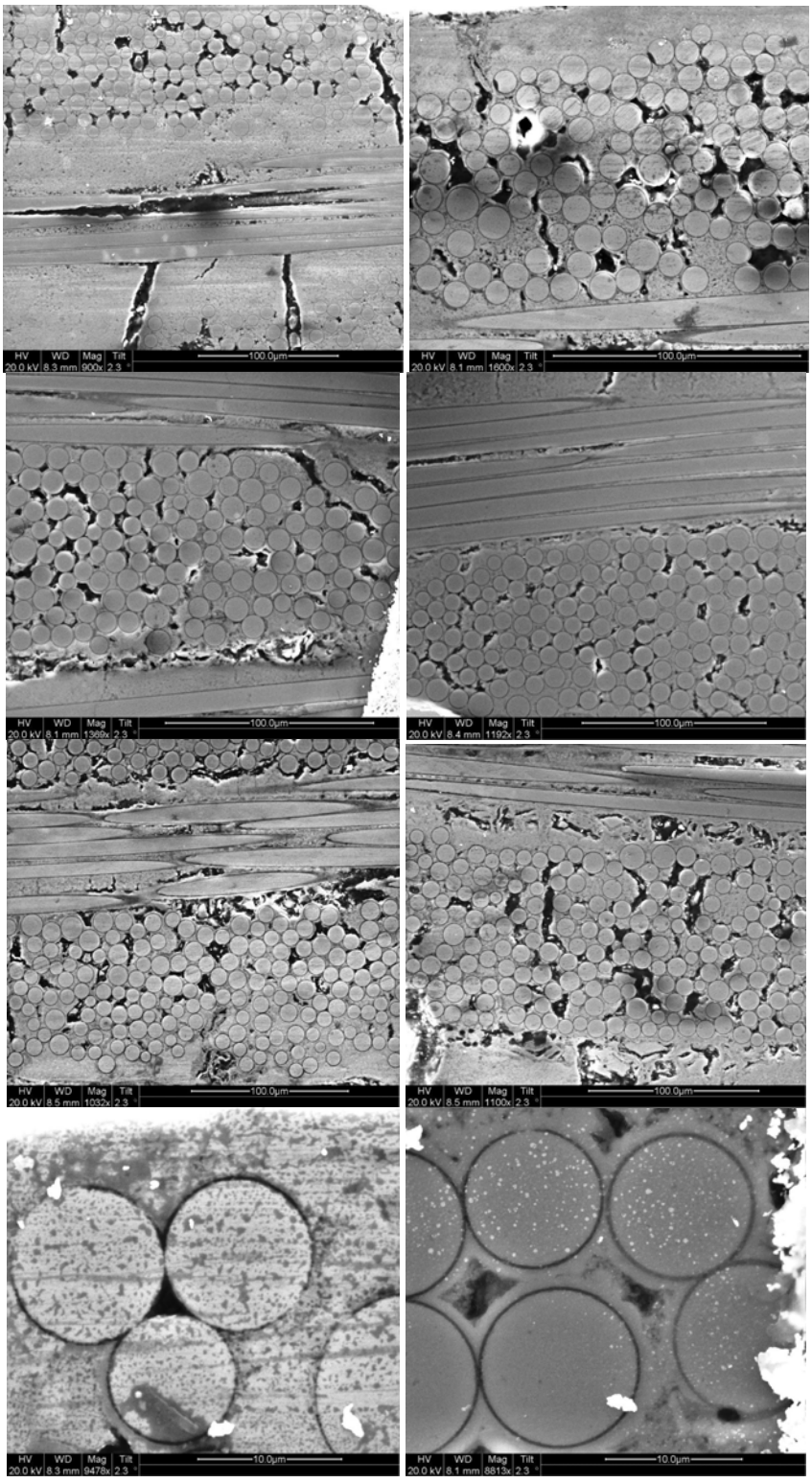

**Figure 102. SEM micrographs of polished material from composite C1 specimen tested at 1300 °C in air with maximum fatigue stress $\sigma_{max}$ = 100 MPa**

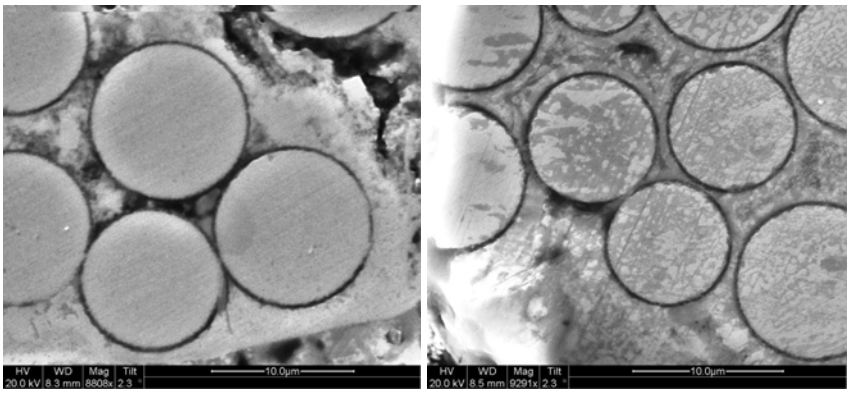

**Figure 103. SEM micrographs of polished material from composite C1 specimen tested at 1300 °C in air with maximum fatigue stress $\sigma_{max}$ = 100 MPa**

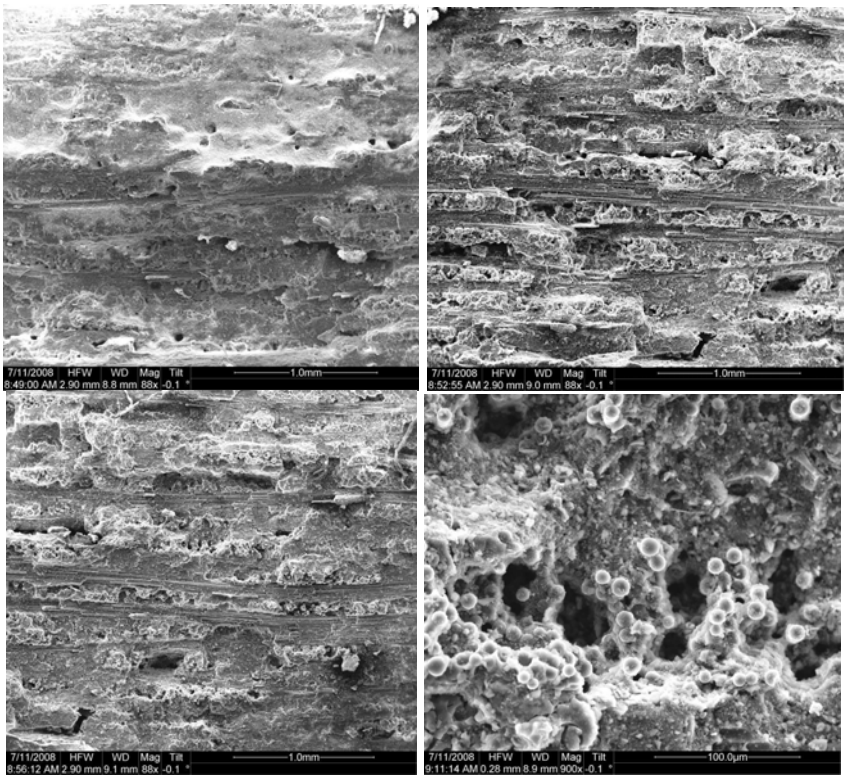

**Figure 104. Fracture surface SEM micrographs of composite C1 specimen tested at 1300 °C in air with maximum fatigue stress $\sigma_{max}$ = 140 MPa**

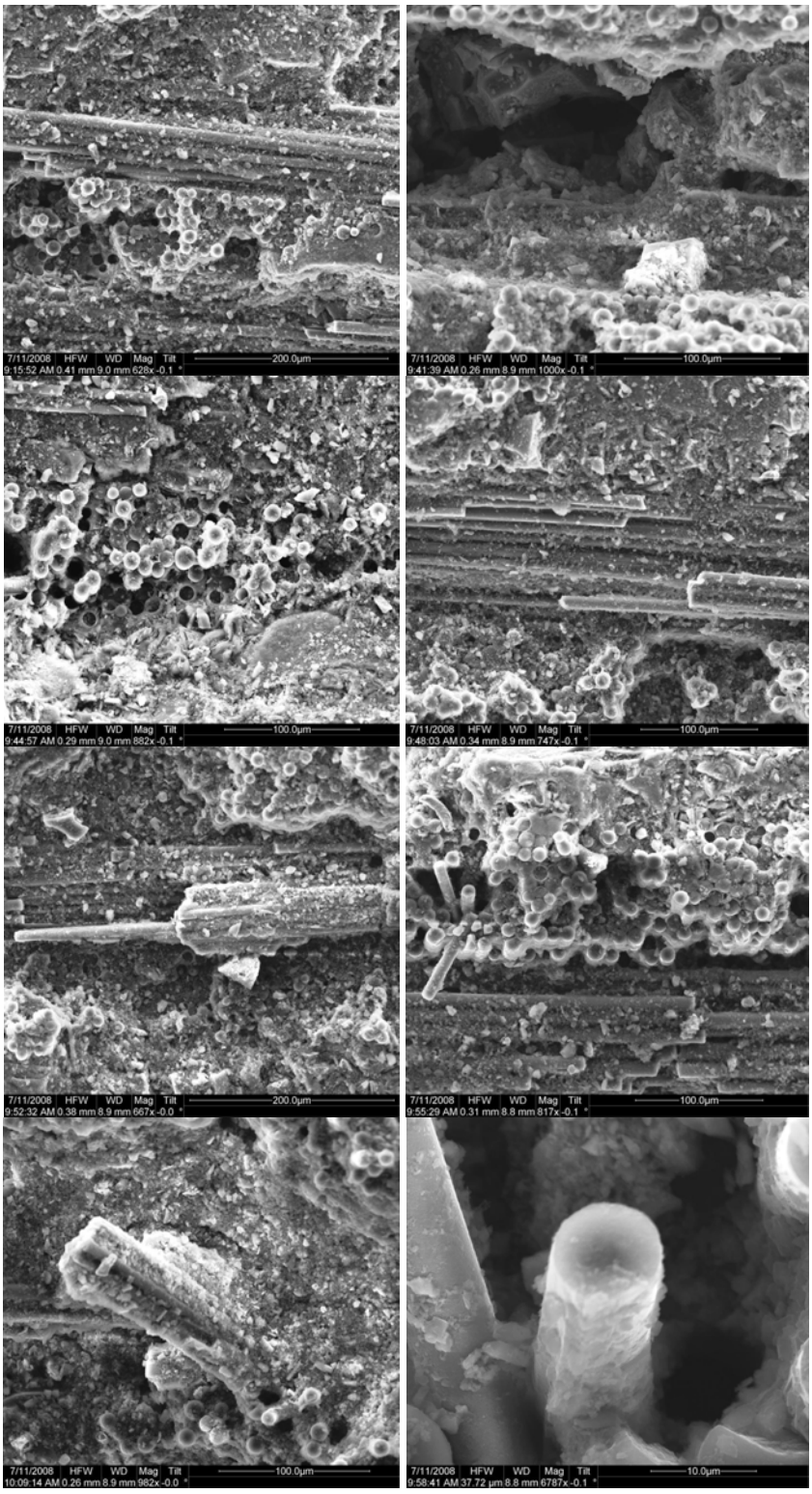

**Figure 105. Fracture surface SEM micrographs of composite C1 specimen tested at 1300 °C in air with maximum fatigue stress $\sigma_{max}$ = 140 MPa**

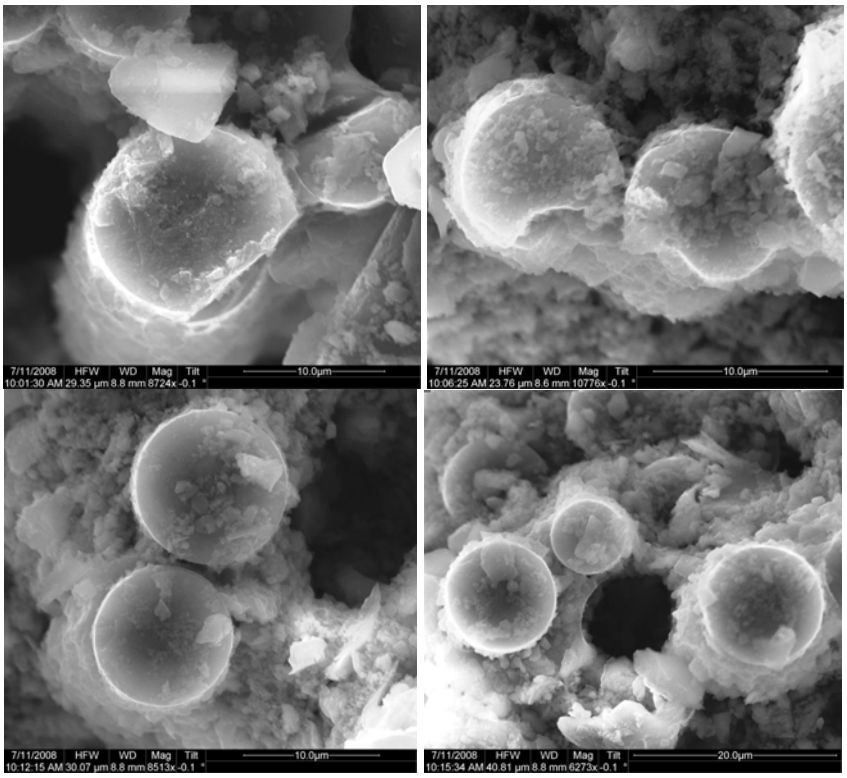

**Figure 106. Fracture surface SEM micrographs of composite C1 specimen tested at 1300 °C in air with maximum fatigue stress $\sigma_{max}$ = 140 MPa**

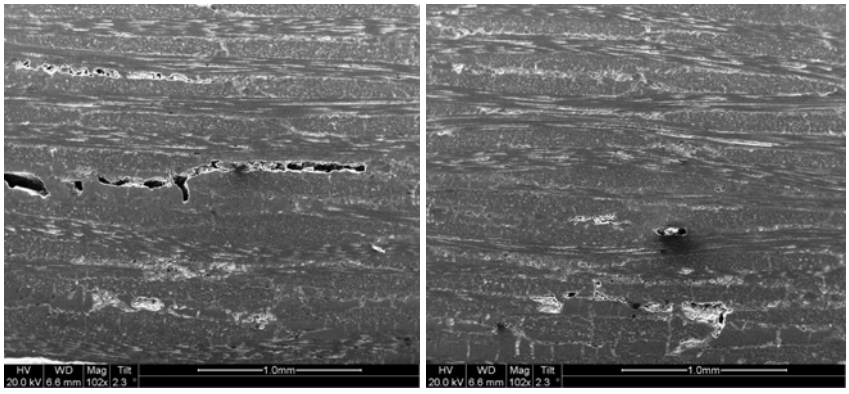

**Figure 107. SEM micrographs of polished material from composite C1 specimen tested at 1300 °C in air with maximum fatigue stress $\sigma_{max}$ = 140 MPa**

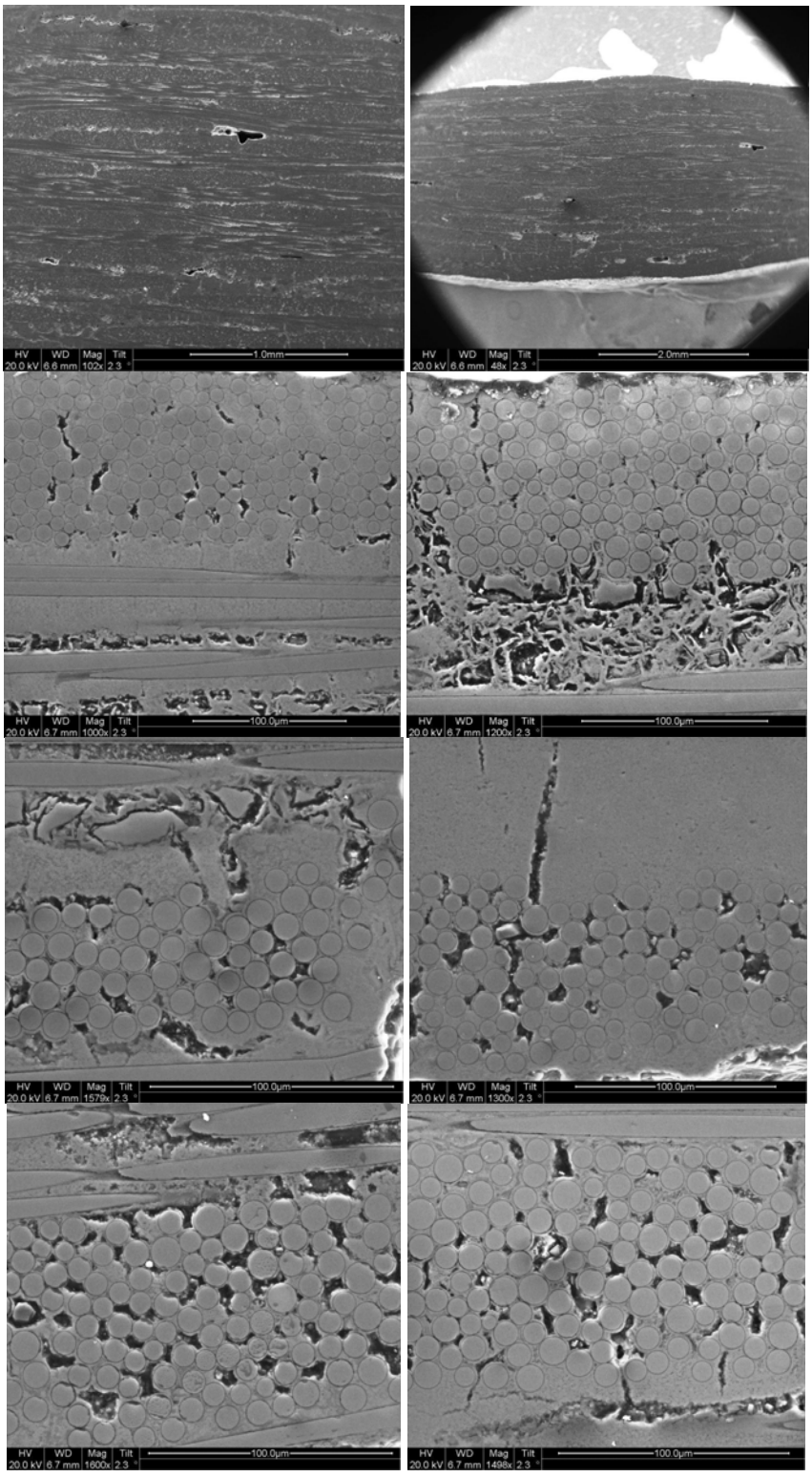

**Figure 108. SEM micrographs of polished material from composite C1 specimen tested at 1300 °C in air with maximum fatigue stress $\sigma_{max}$ = 140 MPa**

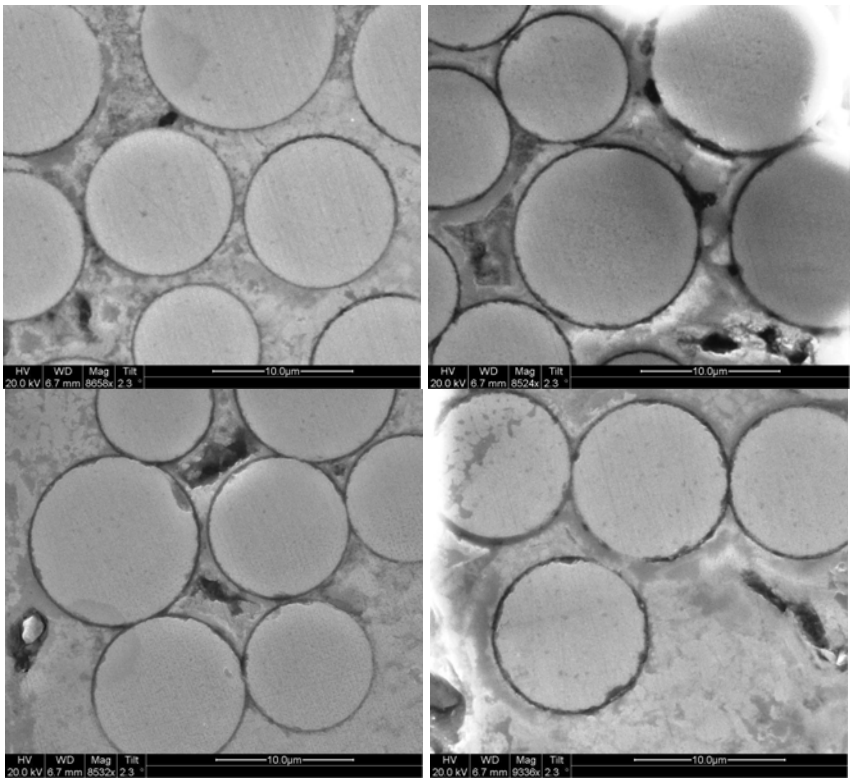

**Figure 109. SEM micrographs of polished material from composite C1 specimen tested at 1300 °C in air with maximum fatigue stress $\sigma_{max}$ = 140 MPa**

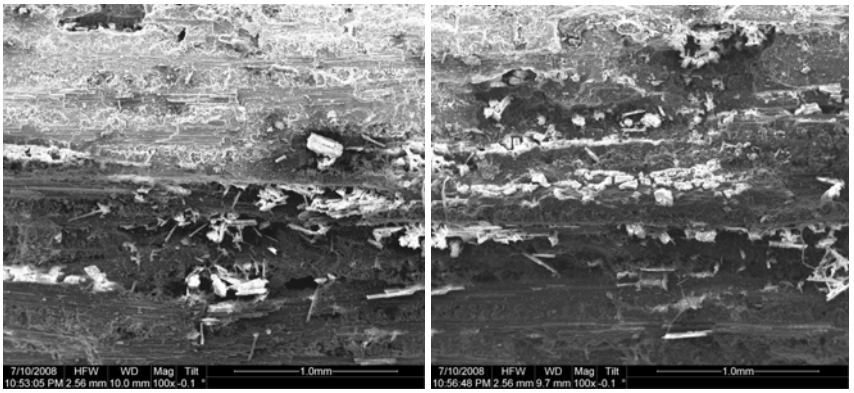

**Figure 110. Fracture surface SEM micrographs of composite C1 specimen tested at 1300 °C in steam with maximum fatigue stress $\sigma_{max}$ = 100 MPa**

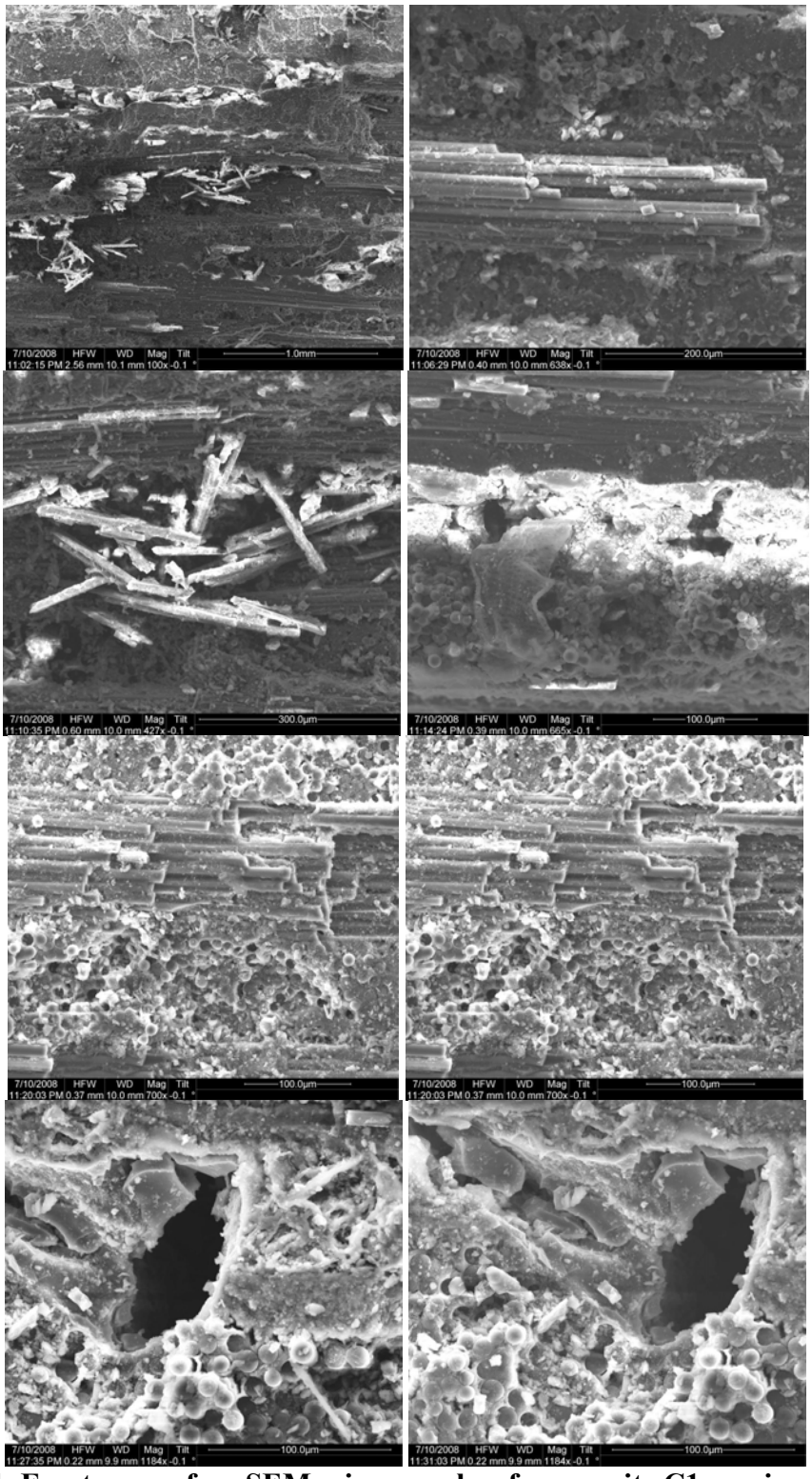

**Figure 111. Fracture surface SEM micrographs of composite C1 specimen tested at 1300 °C in steam with maximum fatigue stress $\sigma_{max}$ = 100 MPa**

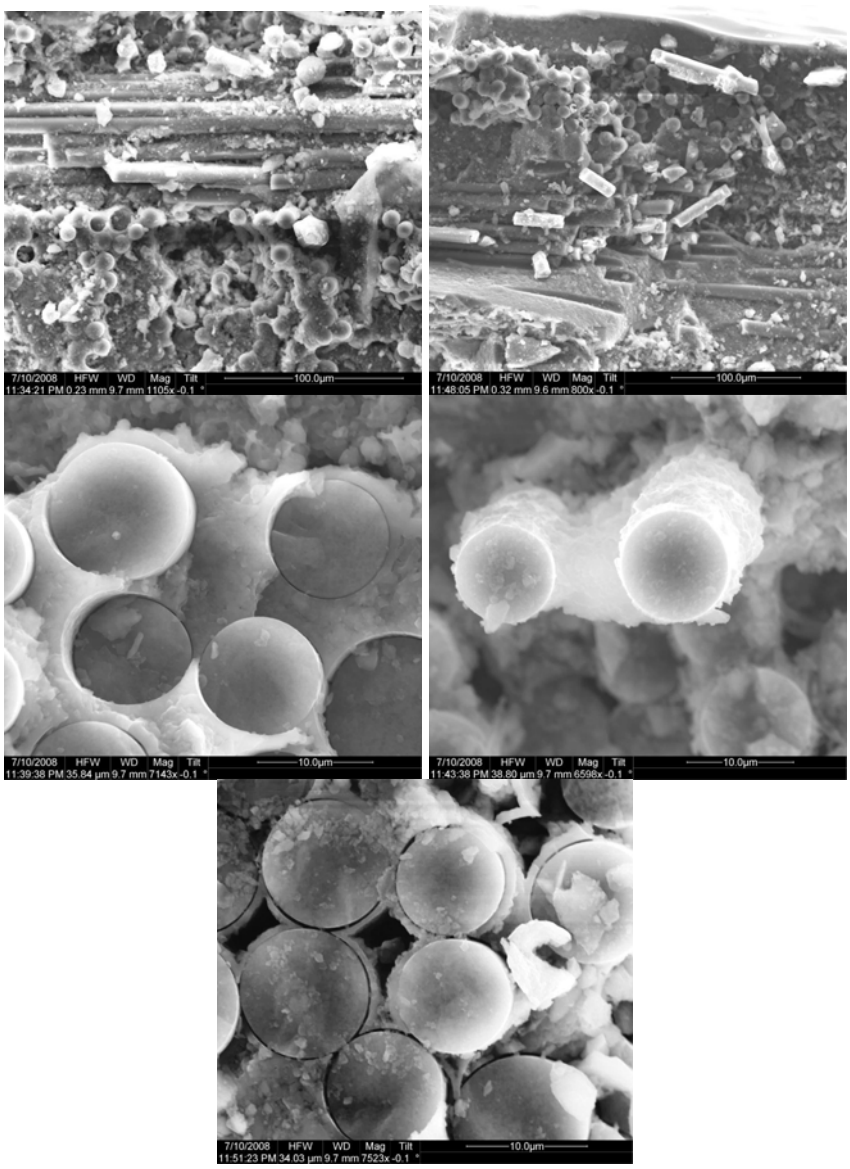

**Figure 112. Fracture surface SEM micrographs of composite C1 specimen tested at 1300 °C in steam with maximum fatigue stress $\sigma_{max}$ = 100 MPa**

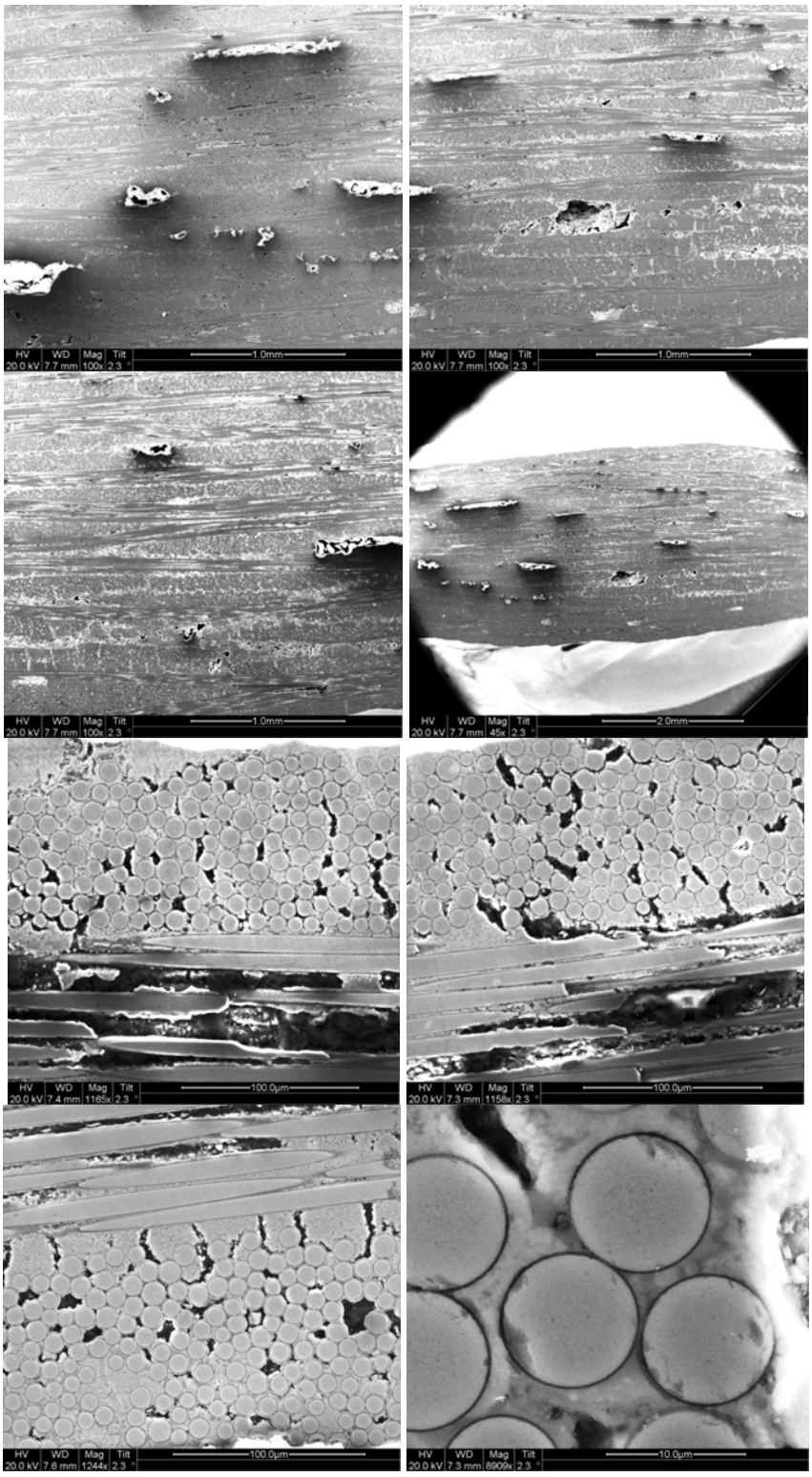

**Figure 113. SEM micrographs of polished material from composite C1 specimen tested at 1300 °C in steam with maximum fatigue stress $\sigma_{max}$ = 100 MPa**

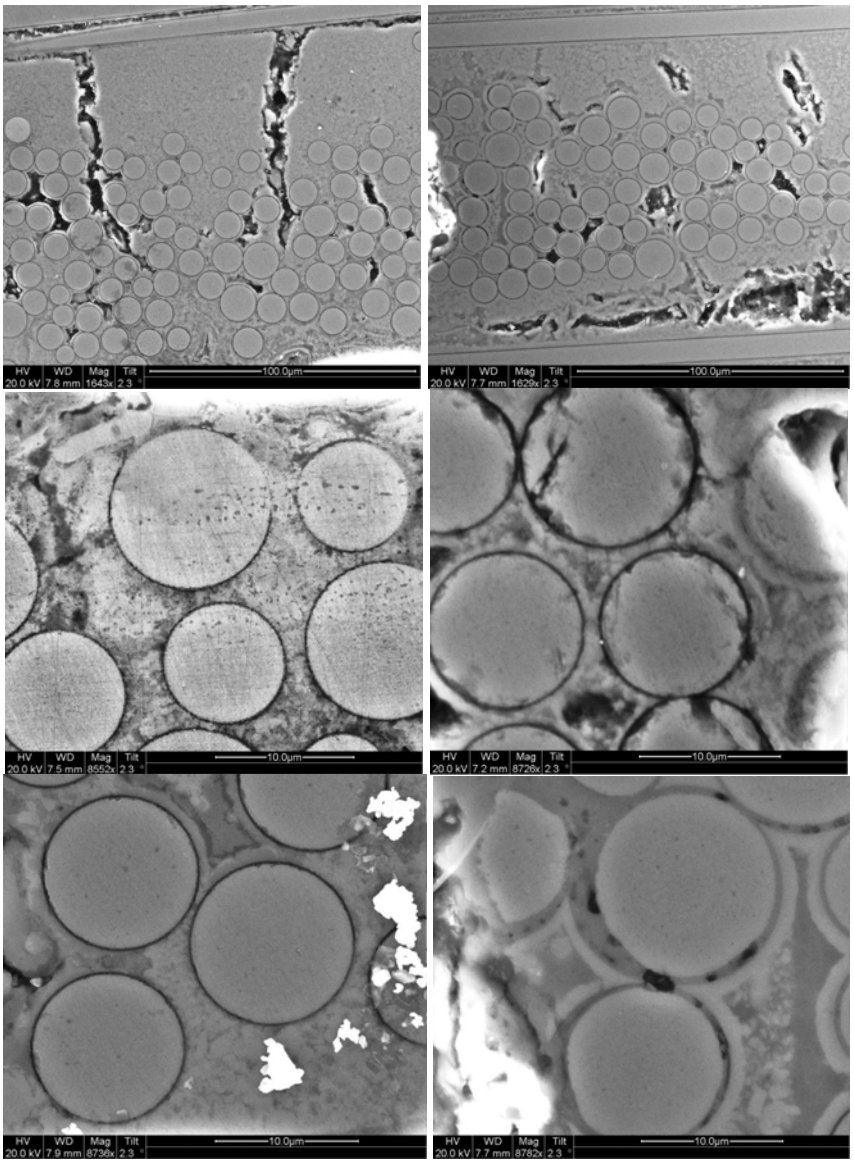

**Figure 114. SEM micrographs of polished material from Composite C1 specimen tested at 1300 °C in steam with maximum fatigue stress $\sigma_{max}$ = 100 MPa**

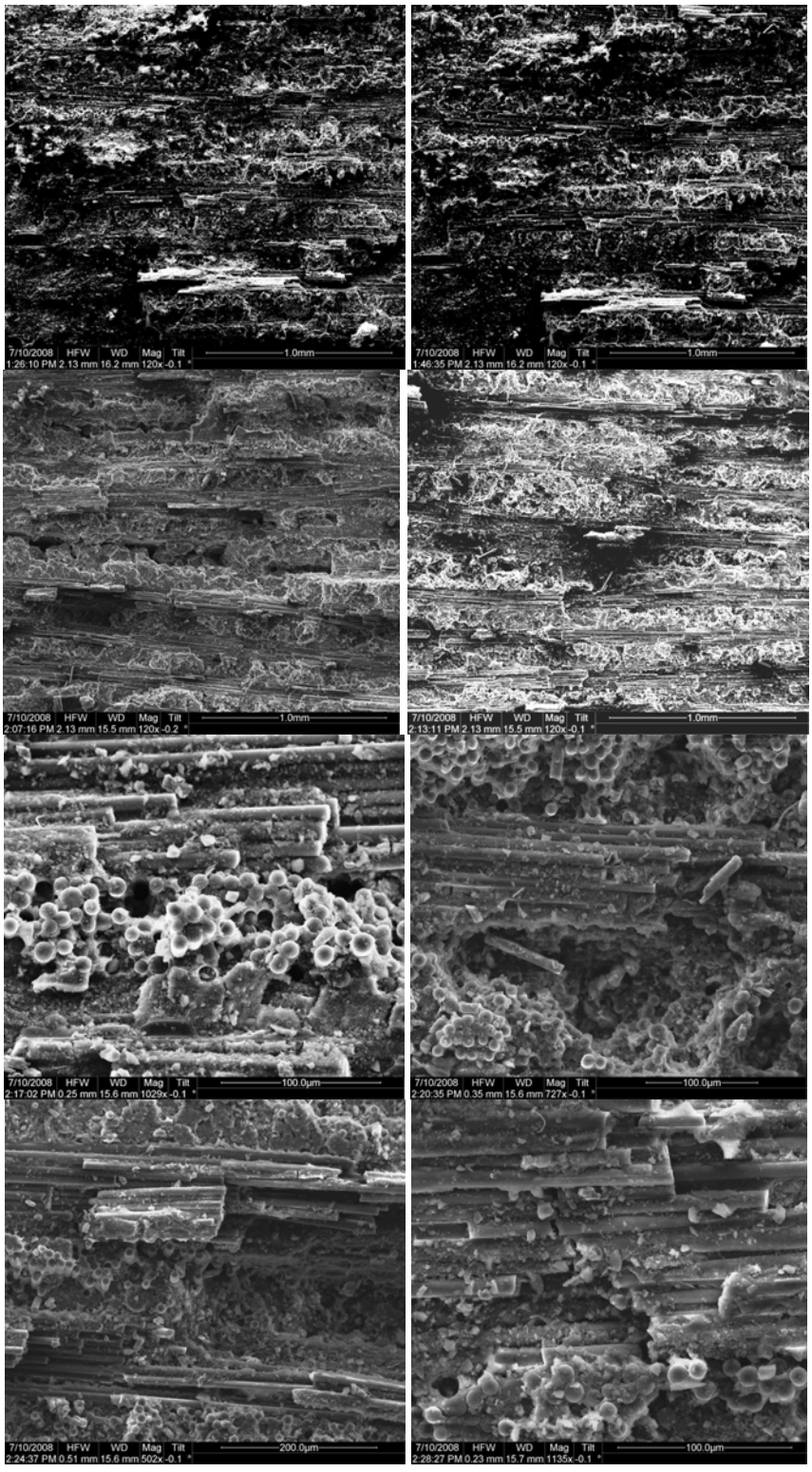

**Figure 115. Fracture surface SEM micrographs of composite C1 specimen tested at 1300 °C in steam with maximum fatigue stress $\sigma_{max}$ = 140 MPa**

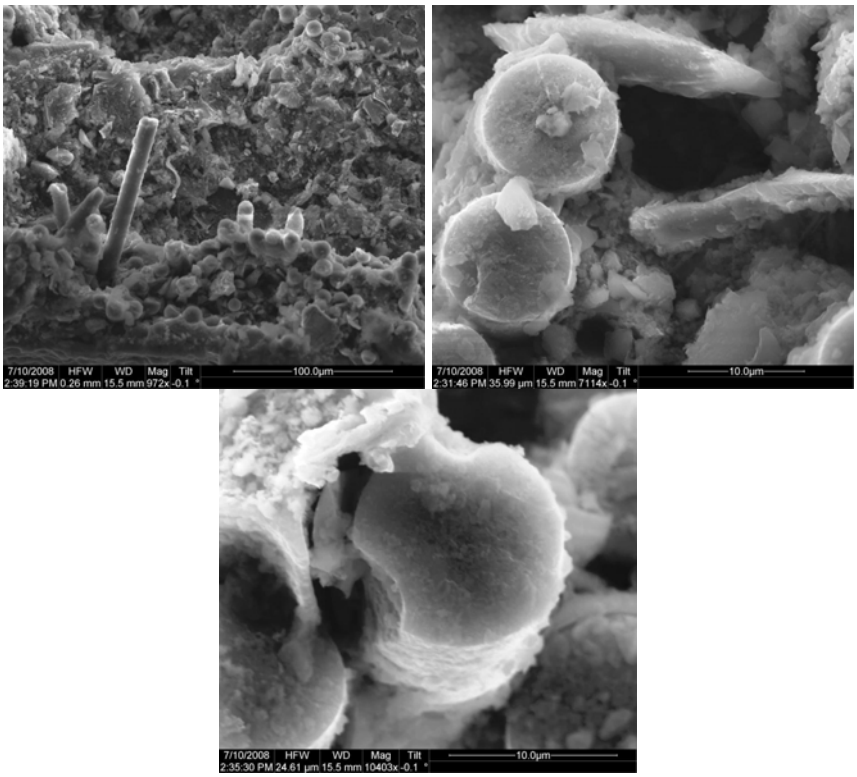

**Figure 116. Fracture surface SEM micrographs of composite C1 specimen tested at 1300 °C in steam with maximum fatigue stress $\sigma_{max}$ = 140 MPa**

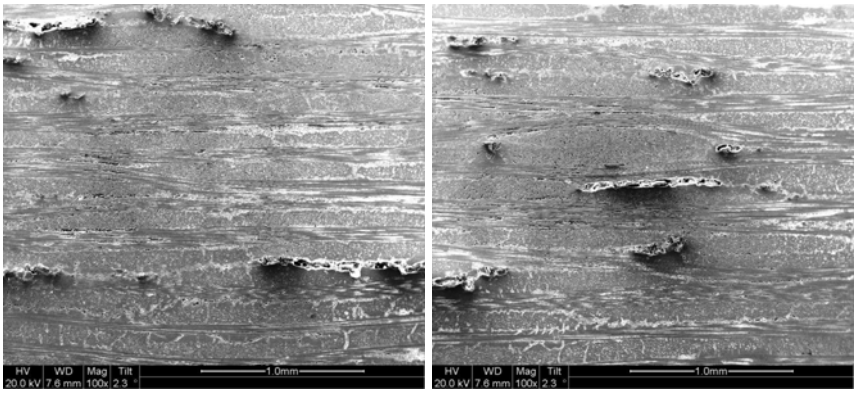

**Figure 117. SEM micrographs of polished material from composite C1 specimen tested at 1300 °C in steam with maximum fatigue stress $\sigma_{max}$ = 140 MPa**

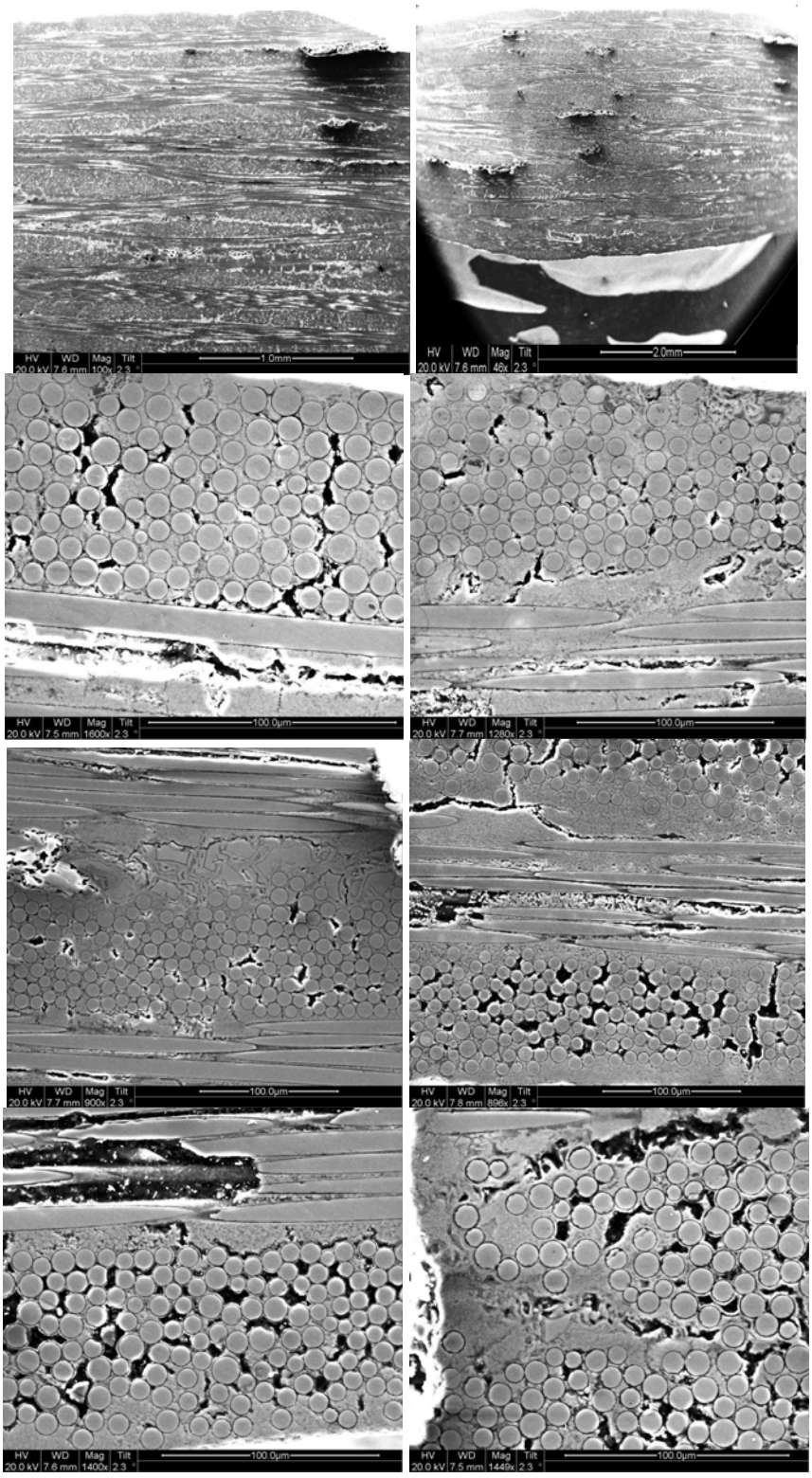

**Figure 118. SEM micrographs of polished material from composite C1 specimen tested at 1300 °C in steam with maximum fatigue stress $\sigma_{max}$ = 140 MPa**

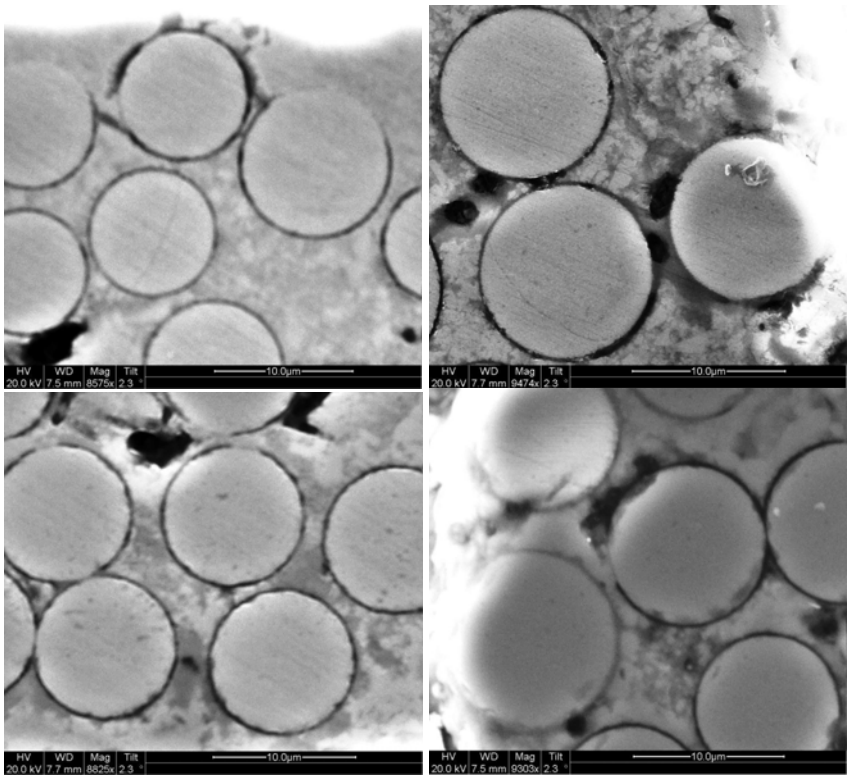

**Figure 119. SEM micrographs of polished material from composite C1 specimen tested at 1300 °C in steam with maximum fatigue stress $\sigma_{max}$ = 140 MPa**

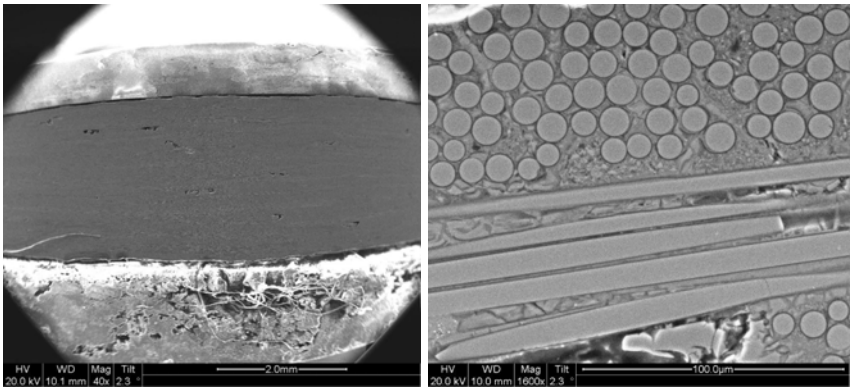

**Figure 120. SEM micrographs of polished composite C2 virgin material**

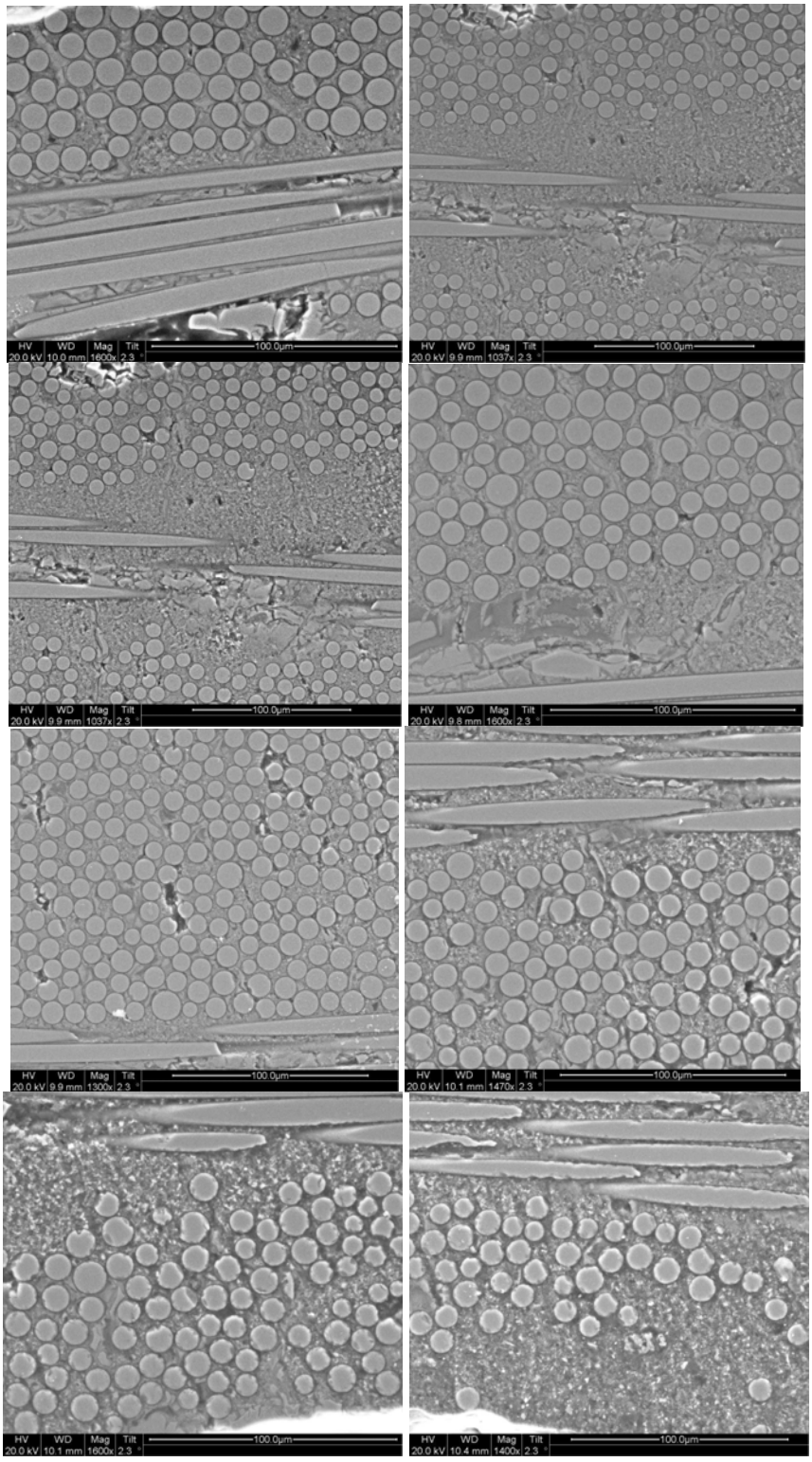

**Figure 121. SEM micrographs of polished composite C2 virgin material**

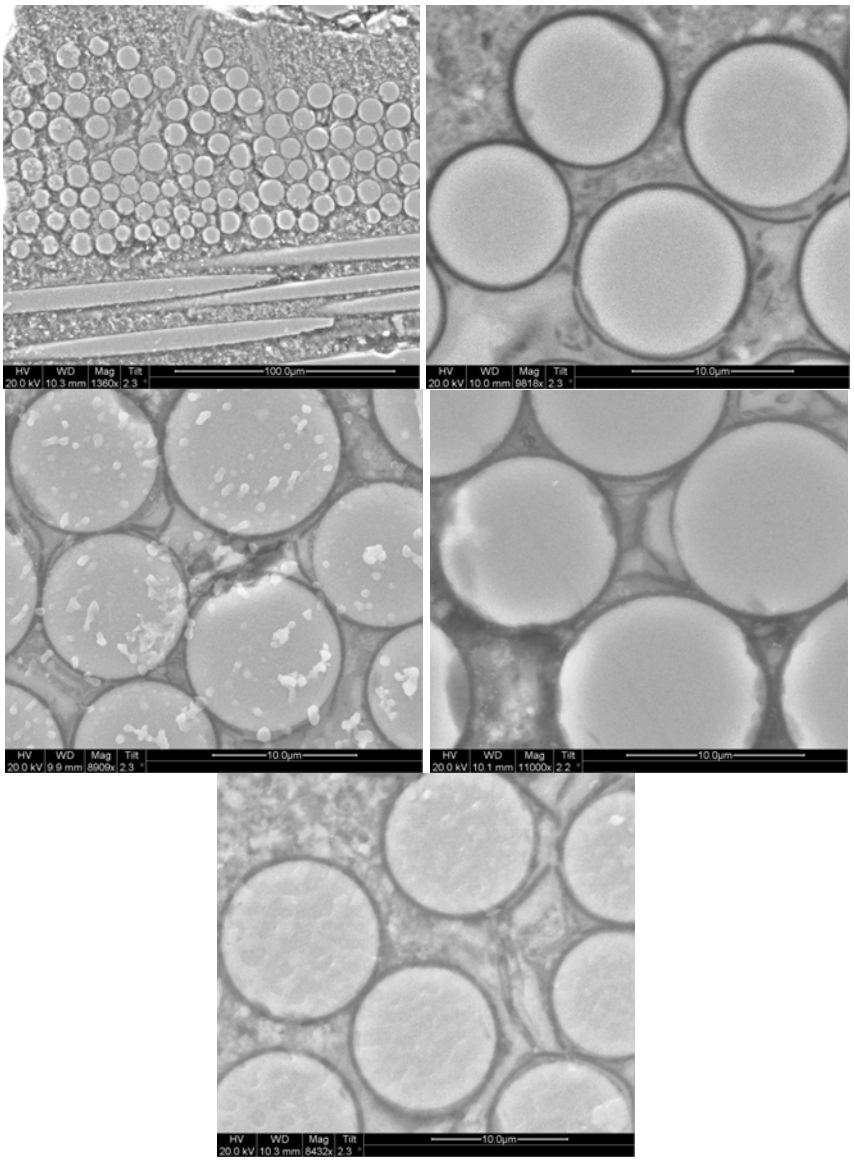


**Figure 122. SEM micrographs of polished composite C2 virgin material**

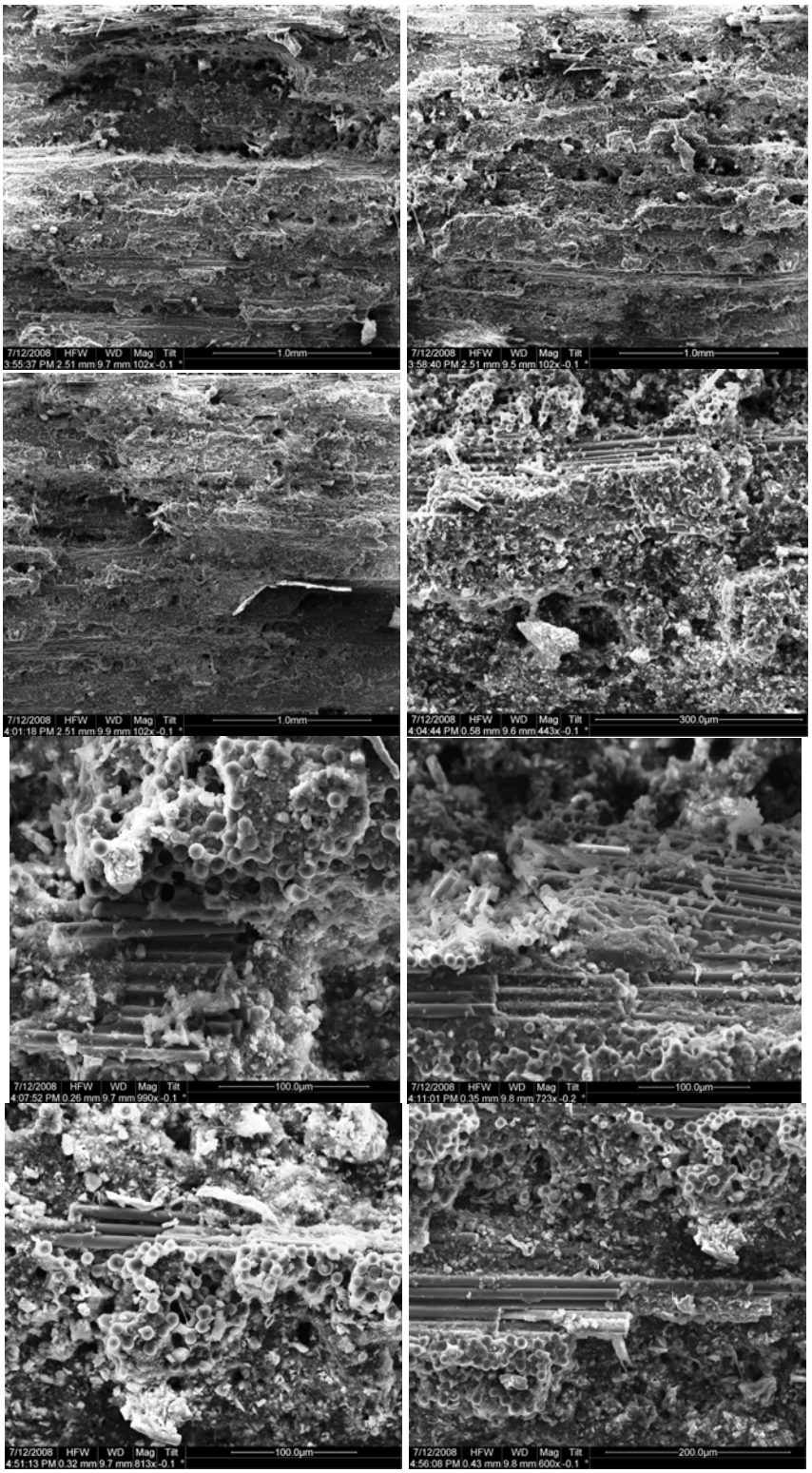

**Figure 123. Fracture surface SEM micrographs of as-processed composite C2 specimen**

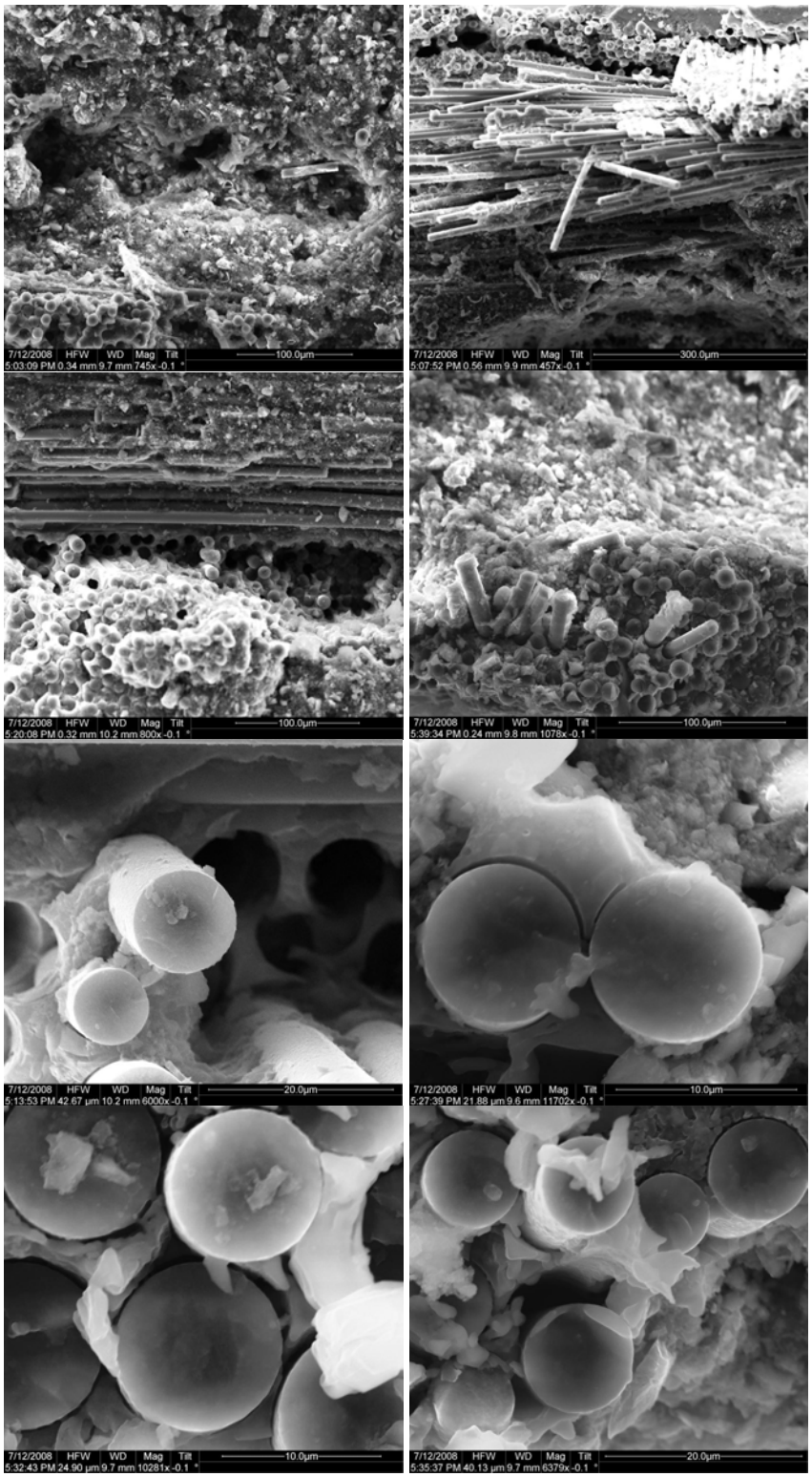


**Figure 124. Fracture surface SEM micrographs of as-processed composite C2 specimen**

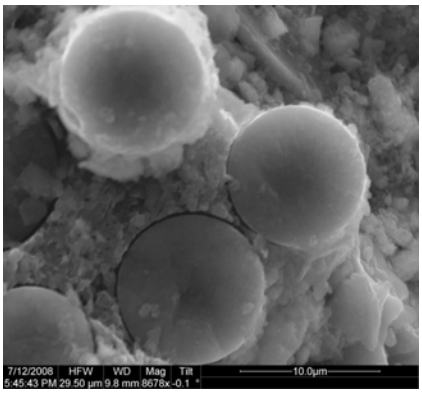


**Figure 125. Fracture surface SEM micrographs of as-processed composite C2 specimen**

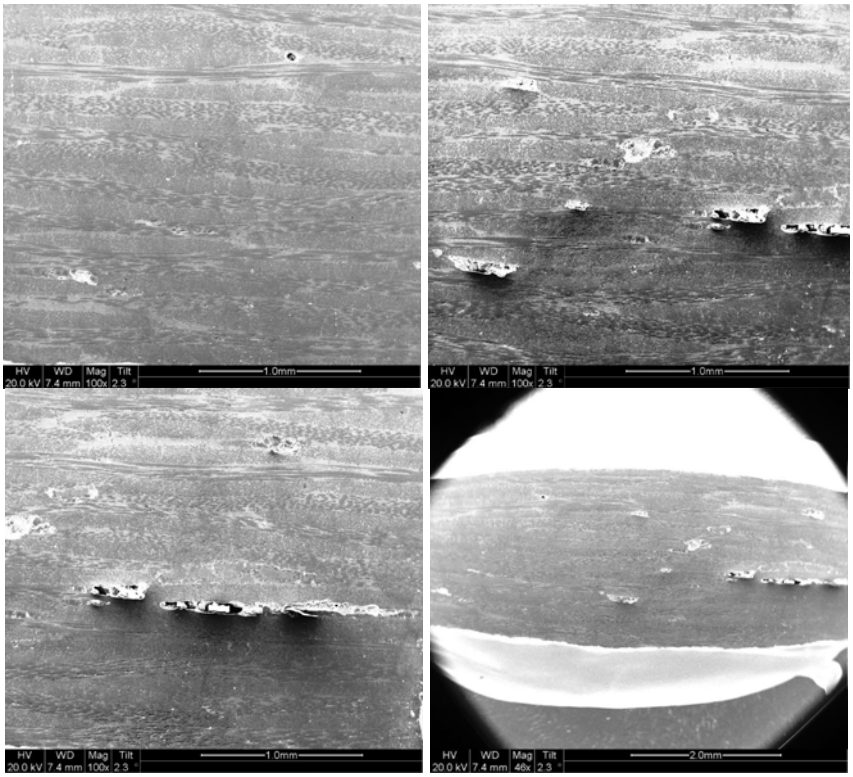


**Figure 126. SEM micrographs of polished as-processed composite C2 specimen**

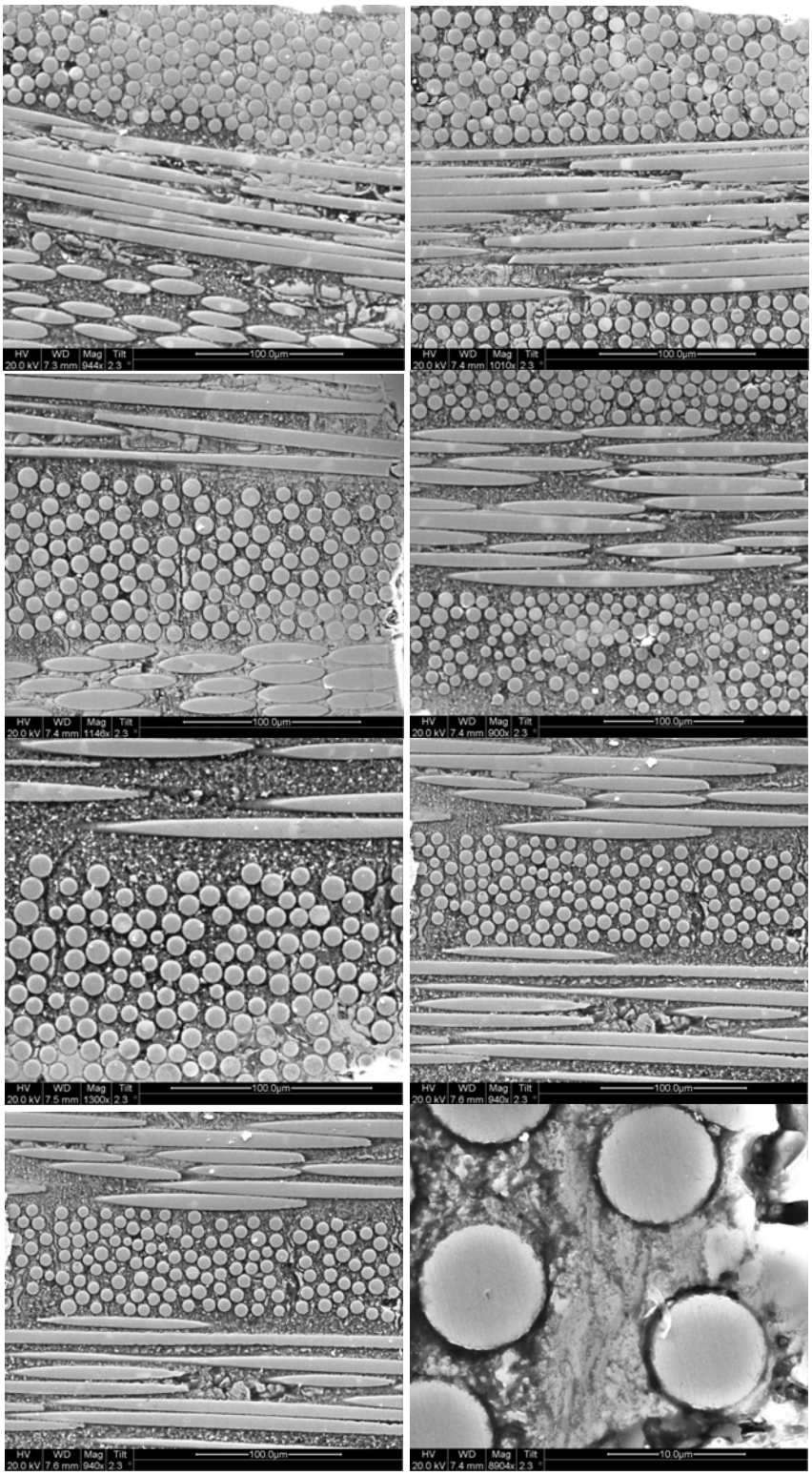


**Figure 127. SEM micrographs of polished as-processed composite C2 specimen**

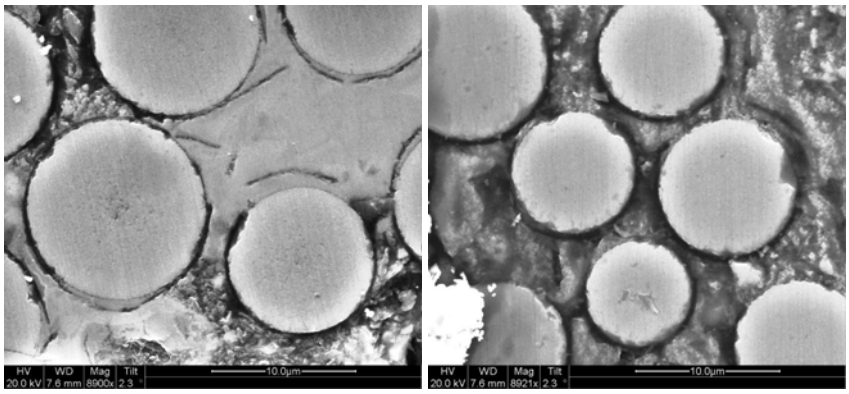

**Figure 128. SEM micrographs of polished as-processed composite C2 specimen**

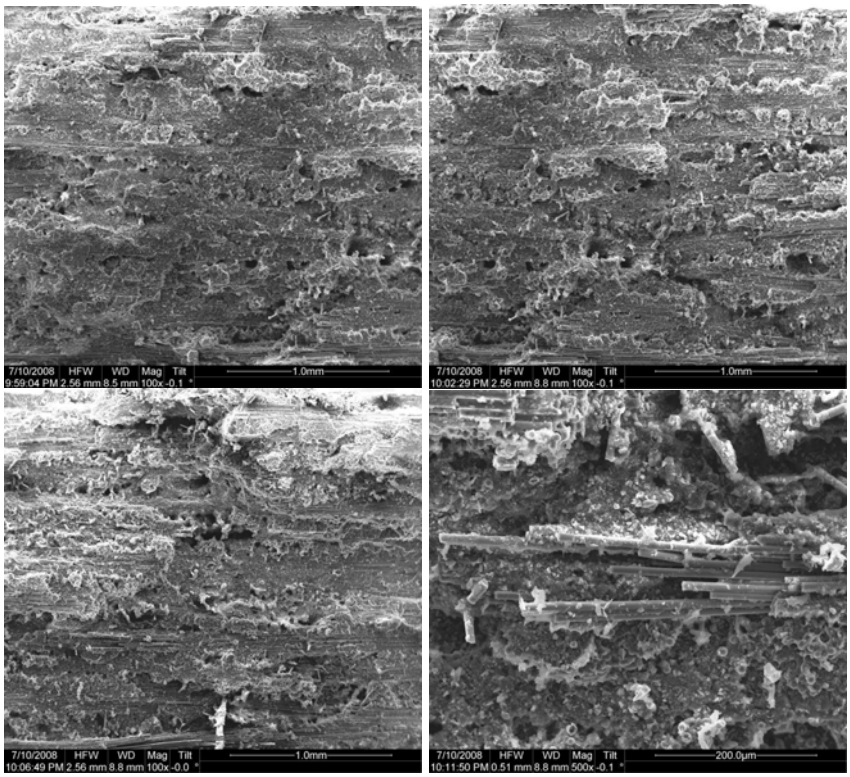

**Figure 129. Fracture surface SEM micrographs of composite C2 specimen tested at 1300 °C in air with maximum fatigue stress $\sigma_{max}$ = 140 MPa**

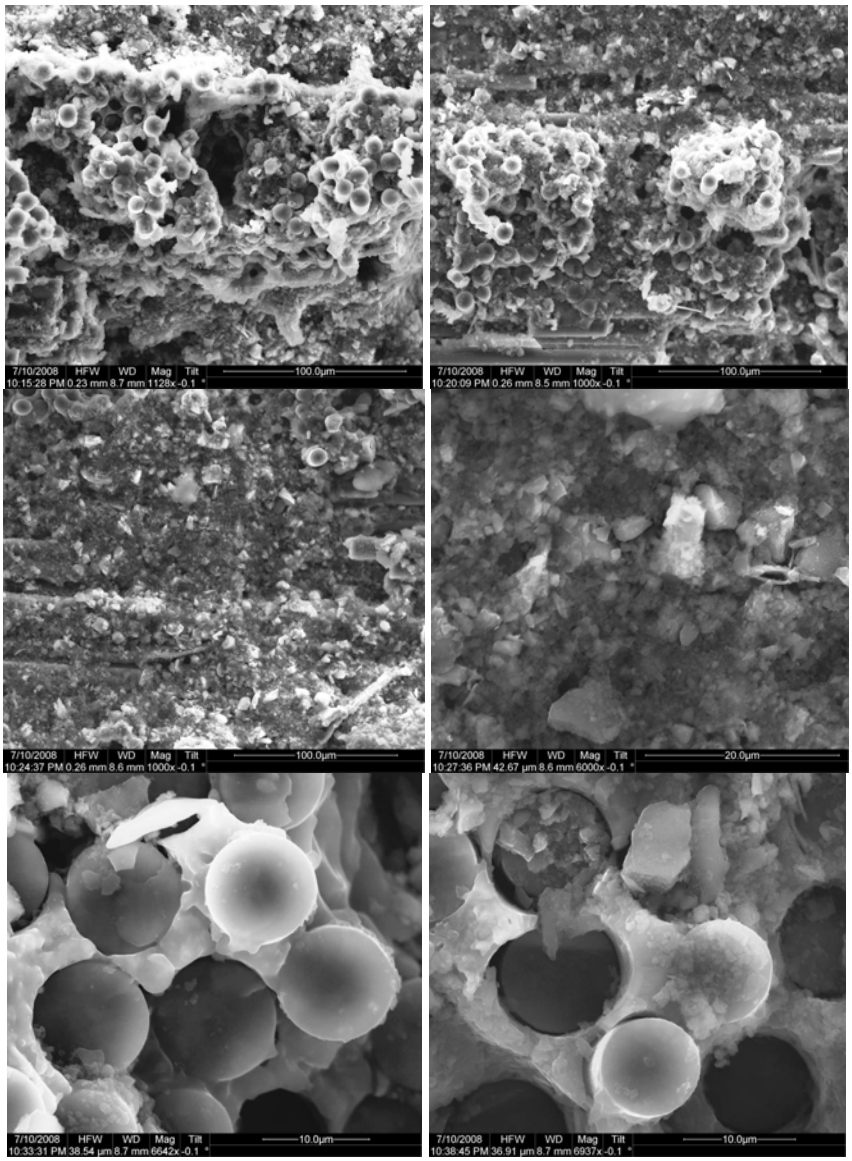


**Figure 130. Fracture surface SEM micrographs of composite C2 specimen tested at 1300 °C in air with maximum fatigue stress $\sigma_{max}$ = 140 MPa**

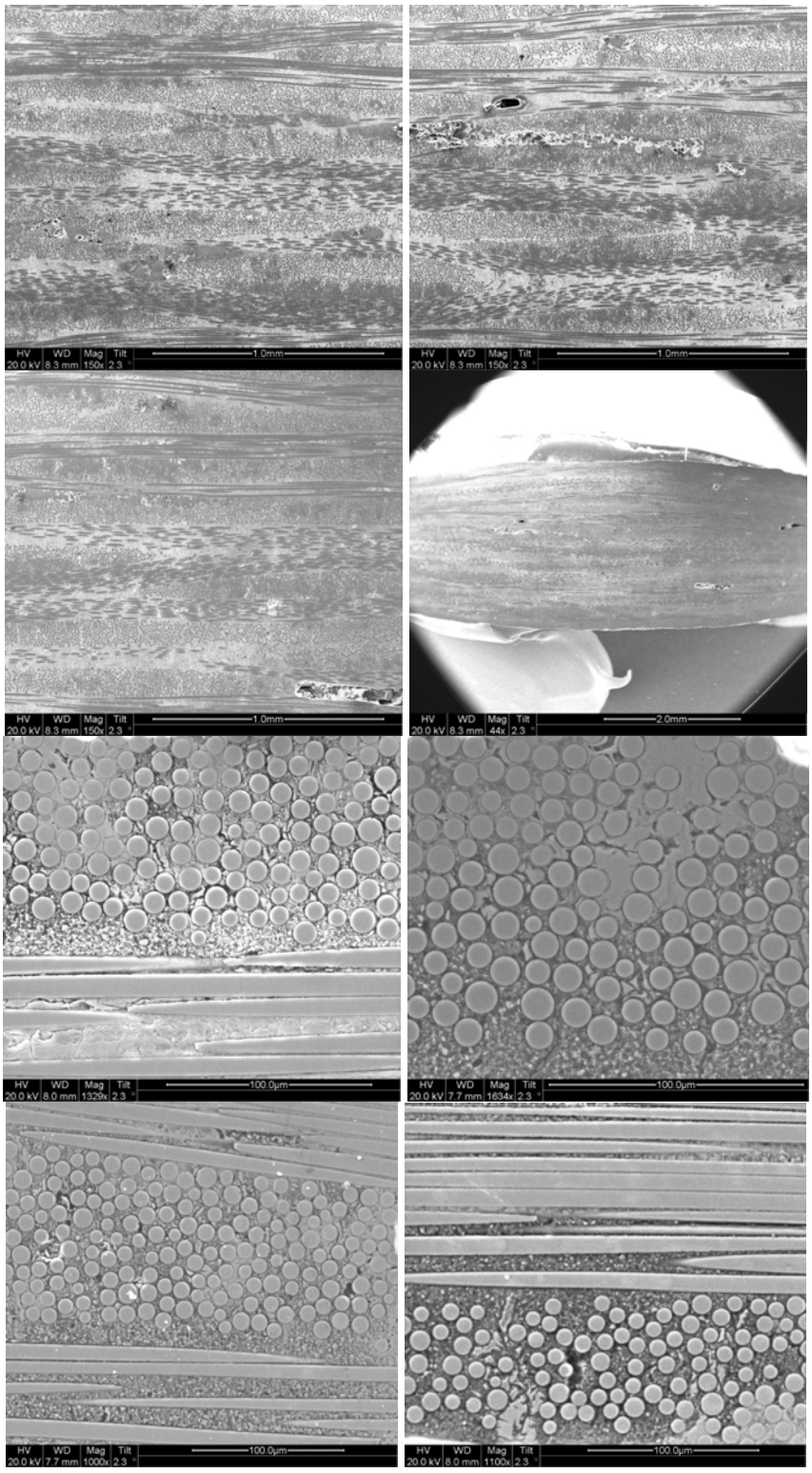

**Figure 131. SEM micrographs of polished material from composite C2 specimen tested at 1300 °C in air with maximum fatigue stress $\sigma_{max}$ = 140 MPa**

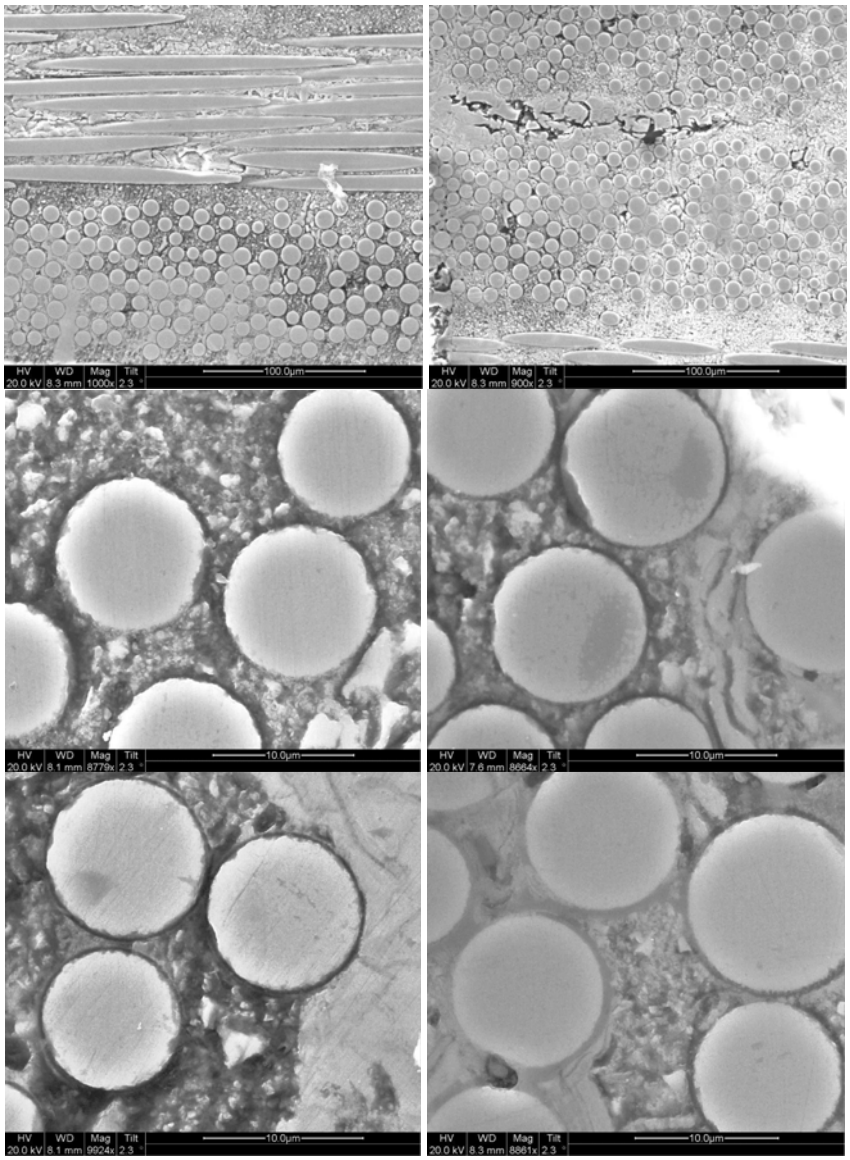

**Figure 132. SEM micrographs of polished material from composite C2 specimen tested at 1300 °C in air with maximum fatigue stress $\sigma_{max}$ = 140 MPa**

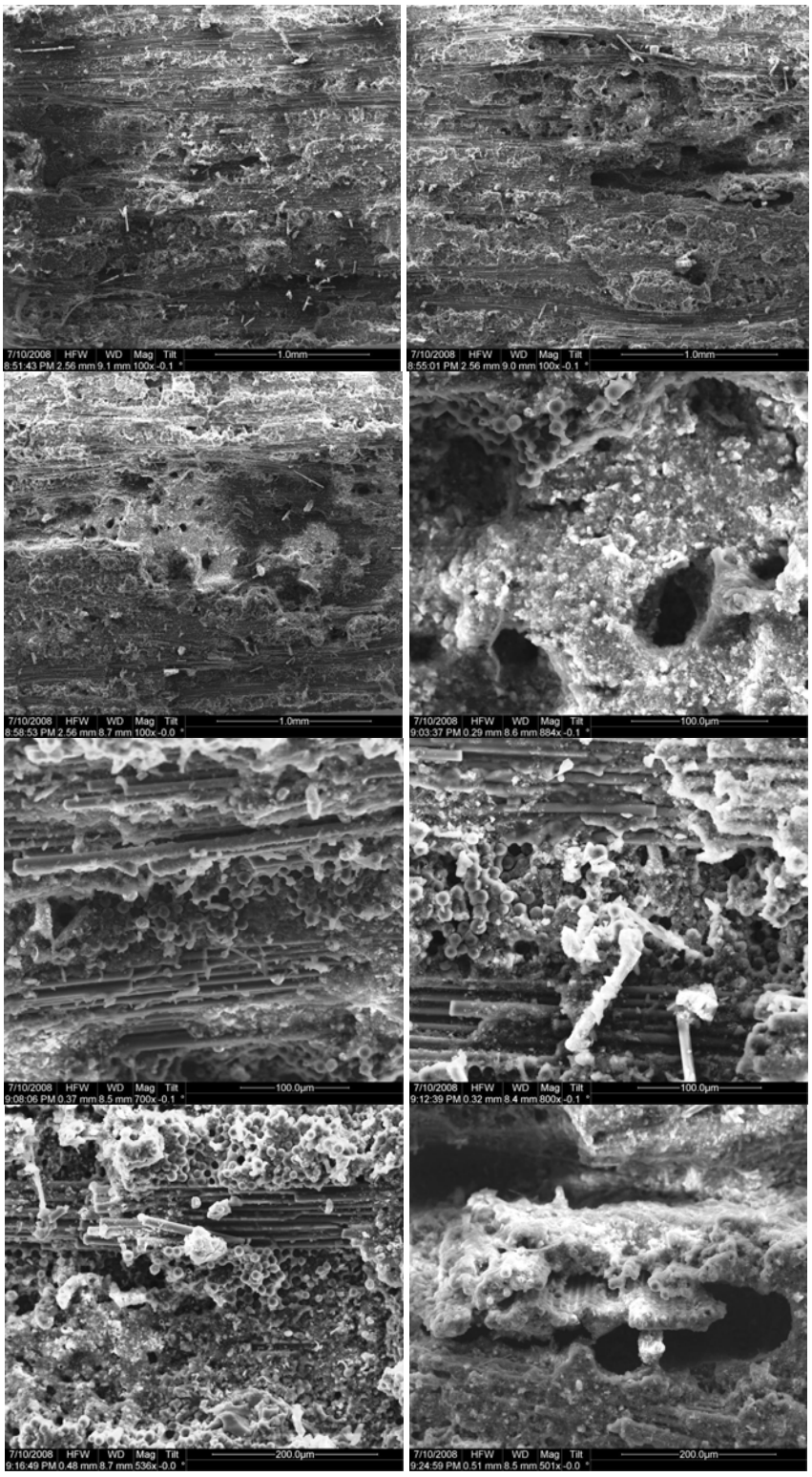

**Figure 133. Fracture surface SEM micrographs of composite C2 specimen tested at 1300 °C in air with maximum fatigue stress $\sigma_{max}$ = 180 MPa**

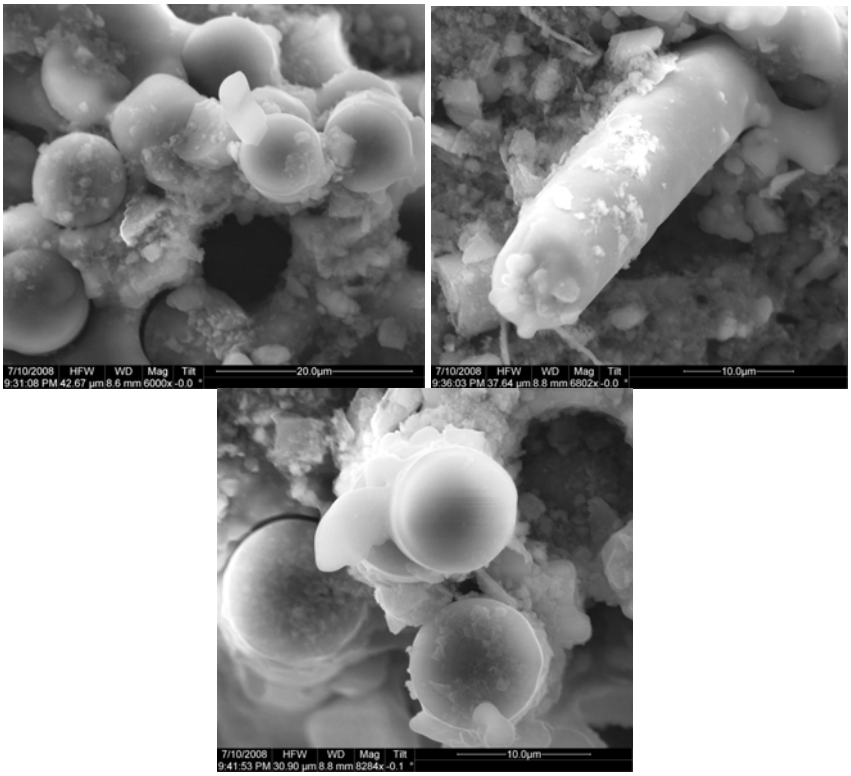

**Figure 134. Fracture surface SEM micrographs of composite C2 specimen tested at 1300 °C in air with maximum fatigue stress $\sigma_{max}$ = 180 MPa**

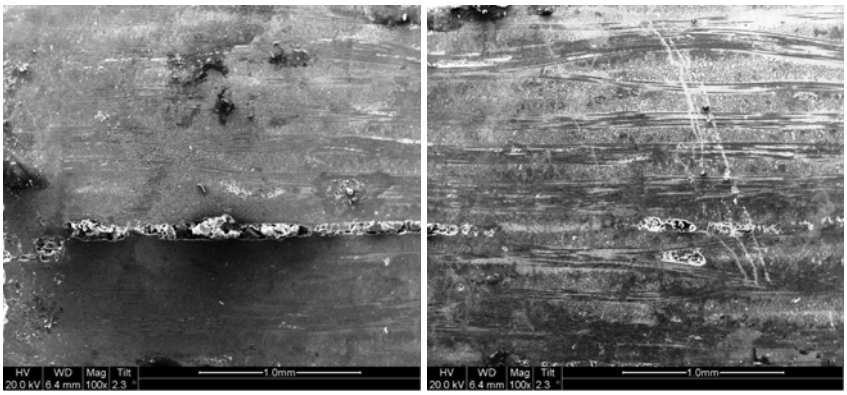

**Figure 135. SEM micrographs of polished material from composite C2 specimen tested at 1300 °C in air with maximum fatigue stress $\sigma_{max}$ = 180 MPa**

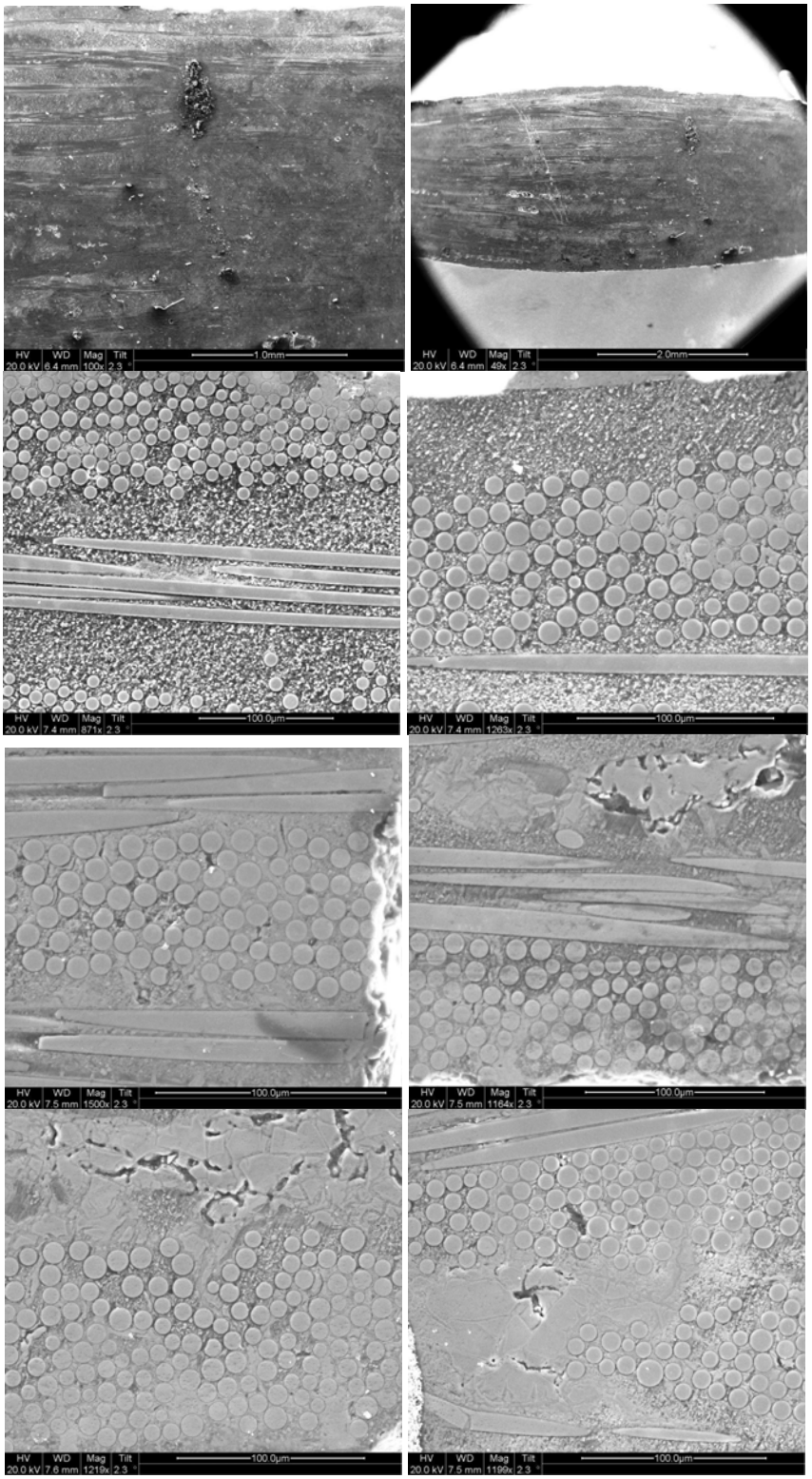

**Figure 136. SEM micrographs of polished material from composite C2 specimen tested at 1300 °C in air with maximum fatigue stress $\sigma_{max}$ = 180 MPa**

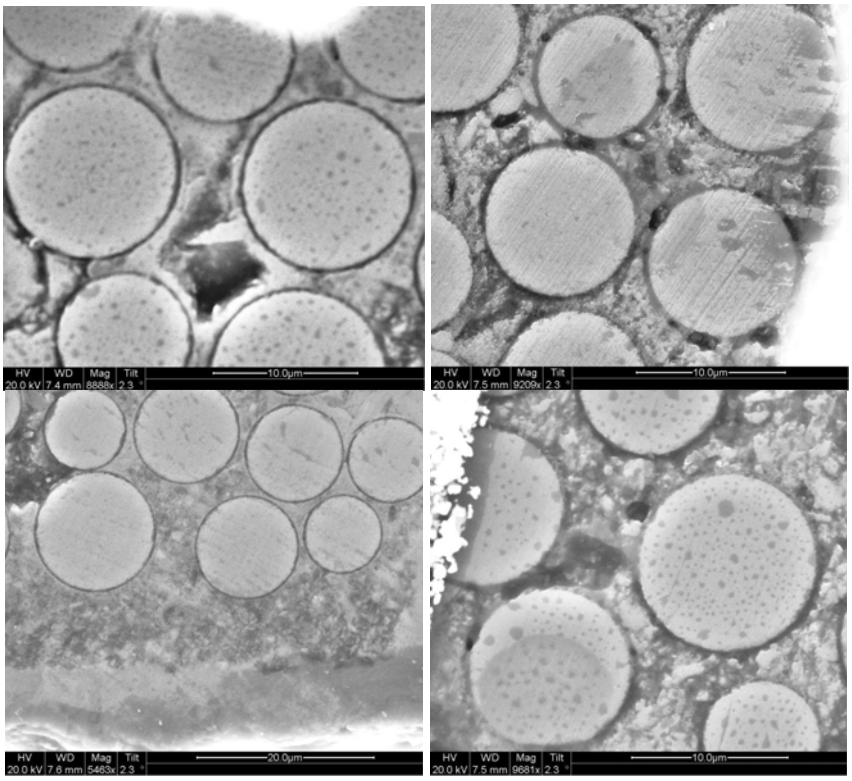

**Figure 137. SEM micrographs of polished material from composite C2 specimen tested at 1300 °C in air with maximum fatigue stress $\sigma_{max}$ = 180 MPa**

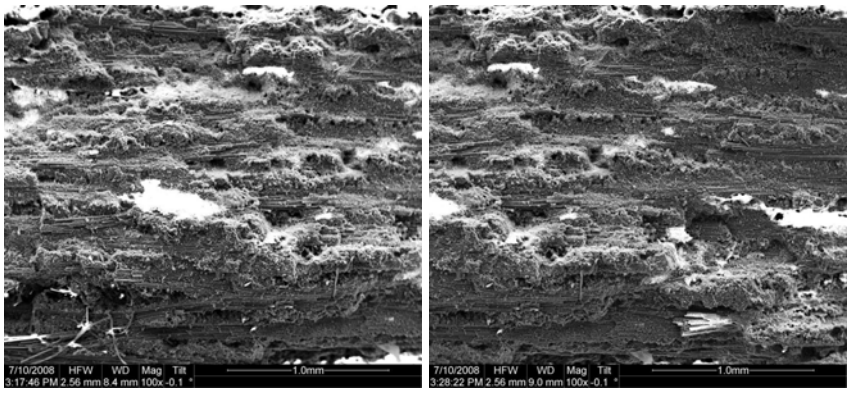

**Figure 138. Fracture surface SEM micrographs of composite C2 specimen tested at 1300 °C in steam with maximum fatigue stress $\sigma_{max}$ = 140 MPa**

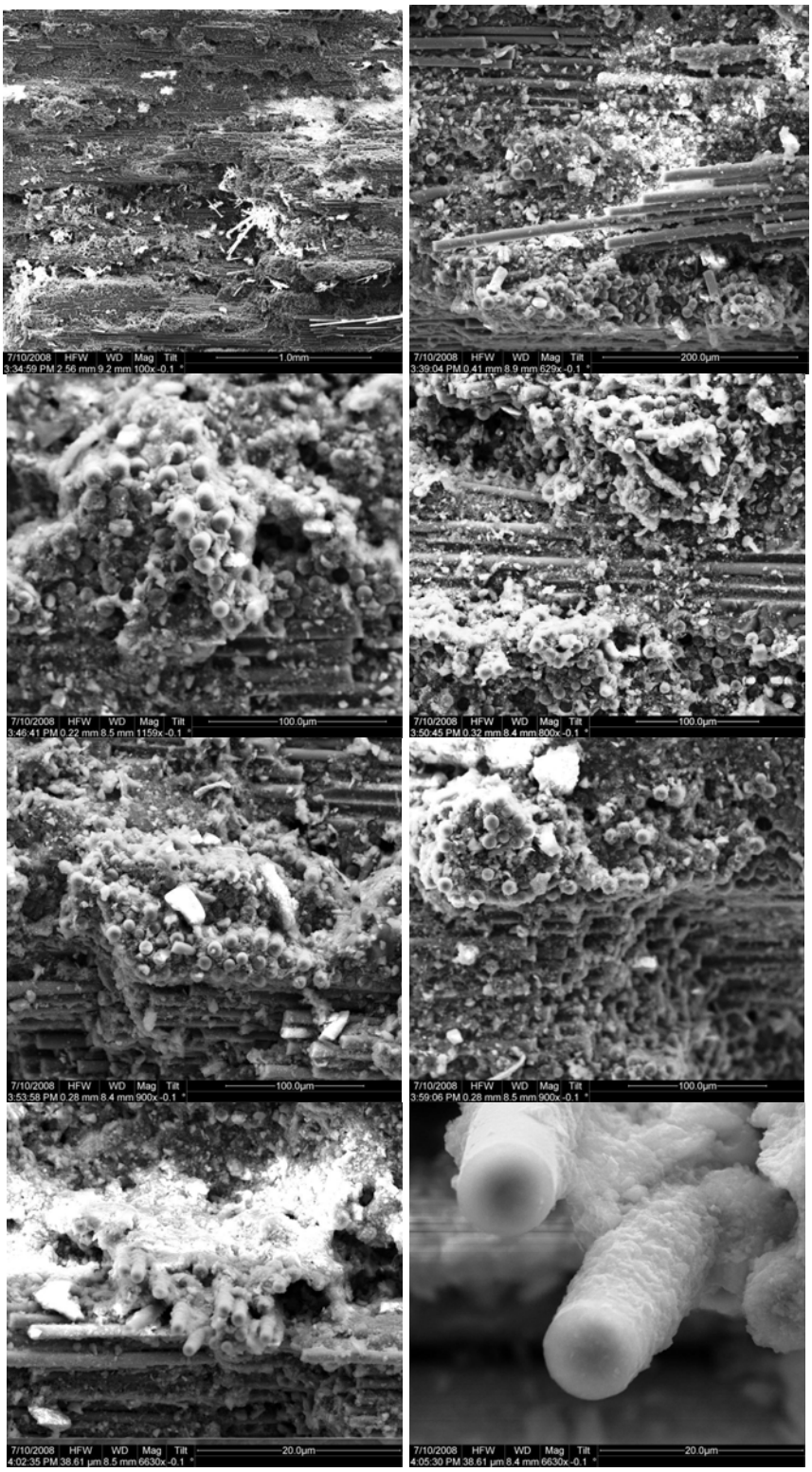

**Figure 139. Fracture surface SEM micrographs of composite C2 specimen tested at 1300 °C in steam with maximum fatigue stress $\sigma_{max}$ = 140 MPa**

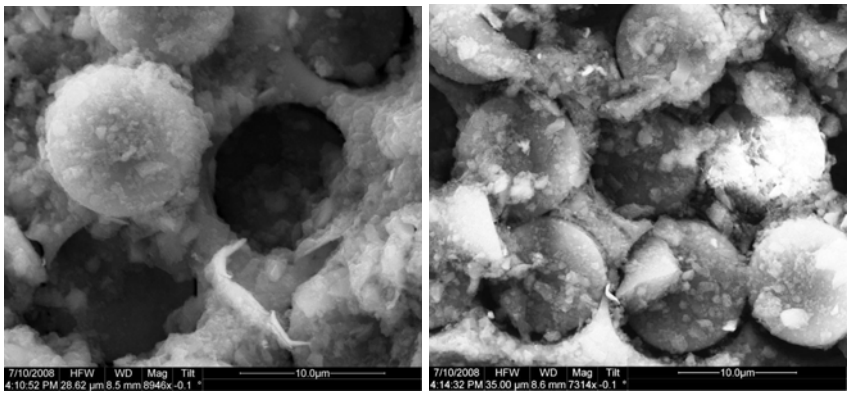

**Figure 140. SEM micrographs of polished material from composite C2 specimen tested at 1300 °C in steam with maximum fatigue stress $\sigma_{max}$ = 140 MPa**

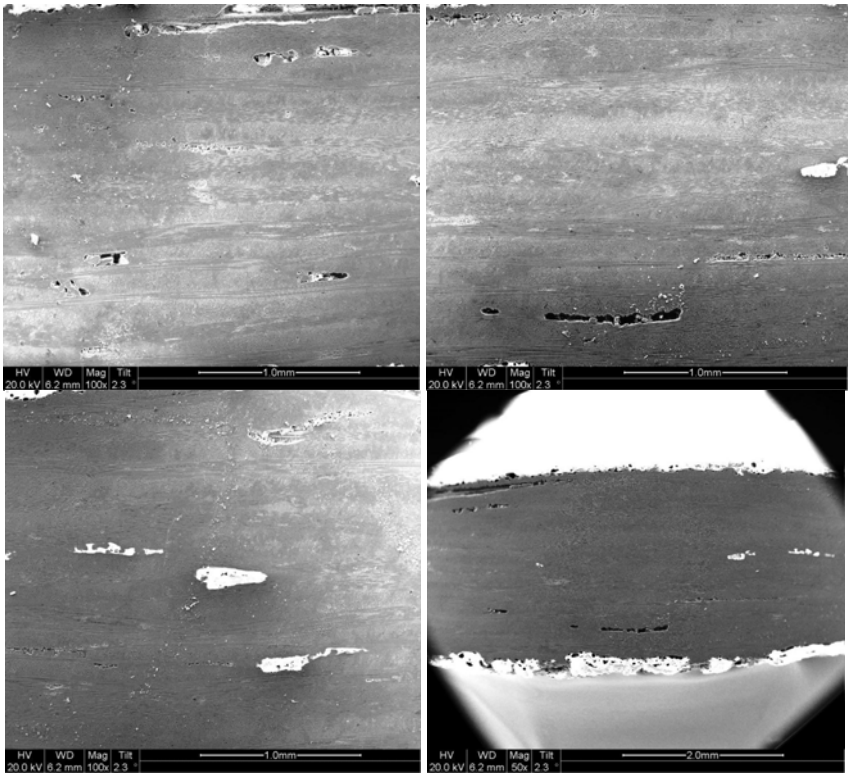

**Figure 141. SEM micrographs of polished material from composite C2 specimen tested at 1300 °C in steam with maximum fatigue stress $\sigma_{max}$ = 140 MPa**

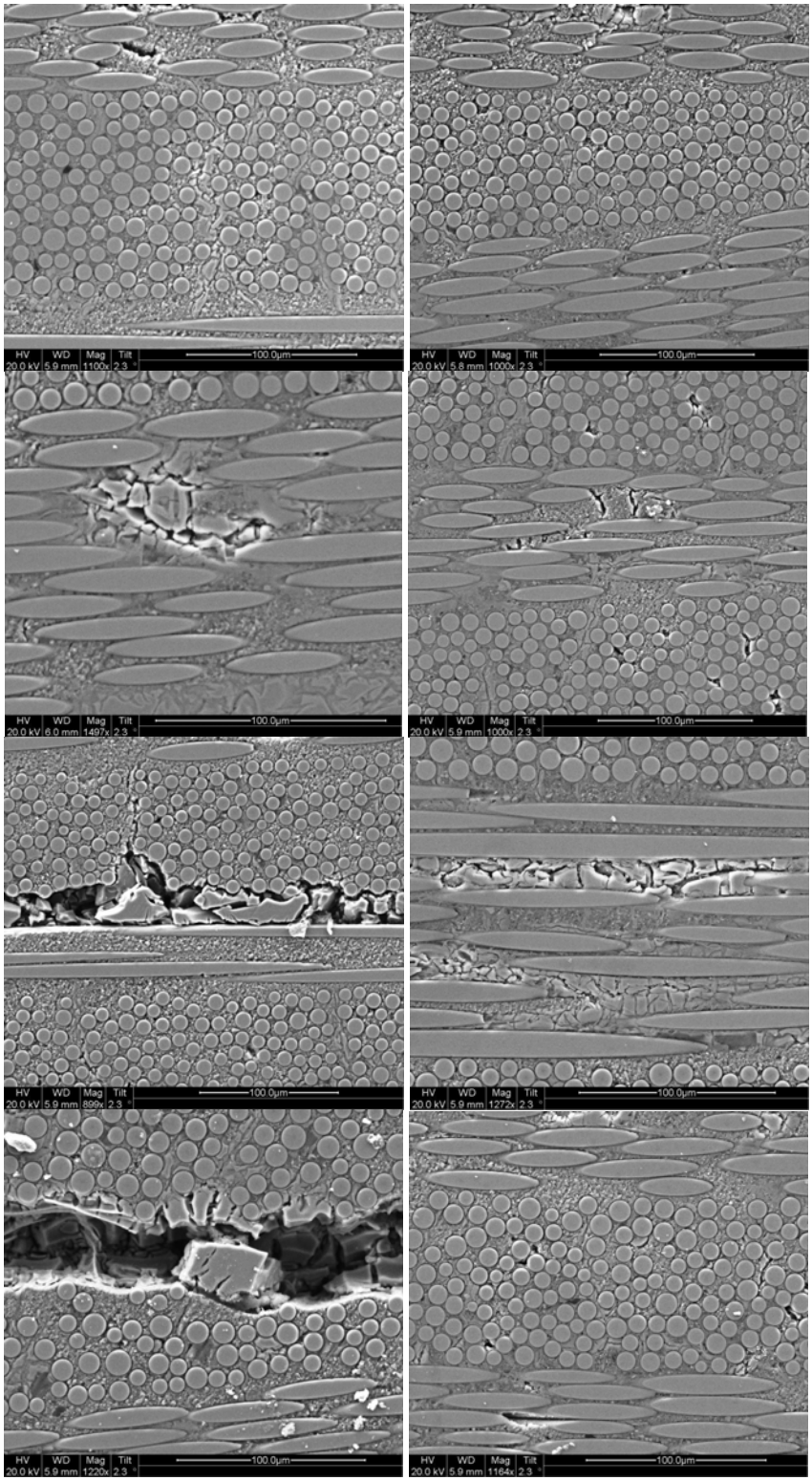

**Figure 142. SEM micrographs of polished material from composite C1 specimen tested at 1300 °C in steam with maximum fatigue stress $\sigma_{max}$ = 140 MPa**

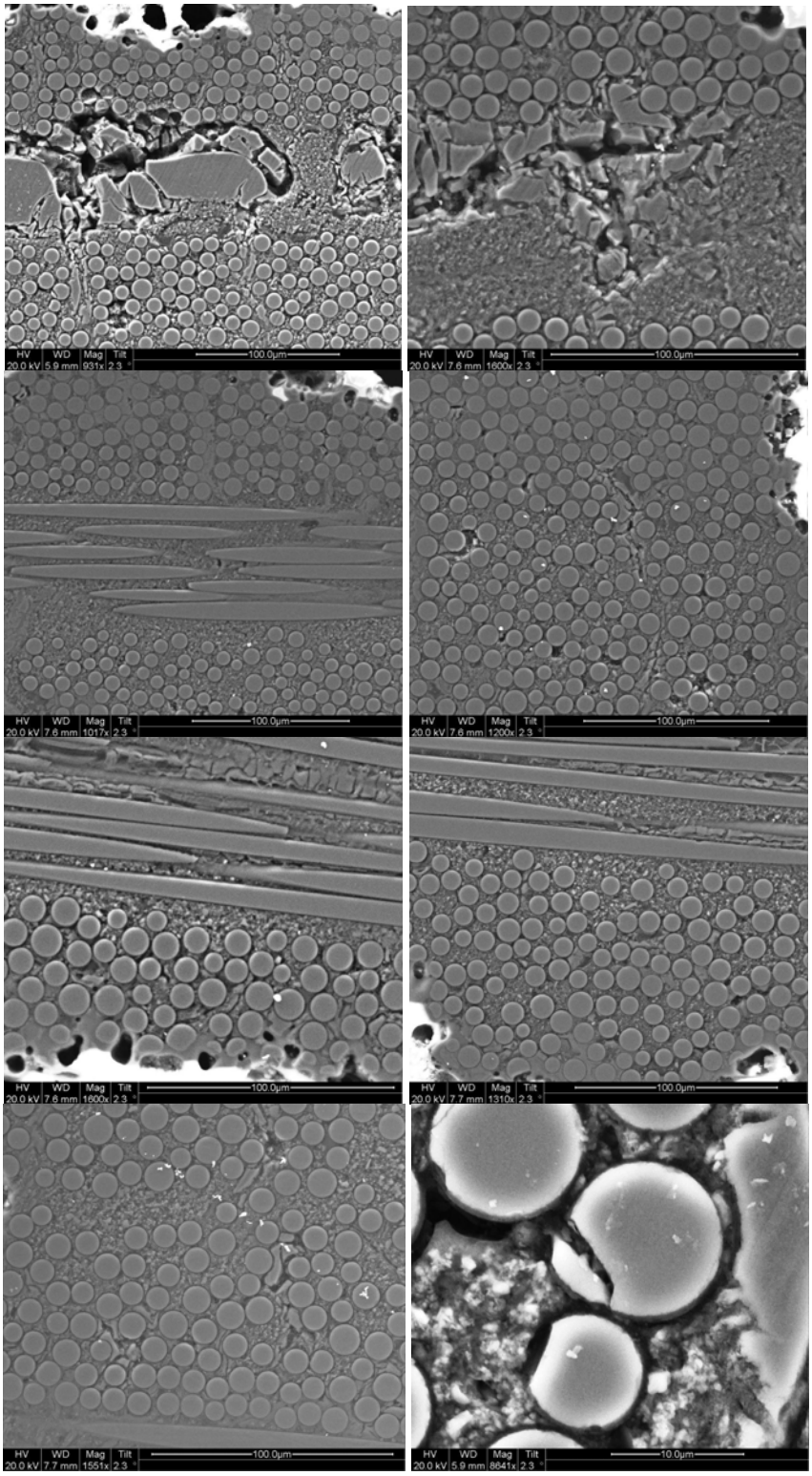

**Figure 143. SEM micrographs of polished material from composite C1 specimen tested at 1300 °C in steam with maximum fatigue stress $\sigma_{max}$ = 140 MPa**

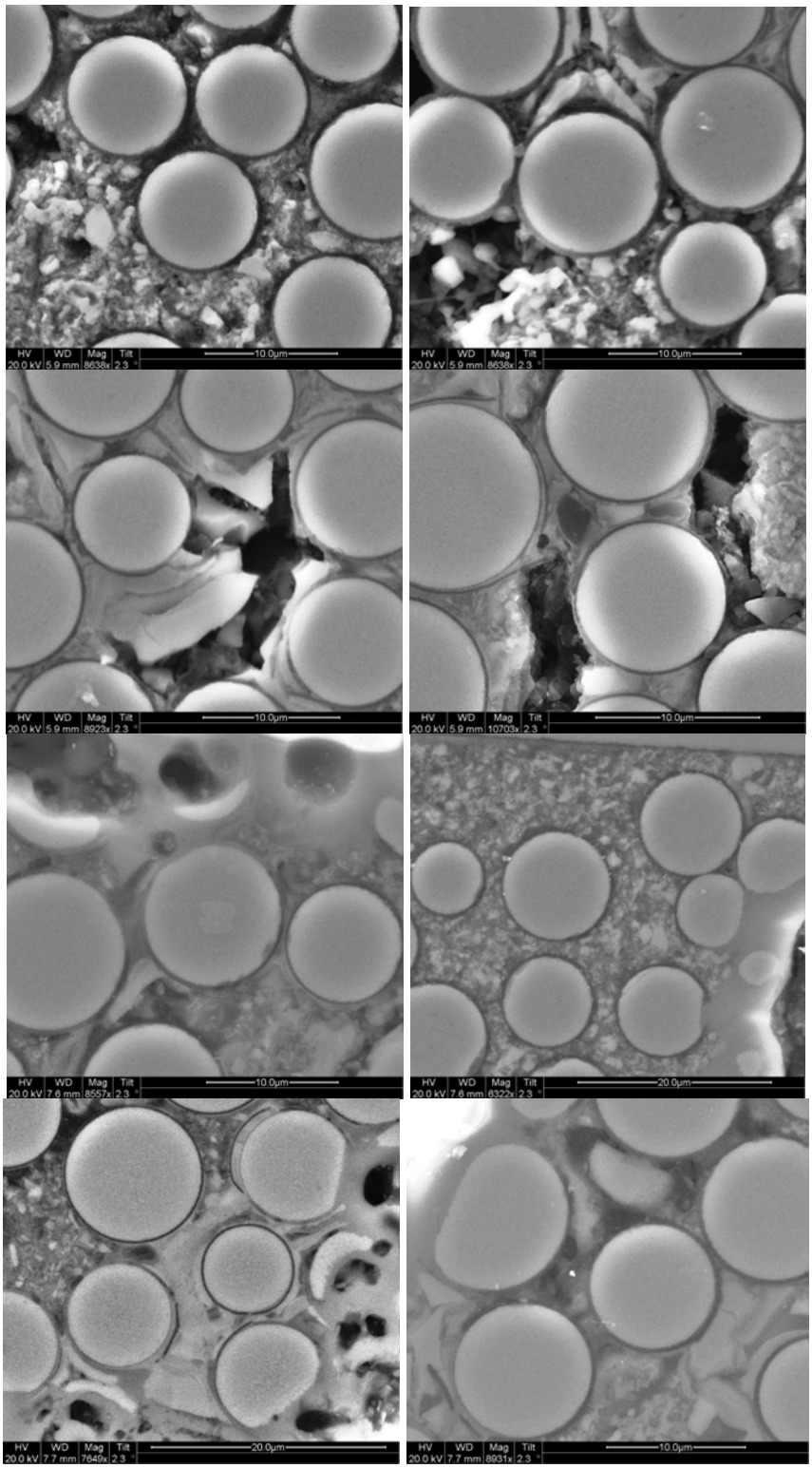

**Figure 144. SEM micrographs of polished material from composite C1 specimen tested at 1300 °C in steam with maximum fatigue stress $\sigma_{max}$ = 140 MPa**

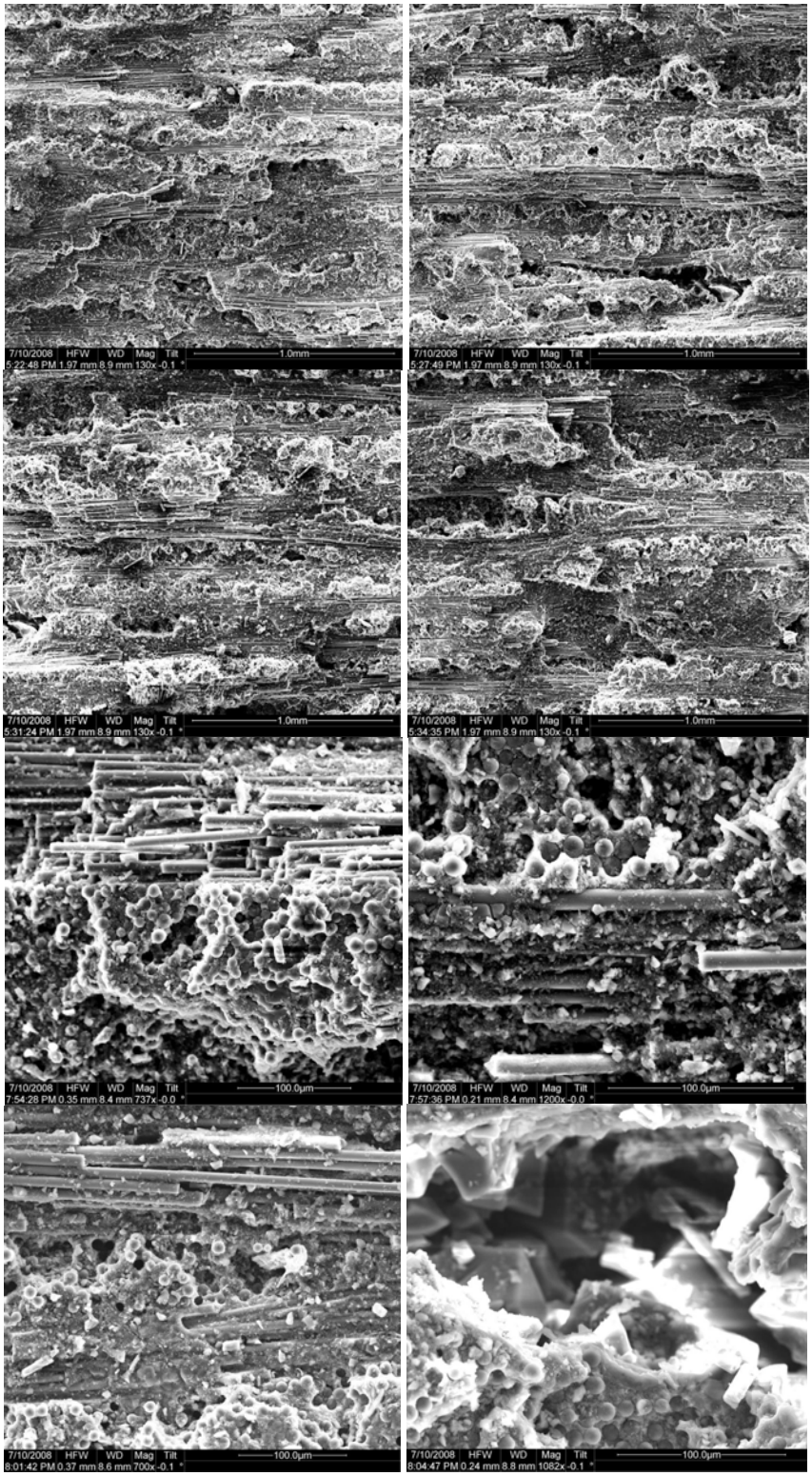

**Figure 145. SEM micrographs of polished material from composite C2 specimen tested at 1300 °C in steam with maximum fatigue stress $\sigma_{max}$ = 180 MPa**

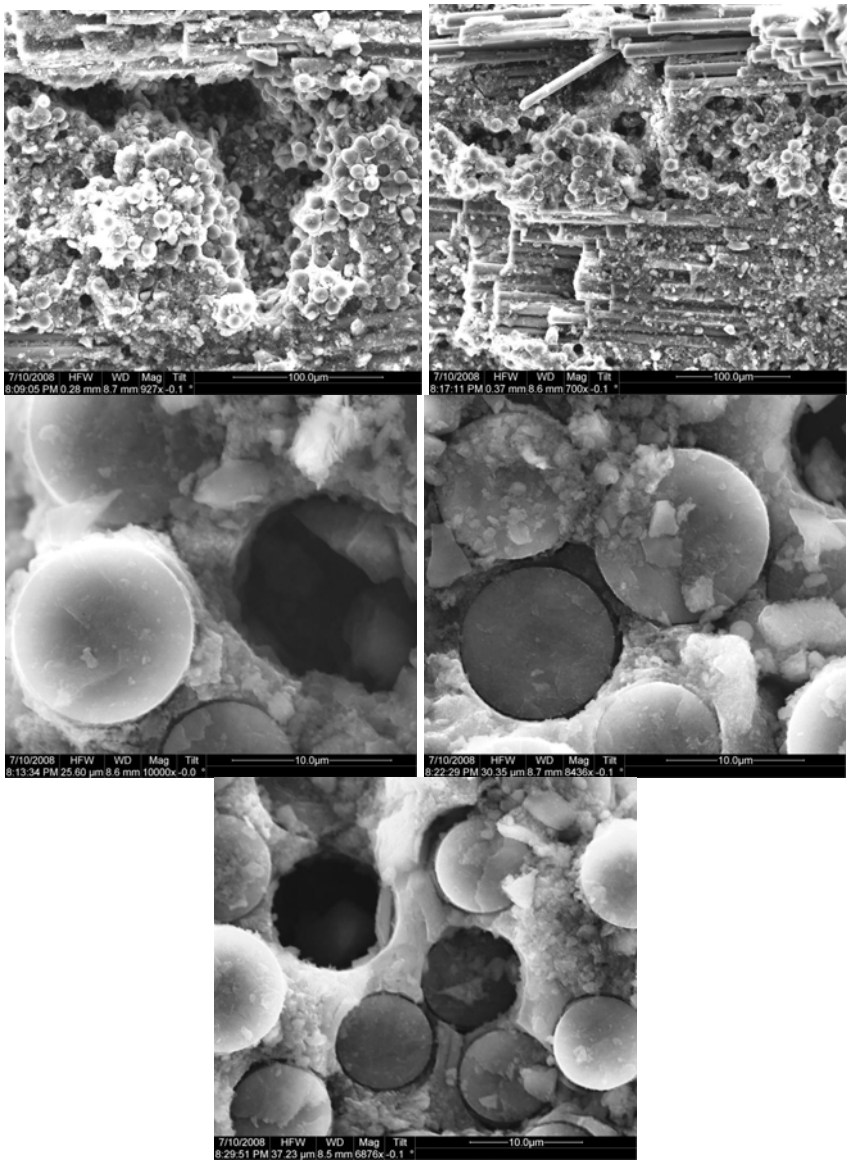

**Figure 146. SEM micrographs of polished material from composite C2 specimen tested at 1300 °C in steam with maximum fatigue stress $\sigma_{max}$ = 180 MPa**

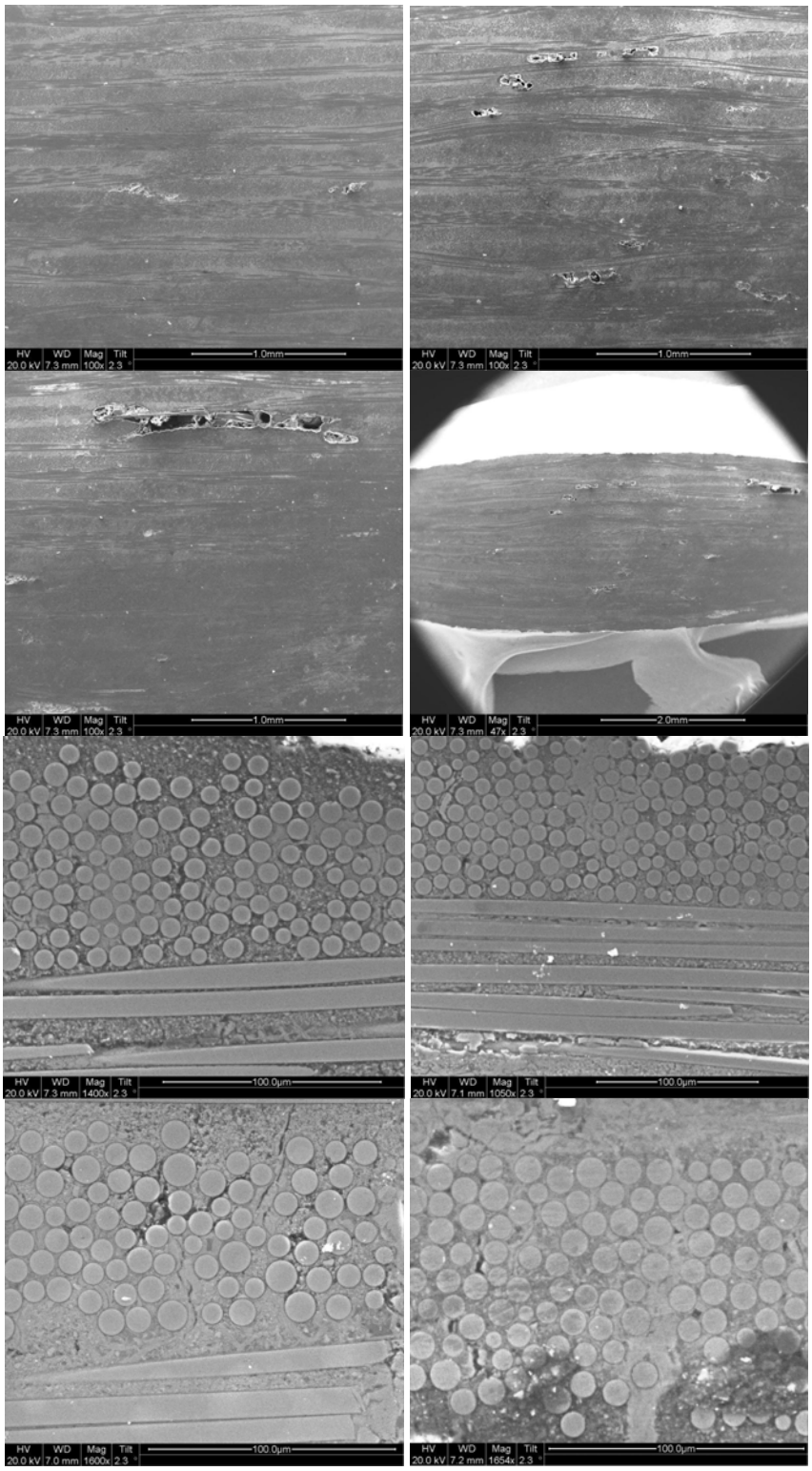

**Figure 147. SEM micrographs of polished material from composite C2 specimen tested at 1300 °C in steam with maximum fatigue stress $\sigma_{max}$ = 180 MPa**

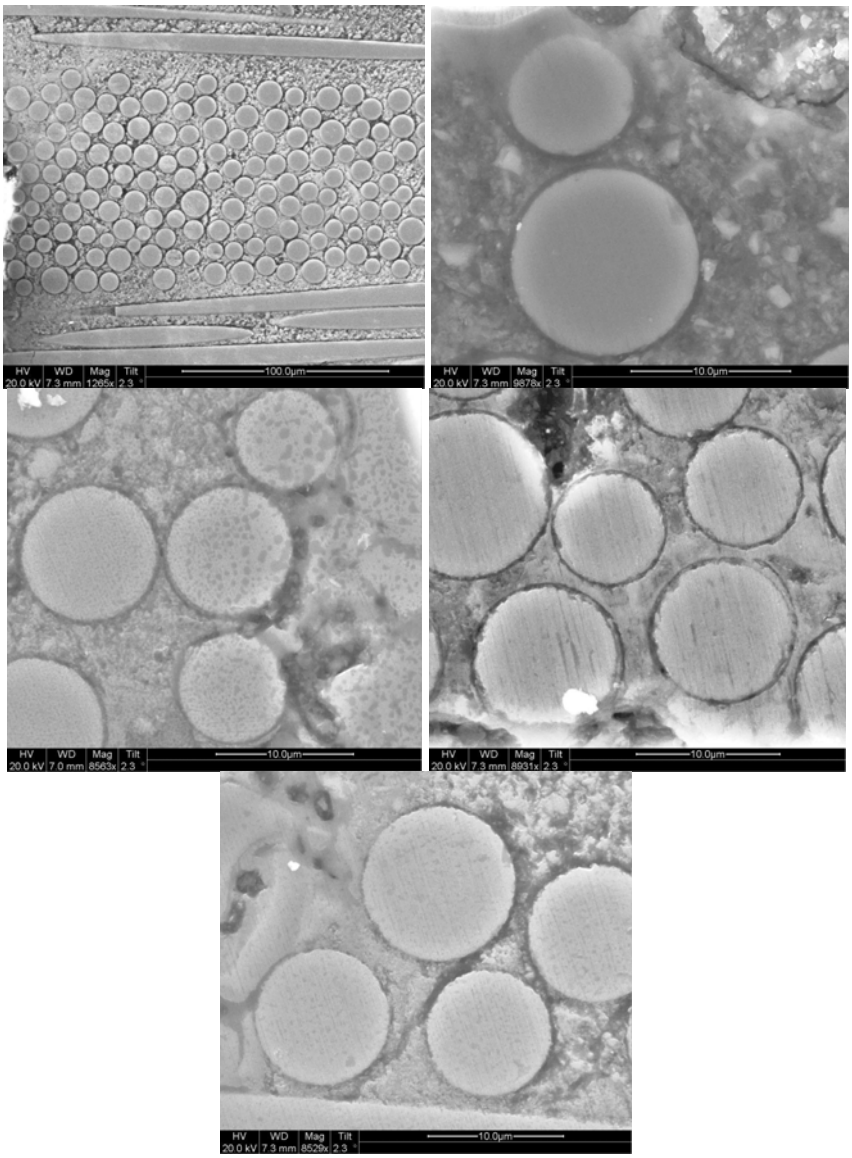

**Figure 148. SEM micrographs of polished material from composite C2 specimen tested at 1300 °C in steam with maximum fatigue stress $\sigma_{max}$ = 180 MPa**

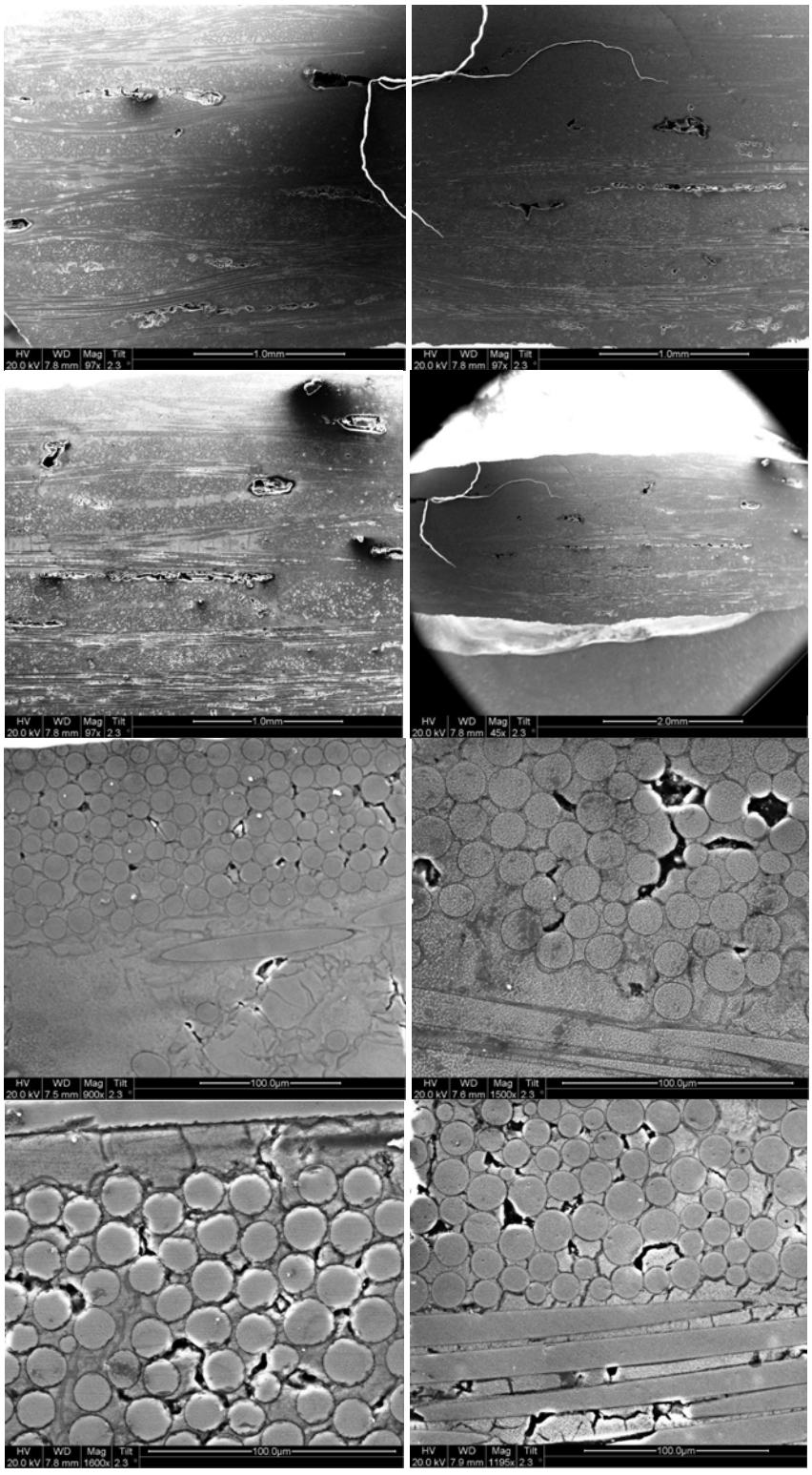


**Figure 149. SEM micrographs of polished composite C3 virgin material**

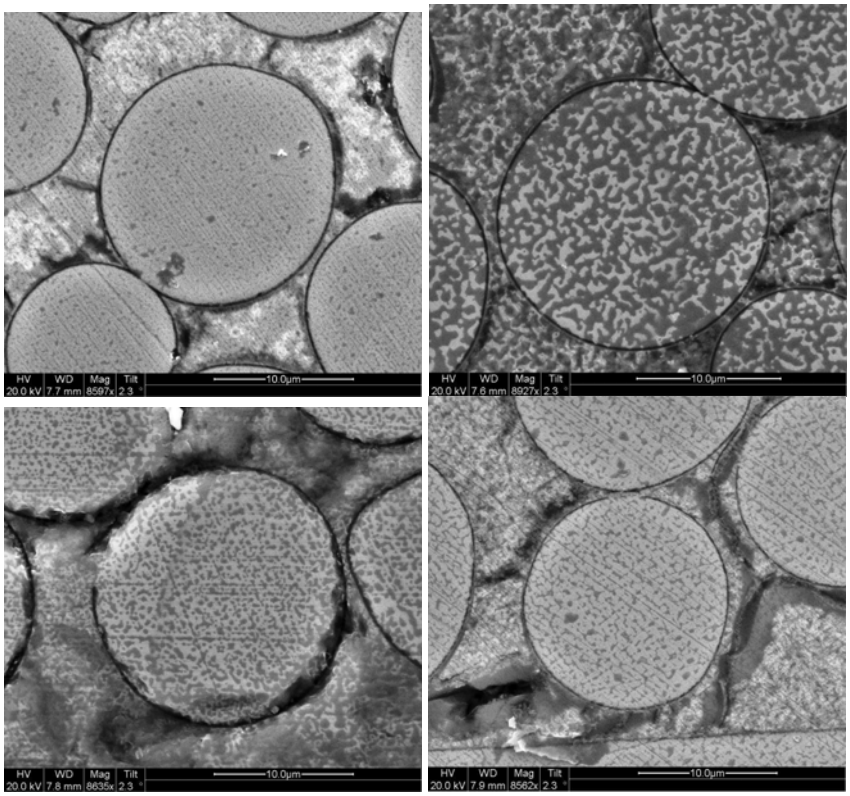


**Figure 150. SEM micrographs of polished composite C3 virgin material**

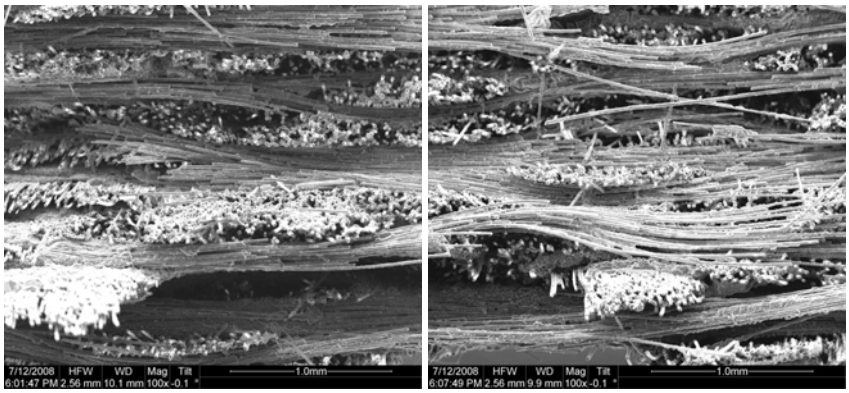


**Figure 151. Fracture surface SEM micrographs of as-processed composite C3 specimen**

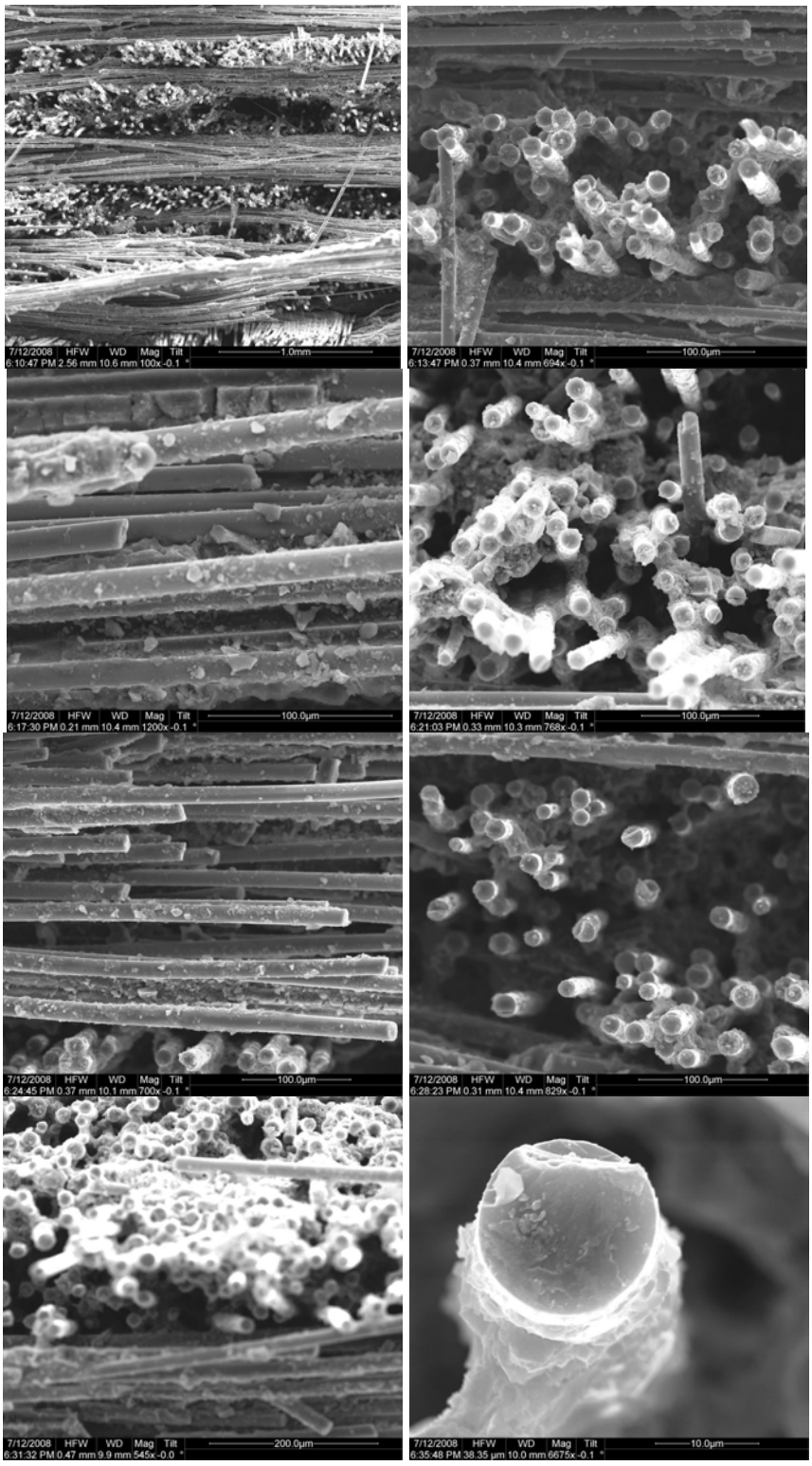


**Figure 152. Fracture surface SEM micrographs of as-processed composite C3 specimen**

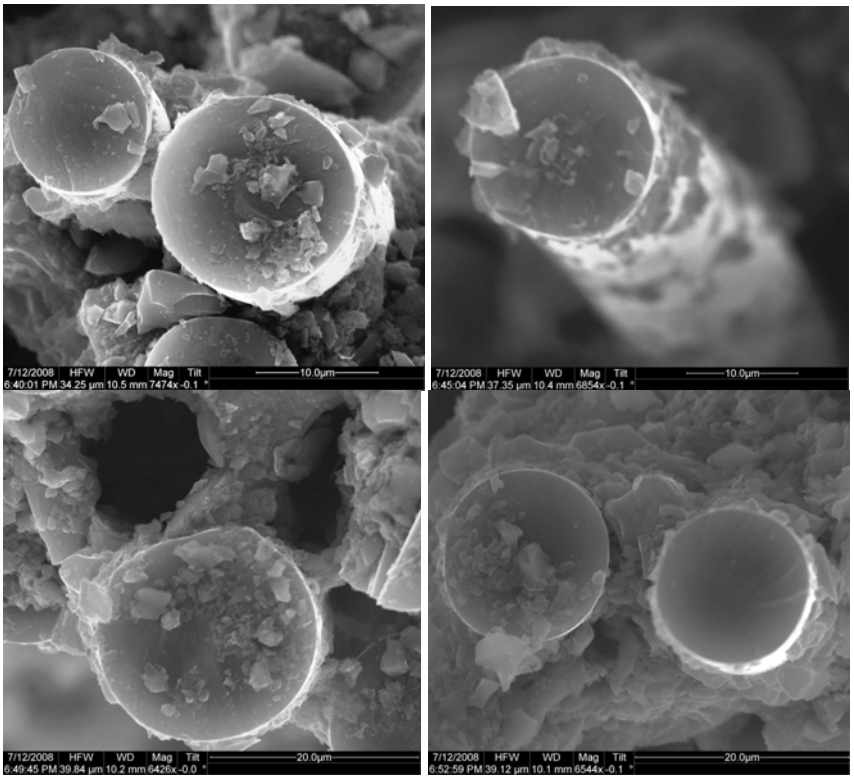

**Figure 153. Fracture surface SEM micrographs of as-processed composite C3 specimen**

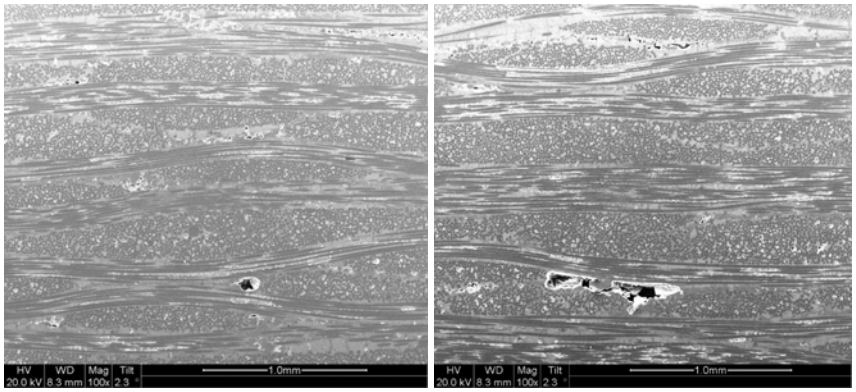

**Figure 154. SEM micrographs of polished as-processed composite C3 specimen**

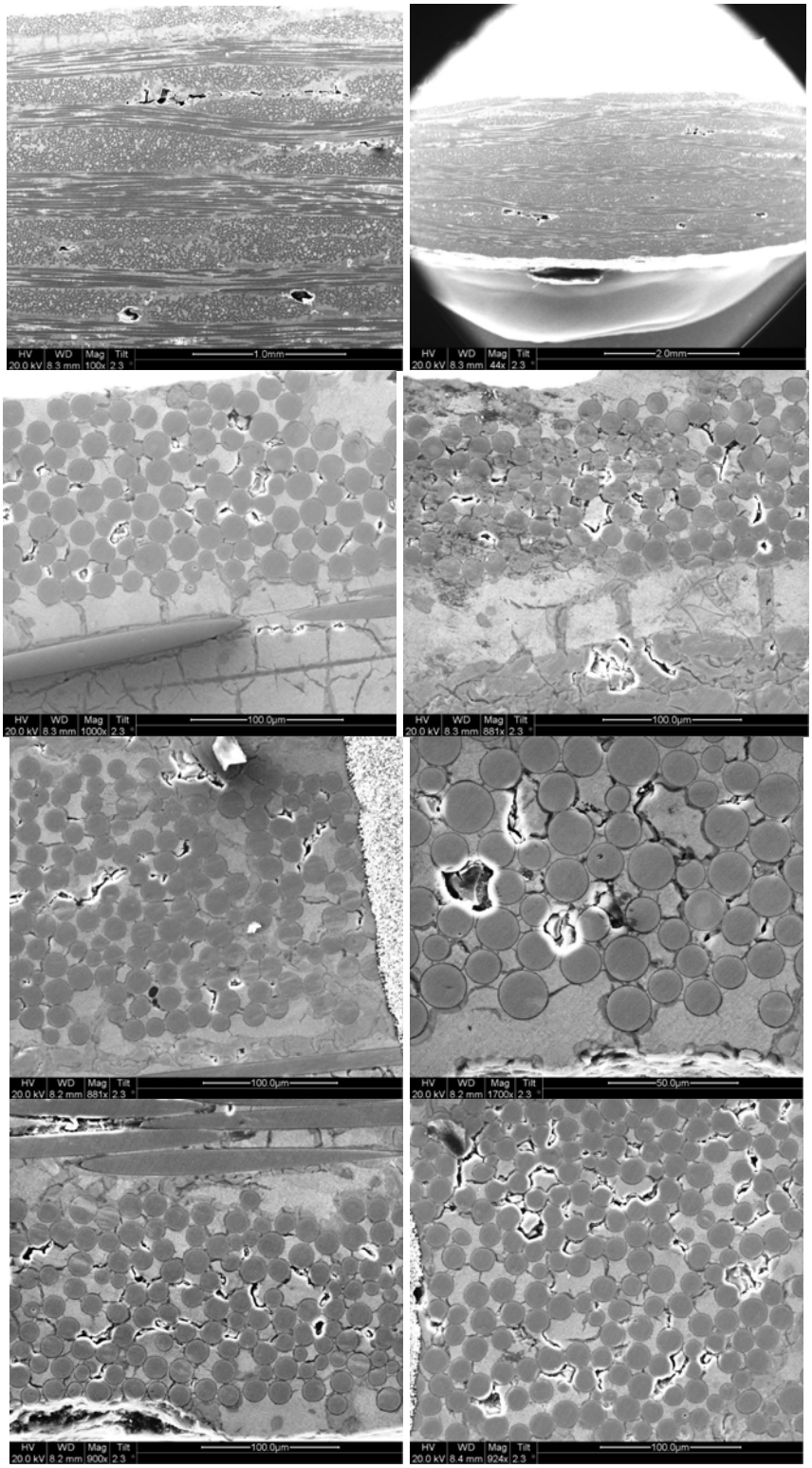


**Figure 155. SEM micrographs of polished as-processed composite C3 specimen**

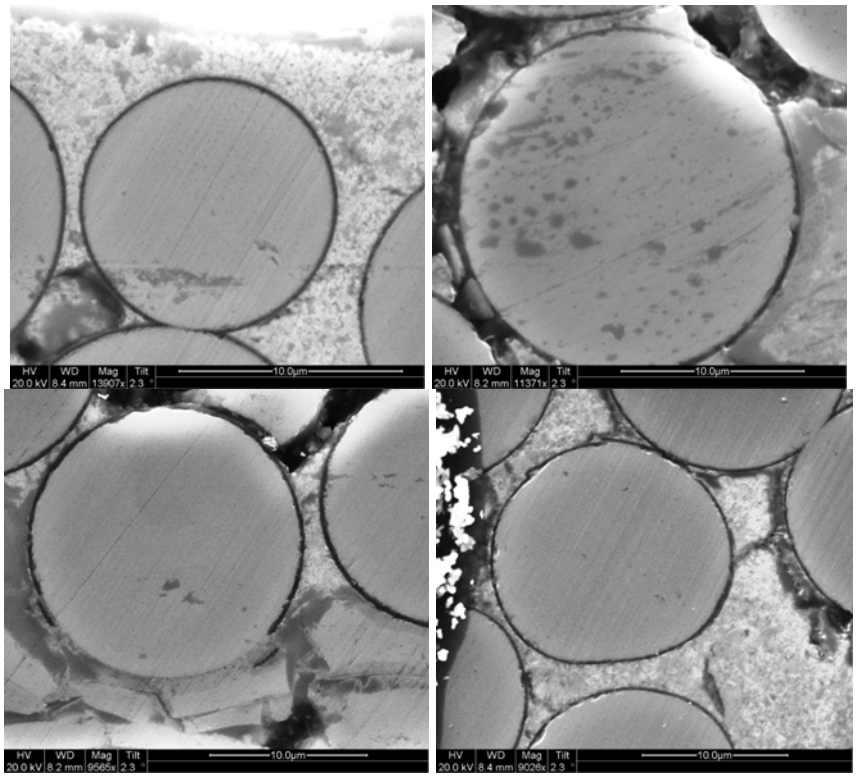


**Figure 156. SEM micrographs of polished as-processed composite C3 specimen.**

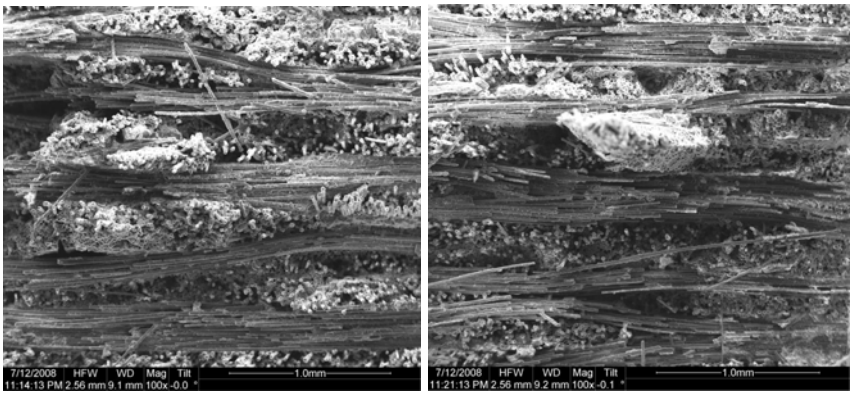


**Figure 157. Fracture surface SEM micrographs of composite C3 specimen aged in air for 8 hours at 815 °C and subjected to a monotonic tension test to failure.**

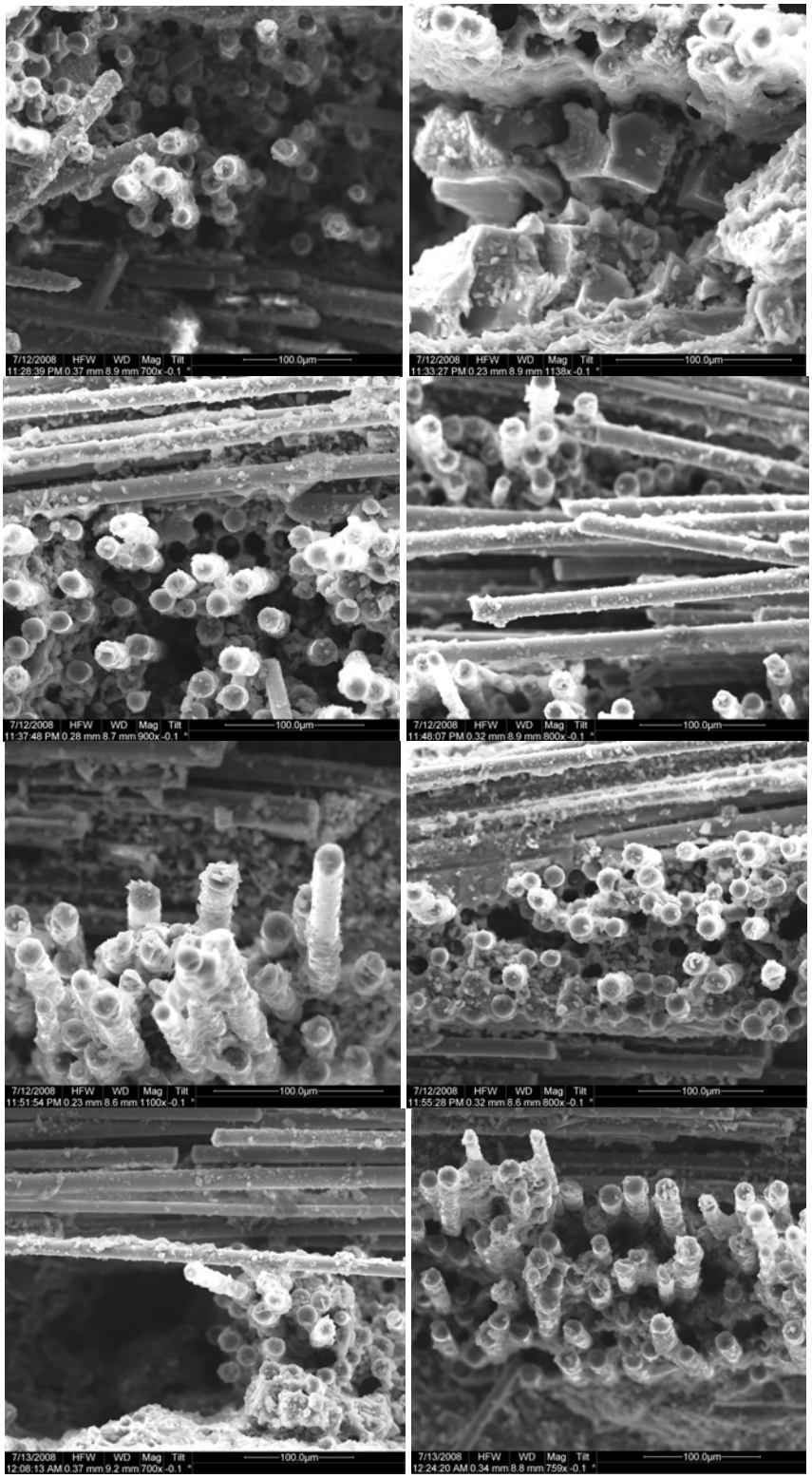

**Figure 158. Fracture surface SEM micrographs of composite C3 specimen aged in air for 8 hours at 815 °C and subjected to a monotonic tension test to failure.**

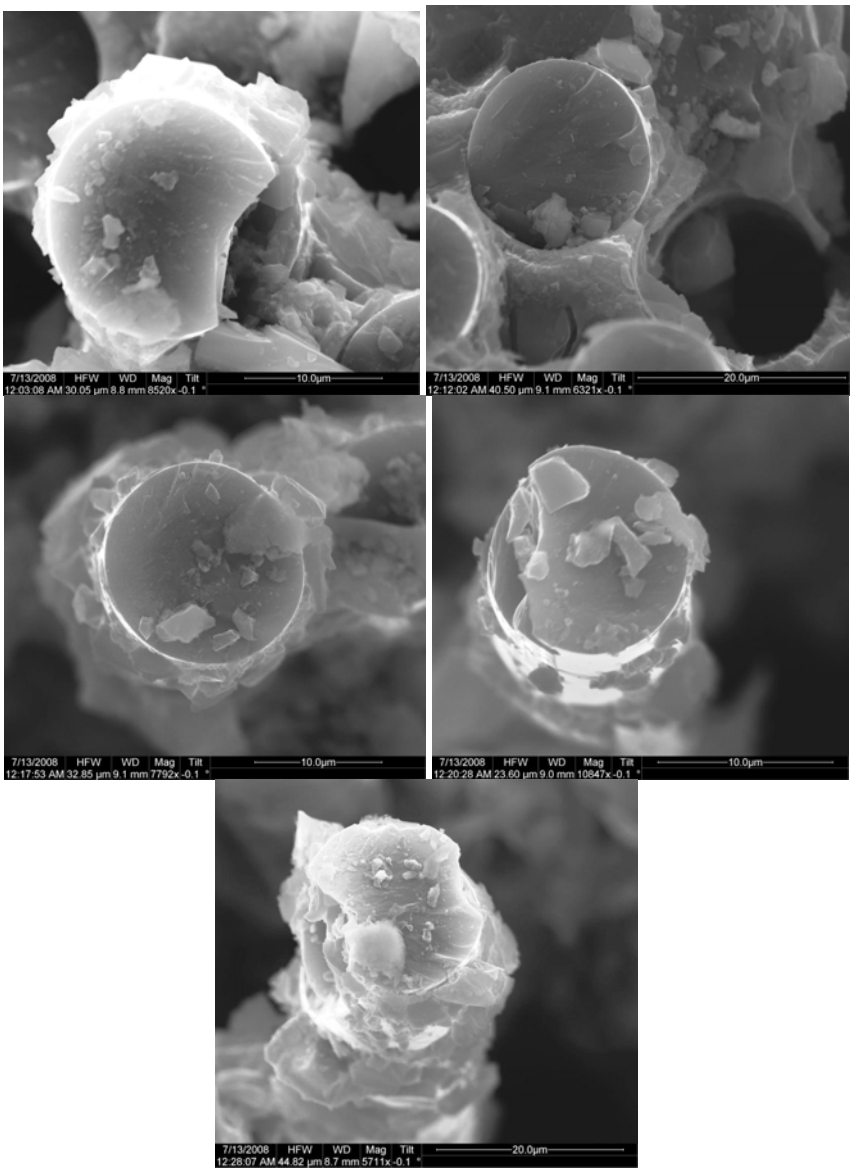


**Figure 159. Fracture surface SEM micrographs of composite C3 specimen aged in air for 8 hours at 815 °C and subjected to a monotonic tension test to failure.**

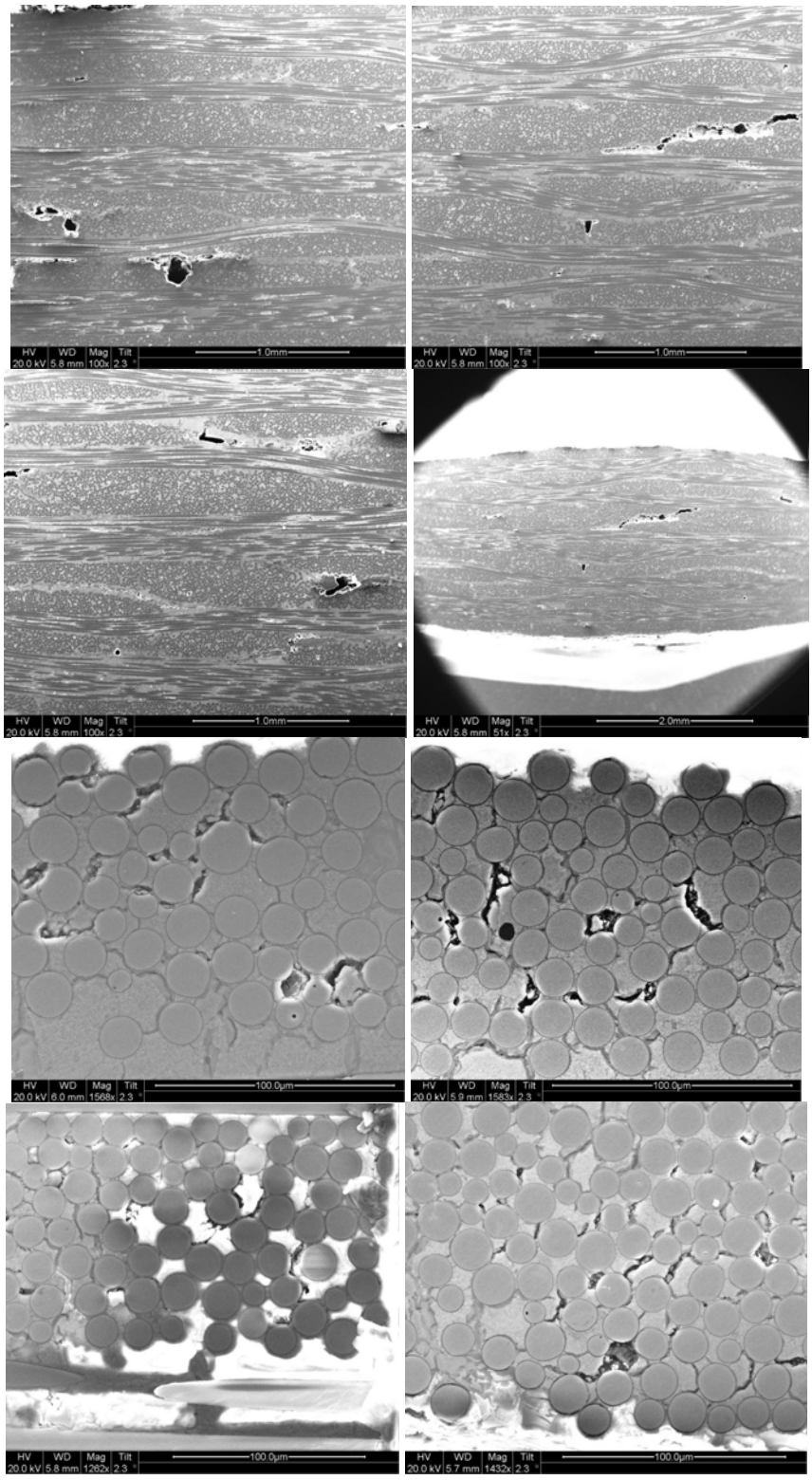

**Figure 160. SEM micrographs of polished composite C3 material aged in air for 8 hours at 815 °C and subjected to a monotonic tension test to failure.**

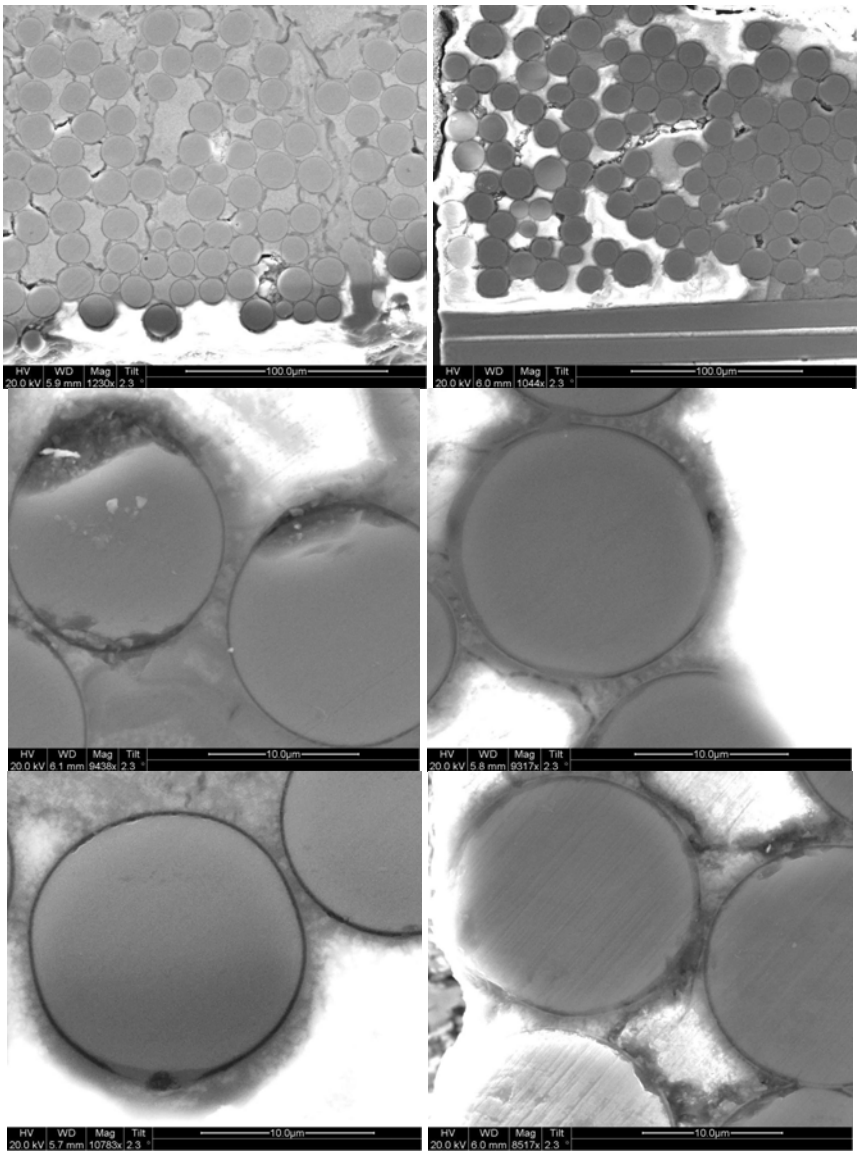


**Figure 161. SEM micrographs of polished composite C3 material aged in air for 8 hours at 815 °C and subjected to a monotonic tension test to failure.**

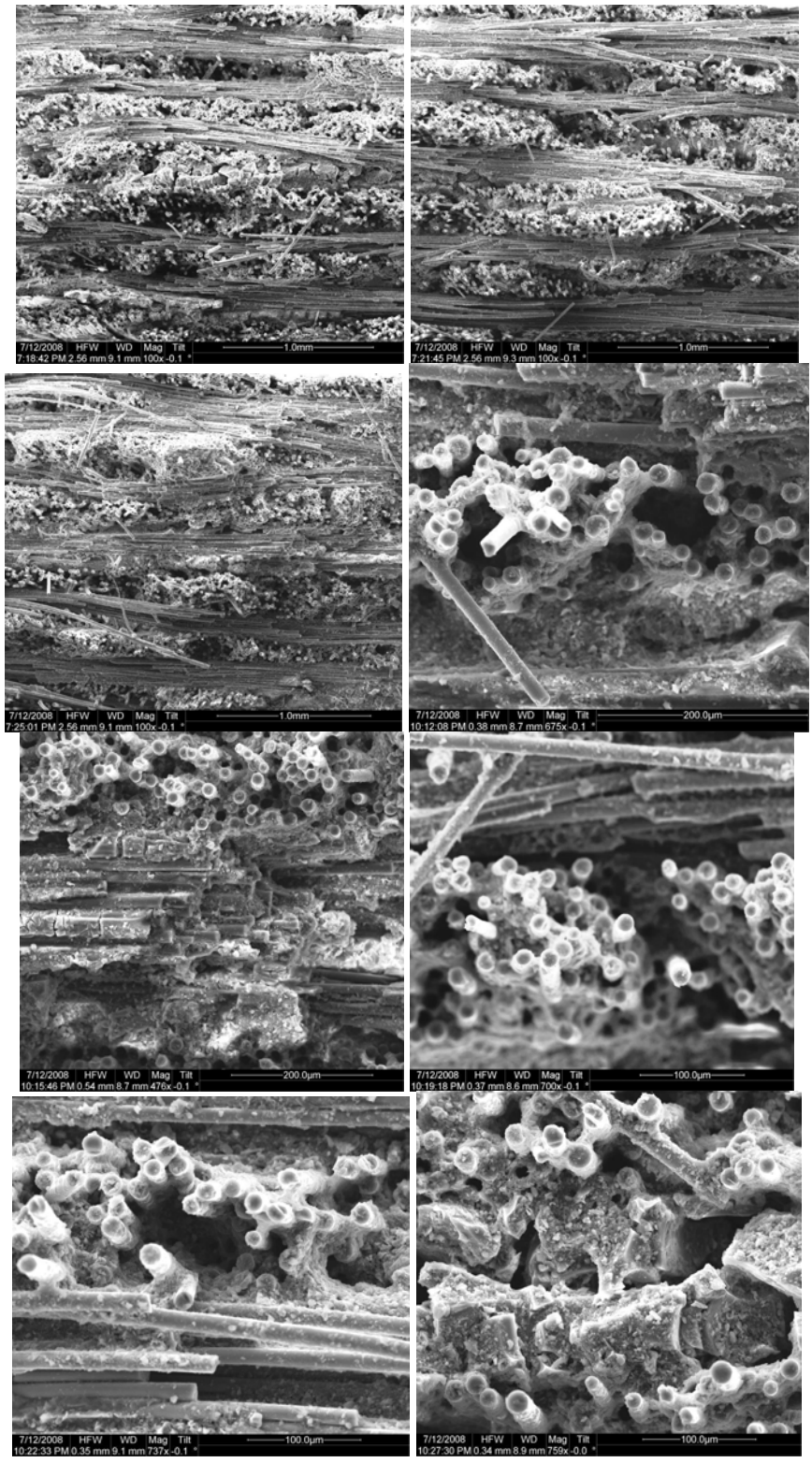

**Figure 162. Fracture surface SEM micrographs of composite C3 specimen aged in steam for 8 hours at 815 °C and subjected to a monotonic tension test to failure.**

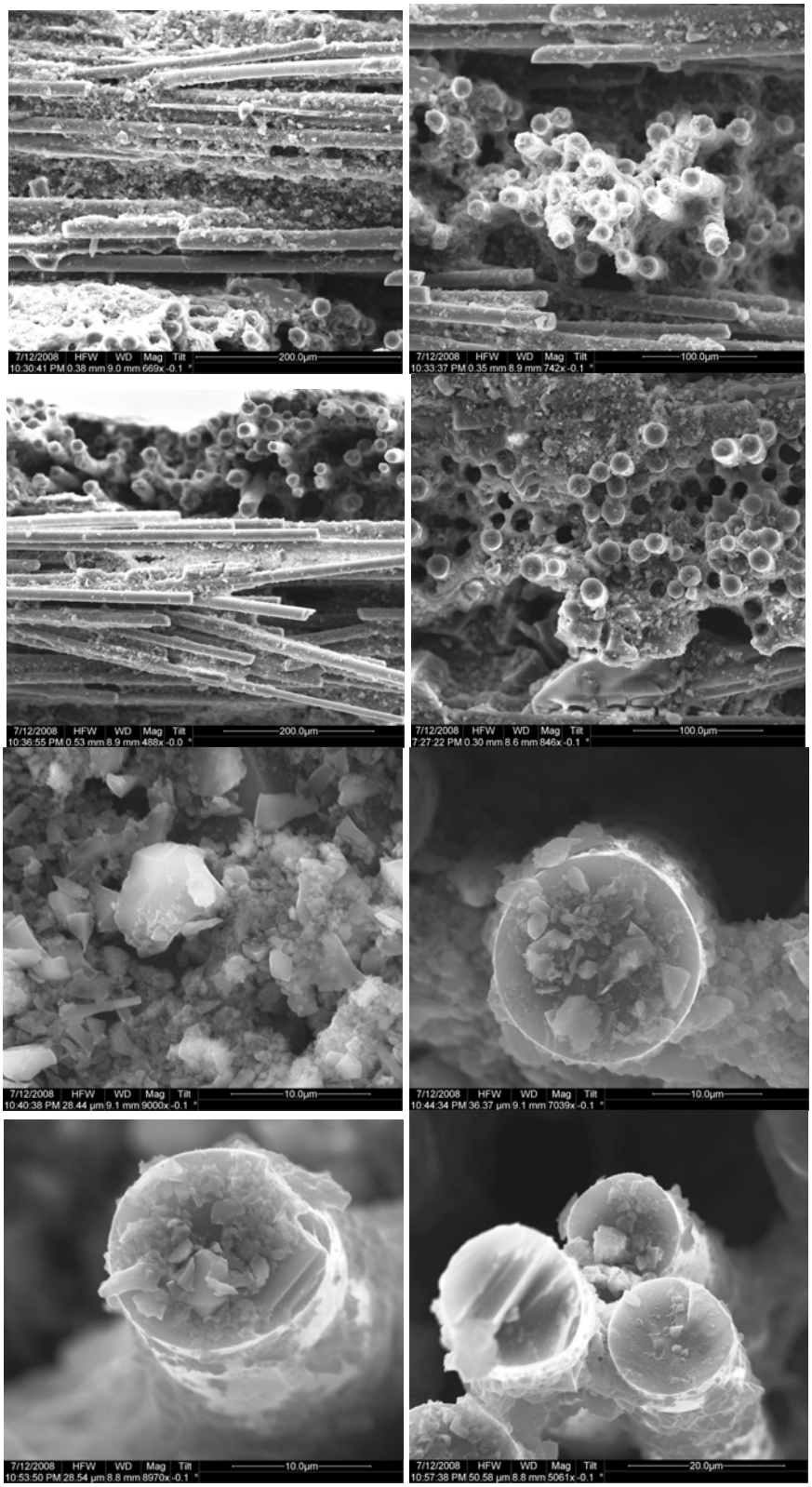


**Figure 163. Fracture surface SEM micrographs of composite C3 specimen aged in steam for 8 hours at 815 °C and subjected to a monotonic tension test to failure.**


**Figure 164. Fracture surface SEM micrograph of composite C3 specimen aged in steam for 8 hours at 815 °C and subjected to a monotonic tension test to failure.**

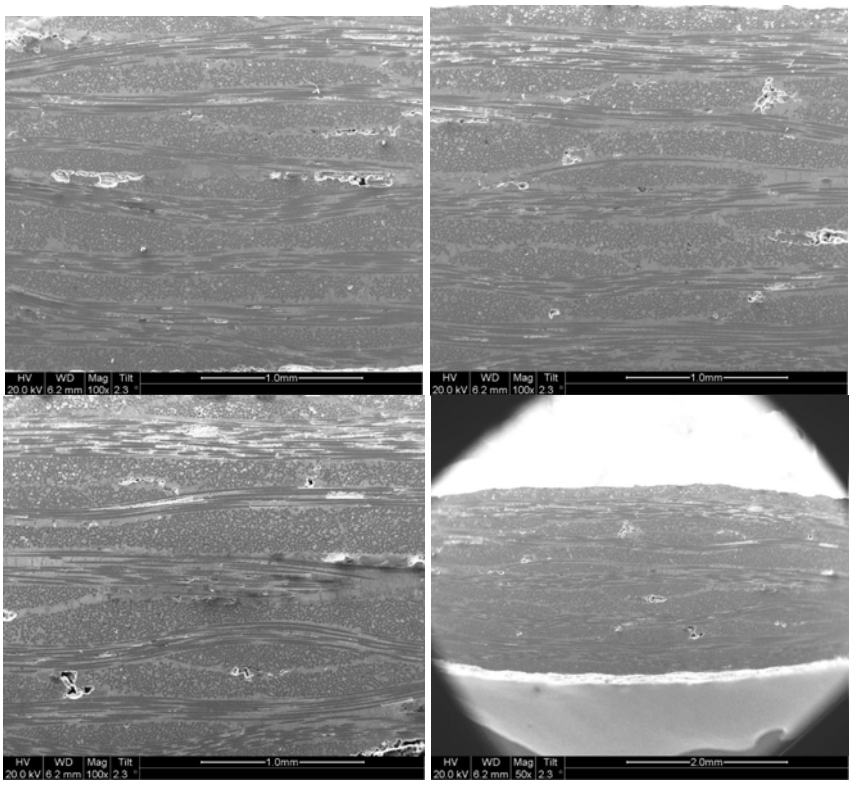


**Figure 165. SEM micrographs of polished composite C3 material aged in steam for 8 hours at 815 °C and subjected to a monotonic tension test to failure.**

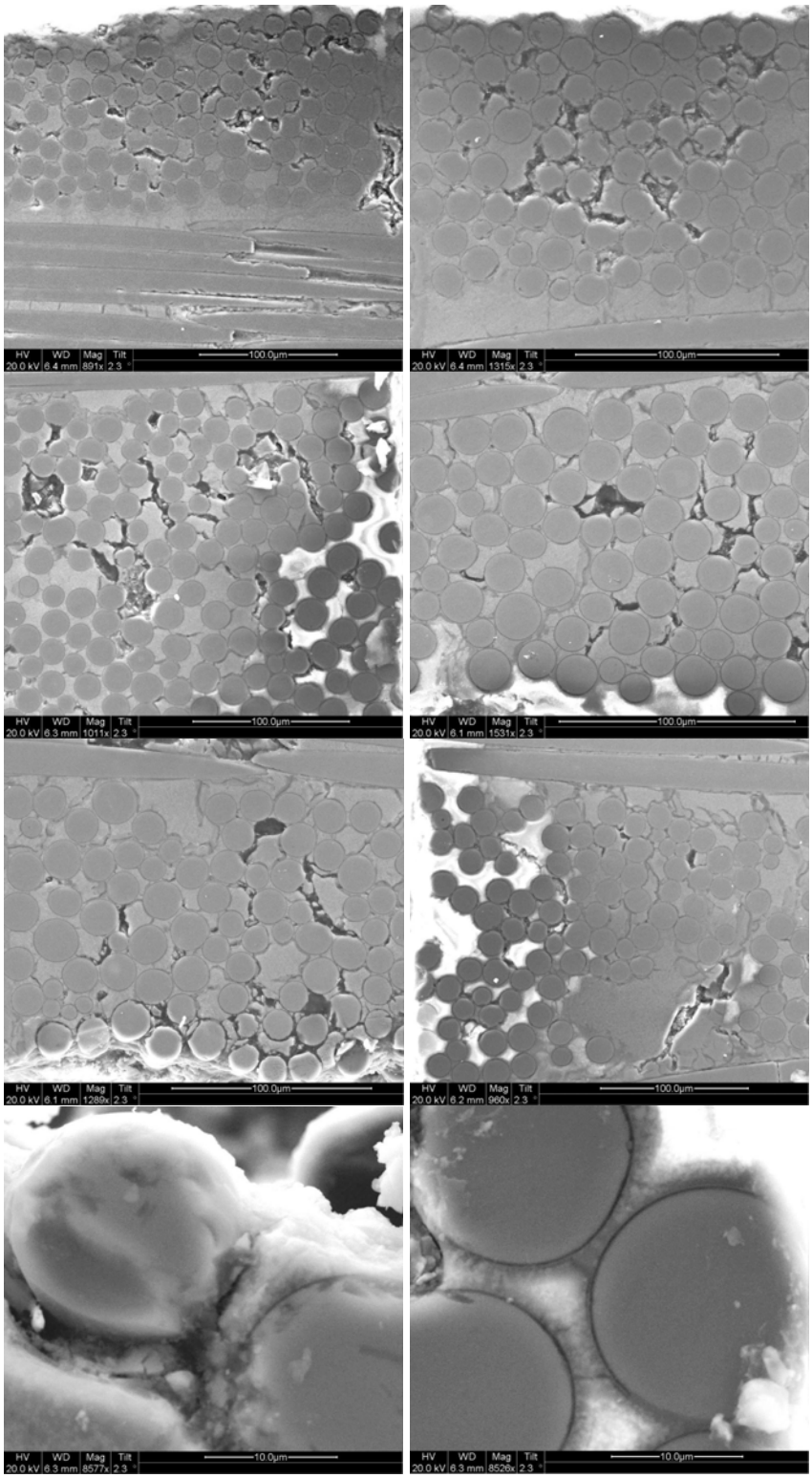


**Figure 166. SEM micrographs of polished composite C3 material aged in steam for 8 hours at 815 °C and subjected to a monotonic tension test to failure.**

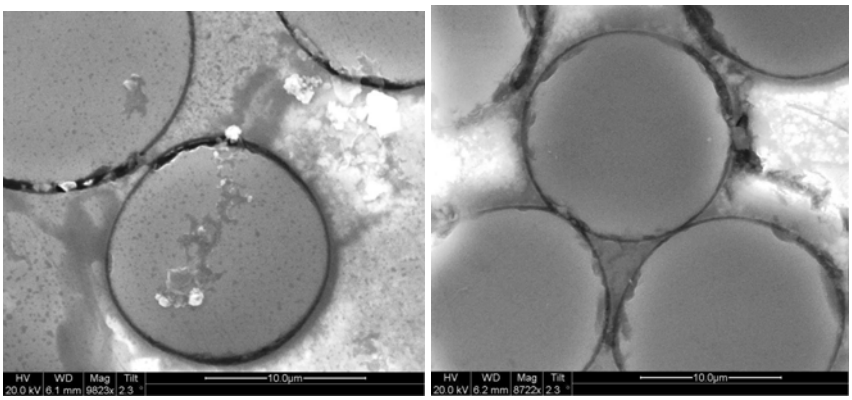

**Figure 167. SEM micrographs of polished composite C3 material aged in steam for 8 hours at 815 °C and subjected to a monotonic tension test to failure.**

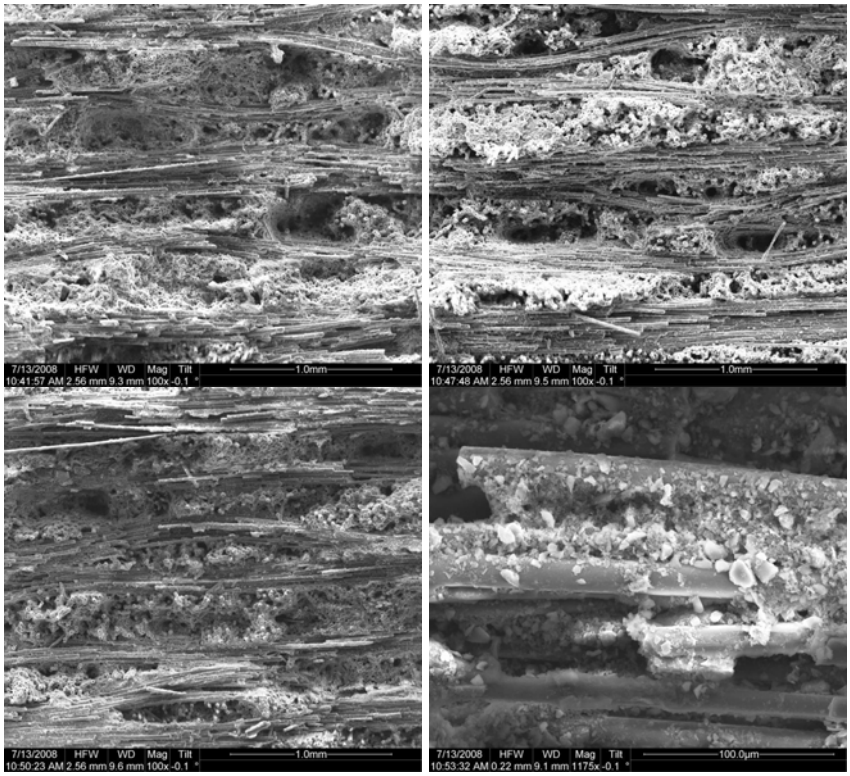

**Figure 168. Fracture surface SEM micrographs of composite C3 specimen pre-fatigued, aged in air for 8 hours at 815 °C, and subjected to a monotonic tension test to failure.**

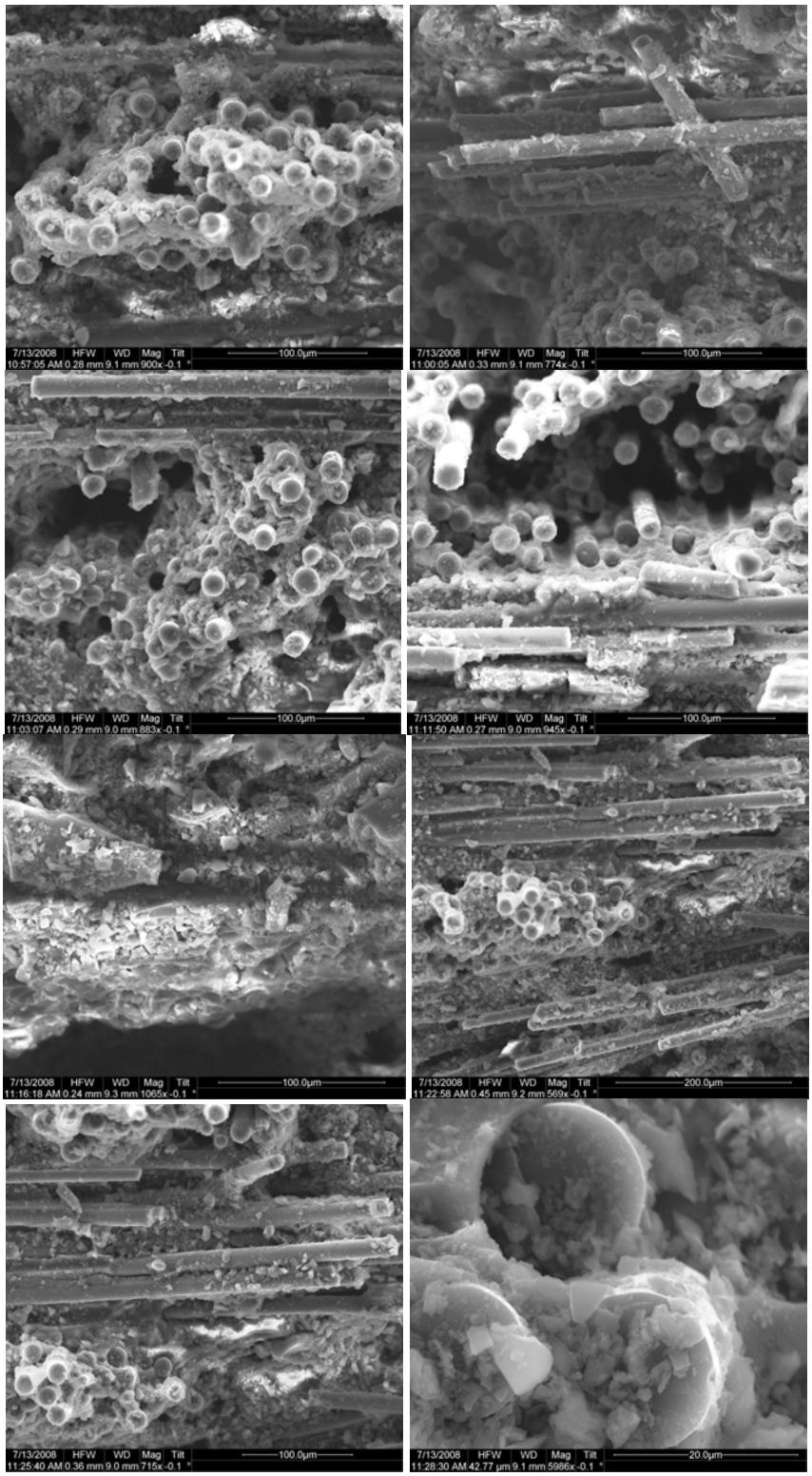


**Figure 169. Fracture surface SEM micrographs of composite C3 specimen pre-fatigued, aged in air for 8 hours at 815 °C, and subjected to a monotonic tension test to failure.**

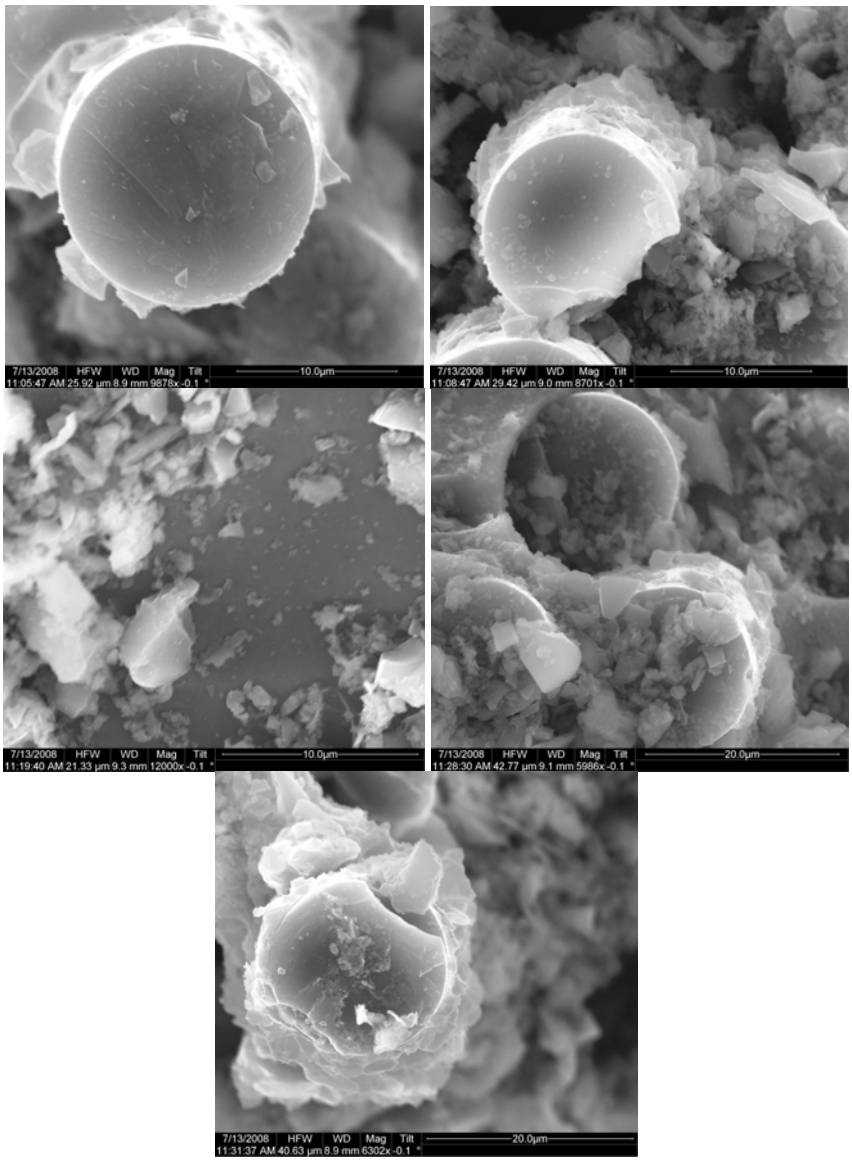


**Figure 170. Fracture surface SEM micrographs of composite C3 specimen pre-fatigued, aged in air for 8 hours at 815 °C, and subjected to a monotonic tension test to failure.**

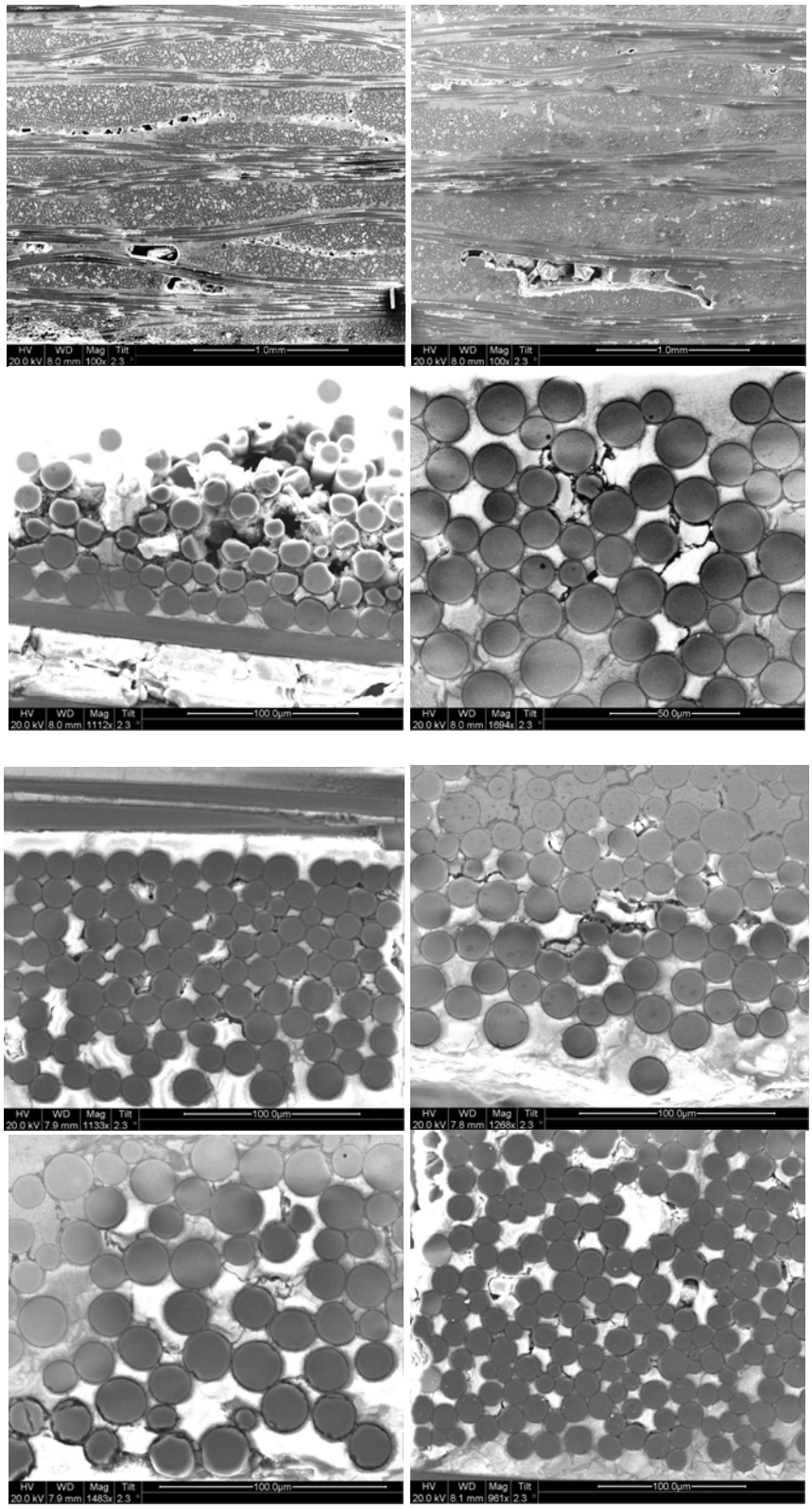

**Figure 171. SEM micrographs of polished composite C3 material pre-fatigued, aged in air for 8 hours at 815 °C and subjected to a monotonic tension test to failure.**

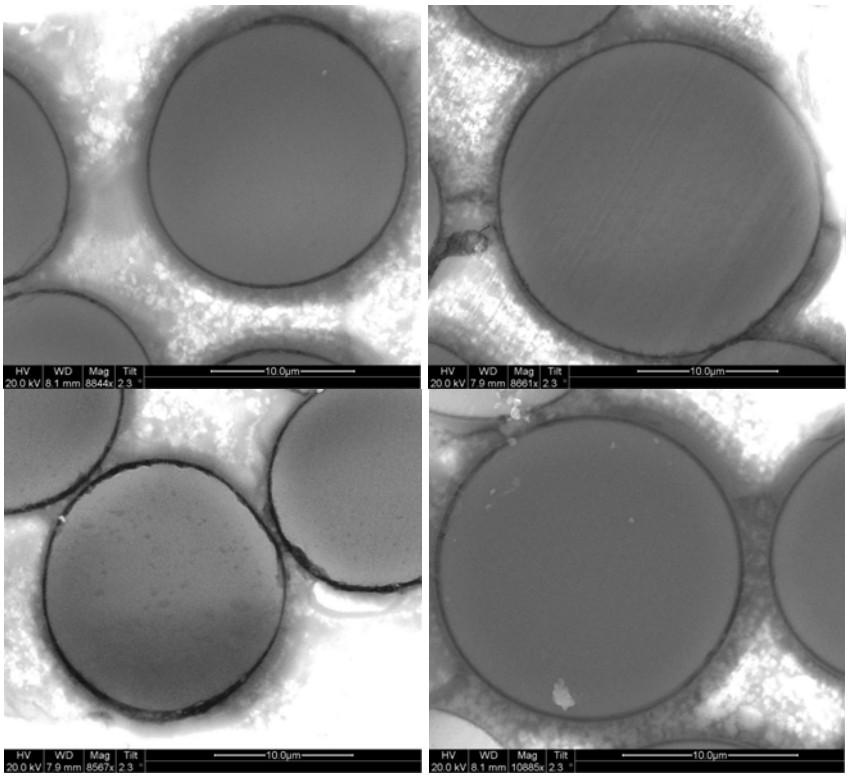


**Figure 172. SEM micrographs of polished composite C3 material pre-fatigued, aged in air for 8 hours at 815 °C and subjected to a monotonic tension test to failure.**

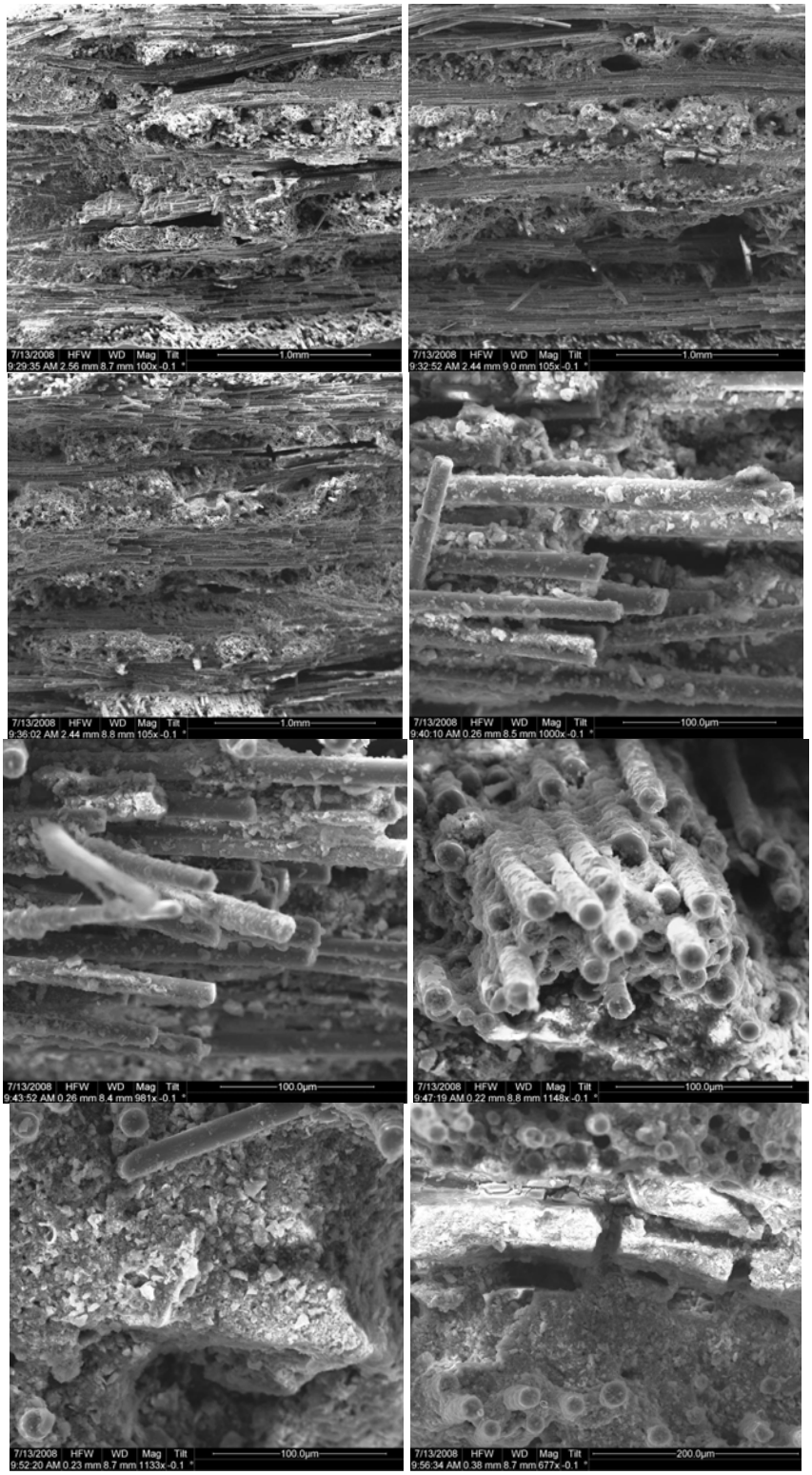

**Figure 173. Fracture surface SEM micrographs of composite C3 specimen pre-fatigued, aged in steam for 8 hours at 815 °C, and subjected to a monotonic tension test to failure.**

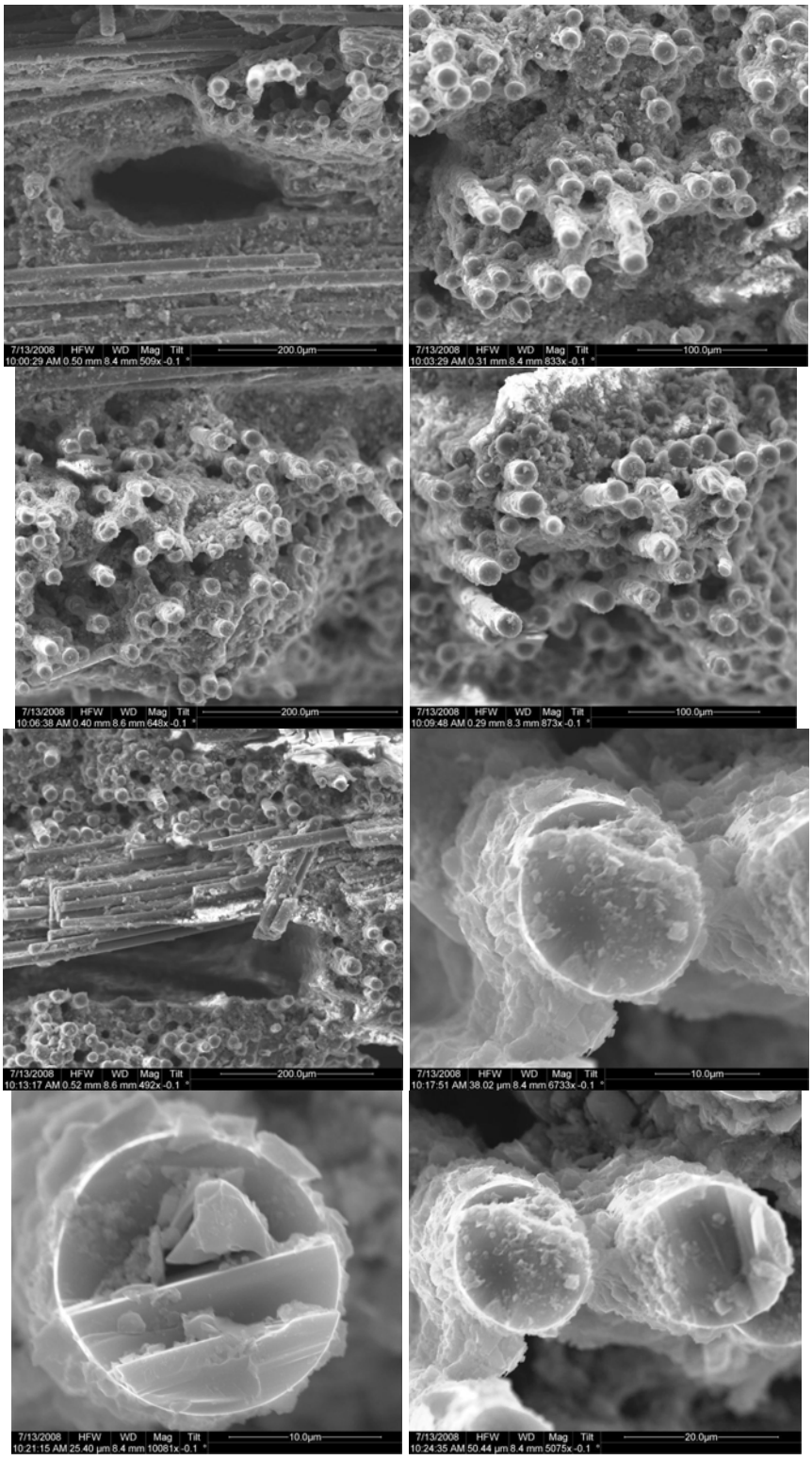


**Figure 174. Fracture surface SEM micrographs of composite C3 specimen pre-fatigued, aged in steam for 8 hours at 815 °C, and subjected to a monotonic tension test to failure.**

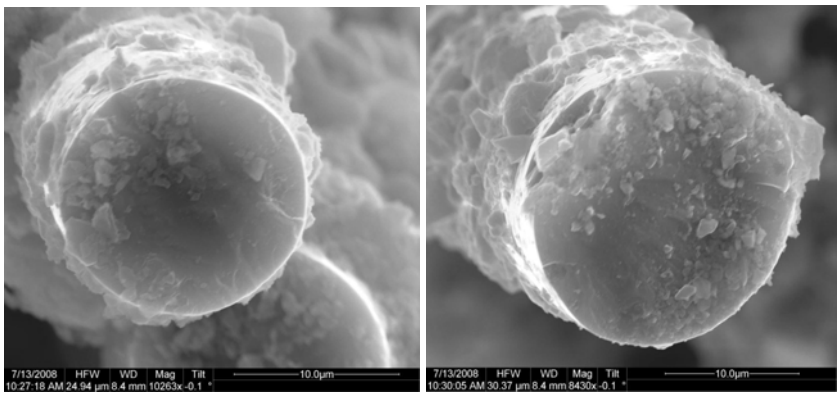

**Figure 175. Fracture surface SEM micrographs of composite C3 specimen pre-fatigued, aged in steam for 8 hours at 815 °C, and subjected to a monotonic tension test to failure.**

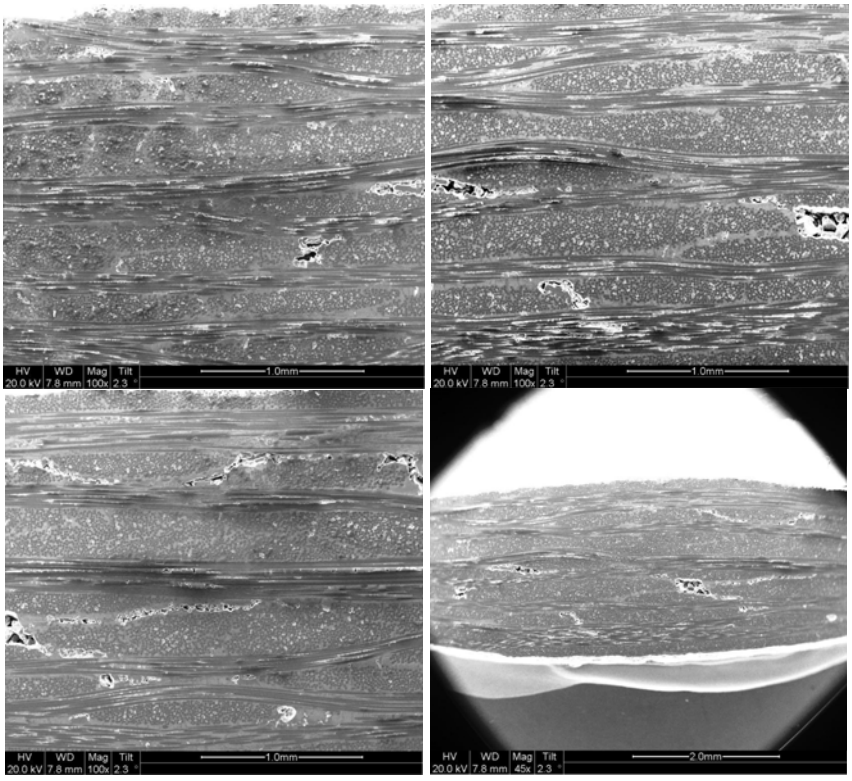

**Figure 176. SEM micrographs of polished composite C3 material pre-fatigued, aged in steam for 8 hours at 815 °C and subjected to a monotonic tension test to failure.**

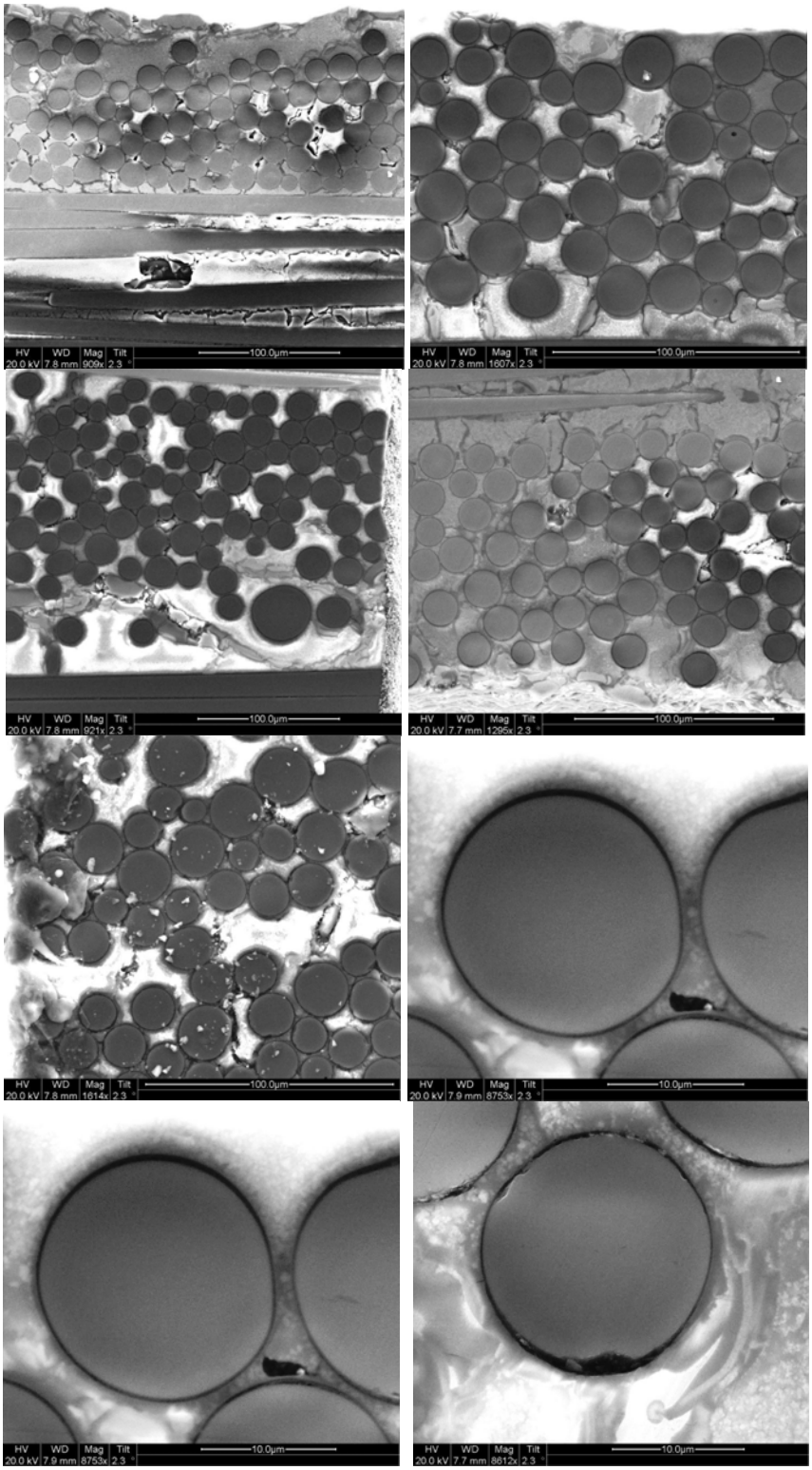

**Figure 177. SEM micrographs of polished composite C3 material pre-fatigued, aged in steam for 8 hours at 815 °C and subjected to a monotonic tension test to failure.**

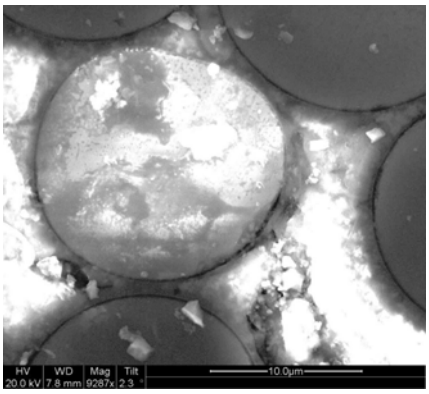


**Figure 178. SEM micrographs of polished composite C3 material pre-fatigued, aged in steam for 8 hours at 815 °C and subjected to a monotonic tension test to failure.**

## Bibliography


1.) Bhatt, R.T., Hull, D.R. "Strength Degrading Mechanisms for CVD SCS-6 SiC Fibers in Aragon Environments," *Prepared for the 17th Annual Conference on Composites, Materials and Structures sponsored by the American Ceramic Society, Cocoa Beach, Florida, January 10-15, 1993*

2.) The Boeing Company, (Sept 2008), http://www.boeing.com.

3.) Budinansky, B., Hutchinson, J.W., Evans, A.G. "Matrix Fracture in Fiber-Reinforced Ceramics," *Journal of the Mechanics and Physics of Solids.* 34:167-189 (1986).

4.) Bunsell, A.R., Piant, A. "A review of the development of three generations of small diameter silicon carbide fibers," *Journal of Material Science.* 41:823-893 (2006)

5.) Chawla, K.K. *Ceramic Matrix Composites* (1st Edition). Boston: Kluwer Academic Publishers, 1993.

6.) Chawla N., Tur Y.K., Holmes J.W., Barber J. R., "High-Frequency Fatigue Behavior of Woven-Fabric-Reinforced Polymer-Derived Ceramic-Matrix Composites," *Journal of the American* Ceramic Society., **81** [5] 1221–30 (1998).

7.) DiCarlo, J.A.; Yun, H.M.; and Brennan, J. J. "SiC/SiC Composites With Improved BN Coating on Fibers," NASA Tech Brief LEW 16864, 2000.

8.) Eber, C.A. *Effect of Temperature and Steam Environment on Fatigue Behaviore of an Oxide-Oxide Continuous Fiber Ceramic Composite.* MS thesis, AFIT/GA/ENY/05-M09. School of Engineering and Management, Air Force Institute of Technology (AU), Wright-Patterson AFB, OH March 2005.

9.) Evans A.G., Zok F.W., McMeeking R.W. "Fatigue of Cermaic Matrix Composites." *Acta metal. mater.* 43:859-875 (1995)

10.)Fair, G.E. private communications (2008).

11.)Filsinger D., Munz S., Schulz A., Wittig S., Andrees G. "Experimental Assesment of Fiber-Reinforced Ceramics for Combustor Walls," *Journal of Engineering for Gas Turbines and Power.* 123:271-275 (2001)

12.)Gonon M.F., Fantozzi G., Murat M., Disson J.P. ''Association of the CVI Process and of the Use of Polysilazane Precursor for the Elaboration of Ceramic Matrix Composites Reinforced by Continuous Fibres,'' *Journal of the European Ceramic Society*, **15**, 185–90 (1995).

13.)Greil P., ''Active-Filler-Controlled Pyrolysis of Preceramic Polymers,'' *Journal of the American Ceramic Society*, 78 [4] 835–48 (1995).

14.) Hetrick, G. *Effects of Frequency and Environment on Fatigue Behavior of an Oxide-Oxide Ceramic Matrix Composite at 1200 °C*. MS thesis, AFIT/GA/ENY/06-J05. School of Engineering and Management, Air Force Institute of Technology (AU), Wright-Patterson AFB, OH March 2005.

15.) Harlen L.B. *Creep-Rupture Behavior of an Oxide/Oxide Ceramic Matrix Composite at Elevated Temperatures in Air and Steam Environments.* AFIT/GA/ENY/05-M05. School of Engineering and Management, Air Force Institute of Technology (AU), Wright-Patterson AFB, OH March 2005.

16.) Jacobsen, T.K., Bronsdsted, P. "Mechanical Properties of Two Plain-Woven Chemical Vapor Infiltrated Silicon Carbide-Matrix Composites," *Journal of the American Ceramic Society*, 84 [5] 1043–1051 (2001).

17.) Jones R.E., Petrak, D., Rabe, J., Szweda, A. "SYLRAMIC™ SiC fibers for CMC reinforcement," *Journal of Nuclear Materials,* 556-559 (2000)

18.) Klemm, H., Herrmann, M., Schubert, C. "High Temperature Oxidation and Corrosion of Silicon-Based Non-Oxide Ceramics," *Journal of Engineering for Gas Turbines and Power,* 122:13-18 (2000)

19.) Jacobson, N.S. "Corrosion of Silicon-Based Ceramics in Combustion Environments" *Journal of the American Ceramic Society,* 76 [1] 3-28 (1993)

20.) Kalluri S, Calomino A.M., and Brewer D. N. "High Temperature Tensile Properties and Fatigue Behavior of a Melt-Infiltrated SiC/SiC Composite,"

21.) Karandikar, P., Chou, T-S., "Characterization and Modeling of Microcracking and Elastic Moduli Changes in Nicalon/CAS Composites," *Composites Science and Technology,* 46:253-263 (1993)

22.) Lee, S.S., Zawada, L.P., Staehler, J.M., Folsom, C.A.

23.) Lipowitz, J., et al. "Structure and Properties of Sylramic Silicon Carbide Fiber. A Polycrystalline, Stoichiometric □-SiC Composition," *Ceramic Engineering and Science Procedings,* 18 [3] 147-157 (1993)

24.) Lundberg, R., Pompe, R., Carlsson, R., Goursat, P., ''Fibre Reinforced Silicon Nitride Composites,'' *Composites Science and Technology*, 37**:**165–176 (1990).

25.) Machida, T., Miyata, H., Usami, S., Ohta, H. "Fatigue Behavior of Structural Ceramics at Elevated Temperatures," *Cyclic Fatigue in Ceramics,* New York: Elsevier Scinece B.V., 1995

26.) McNulty J.C., Zok, F.W., "Low-cycle fatigue of Nicalon™-fiber-reinforced ceramic composites," *Composites Science and Technology*, 59:1597-1607 (1999)

27.) Mehrman, J.M., *Effect of Hold Times on Fatigue Behavior of Nextel™ 720/Alumina Ceramic Matrix Composite at 1200 °C in Air and in Steam Environment*. MS thesis, AFIT/GAE/ENY/06-M23. School of Engineering and Management, Air Force Institute of Technology (AU), Wright-Patterson AFB, OH March 2005.

28.) Mehrman J.M., Ruggles-Wrenn M.B., Baek S.S., "Influence of hold times on the elevated-temperature fatigue behavior of an oxide-oxide ceramic composite in air and in steam environment," *Composites Science and Technology* 67:1425-1438 (2007)

29.) Mizuno, M., Zhu, S., Nagano, Y., Sakaida, Y., Kagawa, Y., Watanabe, M. "Cyclic-Fatigue Behavior of SiC/SiC Composites at Room and High Temperatures," *Journal of American Ceramic Society,* 79 [12] 3065-3077 (1996)

30.) Mizuno, M., Zhu, S., Kagawa, Y., Kaya, H., "Creep and Fatigue Behavior in Hi-Nicalon-Fiber-Reinforced Silicon Carbide Composites at High Temperatures," *Journal of American Ceramic Society,* 82 [1] 117-128 (1999)

31.) More, K.L., Tortoreli, P.F., Ferber, M.K., Walker, L.R., Keiser, J.R., Miriyala, N., Brentall, W.D., Price. J.R., "Exposure of Ceramics and Ceramic Matrix Composites in Simulated and Actual Combustor Environments," *Journal of Engineering for Gas Turbines and Power,* 122:212-218

32.) Gregory N. Morscher, Hee Mann Yun, James A. DiCarlo, Linus Thomas-Ogbuji

33.) Naslain, R.R. "Design, preparation and properties of non-oxide CMCs for application in engines and nuclear reactors: an overview," *Composites Science and Technology,* 64:155-170 (2004)

34.) Naslain, R.R., "SiC-Matrix Composites: Nonbrittle Ceramics for Thermo-Structural Application" *International Journal of Applied Ceramic Technology,* 2 [2] 75-84 (2005)

35.) Raymer, D.P., *Aircraft Design: A Conceptual Approach, 3rd Ed.* Reston, VA: American Institute of Aeronautics and Astronautics, Inc, 1999.

36.) Ruggles Wrenn, M.B. private communications (2008)

37.) Ruggles-Wrenn, M.B., Siegert, G.T., Baek, S.S. "Creep behaviore of Nextel™720/alumina ceramic composite with ±45° fiber orientation at 1200 °C," *Composites Science and Technology,*10:1-8 (2007)

38.) Ruggles-Wrenn M.B., Hetrick G., Baek, S.S., "Effects of frequency and environment on fatigue behavior of an oxide-oxide ceramic composite at 1200 °C," *International Journal of Fatigue*, 10:1-15 (2007)

39.) Sato, K., Morozumi, H., Tezuka, A., Funayama, O., Isoda, T., ed. Evans, A.G., Naslain, R. ''Interface and Mechanical Properties of Ceramic Fiber Reinforced Silicon Nitride Composites Prepared by a Preceramic Polymer Impregnation Method''; *High Temperature Ceramic-Matrix Composites II: Manufacturing and Materials Development*. 58:199-204 (1995).

40.) Sharma, Ramesh, private communications (2008).
41.) Sirieix, F., Goursat, P., Lemcote, A., Dauger, A., ‘‘Pyrolysis of Polysilazanes: Relationship between Precursor Architecture and Ceramic Microstructure,’’ *Composites Science and Technology*, 37:7–19 (1990).

42.) Staehler, J., Zawada, L.P., “Performance of Four Ceramic-Matrix Composite Divergent Flap Inserts Following Ground Testing on an F110 Turbofan Engine,” *Journal of American Ceramic Society,* 83 [7] 1727-1738 (2000)

43.) Verrilli, M.J., Opila, E.J., Calomio, A., Kiser, J.D. “Effect of Environment on the Stress-Rupture Behavior of a Carbon-Fiber-Reinforced Silicon Carbide Ceramic Matrix Composite,” *Journal of the American Ceramic Society*, 87 [8] 1536-1542 (2004)

44.) Yasmin, A., Bowen P., “Fatigue behavior of cross-ply Nicalon/CAS-II glass-ceramic matrix composite at room and elevated temperatures,” *Composites: Part A*, 35:83-94 (2004)

45.) Yun, H.M., DiCarlo, J. A. “Comparison of the Tensile, Creep, and Rupture Strength Properties of Stoichiometric SiC Fibers,” *Ceramaic Engineering and Science Proceedings*, 20 [3] 259-272, (1999)

46.) Yun, H.M., et al. “Tensile Behavior of SiC/SiC Composites Reinforced by Treated Sylramic SiC Fibers,” *Ceramic Engineering and Science Proceedings*, 22 [3] 521-531 (2001).

47.) Yun H.M., Dicarlo J.M., “Thermomechanical Characterization of SiC Fiber Tows and Implications for CMC,” *Prepared for the 12th International Conference on Composite Materials cosponsored by the AMAC, CEA, and SF2M, Paris, France, July 5-9, 1999,* 1-10 (1999)

48.) Zawada, L.P., Staehler, J., Steel, S. “Consequence of Intermittent Exposure to Moisture and Salt Fog on the High-Temperature Fatigue Durability of Several Ceramic-Matrix Composites,” *Journal of the American Ceramic Society,* 86 [8] 1282-1291 (2003)

49.) Zhu, S., Mizuno, M., Kagawa, Y., Mutoh, Y. “Monotonic tension, fatigue and creep behavior of SiC-fiber-reinforced SiC-matrix composites: a review,” *Composites Science and Technology,* 59:833-851 (1999)

50.) Zhu, S., Mizuno, M., Nagano, Y., Kagawa, Y., Kaya, H. “Tensile Creep Behaviore of a SiC-Fiber/SiC Composite At Elevated Temperatures,” *Composites Scinence and Technology,* 57:1629-1637 (1997)

## Vita

2nd Lieutenant Vipul Sharma is a 2003 graduate from Catalina Foothills High School in Tucson, AZ and a 2007 graduate of the United States Air Force Academy where he majored in Mechanical Engineering and minored in Mandarin.

His first assignment was to the Air Force Institute of Technology at Wright Patterson Air Force Base, OH. Upon graduation in the summer of 2008 he will attend undergraduate pilot training at Laughlin Air Force Base, TX.

# REPORT DOCUMENTATION PAGE

*Form Approved*
*OMB No. 074-0188*



| 1. REPORT DATE *(DD-MM-YYYY)* | 2. REPORT TYPE | 3. DATES COVERED *(From – To)* |
|---|---|---|
| 05-09-2008 | Master's Thesis | April 2008 – Sept 2008 |

**4. TITLE AND SUBTITLE**

EFFECTS OF TEMPERATURE AND STEAM ENVIRONMENT ON FATIGUE BEHAVIOR OF THREE SIC/SIC CERAMIC MATRIX COMPOSITES

**5a. CONTRACT NUMBER**

**5b. GRANT NUMBER**

**5c. PROGRAM ELEMENT NUMBER**

**6. AUTHOR(S)**

Sharma, Vipul, 2d Lt, USAF

**5d. PROJECT NUMBER**
2008-107

**5e. TASK NUMBER**

**5f. WORK UNIT NUMBER**

**7. PERFORMING ORGANIZATION NAMES(S) AND ADDRESS(S)**
Air Force Institute of Technology
Graduate School of Engineering and Management (AFIT/EN)
2950 Hobson Way, Building 640
WPAFB OH 45433-8865

**8. PERFORMING ORGANIZATION REPORT NUMBER**
AFIT/GAE/ENY/08-S02

**9. SPONSORING/MONITORING AGENCY NAME(S) AND ADDRESS(ES)**
Dr. Geoff Fair
AFRL/RXLN
Bldg 655
2230 Tenth Street
WPAFB OH 45433-7817

Dr. Michael Cinibulk
Address: Same as Dr. Geoff Fair

Dr. L.P. Zawada
Address: Same as Dr. Geoff Fair

**10. SPONSOR/MONITOR'S ACRONYM(S)**

**11. SPONSOR/MONITOR'S REPORT NUMBER(S)**

**12. DISTRIBUTION/AVAILABILITY STATEMENT**

APPROVED FOR PUBLIC RELEASE; DISTRIBUTION UNLIMITED.

**13. SUPPLEMENTARY NOTES**

**14. ABSTRACT**

The fatigue behavior of two woven SiC-SiNC ceramic matrix composites (CMCs) was investigated at 1300 °C in laboratory air and in steam. The first composite (C1) consists of a PIP SiNC matrix reinforced with Sylramic (Syl) fibers woven in a five-harness satin weave fabric and coated with a proprietary dual-layer interface. The second composite (C2) consists of a modified PIP SiNC matrix reinforced with Sylramic-iBN (Syl-iBN) fibers woven in a five-harness satin weave fabric and coated with a proprietary dual-layer interface. The tensile stress-strain behavior was investigated and the tensile properties measured at 1300°C. Tension-tension fatigue behavior was studied for fatigue stresses ranging from 100 to 180 MPa at 1300 °C in air and in steam. The presence of steam caused noticeable degradation in fatigue performance of both composites at 1300°C. The fatigue limit of the composite C1 (based on a run-out condition of $2 \times 10^5$ cycles) was 100 MPa (53% UTS at 1300°C) in both air and steam. The fatigue limit of the composite C2 was 160 MPa (66% UTS) in air and 140 MPa (58% UTS) in steam. The retained strength and modulus of all specimens that achieved run-out were characterized. Specimens of both composites tested in air retained 100% of their tensile strength, while the specimens of both composites tested in steam retained only about 90% of their tensile strength.

**15. SUBJECT TERMS**
Ceramic Matrix Composites, Fatigue, Silicon-Carbide/Silicon-Carbide, Sylramic, Nicalon, Scanning Electron Microscope,

| 16. SECURITY CLASSIFICATION OF: | | | 17. LIMITATION OF ABSTRACT | 18. NUMBER OF PAGES | 19a. NAME OF RESPONSIBLE PERSON |
|---|---|---|---|---|---|
| a. REPORT | b. ABSTRACT | c. THIS PAGE | | | Dr. Marina B. Ruggles-Wrenn |
| U | U | U | UU | 229 | 19b. TELEPHONE NUMBER *(Include area code)* (937) 785-3636, ext 4641 Email: marina.ruggles-wrenn@afit.edu |